MAGISTERARBEIT

Titel der Magisterarbeit

The Influence of Core Size on Magnetic Field Generation in (Exo-)Planets

Verfasser

Ing. Manfred Gold, Bakk.rer.nat.

angestrebter akademischer Grad

Magister der Naturwissenschaften (Mag.rer.nat.)

Wien, im März 2012

Studienkennzahl lt. Studienblatt:	A 066 861
Studienrichtung lt. Studienblatt:	Astronomie
Betreuerin:	Univ.-Prof. Dr. Maria G. Firneis

Contents

Acknowledgements

I want to express my gratitude to Univ.-Prof. Dr. Maria G. Firneis (Institute for Astronomy, University of Vienna) for supporting me during the time I worked on my master's thesis and for giving me the chance of being part of the Research Platform: Exolife. I want to thank Johannes Leitner (Institute for Astronomy, University of Vienna, Research Platform: Exolife, University of Vienna) for countless discussions about my thesis, planetary processes and exotic life, and science in general as well as for assistance and support in dealing with any problems concerning the completion of this work. Many thanks to Francis Nimmo (University of Santa Cruz, California) for answering my questions regarding his chapter in the "Treatise on Geophysics, Vol. 8" so patiently and extensively, and his help with the derivation of the entropy budget. Finally I want to thank my parents, who spurred my interest in natural sciences, enabled me to pursue my studies in astronomy and physics, and supported but never criticized my late career change.

List of Figures

List of Tables

Terrestrial Planets and Moons General Fact Sheet

Body	**M** (kg)	**R** (km)	ρ ($kg\ m^{-3}$)	**a** (km)	**MoI**	P_O (d)	P_R (h)	M_P ($T\ m^3$)	B_S (nT)
Mercury	$0.33 \cdot 10^{24}$	2439.7	5427	$57.91 \cdot 10^6$	0.33	87.97	–	$3.49 - 3.92 \cdot 10^{12}$ [1]	$250 - 290$ [1]
Venus	$4.8685 \cdot 10^{24}$	6051.8	5243	$108.21 \cdot 10^6$	0.33	224.70	–	$\leqslant 8.4 \cdot 10^{10}$ [2]	–
Earth	$5.9736 \cdot 10^{24}$	6378.1	5515	$149.6 \cdot 10^6$	0.3308	365.26	–	$7.746 \cdot 10^{15}$ [3]	$25000 - 60000$ [4]
Moon	$0.07349 \cdot 10^{24}$	1738.1	3350	$0.3844 \cdot 10^6$	0.394	–	27.3217	$\leqslant 4.4 \cdot 10^8$ [5]	[6]
Mars	$0.64185 \cdot 10^{24}$	3396.2	3933	$227.92 \cdot 10^6$	0.366	686.98	–	$\leqslant 2.0 \cdot 10^{11}$ [7]	$\leqslant 5$ [8]
Ganymede	$1481.9 \cdot 10^{20}$	2631.2	1940	$1070.4 \cdot 10^3$	0.3105 [9]	7.154553	S	$1.4 \cdot 10^{13}$ [10]	719 [11]
Io	$893.2 \cdot 10^{20}$	1821.6	3530	$421.6 \cdot 10^3$	0.37685 [12]	1.769138	S	–	–
Titan	$1345.5 \cdot 10^{20}$	2575	1880	$1221.83 \cdot 10^3$	0.3414 [13]	15.945421	S	$\leqslant 7 \cdot 10^{10}$ [14]	4.1 [14]

Table 1: M=Mass, R=equatorial radius, ρ=mean density, a=semimajor axis, MoI=dimensionless moment of inertia, P_O=sidereal orbit period, P_R=Rotation Period, M_P=dipole moment, B_S=surface field strength, S=synchronous rotation, i.e. rotation period=orbital period; all data are taken from http://nssdc.gsfc.nasa.gov/planetary/factsheet/, except indicated otherwise; [1] Anderson et al. (2001), [2] Phillips and Russel (1987), [3] http://de.wikipedia.org/wiki/Erdmagnetfeld, 01/2012, [4] Hulot et al. (2010), [5] Dyal et al. (1974), [6] magnetized regions with intensities up to 250 nT exist on the moon, [7] Acuña et al. (1998), [8] Acuña et al. (1998) - magnetic signatures with intensities up to 1500 nT exist on Mars, [9] Anderson et al. (1996), [10] Sage (1997), [11] Kivelson (2002), [12] Anderson et al. (2001), [13] Iess et al. (2010), [14] Neubauer et al. (1984).

Chapter 1

Magnetic Fields of Terrestrial Planets and Moons

1.1 Introduction

Since the ancient Chinese have discovered earth's magnetic field, a lot of research has been performed to find the physical laws that govern it and gain insight into the multitude of processes involved in its origin. By now the fundamental principles are known to scientists (see Chapter 2), and although there still remains a lot to be done, highly sophisticated numerical simulations are able to reproduce the key features of planetary magnetic fields fairly well. But research did not come to a halt at earth, and with the dawn of the space age, interest in other planets of the solar system and their magnetic fields grew. During the last decades many bodies of the solar system have been investigated and today all objects possessing a magnetic field, terrestrial planets and moons (see sections below) as well as gas giants, in the solar system are known.

When the first extra-solar planets where detected in the last decade of the last century, scientists where enthusiastic about a new area of research that would develop in the years to come. Naturally the question arose how the magnetic field of extra-solar planets, especially earth-like planets or super-earths, would look like. Due to the limitation of observational methods, theoretical considerations were the only possibility to assess the magnetic field an extra-solar planet would have, depending on its internal structure. The internal structure of a planet has a big influence on the possibility of magnetic field generation, since the size and structure of the core on one hand are crucial parameters for the existence of convection, which is thought to be the main driving mechanism of a planetary dynamo. On the other hand, the thickness of the mantle and the crust determine the rate of cooling, which governs the energetics of the core (see Chapter 3). Since there is no information about the internal structure of extra-solar planets, it would be interesting to use a scaling law to relate different structure models to possible magnetic field strengths of those planets. If this is possible and which conditions are needed to make a statement about magnetic fields of extra-solar planets will be investigated in the following chapters. This thesis will conclude with the consideration of the influence of magnetic fields on the habitability of hypothetical earth-like planets, which also is a key interest of the "Research Platform: Exolife" of the University of Vienna.

In the following section all terrestrial planets and those moons possessing either an intrinsic or remanent magnetic field are described. Since gas giants are not of interest regarding planetary habitability, these are not considered in the following chapters. Because the physics of these planetary interiors are so different from those in terrestrial planets, disregarding gas giants in this work makes sense besides considerations of habitability.

1.2 Mercury

Mercury, the innermost planet of the solar system, is very difficult to observe due to its proximity to the sun. Nevertheless it was already known in ancient Greece and its orbital period around the sun was also known for a long time. But very little was known about its surface which made it very difficult to determine its rotation period. All this was about to change with the first space mission to Mercury, Mariner 10. On March 29, 1974, the space probe had its first encounter with the innermost planet. Approaching the planet from the night side the first impressing pictures from Mercury's surface were taken (Balogh et al., 2007). But what was even more remarkable was the detection of a "very well developed, strong, detached bow shock" (Ness et al., 1974) which was a clear indication of an interaction of the solar wind with a planetary magnetic field. This was completely unexpected, since pre-Mariner 10 models of Mercury suggested a completely solid inner core which would not provide a magnetic field. All other key features of a magnetosphere like the magnetosheath, the magnetopause and a magnetotail were also observed during the first flyby. The third flyby of Mariner 10 on March 16, 1975 confirmed all these signatures of a planetary magnetosphere and the planetary dipole moment was estimated through spherical harmonic analysis to be $5.1 \cdot 10^{22}$ $G\ cm^3$ (Ness et al., 1975). The stagnation point distance of the solar wind flow was found to be $\sim$ 1.6 Mercury radii (Ness et al., 1974), in contrast to 11 earth radii at earth. Hence, Mercury's magnetosphere is much smaller than earth's related to the radius of the planet and Mercury occupies much more volume of this sphere than earth does.

Naturally the question after the origin of this global magnetic field arose. One possibility considered, though very unlikely, was that of a rather complex induction mechanism by the solar wind causing the planetary magnetic field. But this would mean that there should be a correspondence between the global planetary field and the change in the interplanetary field and the solar wind flow, which was not observed during Mariner 10's third flyby (Ness et al., 1975). Moreover, the magnitude of the field was too large to be caused by an induction mechanism (Herbert et al., 1976).

Another explanation would be fossil magnetization, where a spherical shell would be magnetized by either an externally generated field or by an internal dynamo decayed long ago. Depending on whether Mercury had formed a core or not the maximum thickness of this shell below the Curie point would be either 488 km or 244 km (Ness et al., 1975). But such a shell could not have been magnetized uniformly, neither by an external field nor by an internal dynamo, at least not to the level satisfying Mariner 10's observations of Mercury's dipole moment (Ness et al., 1975). Thus, the only plausible explanation for Mercury's global magnetic field was its origin due to an internal planetary dynamo, although this approach was problematic in other ways, since the internal structure of the planet was rather unknown and therefore a modelling of a dynamo a very difficult task.

The most recent observations of Mercury's magnetic field were carried out during two flybys of the MESSENGER (**ME**rcury **S**urface, **S**pace **EN**vironment, **GE**ochemistry, and **R**anging) probe on January 14, 2008 and October 6, 2008, respectively. The mission designers chose the closest approaches of MESSENGER's flybys at different longitudes than those of Mariner 10 in order to gain the possibility to image most of the planet's surface and thereby getting a more global view of the planet than was possible during the encounters with Mariner 10. Another main objective of the mission was a more comprehensive coverage of the magnetic field (Balogh et al., 2007). MESSENGER confirmed the structure of Mercury's magnetosphere as obtained by the Mariner 10 flybys and subsequent analysis yielded a smaller range of values for the magnetic moment($240 - 270\ nT\ R_M^3$ for dipole solutions, $180 - 220\ nT\ R_M^3$ for multipole solutions; R_M is Mercury's radius of $\sim 2440\ km$) and for the field strength of the equatorial surface field ($250 - 290\ nT$, obtained from higher-order terms of the multipole solutions) than established by Mariner 10 observations (Anderson et al., 2009). The tilt of the dipole axis from the planet's spin axis was constrained to less than $5°$, which is also a lower value than the one obtained by Mariner 10 (Anderson et al., 2009). A schematic picture of Mercury's magnetosphere as observed by the MESSENGER probe can be seen in Fig. 1.1.

But in addition to more precise measurements of already well-established properties of Mercury, MESSENGER detected something completely new as well. It was known from earth-bound as well as spacecraft observations that Mercury possessed an exosphere containing light elements like hydrogen and helium as well as heavier species like sodium and calcium. MESSENGER's FIPS (**F**ast **I**maging **P**lasma **S**pectrometer) instrument detected ions of those elements in Mercury's magnetosphere and showed that it was permeated predominantly by Na^+ and other ions in lesser amounts. The ions are originating as neutral particles in Mercury's exosphere, and after photo-ionization, are picked up by the fast magnetosheath flow and thereby gaining energy. Hence, influence of these ions on the interaction between the solar wind and the magnetic field has to be considered (Slavin et al., 2008).

Already the next mission to Mercury is under study. BepiColombo, a joint mission between ESA and JAXA, is planned to set off to its 6-year journey to Mercury in 2014. It comprises two orbiters, MPO (**M**ercury **P**lanetary **O**rbiter), provided from ESA, and MMO (**M**ercury **M**agnetospheric **O**rbiter), contributed by JAXA. The main scientific goals include even more detailed studies of Mercury's magnetic field, detailed observations of its gravity field to gain new insight about Mercury's interior, observations of Mercury's exosphere, verification of the existence of ice on Mercury's polar regions by neutron and gamma-ray observations, remote sensing of IR-, UV-, X-ray-, gamma-ray, neutron and direct measurements of surface gases and observations of the high-energy environment near the sun (ESA Website (2012) and JAXA Website (2012) (web link see Bibliography), Balogh et al. (2007)). Planetary scientists can look forward to gain new knowledge from the innermost planet with its unique environment.

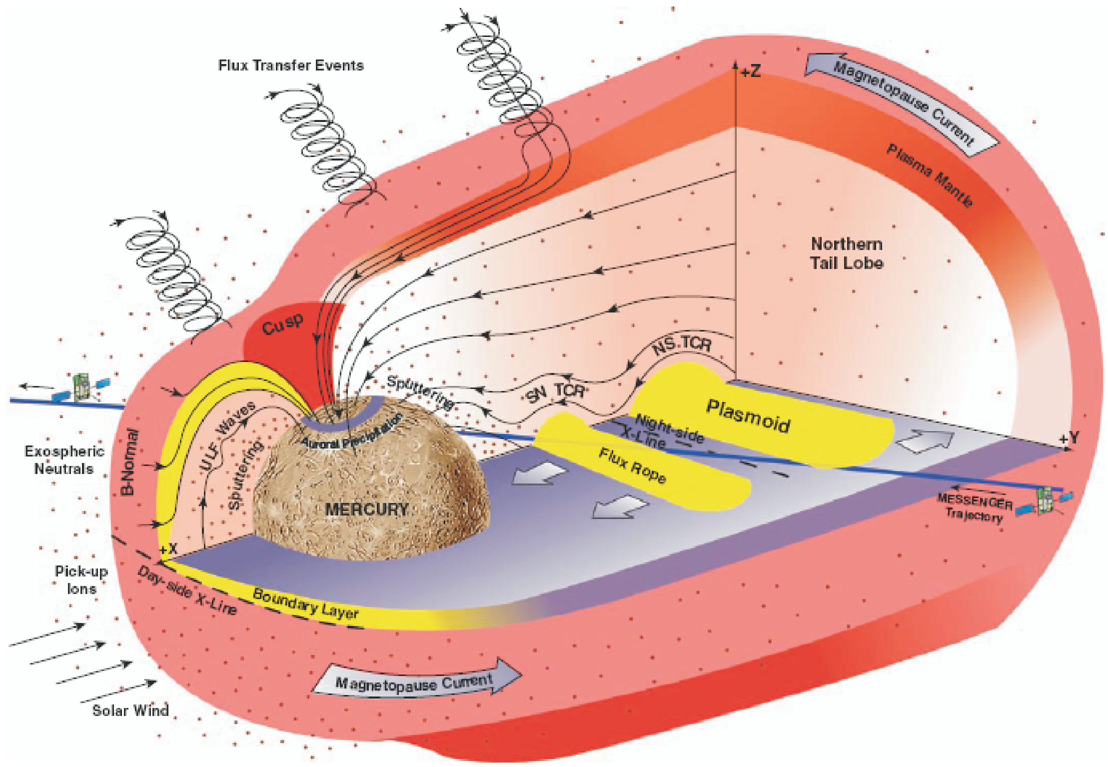

Figure 1.1: Mercury's magnetosphere, image taken from Slavin et al. (2008).

1.3 Venus

From all planets that have been visited by spaceprobes so far, Venus is the one which has been visited most frequently, either by dedicated missions or merely as a target for flyby. The reason for this most likely is the similarity of Venus to our home planet earth regarding its size and mean density, a fact that earned Venus the designation "earth's sibling". Mariner 2 was the first spacecraft to reach another planet at all, and during its Venus flyby in 1962, conducted first magnetometer measurements of Venus' magnetic field. But due to its large distance to the planet no interaction of the solar wind with Venus could be observed, and so five years later it was up to Mariner 5 to put the first upper constraints on the magnitude of a possible planetary magnetic field of Venus, which was 10^{-3} of that of earth's field (Russell, 1981). From now on with every Venusian space mission these constraints constantly declined in magnitude, and when Pioneer Venus Orbiter probed the magnetic dipole moment of Venus in 1978, the value was reduced to $0.87 \pm 3.00 \cdot 10^{21}\ G\ cm^3$ (Russell, 1981). Six years later, another reduction followed and the new upper limit was set to $8.4 \cdot 10^{10}\ T\ m^3$ (Phillips and Russel, 1987), which was approximately 10^{-5} of the magnetic dipole moment of earth and as a consequence Venus was considered to possess no intrinsic magnetic field at all. This was surprising, because although the rotation of Venus is very slow in contrast to earth's, a measurable magnetic field should exist, even though it would be rather small. The reason for this probably is the lack of sufficient energy in the core of Venus to maintain a dynamo against losses due to Ohmic dissipation. Why this is the case is still subject to speculation, but a lower pressure in the core of Venus due to its smaller radius could suffice to prevent the formation of a solid core, which in turn is considered to be one of the main energy sources of the terrestrial dynamo by the release of latent heat during solidification (Russell, 1981). A detailed history of missions to Venus can be found in Leitner (2006).

The latest and first European space mission to Venus, Venus Express, entered into a highly elliptical polar orbit around the planet on April 11, 2006. The main scientific goal was the exploration of Venus' atmosphere but also the interaction of the solar wind with it. Since Venus Express conducted its measurements during solar minimum, they were a perfect supplement to Pioneer Venus Orbiter data, which were taken during solar maximum. Although Venus possesses no intrinsic magnetic field, as was clear by now from Pioneer Venus Orbiter measurements, the ionosphere of Venus (see Fig. 1.2) deflects the solar wind due to its high electrical conductivity and thus forms a so-called induced magnetosphere. Several mechanisms, like acceleration and escape, are acting on planetary ions, and observations indicate a considerable loss of these through the plasma wake. The temporal characteristics of ion loss and its variability is still a matter of discussion but would be an important jigsaw piece on the way to determine the history of water on Venus. Further observations are therefore needed and future missions to Venus will hopefully provide new insights into the secrets of "earth's sibling" (see Titov et al. (2009) for more details).

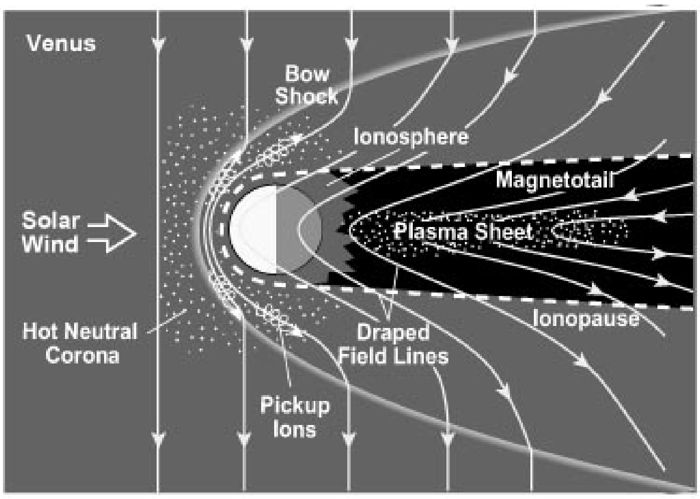

Figure 1.2: Venus' ionosphere, image taken from NASA's Cosmos Website (2012).

1.4 Earth

The magnetic field of earth is the best known planetary magnetic field in the solar system, partly due to the fact that it has been observed and studied since ancient times, but also because of our ability to examine it directly from the surface of the planet. Thus observations were carried out on a regular basis fairly soon, mainly due to the importance of precise knowledge of the magnetic field for navigation purposes. But only at the end of the first half of the 19th century a network of magnetic observatories was built up around the globe, which was initiated by Gauss and Weber. So a lot of data on earth's magnetic field during the last 500 years exist, most of which had been recorded by mariners during their travels over the oceans. Naturally, the amount of these data increased with advancing years and progress in natural sciences, especially geosciences, and related observation programs and extended land and sea surveys.

To make a statement about changes in the magnetic field and the responsible mechanism, a much longer period of time than a couple of hundred years has to be considered. The method of choice is to use data gained by investigations of archeomagnetic, paleomagnetic and seafloor records. Archeomagnetic records are found in human buildings and artefacts or young lava flows with ages up to 50,000 years (Hulot et al., 2010). When these objects are created, the ambient magnetic field at this time is frozen in as the material cools below the Curie temperature, a process called thermal remanent magnetization. Then the three magnetic elements, declination, inclination and field strength, can be recovered by different laboratory procedures, though it is not always possible to recover all of them. This depends on chemical alteration of the sample during analysis or even before collection, or the cooling rate at the time of creation. Naturally the number of particularly human artifacts correlates with the development of human civilizations and the development of settlements and cities. Therefore the possibility to recreate the ancient magnetic field strongly depends on the geographical distribution of human cultures around the globe, a constraint that also has to be considered for lava flows, since they also can be found only in certain regions on earth (Hulot et al., 2010).

To gain information about earth's magnetic field over even longer periods, three major sources of magnetic records are available: igneous rocks, marine sediment records and marine magnetic anomalies, collectively designated as paleomagnetic or seafloor records, respectively. Igneous rocks comprise old lava flows as well as plutonic rocks, which allow to recover the field back in time up to 3.2 Gyr of age (Tarduno et al., 2007). Several effects have to be considered in order to recover the correct orientation of the ancient field, like movement or rotation of sites of old lava flows due to plate tectonics. Basically, intensities can be determined as well, but alteration of the samples prior to collection or uncertainties regarding the cooling rates exacerbate the evaluation of the magnetic record. Moreover, the uneven distribution of samples around the world makes it difficult to create a global view of the magnetic field in the past.
Marine sediment records, which are retrieved from sediment cores by drillings into the seafloor, should in principle yield continuous data on the magnetic field of the past. But different problems with the determination of the original orientation only allow the determination of a relative intensity, and this is only accurate to within 10-25% (Hulot et al., 2010).
Magnetic anomalies can be obtained by measuring the magnetization of the ocean crust with magnetometers mounted on a cable behind a ship. The ocean crust originates at the mid-oceanic ridges and moves away from the ridge axis by sea floor spreading. When the crust leaves the interior of the earth and cools down below the Curie temperature the mechanism of thermal remanent magnetization freezes in the current magnetic field and preserves it for later retrieval (see Fig. 1.3). Therefore reversals of the magnetic field and changes in intensity can be gained from marine magnetic anomaly records fairly well. Since reversals produce very strong

anomalies, these are the anomalies which are known and understood best. The oldest records recovered from magnetic anomalies are approximately 160 Myrs old (Hulot et al., 2010), since crust older than this has been subducted again and is thus no longer available for scientific investigations. Older records can only be obtained from geological or marine sediment records. Taken together these methods reveal a field of dominant axial

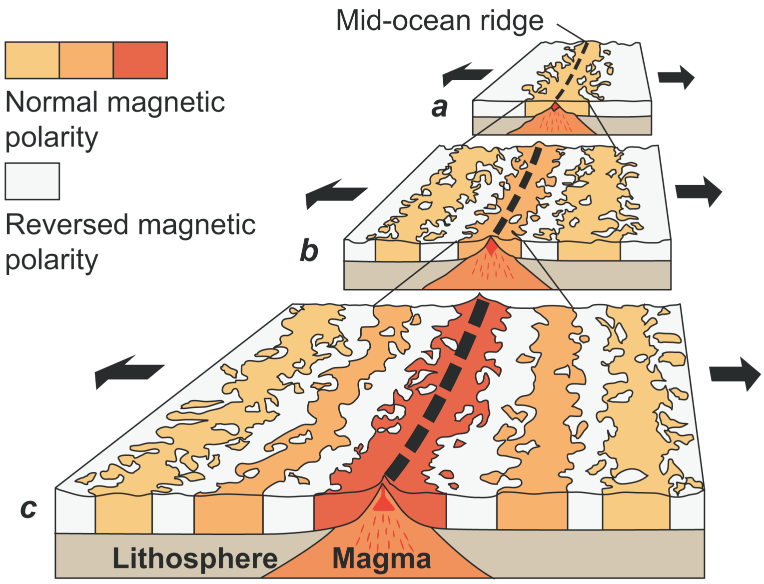

Figure 1.3: Magnetic stripe pattern at mid-oceanic ridges, image taken from Earth Science in Maine Wiki (2012).

dipole character with a field strength between $25 - 60\ \mu T$ (Hulot et al., 2010), which is comparable in strength to the present field. Only during short periods of weakening the field was dominated by none-dipole components before growing back to its average strength with dipole character and same or opposite polarity (Hulot et al., 2010). The structure of the magnetosphere is shown in Fig. 1.5.

The first satellites observing earth's magnetic field were the POGO (Polar Orbiting Geophysical Observatories) satellites, which conducted measurements of the magnetic field of the Equatorial Electrojet between 1965 and 1971 (Onwumechili and Agu, 1980). The Equatorial Electrojet is a phenomenon occurring in the E-region of the ionosphere (see Fig. 1.4), between 90 - 130 km altitude, caused by an electric field generated by the world-wide solar quiet current system. Together with the magnetic field this causes an upward drift of electrons. Therefore a positive charge at the bottom and a negative charge at the top of the E-region results until no further electrons can move upwards. Instead a westward movement develops, causing an eastward electric current, which is called the Equatorial Electrojet (Geomagnetism Website, 2012a). But the POGO satellites only conducted measurements of the scalar field, neglecting the vector components, which led to certain problems in the determination of the magnetic field.

The first vector measurements were carried out by MAGSAT from 1979 to

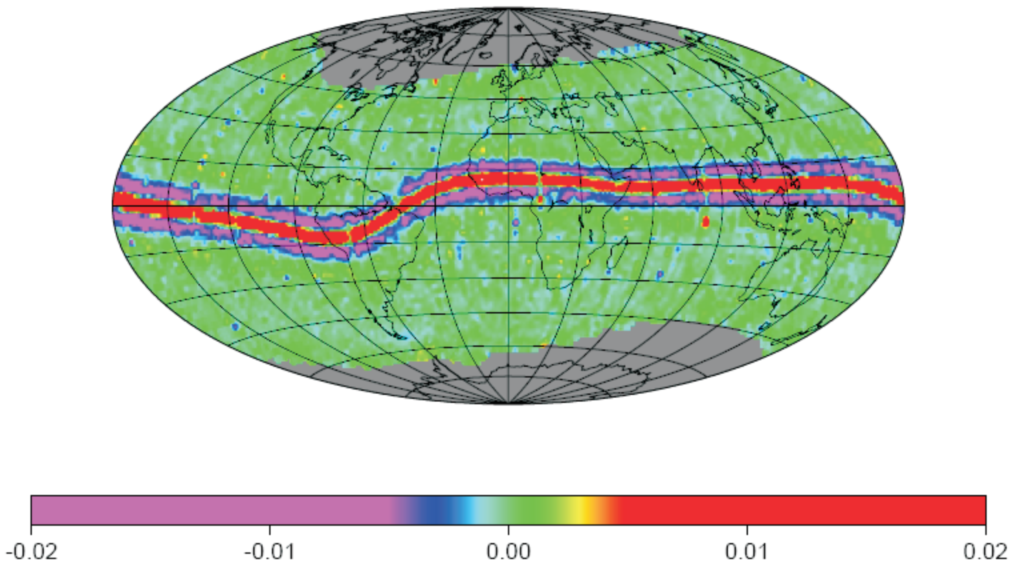

Figure 1.4: The longitudinal field component of the Equatorial Electrojet from CHAMP data in $nT\ s^{-2}$, local time 14:00, image taken from Mouël et al. (2006).

1980 in altitudes between 352 and 561 km (Rajaram, 1993). The data contained contributions from the core and crustal field of earth and from external current systems as well. Although these results were the most accurate ones obtained until this time, the mission was too short to gather sufficient data for an accurate model of the secular variation. Only 20 years later, Ørsted, the first satellite of the International Decade of Geopotential Research, provided measurements of a 14 month-period of observation, long enough to create reasonable models of the secular variation, one of the first geomagnetic field models being the Ørsted Initial Field Model (Hoffmeyer, 2000; Olsen et al., 2006). More recent missions like CHAMP, a German satellite launched on July 15, 2000 (Reigber et al., 2002), and SAC-C, a satellite built by an international cooperation of more than 5 countries and launched on November 21, 2000 (Colomb et al., 2004), yielded even more data that complemented observations by Ørsted, allowed even more accurate determinations of the field intensity and field components, and led to progress in investigations of the ionospheric, crustal and core field of the earth. The next earth observing satellite mission planned is ESA's Swarm mission, due to launch in July 2012, consisting of three satellites, which is aimed to improve our understanding of all different sources of earth's magnetic field by even better separation of internal and external sources (Hulot et al., 2010).

1.5 The Moon

Very little was known about the magnetic properties of the moon, until the USSR spacecraft Luna 1 and Luna 2 carried out first measurements with their magnetometers in 1959 and set an upper limit of 10^{-3} G (Dyal et al., 1974) for the strength of a possible lunar magnetic field. In 1966 Luna 10 encountered a time-varying field near the moon, which was considered a possible indication of a lunar magnetosphere. But in 1967 the U.S. satellite Explorer 35 was placed in an orbit around the moon, approaching it

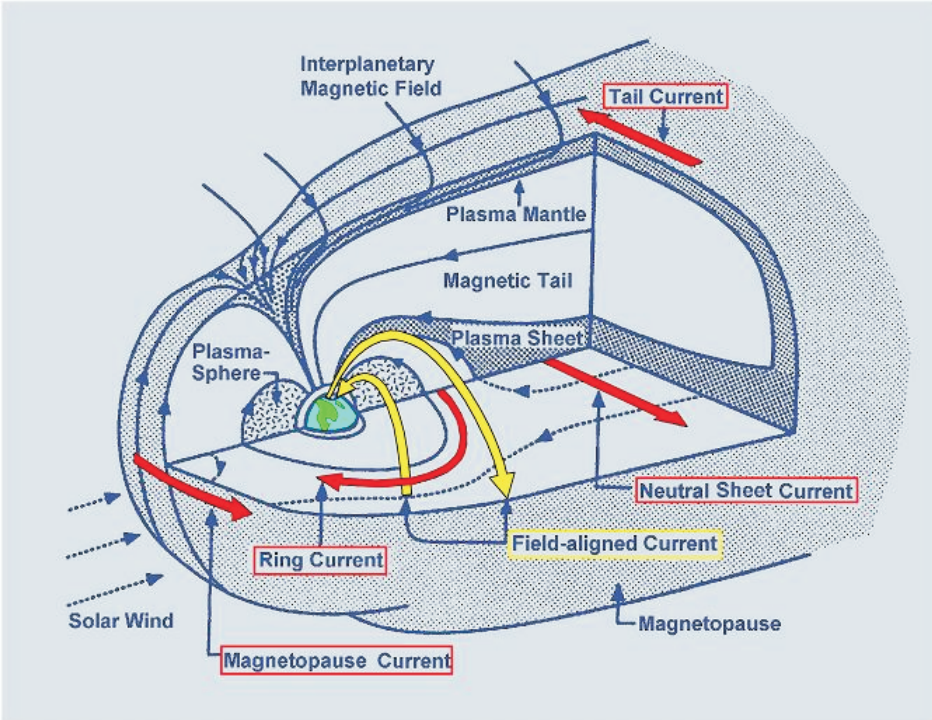

Figure 1.5: Earth's magnetosphere, image taken from the Geomagnetism Website (2012b).

to a distance of 830 km, and could not verify the magnetosphere indicated by Luna 10. Subsequent analysis of Explorer 35 data led to a lower upper limit for a possible magnetic field of less than $2 \cdot 10^{-5}$ G (Dyal et al., 1974) at the satellite's altitude of 830 km, meaning a surface field of $4 \cdot 10^{-5}$ G (Dyal et al., 1974) at most and a permanent dipole moment of 10^{20} $G\ cm^3$ (Dyal et al., 1974), which was less than 10^{-5} of that of the earth's dipole moment.

During the Apollo missions the first lunar rock samples were collected by Apollo 11 astronauts, and scientists were surprised by the presence of natural remanent magnetization in this material between 10^{-3} and 10^{-7} $G\ cm^3\ g^{-1}$ (Dyal et al., 1974), which was attributed to thermoremanent magnetization of metallic iron grains. The first surface magnetometers were deployed at the moon by Apollo 12, 14, 15, and 16, which showed the magnetization of the lunar crust over regions of up to 200 km. The maximum of this permanent magnetic field was measured at the Apollo 16 site with a field intensity of $3.27 \cdot 10^{-3}\ G$ (Dyal et al., 1974) and the sources of this field where thought to be local magnetizations, so-called "magcons". In addition to the surface magnetometers of Apollo 15 and 16, subsatellite magnetometers yielded maps of the larger magnetized regions between 1971 and 1972, which confirmed the assumption that most of the lunar surface exhibited magnetized regions. A new upper limit on the permanent dipole moment was set to $4.4 \cdot 10^{18}\ G\ cm^3$ (Dyal et al., 1974), indicating that no intrinsic magnetic field but only remanent magnetization existed on the moon, since this was $5 \cdot 10^{-8}$ of that of the earth's magnetic moment. The fact that the lunar field did not vary with distance from the center, as would be the case for a planetary field, but with altitude measured from the surface, confirmed this hypothesis even more (Russell et al., 1973). Moreover, magnetic fields induced in the interior of the moon by the external magnetic field of the earth and interaction with the solar wind were discovered, and thereby the deep interior of the moon could be investigated, like its relative magnetic permeability and its electrical conductivity. The solar wind also causes a phenomenon called "limb compression", where electrically conducting solar wind plasma interacts with certain highland regions near the limb of the moon, and produces a weak local shock, which could be detected downstream from the moon by Explorer 35 (Russell and Lichtenstein, 1975). Since this was possibly caused by deflection of the solar wind by magnetic fields originating in regions of high magnetization (Russell et al., 1973), this also indicated the existence of magnetized regions at the moon, although other possible causes where considered plausible as well (Dyal et al., 1974). Several mechanisms were proposed to explain the lunar remanent magnetization, some of which shall be explained in the following.

The influence of a large solar or terrestrial field on the cooling of crustal material of the ancient moon could have caused the thermoremanent magnetization. Although the field of the sun during its T Tauri phase could have been large enough, it also would have been much more variable than today at the earth's orbit, but the observed lunar remanent magnetization would have required relatively steady fields of a few 10^{-2} G (Dyal et al., 1974). On the other hand, a large terrestrial field also could have been responsible, if it either would have been 100 times greater than today (Dyal et al., 1974), which is rather unprobable, since this is not indicated by paleomagnetic data, or if the moon's orbit would have been within 2-3 earth radii (Dyal et al., 1974). But since this is within the Roche limit, this hypothesis is also problematic (Dyal et al., 1974).

One natural explanation seemed to be the thermoremanent magnetization of the crust by a self-sustaining dynamo of an ancient lunar iron core as soon as the crust had cooled down below the Curie temperature. Afterwards the dynamo ceased to operate and meteorite impacts generated a random distribution of the field's sources and destroyed the magnetization of the whole crust. But it was questionable, first, if even the most efficient lunar dynamo could have produced a sufficient surface field to explain the observed remanent magnetization and, secondly, if at mechanically possible rotation speeds of the moon this dynamo would be self-sustaining at all. Moreover, it was possible that the moon's core formed too late in its history to magnetize the crust by dynamo action (Goldstein et al., 1976). Investigations of the lunar interior from magnetic field measurements showed at least that a lunar core would be within the necessary size range, between 385 and 535 km, to support a core dynamo (Dyal et al., 1976). Despite all shortcomings, the lunar dynamo hypothesis seemed to be the most plausible one and explained the observed features best (Russell and Goldstein, 1976).

If no dynamo was operating in the ancient moon's interior, maybe the iron core was magnetized by other mechanisms, like isothermal magnetization by a strong transient field, viscous remanent magnetization by a weak field applied over a long period, depositional remanent magnetization during early lunar formation in a weak field, or thermoremanent magnetization of the core by cooling through the Curie point in a weak field (Dyal et al., 1974). If the core temperature stayed below the Curie point of iron this core could then have magnetized the crust and caused the thermoremanent magnetization during crystallization of the crust. The core magnetization could have then disappeared due to subsequent radioactive heating (Dyal et al., 1974).

Small local dynamos, generated by pockets of iron and iron-sulfide melt, about 100 km in diameter, were also thought to be responsible for the crustal magnetic signatures at the moon. Such sources, though, should be identified by mapping of the lunar surface field, but some scientists considered these shallow Fe-FeS dynamos as the cause for the observed asymmetry in the electromagnetic field fluctuations at the Apollo 15 landing site (Dyal et al., 1974).

An important fact to consider when discussing possible origins of the lunar remanent field was the fact, that different magnetizing mechanisms leave certain characteristic imprints. An external field, for example, would have only been effective in its parallel component when magnetizing the lunar crust, thus causing a distinct north-south magnetization. Or if the responsible mechanism would have been a dynamo, the magnetization would be oriented almost parallel to the rotation axis, again resulting in a north-south magnetization. While this was partly observed on the moon, no effectively large areas showed such signatures (Russell et al., 1975).

More recent missions to the moon were the Lunar Prospector and Clementine missions. While a main task of Clementine was to search for signs of water on the moon, Lunar prospector conducted gravity and magnetic measurements as well. In contrast to the Luna and Apollo missions, Clementine and Lunar prospector also observed the lunar poles in detail. Lunar prospector, the first NASA mission to the moon in 25 years, was launched on the January 7, 1998 and stayed in lunar orbit until its scheduled impact on the surface on July 31, 1999. Although one of Lunar Prospector's main tasks was to find polar water ice deposits, too, in order to map the gravity and magnetic field in detail it was the first spacecraft in low polar orbit around the moon. The magnetic maps (see Fig. 1.6) show strong magnetic fields, at the antipodal regions of Mare Imbrium and Mare Serenitatis, which are strong enough to form a magnetosphere with magnetosheath and bowshock. This is the smallest magnetic system known in the solar system and its existence indicates the importance of shock remanent magnetization in the discussion of the origin of the moon's magnetic fields. Nevertheless, this association of strong surface fields with the antipodal regions of large impact basins suggests enhancement of ambient fields 3.6 to 3.85 Gyr ago, in turn indicating strong fields of lunar origin, possibly generated by a lunar core dynamo (Lin et al., 1998; Wieczorek and Weiss, 2010). The gravity measurements also yielded important results, one of them being the determination of lunar mass concentrations, or "mascons", on the far side of the moon, indicating an Fe rich lunar core of 300 km in size (Binder, 1998). The last spacecraft to visit the moon was JAXA's SELENE(Kaguya), which entered into a polar orbit around the moon in October 2007. Selene's mission was not only to map the strong magnetic fields of the moon, but also to detect weak anomalies with fields $\leqslant 1\ nT$. It could confirm Lunar Prospector's discovery that most of the lunar crust is magnetized and therefore strengthened the hypothesis that the lunar crustal magnetism was acquired in a global magnetic field which was probably provided by a lunar core dynamo (Tsunakawa et al., 2010).

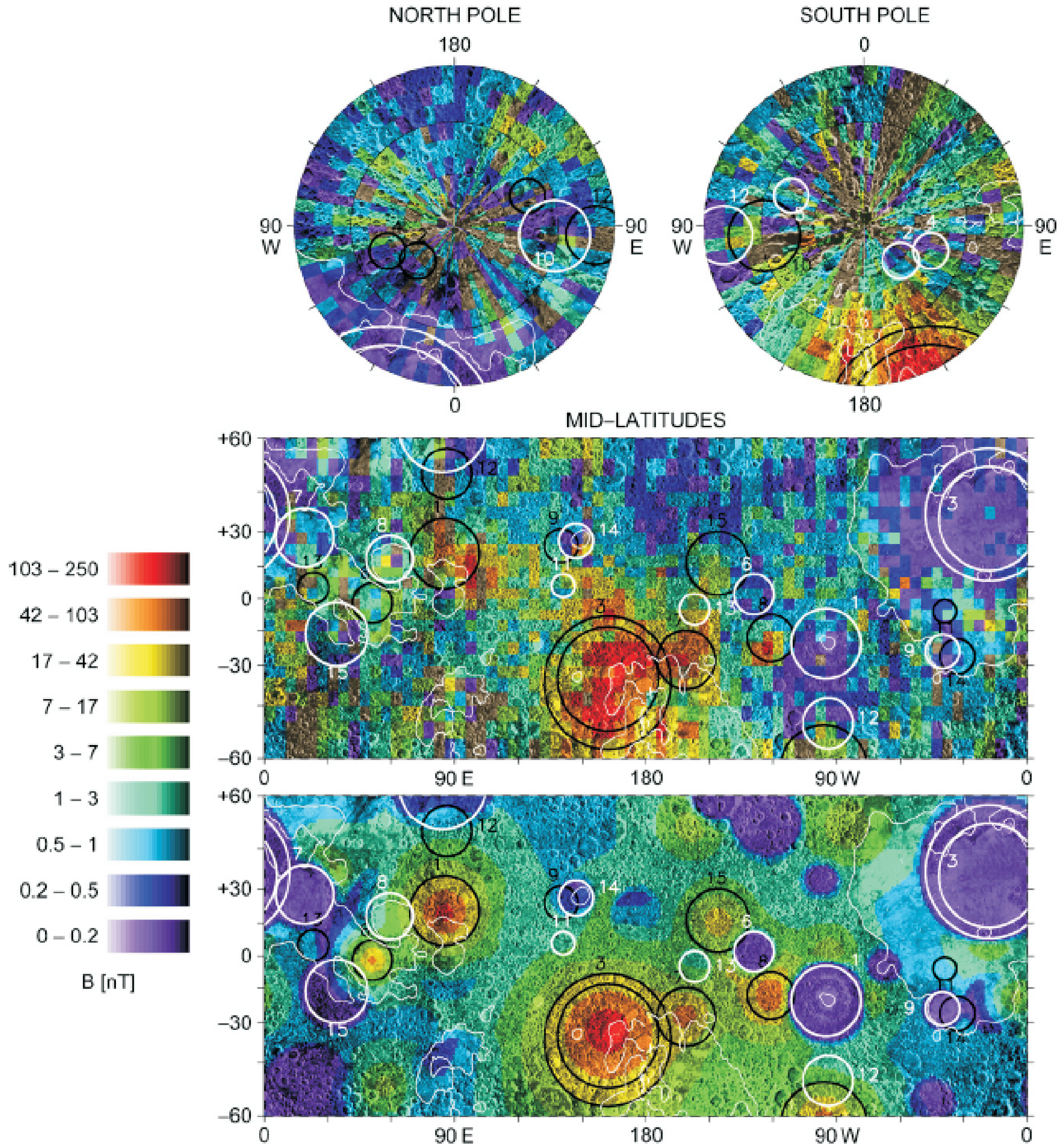

Figure 1.6: The surface crustal magnetic field intensity of the moon from Lunar Prospector Observations. White rings show the 15 most recent impact basins, while black rings are antipodal to white rings. The bottom image represents an empirical model. Image taken from Mitchell et al. (2008).

Summarizing, Lunar magnetic fields and anomalies seem to exhibit a complex history and their origin probably cannot be attributed to one single mechanism alone. Shock remanent magnetization by meteorite impacts seems to play a crucial role and be able to explain some of the observed magnetic features, but from a global view an ancient lunar core dynamo still seems to be the most plausible explanation for the magnetization of most of the lunar crust.

1.6 Mars

The "Red Planet" has been the target of many space missions in the last 50 years, though not all of them reached their destination. Sometimes computer errors were the source of failure, Mars Climate Orbiter being a famous example, where the U.S. imperial and the SI system of units where mixed up. NASA used the SI system of units, but Lockheed Martin, who developed the navigation software, used the imperial units in their programs taken from Mars Global Surveyor, but without repeated testing. This caused the spacecraft to enter a much lower orbit than planned, and as a consequence it was destroyed by the atmospheric friction (WIKIPEDIA, 2012). Many Soviet missions to Mars also failed in one way or the other, some passing by the planet too far to enter into the planned orbit, others experiencing the same destiny like Mars Climate Orbiter. Most of the time, the low-budget and saving politics of Soviet authorities led to failure in electronic components, ending in disaster for the mission. Of those spacecraft arriving at Mars, able to conduct the planned measurements, only some have been carrying magnetometers. The first U.S. spacecraft that made magnetic measurements was Mariner 4 in 1965, but the distance to Mars was too large to probe a possible planetary magnetosphere. In the beginning of the 1970s three Russian space missions were targeted at Mars, Mars 2, Mars 3, and Mars 5. Mars 2 and Mars 3 entered into an orbit around Mars in November and December 1971, respectively. They yielded the first data of a possible planetary magnetic field of Mars, though the existence of one was very disputed and hotly debated at this time. Dolginov (Dolginov et al., 1973; Dolginov, 1978a) argued in favor of an intrinsic planetary magnetic field, claiming that Mars 2 and Mars 3 data on shock front, topology and magnitude of the measured field as well as the intensity of the solar wind indicated an intrinsic magnetic field with a dipole moment of $2.4 \cdot 10^{23}$ $G\ cm^3$ and an intensity at the magnetic equator of $6 \cdot 10^{-4}$ G, the weakness of the field either suggesting an ancient dynamo that had ceased to operate or an ongoing magnetic field reversal. But, as mentioned before, not all scientists shared this point of view. For example, Russell (1978b) doubted the existence of a planetary magnetic field at Mars. He argued that Mars had a core comparable in size to that of Mercury and a rotation rate comparable to that of the earth and hence was expected to have a magnetic field with a field strength intermediate between that of Mercury and earth. Since the observed magnetic moment was by a factor 10^3 smaller than that expected from the scaling of core size and rotation rate from Mercury and earth to Mars, Russell concluded that the Martian dynamo, if one had ever existed, had stopped to operate (Russell, 1981). But Dolginov and Pushkov (1978) pointed out that planetary magnetic fields were not proportional to their constant spin rates but to accelerations in such, the Poincaré acceleration being the largest one of these, indicating that a Martian dynamo was not only physically possible but also probable, and that this assumption was strengthened by Mars 5 data (Dolginov, 1978b). This discussion continued for the next decade and only new data from advanced spacecraft could resolve this puzzle. It was up to Mars Global Surveyor to shed new light on the question whether

Mars possessed a global magnetic field or not.

In January 1989, the Soviet Phobos-2 spacecraft arrived at Mars and entered into an elliptical equatorial orbit. It carried two fluxgate magnetometers onboard, FGMM, and MAGMA, and could collect some data before heading for the Martian moon Phobos, where contact was lost shortly before the rendezvous with it. Phobos-2 was the last Soviet planetary mission due to the huge political changes following in the Soviet bloc in the years after 1989. Phobos-2 data indicated that the main source of the observed features was the interaction of the solar wind with an extended ionosphere, leaving the influence of an intrinsic Martian magnetic field negligible. Nevertheless, a weak planetary field could be supposedly detected by interpretation of a co-rotating part in the measured magnetic field as evidence for an intrinsic planetary field. Whether this intrinsic field was generated by a core dynamo or the result of local magnetic anomalies was a matter of discussion at that time (Möhlmann et al., 1992). The magnetic moment was estimated to be $1.5 \cdot 10^{22}\ G\ cm^3$, resulting in a field strength of $\sim 20\ nT$ (Möhlmann et al., 1991).

On November 7, 1996, the U.S. launched their first spacecraft en route to Mars in 10 years, Mars Global Surveyor (MGS). In September 1997 MGS entered into a highly elliptical orbit around the planet, where it conducted a series of measurements before performing orbit changes, using the aerobraking technique (Murphy and Patterson, 1998), to lower its orbit into the upper parts of the Martian atmosphere. MGS was the first spacecraft to collect data beneath the ionosphere, shielded from the influence of the solar wind. Mars Global Surveyor observations showed that the interaction of the solar wind with the ionosphere dominated over a possible magnetospheric interaction and the weakness of the magnetic field below the ionosphere emphasized this dominance. Although variability of the bow shock position, where the solar wind interacts directly with the ionosphere, indicated the influence of an intrinsic magnetic field, no evidence for such a global field of sufficient strength could be found. This was firm evidence that Mars possessed no global magnetic field deflecting the solar wind and creating a magnetosphere similar to earth or Mercury. On day 262 in Martian orbit a weak magnetic field, $\leqslant 5\ nT$, could be detected below the ionosphere, setting an upper limit for a Mars dipole moment of $2 \cdot 10^{21}\ G\ cm^3$, which is an order of magnitude lower than the dipole moment estimated from Phobos-2 results (Acuña et al., 1998). The fact that Mars obviously lacks a global magnetic field of considerable strength today but most probably had one in the past could simply mean that the Martian dynamo ceased to operate fairly early in Martian history. Moreover, it allows to draw some conclusions about the interior of the planet, since a planetary dynamo requires convection within an electrically conducting fluid and a source of energy, like latent heat released by crystallization, to generate a magnetic field. Maybe there exists no active dynamo today because the core has either completely frozen out or never formed. Because of the important role that sulfur plays in these processes, the knowledge of the point in time the dynamo stopped to operate could allow to derive the amount of sulfur present in the Martian core (Acuña et al., 1998). Mars Global Surveyor also created a detailed map of magnetic anomalies of the Martian crust (see Fig. 1.7). The existence of these anomalies is a telltale sign of an ancient dynamo that magnetized the crust. The maps revealed a very interesting feature of the Martian crust, an apparent dichotomy of magnetic anomalies between the northern and southern hemisphere (see Fig. 1.8). While the northern plains, which exhibit very low crater densities and therefore are one of the youngest regions on Mars, showed only some weakly magnetized anomalies, the heavily cratered and ancient terrain of the southern highlands was full of magnetic signatures covering a wide range of magnetic moment.

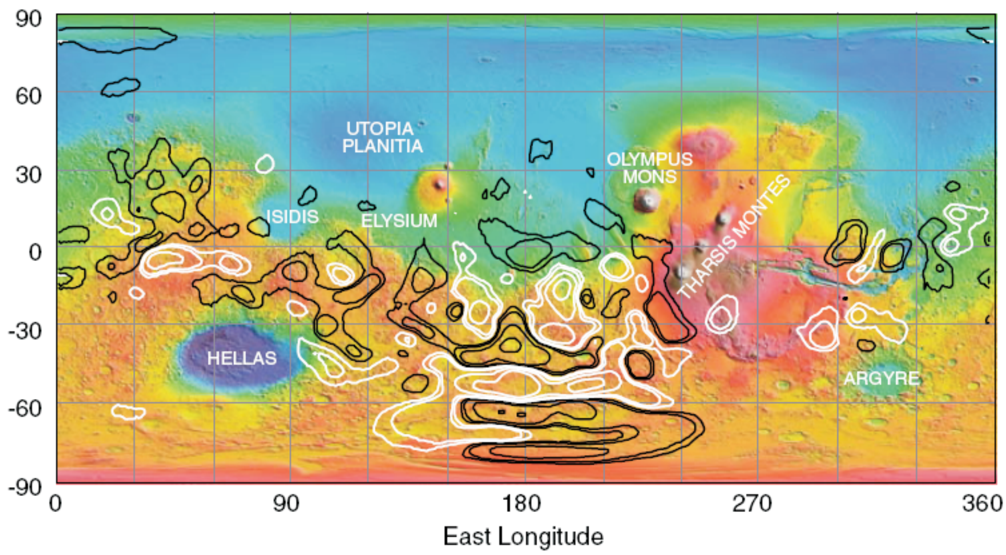

Figure 1.7: Map of the magnetic field of Mars, showing isomagnetic contours for $B = \pm 10, 20, 50, 100, 200$ nT. Image taken from Connerney et al. (2001).

Although there was an obvious correlation between impact crater density and magnetic anomaly density, there was no association between individual craters and magnetic anomalies. For example, no magnetic signatures were found at the Hellas, Argyre, and Isidis impact basins, as well as at Tharsis region, Valles Marineris, and Elysium Planitia. It seems that the ancient dynamo that magnetized the crust shut off before these structures had been formed and subsequent alteration of the crust resulted from impacts and tectonic or magmatic processes. The magnetic signatures with highest intensities exceeded 1500 nT, strong enough to deflect the solar wind, thus creating asymmetries of the bow shock when facing the solar wind. This also could explain the co-rotating part of the magnetic field measurements during Phobos-2 observations, since the magnetic anomaly of Terra Sirenum could be responsible for that periodicity (Acuña et al., 1999). The next mission to Mars will be the MAVEN (**M**ars**A**tmosphere and**V**olatile**E**volutio**N**) Mission, a collaboration of NASA/JPL with several institutions experienced in space research. One of its main scientific goals will be the determination of the loss of volatiles from the Martian atmosphere and its importance for Mars' climate, water abundance and habitability during its history. The spacecraft, which is due to launch in November 2013, will also carry a magnetometer and several particle detectors, to measure the interaction of the solar wind with the ionosphere of Mars and to determine its magnetic properties to an even higher degree than before (Jakosky, 2011; NASA Website, 2012b).

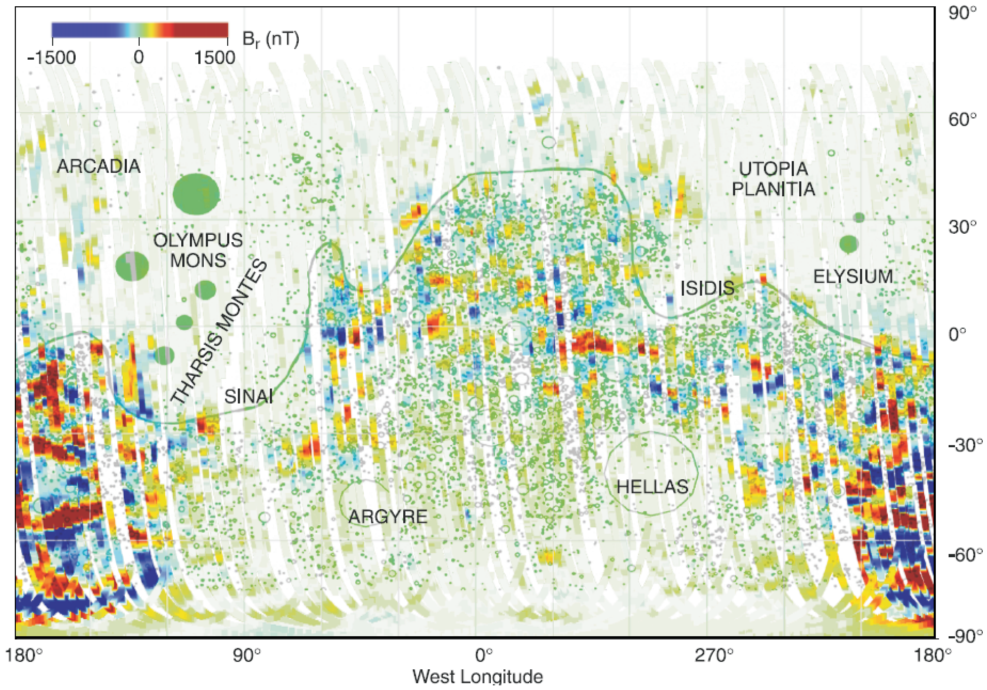

Figure 1.8: Map showing the dichotomy of magnetic anomalies on Mars with a correlation of magnetic crustal sources and high crater densities. Craters with diameters greater than 15 km are superimposed on the distribution of crustal magnetic field sources. The green line is the dichotomy boundary line. Image taken from Acuña et al. (1999).

1.7 Ganymede

Although Jupiter possesses the strongest magnetic field in the solar system, it is not subject of this chapter since it is not a terrestrial planet but a gas giant. But two of its moons, Ganymede and Io, showed characteristics of an intrinsic magnetic field during their observations with the Galileo spacecraft. It was a great surprise to scientists when data obtained during the first encounter of the Galileo spacecraft with Ganymede, Jupiter's largest moon, indicated that the moon possessed an intrinsic magnetic field, since this was something completely unexpected. The field determined by the onboard magnetometers was that of a dipole with a surface field strength at the equator of $\sim 750\ nT$, a magnetic moment of $1.4 \cdot 10^{13}\ Tm^3$ and a tilt of the dipole axis from the spin axis of 10° (Sage, 1997) (a more recent value of the field strength being 719 nT, (Kivelson, 2002)). Although the field strength determined was a little too high, since currents in the magnetosphere of Ganymede could perturb the signature of the intrinsic field, leading to a slight overestimation of the vacuum field, it was considerably stronger than the surrounding field of Jupiter, which is about 100 nT at the orbit of Ganymede (Gurnett et al., 1996). This led to the conclusion that the measured field was definitely associated with Ganymede (Kivelson et al., 1996c), and observations by the plasma-wave instrument of Galileo confirmed these results (Gurnett et al., 1996). Another interesting result of Galileo observations came with the determination of the dimensionless axial moment of inertia, C/MR^2, which allows to set very tight constraints on the internal distribution of mass in a body. The smaller the value, the more the mass is concentrated towards the center. The value obtained by Galileo for Ganymede, $C/MR^2 = 0.3105 \pm 0.0028$, is one of the smallest known of all the terrestrial objects in the solar system, which means that Ganymede is differentiated very strongly and much of its mass is concentrated towards its center (Anderson et al., 1996) (see also Schubert and Limonadi (1994)). Hence, a metallic core is very likely to exist and this, in turn, is one possible origin of a self-sustaining magnetic field (Fig. 1.9 shows the assumed internal structure of Ganymede.) This leads to the question for the origin of the magnetic field and to the various mechanisms and their plausibility. A possible source, discussed again and again for all the terrestrial bodies, is remanent magnetization. Although this seems not to be the most likely case for Ganymede, it would be a feasible solution. This would require the interior of the moon to consist of very iron-rich material and an ambient or ancient intrinsic field of considerably higher strength than is observed today (Kivelson et al., 1996c; Schubert et al., 1996). Crary and Bagenal (1998) argued that the field observed at Ganymede could not result from remanent magnetization generated by the Jovian magnetic field, but by a field of an internal paleodynamo, active 3-4 billion years ago. Although this dynamo had to exhibit field strengths between 10 and 50 μT, or even stronger ones if polarity reversals had to be accounted for, this could be considered likely in light of estimates for a lunar paleodynamo, based on Apollo samples, of about $10 - 100$ μT. Therefore neither an active dynamo nor a convecting core would be necessary. Magnetoconvection is another mechanism

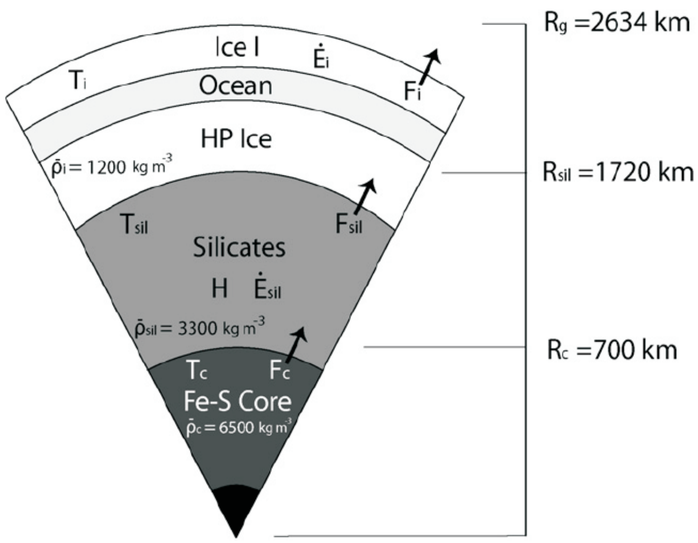

Figure 1.9: The assumed internal structure of Ganymede, taken from Bland et al. (2008).

suggested to explain Ganymede's magnetic field. If an ambient field affects an electrically conducting fluid in convective motion, a perturbation magnetic field is generated, which is similar in strength to the ambient field. Since Ganymede's field is much stronger than the ambient field, this process can not explain Ganymede's magnetic properties. Moreover, magnetoconvection in a possible salty subsurface ocean below the crust of Ganymede would require fluid motions of $1\ ms^{-1}$, which seems improbable considering Kolmogorov scaling (Schubert et al., 1996). At least magneto-convective processes could have an influence on the sense of field (Sarson et al., 1997). The most likely explanation for Ganymede's magnetic field, given its dipolar character and observed field strength, seems to be an active dynamo (Kivelson et al., 1996c; Schubert et al., 1996). For a dynamo to be active over geological timescales, an energy source is needed that drives the dynamo. This energy source is convection, which is either thermal, compositional or both, and it must overcome losses due to Ohmic dissipation to keep the dynamo working. For Ganymede, thermal convection alone would not provide enough energy, and compositional convection depends on the composition of the core and the abundance of light elements like sulfur or oxygen. When the core cools, light elements are segregated into the fluid core and heavy elements like iron or nickel freeze out, releasing latent heat and powering the dynamo. But if cooling happens too fast, the dynamo ceases to operate since the energy to drive convection is used up, and thus prevents the dynamo from being active over geological time. While Hauck et al. (2006) find a broad range of conditions that could support dynamo action via compositional convection, Bland et al. (2008) state that this could only be possible under a very stringent set of parameters, outside of which the core would cool too rapidly to provide an active dynamo until today. If Ganymede had gone through a Laplace-like resonance, however, tidal dissipation could have heated up the mantle and thus insolated the core, preventing it from cooling. As soon as Ganymede had left the resonance, the core would start to cool and the dynamo would begin to operate (Bland et al., 2007). But modelling of this approach showed that even a Laplace-like resonance would not generate enough tidal dissipation to heat the mantle sufficiently and thus would not broaden the conditions favourable for magnetic field generation, although late core formation could provide an alternative solution (Bland et al., 2008). Since an internal dynamo seems the most plausible explanation for Ganymede's magnetic field, either Ganymede meets the criterions stated above, or a combination of several mechanisms is an adequate explanation. As mentioned before, remanent magnetization cannot be ruled out completely. Possibly, oxygen plays an important role in the core, and induction mechanisms are also likely to contribute to the field (Kivelson, 2002). The role of the ambient field of Jupiter and possible interactions with Ganymede's dynamo is also unclear (Bland et al., 2009). As can be seen, Ganymede's magnetic field is very unique, as it not only challenges scientists to explain its existence, but also provides the possibility to study a planetary magnetosphere under the influence of the magnetic field of another planet, and very special physical processes have to be considered here (Kivelson et al., 1997; Paty and Winglee, 2006). Hopefully, the JUNO mission to Jupiter, launched in August, 2011, yields new insight into the magnetosphere of this fascinating moon (for more information about the JUNO mission see NASA Website (2012a)).

1.8 Io

Not only Ganymede surprised scientists on arrival of Galileo at Jupiter. Io, the innermost of the Galilean moons, also showed unexpected signatures of magnetic activity within the moon (Kivelson et al., 1996a,b). Even before Galileo yielded data of Io's environment, suggestions had been made that the moon could possess an intrinsic magnetic field. Wienbruch and Spohn (1995) showed, that if tidal-heating rate and surface heat flow were not in equilibrium but Io would be in a oscillatory phase of its thermal-orbital evolution, a self-sustaining dynamo at Io could be possible as a consequence of convection in the core. But in contrast to Ganymede, it was not clear whether the observed disturbances were caused by an intrinsic magnetic field or are effects of a current-carrying ionosphere of Io. Although Io seems to be sufficiently differentiated to possess a metallic core and adequate heating is present, two prerequisites to drive a dynamo, it also possesses a very special plasma environment, and its contribution to the observed disturbances could not be neglected without further studies. Therefore additional passes of Galileo at Io were needed to gain better data and further constrain the influence of an internal field, and only after the two passes in 2001 it became clear, that if an internal field existed at all, its strength was negligibly small (Bagenal et al., 2006). The field perturbations at Io were hence mainly due to plasma interactions with Io's ionosphere and its neutral cloud.

1.9 Titan

The first attempts to model Titan's magnetic field were undertaken by Neubauer (1978), requiring certain assumptions, like the existence of a liquid inner core consisting of an Fe-FeS eutectic mixture, a silicate outer core, a mantle of water or water-ice and an ice crust, and generation of the field by an internal dynamo. Neubauer (1978) derived a surface field strength for Titan of 100 nT in an ambient field of 13 nT, and a magnetic moment of $4.56 \cdot 10^{-6}\ Tm^3$. Observations by Pioneer 11 during its flyby at Saturn in September 1979 were first interpreted in favour of a magnetic wake at Titan, although there was the possibility that Titan's dense atmosphere hindered plasma to directly flow onto the surface of the moon (Jones et al., 1980). When Voyager 1 encountered Titan in November 1980, though, no evidence for an intrinsic magnetic field was found. Instead these observations indicated that Titan possessed a weak internal field at most, with a dipole magnetic moment $< 2 \cdot 10^{21}\ Gcm^3$, and the ionosphere being the main origin of the observed interaction with the Saturnian magnetoplasma (Ness et al., 1982). After further investigation, Neubauer et al. (1984) concluded that Titan's interaction with Saturn's magnetoplasma was mainly atmospheric, similar to Venus' interaction with the solar wind, and the magnetosphere was caused by induction, resulting in an upper limit for the magnetic moment of $\leqslant 7 \cdot 10^{20}\ Gcm^3$ and a corresponding surface field strength of $\leqslant 4.1\ nT$. When Cassini arrived at Saturn and made its first close encounter with Titan, this view was basically confirmed, since no evidence of any intrinsic field was found (Backes et al., 2005), and so far, this has not changed (Neubauer et al., 2006; Jia et al., 2010).

Chapter 2

Dynamo Theory

2.1 Historical Development of Dynamo Theory

The theory of planetary dynamos describes the generation of a magnetic field due to a rotating, electrically conducting fluid in a planetary core. For many centuries, scientists observed and investigated the surface field, and one well-known result of these efforts is Gauß' representation (Gauß, 1839) of the field at and above the surface of the earth by a scalar potential (Roberts, 2009)

$$\hat{V} = r_e \sum_{n=1}^{\infty} \sum_{m=0}^{n} \Big[\left(\frac{r_e}{r}\right)^{n+1} (g_n^m \cos m\phi + h_n^m \sin m\phi) + \left(\frac{r}{r_e}\right)^{n} (q_n^m \cos m\phi + s_n^m \sin m\phi) \Big] P_n^m(\theta), \tag{2.1}$$

where r, θ, and ϕ describe spherical coordinates, r_e is the earth's radius, g, h, q, and s are time dependent coefficients, g and h describe the field created in the fluid core, q and s describe external sources at infinity, and P is the Schmidt normalized Legendre function. But Gauß never tried to find the origin of the magnetic field he observed, and interest in its theoretical description was rare even until the 1940s. A short paper by Larmor (1920) laid the foundation for dynamo theory, although it took some time to recognize its significance. There he suggested fluid motions within the sun to constitute a possible mechanism for the generation of sunspots, a principle also applicable to the earth's core. His idea was first rejected to be unplausible, and in the 1930s Cowling (1934) proved that axisymmetric fields could not be maintained by a dynamo process, which became known as "Cowlings theorem". In Cowlings opinion it showed that Larmor's idea of fluid motions generating a magnetic field by a self-sustaining dynamo process was false and had to be dismissed completely. Consequently, for the next 20-30 years, theorists all over the world were trying to either prove that self-sustaining dynamos could not produce the earth's magnetic field, or to find a working example that could demonstrate the opposite. The first successful theoretical models by Elsasser (1946a,b,c, 1950), Bullard (1949), Bullard and Gellman (1954), and others appeared in the late 1940s and early 1950s. Although they could not prove the existence of self-sustaining dynamos in a mathematically complete way, their models demonstrated the first efforts of a magnetohydrodynamic theory for the terrestrial magnetic field. Despite the incompleteness of their description, a lot of important results could be achieved, like the derivation of the magnetic induction equation for incompressible flow, the decomposition into poloidal and toroidal fields, recognizing core convection as the main driver of dynamo action, and the definition of a series of dimensionless parameters that govern a self-sustaining dynamo. In the following years, a couple of kinematic dynamo models and anti-dynamo theorems were developed (Zeldovich, 1956; Cowling, 1957). The mathematically rigorous proof was achieved by Herzenberg (1958) and Backus (1958), who could show that despite Cowling's theorem self-sustaining dynamos were possible. But the next big step was taken by Parker (1955), who introduced the concept of mean-fields into dynamo theory and suggested the induction of a poloidal magnetic field by helical flows that twist purely toroidal field lines. Out of this idea originated a whole new field of research, called "mean field electrodynamics", which is in its formalism used today due to

Steenbeck et al. (1966) and Steenbeck and Krause (1969) (see also Roberts and Stix (1971), Rädler (1968), and Moffatt (1978)). The interest more and more shifted from large-scale kinematic dynamos towards the study of mean field dynamos, and in the 1970s the importance of rotation on convection and thus on the dynamo process became apparent. For the case of rapidly rotating systems, like the earth's core, in which convection is influenced by the Coriolis force, Busse (1970) developed theoretical models that showed the development of small-scale columns aligned parallel to the axis of rotation (see 2.1), in which convection could produce magnetic field through the α^2-mechanism. Despite all the achievements in dynamo theory, in the question of dynamo equilibration only marginal successes could be achieved. Equilibration deals with the question how the magnetic field that is generated by the dynamo process interacts with the flow that created the field through the Lorentz force. Two important field equilibration models were developed by Taylor (1963), who proved the so-called Taylor constraint, and Braginsky (1964), who proposed an alternative way of equilibration with his "model-z". But neither of both models could produce convincing results, which could only be achieved with computers powerful enough for full 3D numerical simulations. The first 3D spherical magnetohydrodynamic models were created by Glatzmaier and Roberts (1995), and Kageyama and Sato (1995). Most MHD models developed since then use the Boussinesq approximation (like, for example, Kuang and Bloxham (1999)) although some relied on theories of convection in a compressible fluid, like the one derived by Braginsky and Roberts (1995). An extensive review on numerical dynamo simulations is given in Christensen and Wicht (2009), and in Roberts and Glatzmaier (2000).

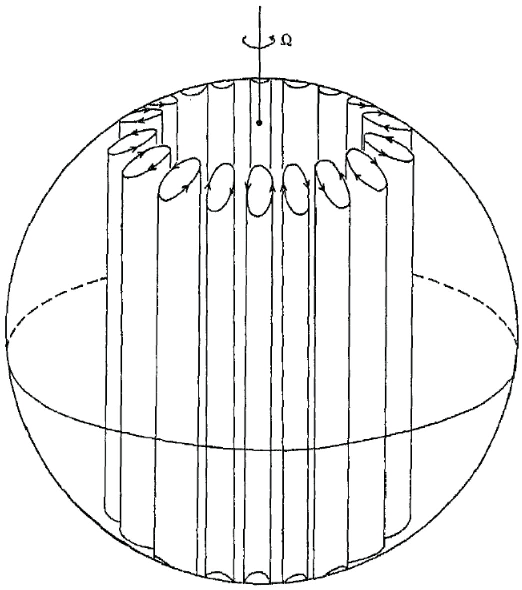

Figure 2.1: Development of vertical columns parallel to the axis of rotation, taken from Busse (1970).

2.2 Basic Theory

Dynamo theory is based upon the equations of electromagnetic theory that were in use before Maxwell introduced the displacement current, which are therefore called "pre-Maxwell equations" ($\mathbf{E}$ and $\mathbf{B}$ are the electric and magnetic field, respectively, μ is the permeability and ϵ the permittivity of the medium considered, $\mathbf{j}$ is the current density, and ρ_c is the charge density):

$$\nabla \times \mathbf{E} = -\frac{\partial \mathbf{B}}{\partial t} \tag{2.2}$$

$$\nabla \times \mathbf{B} = \mu \mathbf{j} \tag{2.3}$$

$$\nabla \cdot \mathbf{B} = 0 \tag{2.4}$$

$$\nabla \cdot \mathbf{E} = \frac{\rho_c}{\epsilon} \tag{2.5}$$

The reason for this is the fact, that in studies concerning the interior of the earth the characteristic velocity of the conductor is much smaller than the speed of light, and therefore the term representing the displacement current can be neglected. In addition, Ohm's law in its generalized form for a conductor moving with the velocity $\mathbf{u}$ is used,

$$\mathbf{j} = \sigma(\mathbf{E} + \mathbf{u} \times \mathbf{B}) \tag{2.6}$$

which results from the form of the law in a stationary medium, after a Galilei transformation to the moving frame of reference. Applying the curl operator on Ohm's law and dividing the whole equation by σ, the electrical conductivity, yields an equation where the electric field is eliminated in favor of $\mathbf{B}$, an indication of the fact that $\mathbf{E}$ only plays a minor role in dynamo theory. This "induction equation" is one of the most fundamental equations in dynamo theory:

$$\frac{\partial \mathbf{B}}{\partial t} = \nabla \times (\mathbf{u} \times \mathbf{B}) - \nabla \times \eta(\nabla \times \mathbf{B}), \tag{2.7}$$

or, assuming $\eta = \frac{1}{\mu_0 \sigma} = const.$:

$$\frac{\partial \mathbf{B}}{\partial t} = \nabla \times (\mathbf{u} \times \mathbf{B}) + \eta \nabla^2 \mathbf{B}. \tag{2.8}$$

When inspecting the induction equation one finds that the temporal variation of the $\mathbf{B}$-field is governed by a "competition" between the induction of the electromagnetic field (the first term on the right-hand side) and diffusion of the field by ohmic dissipation (the second term on the right-hand side). If the velocity $\mathbf{u} = 0$, the first term (=induction term) disappears, and the field diffuses away on a timescale that depends on the characteristic magnitudes (velocity and length) of the system considered. In the case of the earth, it would take 2×10^5 yrs for the field to disappear, which is in stark contrast to the earth's possessing a magnetic field over geological time scales, i.e. the last 3.5 billion years (Roberts, 2009). Therefore there must exist a mechanism that prevents the field from decaying away and maintaining the field by electromagnetic induction, which is represented by the term $\nabla \times (\mathbf{u} \times \mathbf{B})$. On the other hand, if the magnetic diffusivity $\eta = 0$ (=perfect conductor), only the induction term remains, which is called the frozen flux limit, because the magnetic field lines appear to be frozen to the fluid. There's an important theorem that deals with that case, Alfvéns theorem, which will be discussed below. To quantify the relative importance of induction and ohmic dissipation one can start by non-dimensionalizing the induction equation by introducing dimensionless quantities for length, time and velocity (Jones, 2007):

$$\tilde{t} = \frac{t \cdot \mathcal{U}}{\mathcal{L}} \tag{2.9}$$

$$\tilde{x} = \frac{x}{\mathcal{L}} \tag{2.10}$$

$$\tilde{\mathbf{u}} = \frac{\mathbf{u}}{\mathcal{U}}, \tag{2.11}$$

where $\mathcal{L}$ is a typical length scale and $\mathcal{U}$ a typical velocity of the problem considered. After inserting these into the induction equation and considering the change of the nabla operator,

$$\tilde{\nabla} = \nabla \cdot \mathcal{L}, \tag{2.12}$$

the induction equation can be rewritten in the following way (Jones, 2007):

$$\frac{\partial \mathbf{B}}{\partial \tilde{t}} = \tilde{\nabla} \times (\tilde{\mathbf{u}} \times \mathbf{B}) + Rm^{-1} \tilde{\nabla}^2 \mathbf{B}. \tag{2.13}$$

Here, Rm is the magnetic Reynolds number, defined by $Rm = \frac{\mathcal{U} \cdot \mathcal{L}}{\eta}$, and it controls the importance of the ohmic diffusion term. If the magnetic Reynolds number is large, the diffusion term becomes small and induction is the dominating process. On the other hand, if the magnetic Reynolds number is small, the diffusion term is large and therefore dominates the induction term. This requires $Rm > 1$ (it can be shown that $Rm > \pi^2$ suffices for dynamo action to occur in spherical geometry (Jones, 2010)) for a self-sustaining dynamo to work, but many models require Rm to be as large as 50 and in the earth, assuming velocities in the core of

$4 \times 10^{-4}\ m\ s^{-1}$ and a length scale of the size of the earth's core, $Rm = 100$ (Roberts, 2009; Jones, 2007).
For the case of a perfect conductor, $\sigma = 0$ and therefore $\eta = 0$, which means that $Rm = \infty$. Although this case is obviously never realized in nature, it can simplify some considerations by appealing to a theorem due to Alfvén, which states that "magnetic flux tubes move with a perfect conductor as though frozen to it" (Roberts, 2009). Following this idea, it is straightforward to determine the conversion of kinetic energy into magnetic energy by stretching and bending of flux tubes, caused by the fluid flow. The increase in magnetic energy for a tube stretched by an amount of δ is then $(B_0^2/\mu_0)A_0\delta$ (Roberts, 2009), where A_0 is the area of the cross section of the flux tube, B_0 is the magnetic field within this area, and μ_0 is the permeability. Another result obtained is the concept of "Alfvén waves", a concept first suggested in a work on comet tails by Alfvén (1957). Alfvén waves are also caused by the tension of the flux tubes, comparable to a stretched string on a guitar, on which, when released, a wave can travel along. The stretching is caused by perturbations by the flow (the "plucking of the string") and the resulting wave travels along the flux tube with the Alfvén speed, $\mathbf{V}_A = \mathbf{B}/\sqrt{\mu_0\rho}$ (Roberts, 2009). One very important phenomenon is the ω-effect, shown in Fig. 2.2, which creates a zonal field component out of purely meridional field due to shearing of field lines by a zonal flow. If there is no diffusion of the magnetic field, the field lines will be wound around the symmetry axis by the flow (and the field will increase monotonically) as long as the fluid motion is strong enough to act against the growing stresses of the field lines. If the stresses become too strong to allow any further motion, the growth of the field will cease again (Roberts, 2009).

In the more realistic case of an imperfect conductor, the conductivity

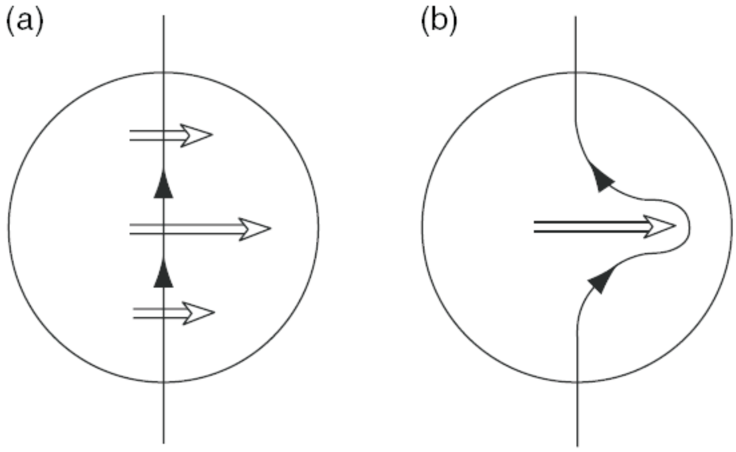

Figure 2.2: Creation of a ϕ-component of $\mathbf{B}$ by shearing of a field line by zonal flow, called the ω-effect. Image taken from Roberts (2009).

σ and the magnetic Reynolds number Rm are finite. This means that diffusion takes place and Alfvén's theorem no longer holds. Therefore the magnetic field no longer has to keep its field line topology for ever and reconnection processes can appear. Reconnection takes place if field lines "break up" and reconnect in some other configuration. It "is essentially a topological restructuring of a magnetic field caused by a change in the connectivity of its field lines" (Priest and Forbes, 2006) and as a consequence stored magnetic energy is released. For example, if two opposing field lines with opposite sign approach each other within a narrow diffusion region, the field lines can break up and rejoin in a different way from the one before (Fig. 2.3). For a self-sustaining dynamo to work, reconnection is an essential process. Without it, the field lines could only be rearranged (due to Alfvén's theorem), but to generate new flux, diffusion is needed in order to enable reconnection.

Besides other important aspects of reconnection (see Roberts (2009); Priest and Forbes (2006)), it also has an impact on the ω-effect described above. When the field is wound by the flow, diffusion has the effect of

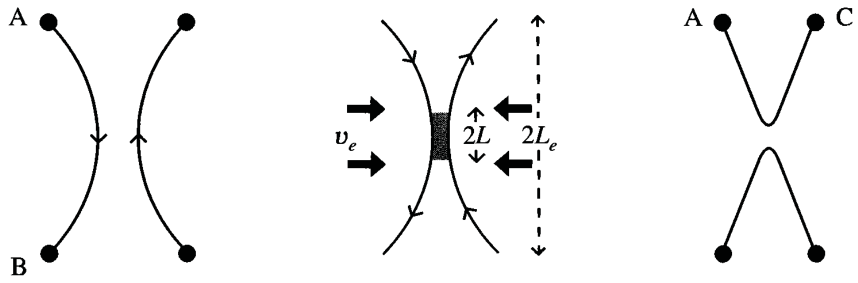

Figure 2.3: Two oppositely directed field lines break up and reconnect. Between the two field lines a narrow diffusion region is formed before reconnection occurs. Image taken from Priest and Forbes (2006).

bending the field lines back to their original state. The field lines begin to move in the opposite direction with a certain drift velocity, proportional to the field line curvature, thus counteracting the process of zonal field production and finally stopping it.

Probably the most famous effect in dynamo theory, which is also a consequence of finite conductivity and reconnection, is the α-effect, which was originally suggested by Parker (1955), but is in its form used today due to Steenbeck et al. (1966). Although it was proposed by Parker in the context of meanfield dynamos (see below), it would not exist in an infinitely conducting fluid, since then no reconnection would happen. In an imperfect conductor, though, it appears when screw-like fluid motion twists magnetic flux ropes until they can disconnect and reconnect as independent flux loops. These screw-like motions are called "helical", and are described by the helicity, which is the dot product of velocity and vorticity (which is the cross product of the nabla operator and the velocity):

$$\omega = \nabla \times \mathbf{u} \tag{2.14}$$

$$\mathbf{H} = \mathbf{u} \cdot \omega \tag{2.15}$$

In Fig. 2.4 , (b), the field gradients are very large at the point marked with an 'R', and there diffusion can have the effect of separating an autonomous

loop from the flux rope. This is a direct effect of the imperfect conductor, because without diffusion the large gradients would not have any effect, since conductivity would be the same, viz. infinity, in all directions.
As mentioned above, $Rm \gg 1$ is assumed for planetary dynamos. Although without relevance in the context of this work, the opposite case, $Rm \ll 1$, also exists and is called "low conductivity approximation" (for details see Roberts (2009), p.78).
Another very important aspect of dynamo theory are anti-dynamo theorems, which shall be described in the context of kinematic dynamos. In simple terms, kinematic dynamos are solutions of the induction equation for a given velocity field. In contrast, the MHD dynamo problem requires in addition the solving of a momentum equation, like the Navier-Stokes equation, and an energy equation. Here the Lorentz force, which is included in the Navier-Stokes equation, is the main nonlinear term, which makes not only the process of solution finding harder, but also requires more computational power in order to generate numerical simulations of planetary dynamos. Although the kinematic dynamo problem is linear in $\mathbf{B}$, it is nevertheless demanding, and it required a lot of work to find solutions for it. The basic problem was either to find a configuration that resulted in a working self-sustaining dynamo, or to formally prove that self-sustaining dynamos could not exist at all. This resulted in a series of theorems, all of which stated certain circumstances under which dynamo action was not possible. The first and most famous of these theorems is Cowling's theorem (Cowling, 1934): "Axisymmetric magnetic fields cannot be maintained by a dynamo". It was followed by many others, e.g. 2D-field theorem, toroidal velocity theorem (see Roberts (2009); Jones (2007) for details), but the first successful models of Herzenberg (1958) and Backus (1958) made it clear that no general anti-dynamo theorem could exist. In the early 70s of the last century another class of dynamos appeared,

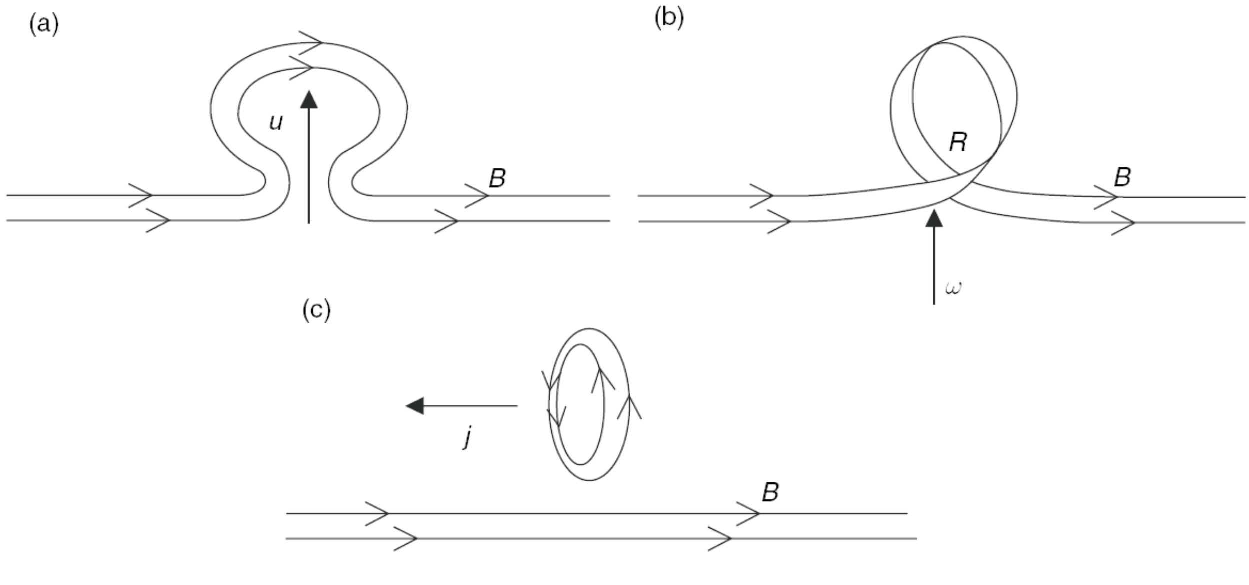

Figure 2.4: The α-effect: A flux rope is bent by the flow (a), and then twisted by the vorticity (b) of a cyclonic eddy. Due to the large field gradients at the point marked with R in (b), a flux loop detaches from the flux rope(c), thereby creating new flux. Image taken from Roberts (2009).

laminar dynamos, which are a special case of kinematic dynamos, where a non-axisymmetric field is generated by laminar flows. The first two simple models were presented by Gailitis (1970) and Ponomarenko (1973), and more complicated models have been developed until today, like dynamos employing the Arnold-Beltrami-Childress (ABC)-flow, which is an example for a 3D laminar dynamo (see Roberts (2009)). In contrast to laminar flows, turbulence has been considered in conjunction with dynamos already in the 1950s. Parker (1955) realized that turbulence could help in defeating Cowling's theorem. By using turbulent fields for velocity and magnetic field,

$$\begin{aligned} \mathbf{u} &= \overline{\mathbf{u}} + \mathbf{u}' \\ \mathbf{B} &= \overline{\mathbf{B}} + \mathbf{B}', \end{aligned} \tag{2.16}$$

where the variable with the overbar is the ensemble average, and the primed variable the fluctuating part of the turbulent quantity, and inserting these fields in the equation for the electric field,

$$\mathbf{E} = -\mathbf{u} \times \mathbf{B} + \eta \nabla \times \mathbf{u}, \tag{2.17}$$

and averaging the whole equation, a new form of the induction equation can be derived:

$$\begin{aligned} \eta \nabla \times \overline{\mathbf{B}} &= \overline{\mathbf{E}} + \overline{\mathbf{u}} \times \overline{\mathbf{B}} + \overline{\mathcal{E}}, \\ \mathcal{E} &= \mathbf{u}' \times \mathbf{B}' \end{aligned} \tag{2.18}$$

Eq. (2.17) is obtained by using Maxwell's equation for the current density from eq. (2.2), and Ohm's law, eq. (2.6), and when averaging it has to be considered, that the average of the fluctuating part is zero. Eq. (2.18) is Ohm's law for the average magnetic field $\overline{\mathbf{B}}$, and contains a new term $\overline{\mathcal{E}}$, which is discussed in detail in Roberts (2009). This term led to the development of a new category of dynamos, mean field dynamos, and a new area of research, mean field electrodynamics. The induction equation for the mean field then can be written as (Roberts, 2009)

$$\frac{\partial \mathbf{B}}{\partial t} = \nabla \times (\alpha \mathbf{B} + \mathbf{u} \times \mathbf{B}) + \overline{\eta} \nabla^2 \mathbf{B} \tag{2.19}$$

where α and β are constants of proportionality, the first one being the constant that gave the α-effect its name. In addition to the α- and ω-effect, new types of dynamos were discovered, the $\alpha\omega$, α^2, and $\alpha^2\omega$-dynamos. Despite their theoretical importance, in geophysics mean field electrodynamics are ignored, since it is assumed that global motions control the geodynamo, and thus the term $\mathcal{E}$ is neglected. Today, most dynamo research is concentrated on full 3D simulations of magnetohydrodynamic dynamos, where the induction equation is solved together with an equation of motion (usually the Navier-Stokes equation in the Boussinesq approximation, including rotation and Lorentz force), an energy equation and an equation of state. Obviously, this requires a lot of computational power, and only since the availability of super computers and highly parallelized dynamo codes these 3D simulations have been successful (Fig. 2.5 shows the 3D simulation of a magnetic field reversal). Although 3D MHD simulations represent the forefront of dynamo research, sometimes it can be more useful to do parameter studies and yield scaling laws, which can give interesting insights into the magnetic fields of planets in the solar system, and possibly on those outside as well.

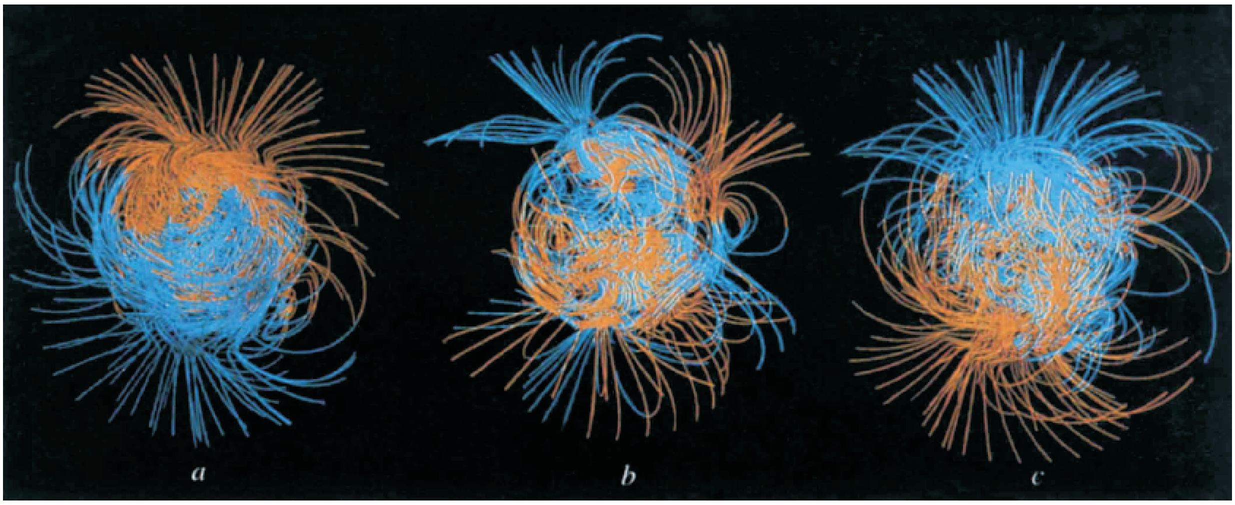

Figure 2.5: Three-dimensional structure of the magnetic field during a magnetic field reversal, shown 9000 years before (a), midway through (b), and at the end of the reversal. Image taken from Glatzmaier and Roberts (1995).

2.3 Scaling Laws

When the first space missions enabled scientists to determine the magnetic moments of the terrestrial planets' magnetospheres (see Chapter 1), it was tempting to come up with empirical laws that lacked the complexity of the usual MHD equations used to describe planetary magnetic fields. The first of such scaling laws is due to Blackett (1947) and is called "magnetic Bode's law" or "Blackett's law" (see Fig. 2.6), and connects the magnetic moment of a planet with its moment of inertia. This is in analogy to the famous

”Titius-Bode law”, which relates the distance of a planet from the sun to its number in position outwards from the sun. For both, the magnetic and the Titius-Bode law, the lack of physical explanations for such simple relations cast doubt on their validity. In the case of the Titius-Bode law, the validity holds out to Uranus, but Neptune's and Pluto's distance deviate strongly from the predicted value. For other solar systems than our own its even unclear, if Bode's law is applicable, because usually too few planets are known to test it. Nevertheless, dynamical stability arguments could be used to show that any planetary system is likely to exhibit some kind of Bode's law, if similar errors in real distances from the predicted ones of a few percent are accepted. Regarding the magnetic Bode's law, planets that do not have a currently active dynamo, like Venus or Mars, do not follow the law (Russell, 1978a; Vallée, 1998), and therefore it is more a dipole dynamo law than a general magnetic scaling law. But even planets like Saturn that have an active dynamo, fall below the predicted value. And in the case of the earth it is not clear whether the angular momentum of the earth-moon system or of the earth alone should be used (Russell, 1978a), and therefore the validity of a magnetic Bode's law is heavily disputed, even more so as no physical explanation for this law could be found so far. Nevertheless, today this law is still used to estimate planetary magnetic moments, for example to estimate the radio flux caused by the interaction of stellar winds with hypothetical exoplanetary magnetospheres that reaches the earth (Stevens, 2005).

However, even in the 1970s it seemed more fruitful to base even empirical laws on some theoretical considerations, as was already exemplified by Busse (1976). But Busse's derivation of Venus' surface field of $1/430$ of the geomagnetic field was definitely too high (see Section 1.3), which shows the difficulty in deriving scaling laws for different kinds of planets from purely theoretical considerations. Nevertheless, new scaling laws have been de-

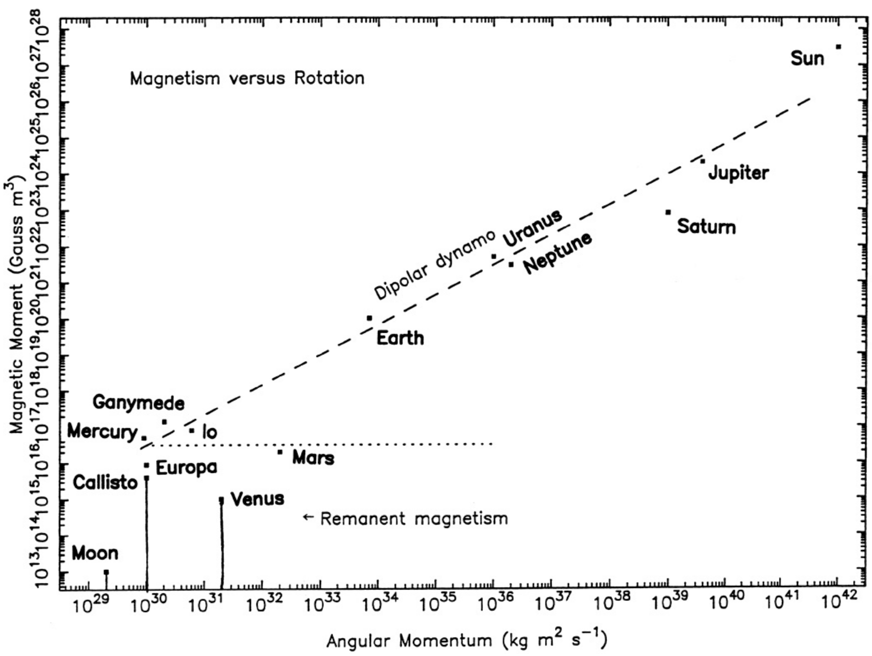

Figure 2.6: The magnetic Bode's law, showing the empirical relation between angular momentum and magnetic moment for planets, moons and the sun. Image taken from Vallée (1998).

rived in the following decades. While Busse (1976) assumed geostrophic balance, i.e. balance between Coriolis and pressure gradient forces, Curtis and Ness (1986) argued that geostrophic balance led to magnetic fields much greater than observed in the case of terrestrial planets, and too low for the gas giants. They advanced an idea originally developed by Eltayeb and Roberts (1970), where balance between Coriolis and Lorentz force was assumed, which is called magnetostrophic balance (Curtis and Ness, 1986):

$$2\omega_{\mathbf{c}} \times \mathbf{v}_c \sim \mathbf{J}_c \times \mathbf{B}_c/\rho_c, \tag{2.20}$$

where $\omega_{\mathbf{c}}$ is the angular velocity of the core, $\mathbf{v}_c$ is the fluid velocity in the core, $\mathbf{J}_c = \nabla \times \mathbf{B}_c/4\pi$ is the current density in the core, $\mathbf{B}_c$ is the magnetic field within the core, and ρ_c is the core density. By assuming right angles in the vector product and the nabla operator to be proportional to the inverse core radius one obtains (Curtis and Ness, 1986)

$$B_c \sim (\rho_c r_c \omega_c v_c)^{\frac{1}{2}}. \tag{2.21}$$

In contrast to Busse, Curtis and Ness (1986) assumed a relation between the heat flux and the energy flux of the convection in the core, which yields

$$\rho_c v_c^3 \sim E \rightarrow v_c \sim E^{\frac{1}{3}} \rho_c^{-\frac{1}{3}}. \tag{2.22}$$

By using the relations between the magnetic moment and the core magnetic field (Curtis and Ness, 1986)

$$M \sim B_c r_c^3 \tag{2.23}$$

and the magnetic moment and the equatorial magnetic field strength at the surface of the planet (Curtis and Ness, 1986)

$$M = B_p r_p^3 \tag{2.24}$$

a relation between the field strength in the core and at the surface is obtained:

$$B_c^2 \sim \frac{B_p^2 r_p^6}{r_c^6}. \tag{2.25}$$

Using the empirical relation between core radius and planetary mass (Curtis and Ness, 1986)

$$r_c \sim M_p^{0.44} \tag{2.26}$$

and eqns. (2.21)-(2.25) the scaling law of Curtis & Ness is obtained:

$$B_p \sim r_p^{-3} \rho_c^{\frac{1}{3}} M_p^{1.54} \omega^{\frac{1}{2}} E^{\frac{1}{6}}. \tag{2.27}$$

A comparison of observed and calculated magnetic fields can be seen in Fig. 2.7.

Since almost all of the calculated field strengths lie below the observed ones, Curtis and Ness (1986) argued that magnetostrophic balance, which they considered as the governing balance in planetary dynamos, obviously yielded an upper limit to the observable magnetic fields of the planets. Mizutani et al. (1992) also based their scaling on the magnetostrophic

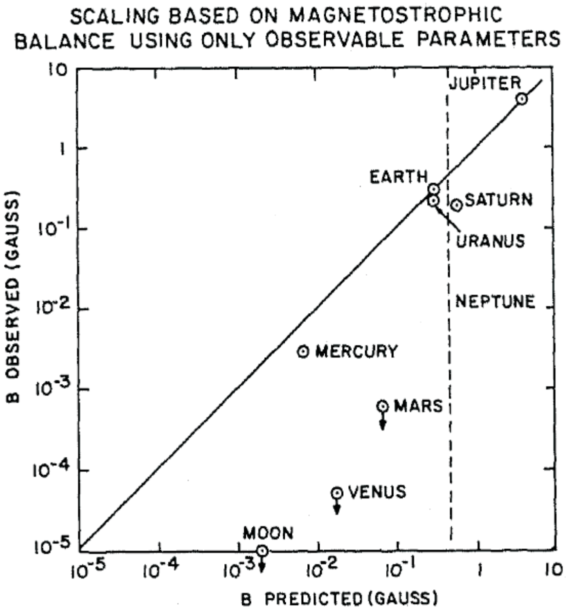

Figure 2.7: Comparison between values predicted by the scaling law of Curtis and Ness (1986) and observed field strengths. Image taken from Curtis and Ness (1986).

balance, but used another estimation of the convection velocity v_c. Following Backus (1958) they first required as a necessary condition for dynamo action a bound on the magnetic Reynolds number, which means that generation of magnetic field dominates Ohmic diffusion:

$$R_m = \frac{v_c R_c}{\lambda} \geqslant \pi, \tag{2.28}$$

R_c being the core radius, v_c the convection velocity, and λ the magnetic diffusivity. Secondly, the fluid velocity within the core had to be lower than the rotation of the planet, and therefore the inequality

$$\lambda / R_c \leqslant v_c \leqslant R_c \Omega, \tag{2.29}$$

had to hold, which constitutes a lower and upper bound for the fluid velocity v_c. Taking the geometric mean of the lower and upper bound directly yields

$$v_c = (\lambda / R_c \cdot R_c \Omega)^{\frac{1}{2}} = (\lambda \Omega)^{\frac{1}{2}} \,. \tag{2.30}$$

From eq. (1) in Mizutani et al. (1992), which describes the fluid velocity in a constantly rotating sphere,

$$\rho_c \left[\frac{\partial \mathbf{v_c}}{\partial t} + (\mathbf{v_c} \nabla) \mathbf{v_c} \right] = 2\rho_c \mathbf{v_c} \times \mathbf{\Omega} + \rho_c \mathbf{\Omega} \times (\mathbf{r} \times \mathbf{\Omega}) - \nabla p + \frac{1}{4\pi\mu} (\nabla \times \mathbf{B_c}) \times \mathbf{B_c} ..., \tag{2.31}$$

where ρ_c is the core density, $\mathbf{v_c}$ the velocity of the convecting fluid, $\mathbf{\Omega}$ the angular velocity, $\mathbf{r}$ the radius at which the velocity is considered, and $\mathbf{B_c}$ the magnetic flux, the first and fourth term on the right-hand side, describing Coriolis force and Lorentz force, respectively, can be equated (i.e. magnetostrophic balance). Assuming again all angles to be perpendicular and the nabla operator $\nabla \propto 1/R$ results in

$$B_c \sim (8\pi\mu\rho_c R_c \Omega v_c)^{\frac{1}{2}}. \tag{2.32}$$

Using the estimation for the fluid velocity described above results in the scaling law used by Mizutani et al. (1992):

$$B_c \sim (8\pi\mu\rho_c R_c)^{\frac{1}{2}} \Omega^{\frac{3}{4}} \lambda^{\frac{1}{4}}. \tag{2.33}$$

Employing the relations from eq. (2.23) and eq. (2.24) yields the scaling law by Mizutani et al. (1992) for the magnetic field at the surface of a planet:

$$B_p \sim (8\pi\mu\rho_c)^{\frac{1}{2}} R_c^{\frac{7}{2}} \Omega^{\frac{3}{4}} \lambda^{\frac{1}{4}} R_p^{-3}. \tag{2.34}$$

(There is an error in the paper by Mizutani et al. (1992) in eq. (11), where $\lambda^{\frac{1}{2}}$ is used instead of $\lambda^{\frac{1}{4}}$. In Table 1, however, this error does not occur.) Fig. 2.8 shows this scaling law in comparison with observed magnetic dipole moments of moons and planets in the solar system.

Starchenko and Jones (2002) took another approach by using the anelastic approximation for self-consistent MHD based on the work by Braginsky and Roberts (1995), since their application covers gas giants as well, for which the Boussinesq approximation does not hold anymore. Employing MAC balance (Magnetic, Archimedean, Coriolis = balance between

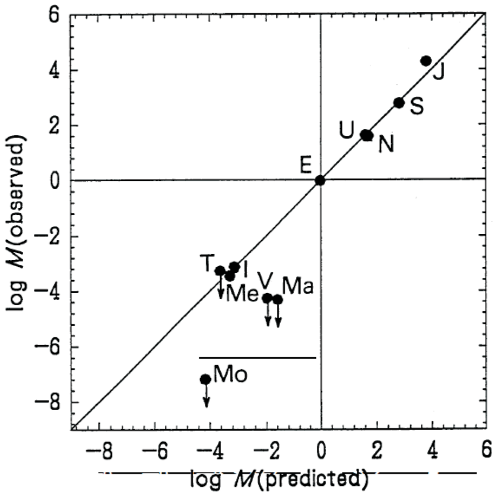

Figure 2.8: The scaling law by Mizutani et al. (1992) in comparison with observed values of the magnetic moment of moons and planets in the solar system. Image taken from Mizutani et al. (1992).

magnetic, buoyancy and pressure, and Coriolis forces) and assuming that compositional convection dominates thermal convection in the earth's core they arrive at the following scaling law for the magnetic field inside the core:

$$B_* = (\mu_0 \overline{\rho_*} \Omega r_* V_*)^{\frac{1}{2}}. \tag{2.35}$$

Here μ_0 is the permeability of free space, $\overline{\rho_*}$ is the typical average density in the core, Ω is the angular velocity, r_* is the mixing length or magnetic length scale of 10^5 m, and V_* is the typical velocity in the core. Using the values for these quantities estimated in Starchenko and Jones (2002) results in a field strength in the earth's core of $B_* \sim 4 \cdot 10^{-3}\ T$. The question, how the internal field is related to the surface field is still a matter of debate. From kinematic dynamo theory it is assumed that only 1% or even less of the core field escapes to the surface, while dynamo simulations suggest values of 10%, and these are even uncertain due to the limitation of parameter space covered by recent simulations. However, a value of 1% of the core field for the surface field would fit current knowledge of the earth's surface field strength of $\sim 30 - 60\ \mu\ T$ fairly well. All these scaling laws assume some kind of balance, be it geostrophic, magnetostrophic, MAC balance, or a balance between buoyancy, Coriolis force and inertia in the so-called mixing length theory. Naturally, this poses a problem, since it is anything else than clear what kind of balance (if one at all) governs planetary dynamos. Although most scientist consider a geostrophic balance as very improbable, there is no clear evidence that favours any of the other three possibilities. Despite the fact that the Elsasser number,

$$\Lambda = \frac{\sigma B^2}{\rho\Omega}, \tag{2.36}$$

which measures the ratio of Coriolis and Lorentz force, is distributed over a fairly wide range in dynamo simulations ($\sim 10^{-2} - 10^2$, (Christensen and Aubert, 2006)), which could tempt one to doubt its significance, there is no evidence that magnetostrophic balance is an erroneous assumption. It could simply be the case that the Elsasser number is a bad measure for the ratio of the two forces, since it neglects important length scales (Christensen and Aubert, 2006). Therefore the results of numerous dynamo simulations have been included in studies of scaling laws, and hence, in contrast to the works described above, Christensen and Aubert (2006) did not employ purely theoretical considerations but simulation results and subsequent parameter studies to derive their scaling law of the magnetic field. An extensive study of several dimensionless parameters and the insight that the heat flux that governs the convection in the core also is a main driver of the geodynamo led them to the following scaling of the magnetic field inside the core (Christensen and Aubert, 2006):

$$B \sim 0.9\mu^{\frac{1}{2}}\rho^{\frac{1}{6}}\left(\frac{g_0 Q_B D}{4\pi r_0 r_i}\right)^{\frac{1}{3}}, \tag{2.37}$$

where μ is the magnetic permeability, ρ the core density, g_0 the gravitational acceleration at the core-mantle boundary, i.e. at the radius r_o, r_i is the radius of the inner core, D is the shell thickness, which is the thickness of the fluid outer core without the inner core, and $Q_B = \alpha Q_{adv}/c$ is the buoyancy flux, where α is the thermal expansivity, c is the heat capacity, and Q_{adv} is the advected heat flux, which is the total heat flux minus the heat flux conducted down the adiabat. Christensen (2010) reformulated this scaling law in terms of the convected heat flux q_c and the radius of the outer core R_c:

$$B^2 \propto \rho R_c^{\frac{4}{3}} q_c^{\frac{2}{3}}. \tag{2.38}$$

A comparison of observations of different solar system planets with the values predicted by the scaling law is shown in Fig. 2.9. As can be seen, not all calculations fit the observations well, and not all planets are represented, due to the lack of knowledge of the energy flux (Mercury and Ganymede). Here an intrinsic problem of this scaling law becomes clear: Although a derivation from numerical simulations and theoretical considerations should involve more physical reality, this is counteracted by the fact that parameters like the buoyancy flux at the core-mantle boundary are very difficult to constrain and not directly observable. Moreover, this scaling law assumes a planetary dynamo like the one working in the earth's interior, which means that a deep convective shell is assumed. But planetary dynamos could also be active in thin convective shells, a fact that is not accounted for by this scaling law.

The disadvantage of this scaling law, the dependence on the energy flux, which is not equally well constrained for all planets, is an advantage at the same time. By employing different structure models for hypothetical exoplanets and using analytic equations for the energetics of the core (see next chapter), it is possible to calculate the different contributions to the heat flow at the core-mantle boundary that originate in the core. By subtracting the heat conducted down the adiabat from the total heat flow, the advected heat flow, and hence, the buoyancy flux can be determined,

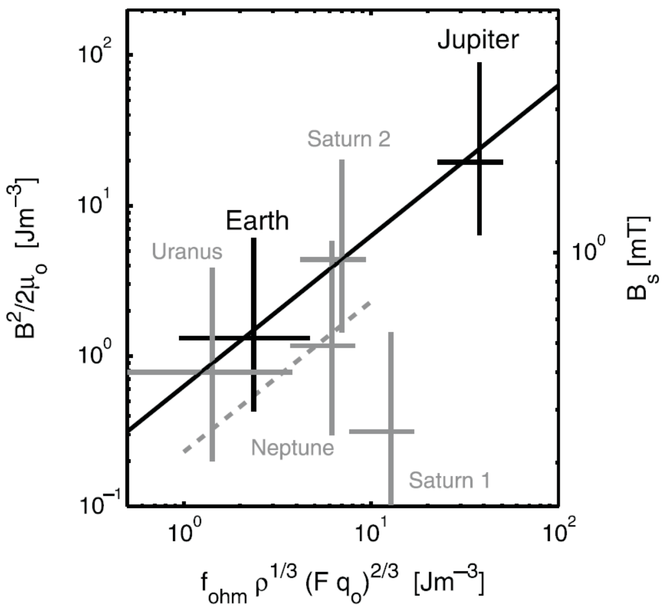

Figure 2.9: The scaling law by Christensen (2010), showing magnetic energy density vs. 2/3-power of the available heat flux given by the solid and dashed line, in comparison with observed values of the magnetic moments of the Earth, Uranus, Neptune, Saturn and Jupiter. Image taken from Christensen (2010).

which can then be used in conjunction with the scaling law eq. (2.37) or eq. (2.38) to estimate the magnetic field strength inside the core. As mentioned above, the ratio of core to surface field is still not clear and the kind of dependence of the one from the other is also not well established. Since dynamo simulations suggest that the surface field strength is 1% to 10% of the core field strength, this range could be used for estimations of the surface field in absence of any other scientifically justifiable estimations.

Chapter 3

Energetics and Composition of the Core

3.1 Overview

One of the main questions regarding planetary magnetic fields is the source of energy powering the planetary dynamo. Although the theoretical foundations of thermodynamics are now known for a fairly long time, the special conditions in a planetary core have hampered the attempt to resolve the question of the energy source of the geodynamo (and the dynamo of other planets as well) and only in the second half of the last decade major advances in this area of research have been achieved. Already in the 1960s Braginsky realized that the release of one ore more light element(s) at the ICB could contribute a substantial part of buoyancy to drive the dynamo (Braginsky, 1963), but it took some time for this idea to find general approval. Today the general view is that this process termed compositional convection outweighs thermal convection by a factor of 2 to 3 (Olsen, 2009). Of course, compositional convection can only occur if a solid core is present, but this has not been the case throughout all the history of the earth. Thus, when the inner core was still fluid in the early days thermal convection was the only energy source present to drive the dynamo. And since paleomagnetic data clearly show that a magnetic field has been present for at least the last 3.2 (possibly up to 3.9) Gyr (Tarduno et al., 2007), thermal convection had to be strong enough when the earth was young to support a magnetic field. This implies a much faster cooling rate, up to 3 times as fast as today (Nimmo, 2009). Thus, the energetics of the core and the history of the dynamo are constrained by the age of the core and its cooling rate, which in turn is constrained by the thermal behavior of the mantle. These facts have to be kept in mind when considering calculations and theoretical derivations of core energetics.

Unfortunately, the core cooling rate and the age of the core are pretty poorly constrained numbers even for the earth, and for other planets they are completely unknown. In the case of the earth one can estimate the dissipation entropy of the geodynamo (see below) to determine the core cooling rate and then calculate all contributing terms of the heat flow across the core-mantle boundary. This is not possible for planets whose magnetic fields (or their existence at all) are totally out of reach. Therefore the possibilities carefully have to be considered how to estimate magnetic fields for extra-solar planets in dependence of their supposed inner structure. In the following sections the thermodynamics of the core using the example of the earth shall be presented. First the structure and composition of the core, which are crucial to its energetics, will be discussed. Then the basic equations how to calculate the energy and entropy for a given core structure are presented, following Gubbins (2003, 2004), and Nimmo (2009). Results from these calculations are demonstrated for the earth and the importance of the mantle for core cooling is briefly discussed. Finally the question is assessed how these considerations can be projected onto extra-solar planets.

3.2 Core Structure and Composition

Although the idea of a layered structure of the earth's interior was already proposed by Halley at the end of the 17th century, it was not clear until the end of the 19th century whether the innermost part of our planet was solid or fluid. Jeffreys (1926) finally succeeded with a model that incorporated a core that was at least partly fluid, and in 1936 Inge Lehmann could show that even deeper within that fluid core was a solid one by discovering the inner-core boundary(Lehmann, 1936). Eventually, the question of the coarse radial structure of the earth was settled (Fig. 3.1).

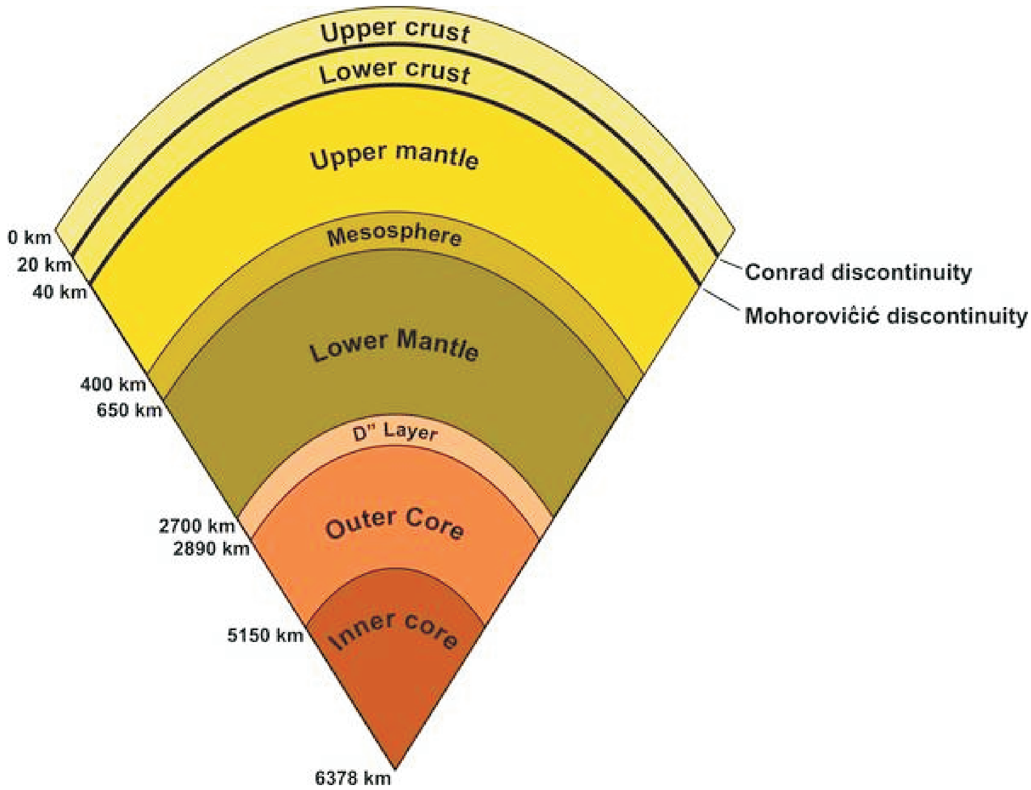

Figure 3.1: The structure of earth's interior. Image taken from Leitner (2006).

Today the knowledge of the deep interior goes even further. The existence of the core-mantle boundary, separating the fluid outer core from the overlying mantle, and the inner-core boundary are firmly established.

But other features, like a laterally varying ultralow velocity zone at the base of the mantle (Wen et al., 1998), or a magma ocean, also at the base of earth's mantle (Labrosse et al., 2007), are still a matter of ongoing research and far from completely explored.
Most information on composition and structure of the earth and its core have been gained by seismic studies, where mainly two methods have been applied. In their PREM (Preliminary Reference Earth Model), Dziewonski and Anderson (1981) used normal mode data, while Shearer and Masters (1990) employed reflected body waves amplitude ratios. Although the results of these works did not agree very well (Nimmo, 2009), recent research has achieved fairly similar conclusions (Master and Gubbins, 2003; Cao and Romanowicz, 2004). Fig. 3.2 shows how the density within the earth changes with increasing depth, Fig. 3.3 shows the density, gravity and temperature gradients only for the inner and outer core.

Of course, besides the density, also the temperature and therefore the pressure are functions of depth. Since the outer core is assumed to be convecting vigorously it seems to be a good idea to approximate the temperature gradient with that of an adiabat. The temperature at the inner-core boundary must be equal to the melting temperature of iron (mixed with some light elements) at the pressure of this depth, since the inner core is solid. Therefore one could determine the temperature at the core-mantle boundary by extrapolating the adiabat radially outwards from the inner core to the CMB.

The behaviour of iron at core pressures is a research area of its own, though, and such pressures are very difficult to produce in laboratories. Moreover, light elements in the core are supposed to reduce the melting temperature, but it is very unsure as to which amount. Nevertheless, Alfe et al. (2002) obtained a melting curve accounting for a melting tempera-

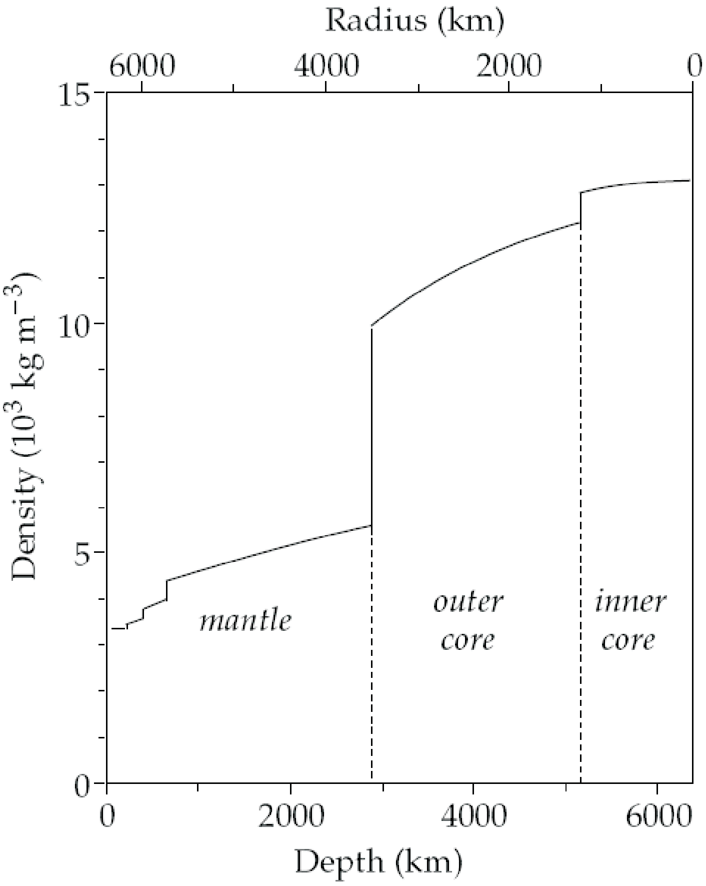

Figure 3.2: The density distribution within the earth according to the PREM model (Dziewonski and Anderson, 1981). Image taken from Lowrie (2006).

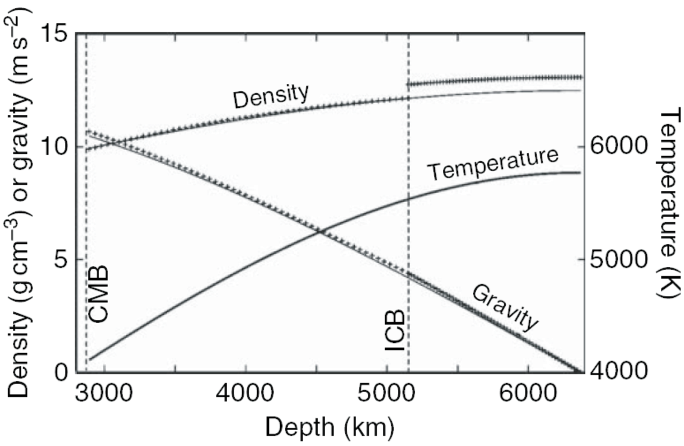

Figure 3.3: Density, temperature and gravity distribution within the earth's core. Crosses indicate data points from the PREM model (Dziewonski and Anderson, 1981), solid lines show analytical solutions according to the model described in Nimmo (2009). Image taken from Nimmo (2009).

ture reduction of 11% due to light elements in the core (Fig. 3.6). The temperature gradient and the change of the solidus with depth for the whole earth is shown in Fig. 3.4. In Fig. 3.5 the change of pressure and gravity, resp., in the earth's interior are plotted.

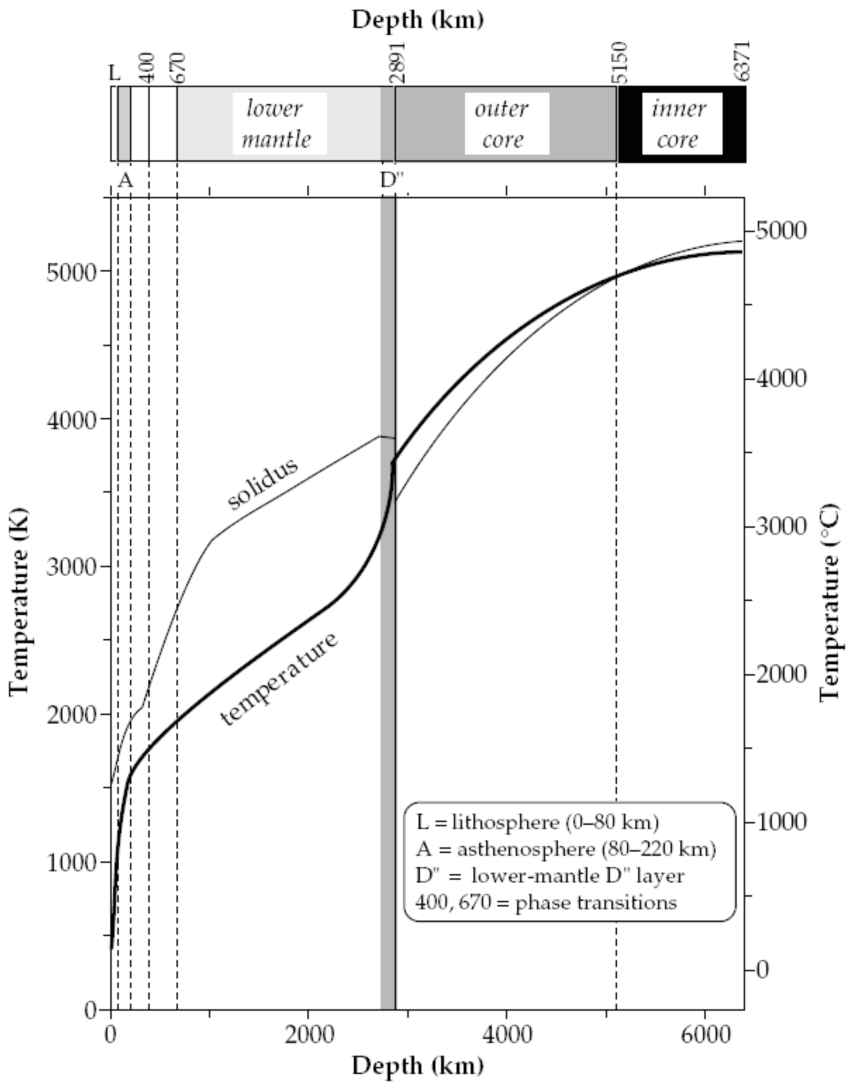

Figure 3.4: Distribution of temperature and melting point within the earth. Image taken from Lowrie (2006).

Another important and also hotly debated question is the composition of the core. Although in the beginning geophysicists assumed the core to be composed of pure iron, Birch (1952) already suspected the existence of light elements in the core due to his interpretation of seismic measurements. Birch's favored elements, carbon and silicon, have been extended by sulfur, oxygen, hydrogen by Poirier (1994), but ab initio calculations by Alfe et al. (2002) resulted in the preference of only sulfur, silicon, and oxygen. The reason was that only sulfur and silicon could not explain the density jump at the ICB, but the inclusion of oxygen in the liquid iron could solve the puzzle.

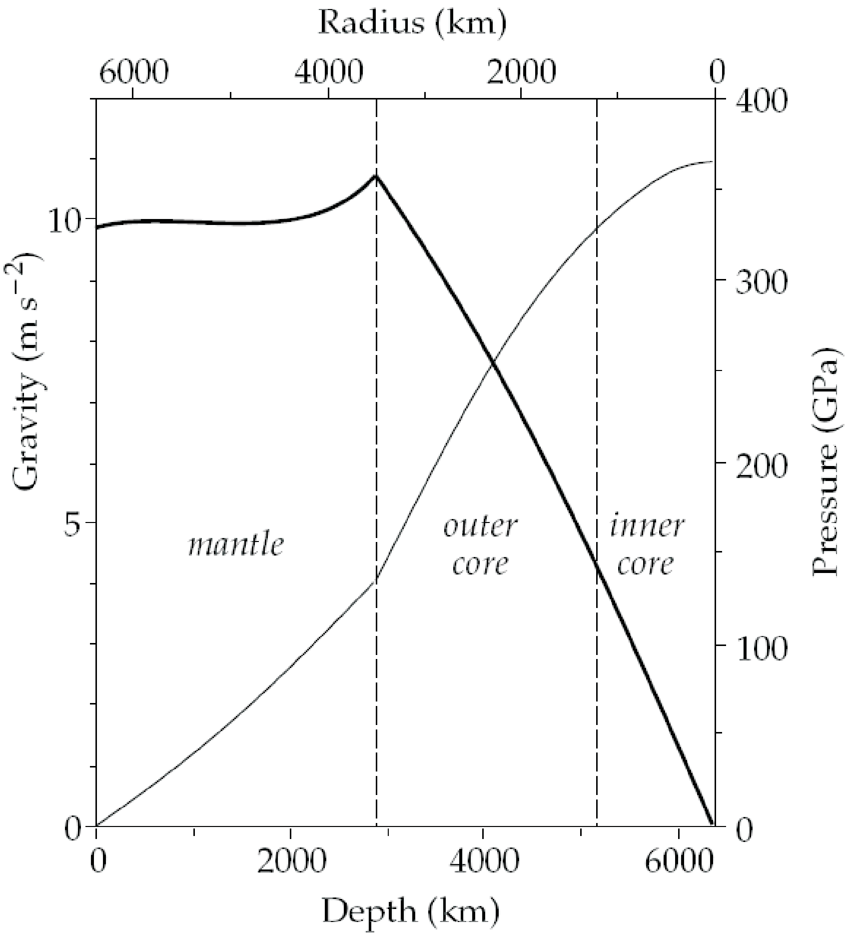

Figure 3.5: The pressure and gravity gradient within the earth, according to PREM data (Dziewonski and Anderson, 1981). Image taken from Lowrie (2006).

But still there is much debate about which light elements are present in the core, since there are geophysical and geochemical arguments for different combinations, which partly contradict each other. In spite of all this, most models assume sulfur, silicon and oxygen to be present in the core in varying abundances. Whatever light elements are present (and seismic data implicate THAT some are present), these elements drive compositional convection, which is thought to be the main driver for the geodynamo today (see section below). Apart from the discussion concerning light elements in the core, scientists are confronted with another problem, which is the possible existence of radioactive elements in the core. Of course, the presence of radiogenic material would have huge implications on the energetics, since the heat produced by radioactive decay would add up to the total heat flow across the core-mantle boundary, and therefore would be of crucial importance for the thermal evolution of the core and the energy supply of the geodynamo. The influence of different radioactive species on heat production is discussed in Chapter 4.

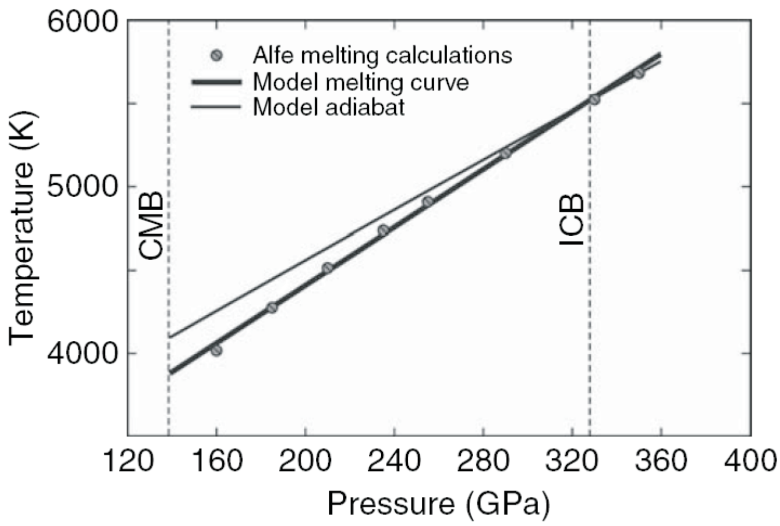

Figure 3.6: Melting curve and adiabatic temperature gradient as a function of pressure in the earth's core. Image taken from Nimmo (2009).

3.3 Governing Equations

So the question remains which energy sources are present in the core and how can they be described? The thermodynamics of the core are often formulated in terms of a so-called basic state. This basic state is produced by taking an intermediate time scale between the lifetime of a convective cell and the evolution of the earth, and averaging thermodynamic properties over this time. Thus, the pressure is averaged to hydrostatic, the temperature to adiabatic, and the gravity to spherically symmetric density distribution values. Despite for the velocity, no difference is made between convective and basic state values. More details on this basic state can be found in Braginsky and Roberts (1995).

To find a quantitative description of core energetics, the energy conservation of the core is considered. Before this, some important quantities have to be defined, which will be used in the following. As mentioned before, by averaging over an intermediate timescale the pressure is hydrostatic and is given by

$$\nabla P = \rho \nabla \psi. \tag{3.1}$$

Assuming an isentropic and isochemical outer core the adiabatic temperature gradient can be written as (Nimmo, 2009),

$$\nabla T_a = \frac{\alpha g T_a}{C_p}, \tag{3.2}$$

with α the coefficient of thermal expansivity, g the gravitational acceleration, T_a the temperature along the adiabat, and C_p the specific heat capacity. Using Grüneisen's parameter γ and the seismic velocities v_p and v_s, this can be rewritten, giving

$$\nabla T_a = \frac{\gamma g}{v_p^2 - \frac{4}{3} v_s^2}. \tag{3.3}$$

Of course, a continuity equation also holds for the core

$$\frac{\partial \rho}{\partial t} + \nabla(\rho \mathbf{v}) = \frac{D\rho}{Dt} + \rho(\nabla \cdot \mathbf{v}) = 0, \tag{3.4}$$

where $\frac{D\rho}{Dt}$ is the total derivative, and when considering a two-mixture composition, with c the mass fraction of the light element, conservation of mass of the light element in the core is given by

$$\rho \frac{\partial c}{\partial t} + \rho \mathbf{v} \cdot \nabla c + \nabla \cdot \mathbf{i} = \rho \frac{Dc}{Dt} + \nabla \cdot \mathbf{i} = 0 \tag{3.5}$$

(Nimmo, 2009). The flux vector of the light element, $\mathbf{i}$, and the heat flux vector, $\mathbf{q}$, are defined by the Onsager reciprocal relationship (Landau and Lifschitz, 1959; Nimmo, 2009):

$$\mathbf{q} = -k\nabla T + \mathbf{i}\left(\mu + \frac{\beta T}{\alpha_D}\right) \tag{3.6}$$

$$\mathbf{i} = -\alpha_D \nabla \mu - \beta \nabla. \tag{3.7}$$

Besides these quantities, two important theorems are employed: the divergence theorem (also known as Gauss' theorem)

$$\int_V \nabla \cdot \mathbf{F} dV = \oint_S \mathbf{F} \cdot \mathbf{n} dS \tag{3.8}$$

which states that the integral of the divergence of a continuously differentiable vector field F over a volume V is equal to the integral of this vector field over the surface of that volume; and Reynolds' transport theorem (Dorfi, 2007):

$$\frac{dF}{dt} = \int_{V(t)} \left[\frac{\partial f}{\partial t} + \nabla \cdot (f\mathbf{u})\right] dV, \tag{3.9}$$

$$F(t) = \int_{V(t)} f(\mathbf{x}, t) dV \tag{3.10}$$

where the change of the volume element $dV_0 = dV(t = 0)$ is described by the Jacobian, $dV = JdV_0$. Reynold's transport theorem states that the total rate of change of a property within a volume of fluid is equal to the rate of accumulation of that property within the volume added to the flux of that property over the surface of the volume. If we set $f(\mathbf{x}, t) = \rho A$, where A is an arbitrary quantity within the volume, then the following form of transport theorem can be deduced (Gubbins, 2003):

$$\frac{d}{dt}\int \rho A dV = \int \rho\left(\frac{\partial A}{\partial t} + \mathbf{v}\cdot\nabla A\right) dV = \int \frac{\partial(\rho A)}{\partial t} dV + \oint \rho A \mathbf{v}\cdot d\mathbf{S} \quad (3.11)$$

To estimate individual terms that contribute to the energy budget of the core, we can start by formulating the energy equation for the core (Gubbins, 2003):

$$\frac{\partial}{\partial t}\left(\rho e + \frac{1}{2}\rho \mathbf{v^2} + \frac{\mathbf{B^2}}{2\mu_0}\right) = -\nabla\cdot\left[\rho\mathbf{v}\left(\frac{1}{2}\mathbf{v^2} + e + \frac{p}{\rho}\right) + \frac{\mathbf{E}\times\mathbf{B}}{\mu_0} - \quad (3.12)$$

$$\left.\mathbf{v}\cdot\tau' - k\nabla T\right] + \rho h + \rho\mathbf{v}\cdot\nabla\psi, \quad (3.13)$$

ρ being the density, e the internal energy, v the velocity of the entire core fluid flow (convection plus contraction), $\mathbf{B}$ the magnetic field, μ_0 the permeability of free space, p the pressure, $\mathbf{E}$ the electric field, τ' the deviatoric stress, k the thermal conductivity, h the local heat generation, and ψ the gravitational potential. The terms in this equation have the following meaning: On the left hand side, the first term within the brackets is the internal energy, the second term is the kinetic energy, and the third term is the magnetic energy, therefore the whole left hand side describes the rate of change of these energies per unit volume. On the right hand side the terms within the brackets are the kinetic, internal, compressional, and electromagnetic energy and the conducted heat, the divergence thus describes an inward flux of these quantities. Finally, the last two terms are the heat generated per unit volume and work done by gravitational forces. The next step is to integrate the last equation over the entire core

$$\int_V \frac{\partial}{\partial t}\rho e dV + \int_V \frac{\partial}{\partial t}\frac{1}{2}\rho \mathbf{v^2} dV + \int_V \frac{\partial}{\partial t}\frac{\mathbf{B^2}}{2\mu_0} dV =$$
$$-\int_V \nabla\rho\mathbf{v}\left(\frac{1}{2}\mathbf{v^2} + e + \frac{p}{\rho}\right) dV - \int_V \nabla\frac{\mathbf{E}\times\mathbf{B}}{\mu_0} dV + \int_V \nabla\mathbf{v}\tau' dV$$
$$+\int_V \nabla\left(k\nabla T\right) dV - \int_V \rho h dV - \int_V \rho\mathbf{v}\cdot\nabla\psi dV \tag{3.14}$$

and use the divergence theorem for the divergence terms on the right-hand side and Reynolds' transport theorem for the first two terms on the left hand side:

$$\frac{d}{dt}\int_V \rho e dV - \oint\limits_{\partial V} \rho e\mathbf{v} d\mathbf{S} + \frac{d}{dt}\int_V \frac{1}{2}\rho\mathbf{v^2} dV - \oint\limits_{\partial V} \frac{1}{2}\rho\mathbf{v^2}\cdot\mathbf{v} d\mathbf{S} +$$
$$\int_V \frac{\partial}{\partial t}\frac{\mathbf{B^2}}{2\mu_0} dV = -\oint\limits_{\partial V} \rho\mathbf{v}\frac{1}{2}\mathbf{v^2} d\mathbf{S} - \oint\limits_{\partial V} \rho e\mathbf{v} d\mathbf{S} - \oint\limits_{\partial V} p\mathbf{v} d\mathbf{S} - \oint\limits_{\partial V} \frac{\mathbf{E}\times\mathbf{B}}{\mu_0} d\mathbf{S}$$
$$+\oint\limits_{\partial V} \mathbf{v}\tau' d\mathbf{S} + \oint\limits_{\partial V} k\nabla T d\mathbf{S} + \int_V \rho h dV + \int_V \rho\mathbf{v}\cdot\nabla\psi dV. \tag{3.15}$$

Eliminating equal terms on both sides yields the following result:

$$\frac{d}{dt}\int_V \rho e dV + \frac{d}{dt}\int_V \frac{1}{2}\rho\mathbf{v^2} dV + \int_V \frac{\partial}{\partial t}\frac{\mathbf{B^2}}{2\mu_0} dV = -\oint\limits_{\partial V} p\mathbf{v} d\mathbf{S} -$$
$$\oint\limits_{\partial V} \frac{\mathbf{E}\times\mathbf{B}}{\mu_0} d\mathbf{S} + \oint\limits_{\partial V} \mathbf{v}\tau' d\mathbf{S} + \oint\limits_{\partial V} k\nabla T d\mathbf{S} + \int_V \rho h dV + \int_V \rho\mathbf{v}\cdot\nabla\psi dV. \tag{3.16}$$

To simplify this equation several assumptions can be made (see Gubbins (2003) for details): First, the velocity $\mathbf{v}$ of the convective motion can be averaged to the radial velocity $\mathbf{u}$ of the slow contraction. Next, contributions by the electromagnetic field are neglected by assuming the mantle to be a perfect insulator. And at last, a stress-free boundary condition is adopted, which allows to drop the term including the deviatoric stress. This results in an equation describing the heat flow across the core-mantle boundary

$$Q_{cmb} = -\oint_{\partial V} k\nabla T d\mathbf{S} = \int_V \rho h dV - \int_V \rho \frac{De}{dt} dV + \int_V \rho \mathbf{u} \cdot \nabla \psi dV - \int_V \nabla \cdot (p\mathbf{u}) dV \tag{3.17}$$

where Reynolds' transport theorem has been applied to the term containing the internal energy.

Each of these terms can be scrutinized to derive the energy budget for the core. The first term can be identified with the heat generated by radioactive elements in the core when neglecting contributions by tidal dissipation (Greff-Lefftz and Legros, 1999) or core-mantle coupling (Touma and Wisdom, 2001)

$$Q_R = \int_V \rho h dV. \tag{3.18}$$

The influence of radioactive elements on heat production in the core is discussed in more detail in Chapter 4. The second term in the energy budget is the internal energy which can be transformed in the following way: By considering the differential of the internal energy in the presence of a light element $de = TdS + \frac{Pd\rho}{\rho^2} + \mu dc$ it follows that

$$\int_V \rho \frac{De}{Dt} dV = \int_V \rho T \frac{Ds}{Dt} dV + \int_V \frac{P}{\rho} \frac{D\rho}{Dt} dV + \int_V \rho \mu \frac{Dc}{Dt} dV. \tag{3.19}$$

Here the total derivatives of s, ρ, and c can be replaced by $\frac{Ds}{Dt}$, $\frac{D\rho}{Dt}$, and $\frac{Dc}{Dt}$, which is obviously identical. By using the continuity equation and substituting for $\frac{D\rho}{Dt}$ in the second term on the right hand side this can be written as

$$\int_V \rho \frac{De}{Dt} dV = \int_V \rho T \frac{Ds}{Dt} dV + \int_V P \nabla \cdot \mathbf{u} dV + \int_V \rho \mu \frac{Dc}{Dt} dV. \tag{3.20}$$

Now the first term on the right hand side can be expanded by considering the dependence of the entropy s on the three state variables T, P, and c:

$$\int_V \rho \frac{De}{Dt} dV = \int_V \rho T \left(\frac{\partial s}{\partial T}\right)_{P,c} \frac{DT}{Dt} dV + \int_V \rho T \left(\frac{\partial s}{\partial P}\right)_{T,c} \frac{DP}{Dt} dV + \\ \int_V \rho T \left(\frac{\partial s}{\partial c}\right)_{T,P} \frac{Dc}{Dt} dV + \int_V P \nabla \cdot \mathbf{u} dV + \int_V \rho \mu \frac{Dc}{Dt} dV. \tag{3.21}$$

Using Maxwell's relation

$$\left(\frac{\partial \mu}{\partial t}\right)_{P,c} = \left(\frac{\partial s}{\partial c}\right)_{P,T} \tag{3.22}$$

and the definition of the specific heat capacity

$$C_P = T \left(\frac{\partial s}{\partial T}\right)_{P,c} \tag{3.23}$$

and the thermal expansivity

$$\alpha = -\rho \left(\frac{\partial s}{\partial P}\right)_{T,c} \tag{3.24}$$

this equation can be rewritten in the following way:

$$\int_V \rho \frac{De}{Dt} dV = \int_V \rho C_P \frac{DT}{Dt} dV - \int_V \alpha T \frac{DP}{Dt} dV - \int_V \rho T \left(\frac{\partial \mu}{\partial T}\right)_{P,c} \frac{Dc}{Dt} dV + \\ \int_V P \nabla \cdot \mathbf{u} dV + \int_V \rho \mu \frac{Dc}{Dt} dV. \tag{3.25}$$

This equation is one term in Q_{cmb}, equation (3.17). The last two terms in equation (3.17) and the next to last term in equation (3.25) cancel each other out when using the hydrostatic pressure gradient $\nabla P = \rho \nabla \psi$. Therefore the following result is yielded:

$$\int_V \rho \frac{De}{Dt} dV = \int_V \rho C_P \frac{DT}{Dt} dV - \int_V \alpha T \frac{DP}{Dt} dV + \int_V \rho\mu \frac{Dc}{Dt} dV$$
$$- \int_V \rho T \left(\frac{\partial \mu}{\partial T}\right)_{P,c} \frac{Dc}{Dt} dV = \int_V \rho C_P \frac{DT}{Dt} dV - \int_V \alpha T \frac{DP}{Dt} dV +$$
$$\int_V \rho \left[\mu - T\left(\frac{\partial \mu}{\partial T}\right)_{P,c}\right] \frac{Dc}{Dt} dV. \tag{3.26}$$

The first term on the right hand side is the secular cooling term, Q_S ,which arises due to the heat released by core cooling. The Lagrangian derivative includes a contraction term, and the latent heat released as the inner core solidifies could also be included in this term by using a modified C_P, but will be used separately in the final heat balance. The second term describes the additional heat generated by increase in pressure, Q_P, which can be rewritten by using a numerical coefficient, P_T, which relates the rate of pressure change at the core-mantle boundary to the core cooling rate (Gubbins, 2003)

$$\int_V \alpha T \frac{DP}{Dt} dV = \int_V \alpha T P_T \frac{dT_{cmb}}{Dt} dV, \quad \frac{DP}{Dt} = P_T \frac{dT_{cmb}}{dt}. \tag{3.27}$$

Here $\frac{dT_{cmb}}{dt}$ is the rate of change of the temperature at the core-mantle boundary, which is identical to the core cooling rate. The last term is associated with compositional variations and hence is termed heat of reaction, Q_H, describing the change of internal energy due to chemical reactions between iron and the light element. The term within the square brackets is the actual heat of reaction, R_H.
Although the gravitational energy term dropped out by using the hydrostatic pressure gradient in the heat balance as described above, by release of the light element at the inner core boundary a change in gravitational

energy takes place. This can be allowed for by taking into account only density changes caused by separation of the light element, and the resulting term, Q_G, is another compositional energy term, in addition to Q_H (Nimmo, 2009):

$$Q_G = \int_V \rho\mathbf{v} \cdot \nabla\psi dV = \int_V \psi \left(\frac{\partial\rho}{\partial t}\right)_{P,T} dV = \int_V \rho\psi\alpha_c \frac{Dc}{Dt} dV. \quad (3.28)$$

The transformation from the first to the second integral on the right hand side can be understood in the following way (Gubbins, 2003):

$$\int_V \rho\mathbf{v} \cdot \nabla\psi dV = \int_V \nabla \cdot (\rho\psi\mathbf{v}) dV - \int_V \rho\nabla \cdot (\rho\mathbf{v}) dV = \oint_{\partial V} \rho\psi\mathbf{v} d\mathbf{S} + \int_V \psi\frac{\partial\rho}{\partial t} dV = \int_V \psi\frac{\partial\rho}{\partial t} dV \quad (3.29)$$

where the surface integral vanishes, since $\mathbf{v} \cdot d\mathbf{S} = 0$ at ∂V, and the continuity equation has been used for the second term on the right hand side. The last step is to insert the definition of the compositional thermal expansivity (Gubbins, 2004)

$$\alpha_c = -\frac{1}{\rho}\left(\frac{\partial\rho}{\partial c}\right)_{P,T} \quad (3.30)$$

into the last equation

$$\int_v \psi \left(\frac{\partial\rho}{\partial t}\right)_{P,T} dV = \int_v \psi \left(\frac{\partial\rho}{\partial c}\right)_{P,T} \frac{Dc}{Dt} dV \overset{eq.3.20}{=} \int_V \rho\psi\alpha_c \frac{Dc}{Dt} dV. \quad (3.31)$$

Since the inner core cools, latent heat is released due to the phase transition of iron at the inner core boundary. The amount of heat released depends on the advance of the inner core and the latent heat released during phase transition. Therefore this contribution to the core energy budget can be written as (Nimmo, 2009)

$$Q_L = 4\pi r_i^2 L_H \rho_i \frac{dr_i}{dt}. \tag{3.32}$$

Here r_i is the radius of the inner core, L_H is the laten heat, ρ_i is the density at the inner-core boundary, and $\frac{dr_i}{dt}$ is the rate of change of the inner-core radius.

Due to core cooling the earth is contracting slowly with time. This means that for most of the planet, except near the surface, the pressure increases since more material is inside some fixed radius r. This increase in pressure gives rise to an increase of the melting temperature of iron, which in turn causes the inner core to grow. Therefore additional latent heat is released due to the effect of pressure increase. This effect can be written separately in the following way (Nimmo, 2009)

$$Q_{PL} = \frac{4\pi r_i^2 L_H T'_m P_T}{(T'_m - T')g} \frac{dT_{cmb}}{dt} \tag{3.33}$$

or included in the latent heat term by using a modified latent heat (Nimmo, 2009)

$$L'_H = L_H \left(1 + P_T \frac{dT_m}{dP} \frac{T_{cmb}}{T_i}\right). \tag{3.34}$$

Summing up, the energy balance of the core can be expressed by the following equation:

$$\begin{gathered} Q_{cmb} = Q_R + Q_S + Q_P + Q_H + Q_G + Q_L = \\ \int_V \rho h dV + \int_V \rho C_P \frac{DT}{Dt} dV - \int_V \alpha T \frac{DP}{Dt} dV + \int_V \rho R_H \frac{Dc}{Dt} dV + \\ \int_V \rho \psi \alpha_c \frac{Dc}{Dt} + 4\pi r_i^2 L'_H \rho_i \frac{dr_i}{dt}. \end{gathered} \tag{3.35}$$

All these terms, except the radioactive heat generation, can be expressed in terms of the core cooling rate by substituting the total derivatives by the core cooling rate (see above and next section), which can then be taken out of the integral (see also next section). Then the following equation is yielded (Nimmo, 2009):

$$Q_{cmb} = Q_R + \tilde{Q}_T \frac{dT_{cmb}}{dt}, \tag{3.36}$$

where all terms depending on the core cooling rate are combined to give the term $\tilde{Q}_T$. This gives a concise overview over the energy budget of the core, and could in principle be used to estimate the magnetic field of a planet via scaling laws that use the heat flow (see 2.3). An interesting aspect of this equation is the fact that dissipation due to Ohmic resistance within the (not perfectly) conducting fluid, causing further heating, does not occur, and so does neither the adiabatic heat flow, Q_k. Since Ohmic heating is representing a transformation of energy, from buoyancy to kinetic and to magnetic energy, back to heat by ohmic dissipation, it does not contribute to the overall energy budget. But the dissipative effect represents a source of entropy, since it is a nonreversible process, and has to be considered since it could control the possibility and effectiveness of dynamo action in the core. The entropy budget of the core can be expressed as (Hewitt et al., 1975)

$$\rho \frac{Ds}{Dt} = -\frac{\nabla \cdot \mathbf{q}}{T} + \frac{\mu \nabla \cdot \mathbf{i}}{T} + \frac{\rho h}{T} + \frac{\Phi}{T}. \tag{3.37}$$

This equation can be transformed by a couple of steps. The term on the left hand side can be transformed completely analogously to the first term on the right hand side in equation (3.20), considering this time that the multiplicative factor of T is missing. The first term two terms on the right hand side can be rewritten by considering the chain rule,

$$\nabla \cdot \left(\frac{\mathbf{q}}{T}\right) = \frac{\nabla \cdot \mathbf{q}}{T} - \frac{\mathbf{q} \cdot \nabla T}{T^2}, \tag{3.38}$$

and using the definition of $\mathbf{q}$, eq.(3.6), yielding the following intermediate result:

$$-\frac{\nabla \cdot \mathbf{q}}{T} + \frac{\mu \nabla \cdot \mathbf{i}}{T} = -\nabla \cdot \left(\frac{\mathbf{q}}{T}\right) - \frac{\mu \mathbf{i} \nabla T}{T^2} - \frac{\beta \mathbf{i} \nabla T}{\alpha_D T} + \frac{k(\nabla T)^2}{T^2} + \frac{\mu \nabla \mathbf{i}}{T}. \tag{3.39}$$

Using again the chain rule for the term including $\mathbf{i}$ and T,

$$\nabla \left(\frac{\mathbf{i}}{T}\right) = \frac{\nabla \mathbf{i}}{T} - \frac{\mathbf{i} \nabla T}{T^2}, \tag{3.40}$$

and integrating over the whole core gives

$$\begin{aligned} \int_V \left[-\frac{\nabla \cdot \mathbf{q}}{T} + \mu \frac{\nabla \cdot \mathbf{i}}{T}\right] dV = -\int_V \nabla \left(\frac{\mathbf{q}}{T}\right) dV + \\ \int_V \left[\mu \nabla \cdot \left(\frac{\mathbf{i}}{T}\right) - \frac{\beta}{\alpha_D} \frac{\mathbf{i} \cdot \nabla T}{T} + k \left(\frac{\nabla T}{T^2}\right)\right] dV. \end{aligned} \tag{3.41}$$

Since the heat flow across the core-mantle boundary $Q_{cmb} = \oint_{\partial V} \mathbf{q} d\mathbf{S} = -\oint_{\partial V} k \nabla T \cdot d\mathbf{S}$, when assuming that there's no flux of light element across the core-mantle boundary, and hence, $\mathbf{i} \cdot d\mathbf{S} = 0$, the first term on the right hand side can be written as (Nimmo, 2009)

$$\int_V \nabla \cdot \left(\frac{\mathbf{q}}{T}\right) dV = \frac{Q_{cmb}}{T_{cmb}}, \tag{3.42}$$

where T_{cmb} is the temperature at the core-mantle boundary. Considering the definition of $\mathbf{i}$, eq. (3.7), and its square,

$$\mathbf{i}^2 = \alpha_D^2 (\nabla \mu)^2 + 2\alpha_D \nabla \mu \beta \nabla T + \beta^2 \nabla T^2, \tag{3.43}$$

as well as

$$\mathbf{i} \cdot \nabla T = -\alpha_D \cdot \nabla \mu \cdot \nabla T - \beta \cdot (\nabla T)^2, \tag{3.44}$$

yields, by comparison of these two equations (F.Nimmo, pers. comm., 2012)

$$\mathbf{i} \cdot \nabla T = -\frac{\mathbf{i}^2}{\beta} - \frac{\alpha_D}{\beta}\mathbf{i} \cdot \nabla \mu. \tag{3.45}$$

Inserting this into eq. (3.41) yields

$$\begin{aligned} \int_V \left[-\frac{\nabla \cdot \mathbf{q}}{T} + \mu \frac{\nabla \cdot \mathbf{i}}{T} \right] dV &= -\frac{Q_{cmb}}{T_{cmb}} + \\ \int_V \left[\mu \nabla \cdot \left(\frac{\mathbf{i}}{T} \right) + \frac{\mathbf{i}^2}{\alpha_D T} + \frac{\mathbf{i} \nabla \mu}{T} + k \left(\frac{\nabla T}{T^2} \right) \right] dV. \end{aligned} \tag{3.46}$$

Combining the first and third term in brackets on the right-hand side gives

$$\begin{aligned} \int_V \left[-\frac{\nabla \cdot \mathbf{q}}{T} + \mu \frac{\nabla \cdot \mathbf{i}}{T} \right] dV &= -\frac{Q_{cmb}}{T_{cmb}} + \\ \int_V \nabla \left(\frac{\mu \cdot \mathbf{i}}{T} \right) + \int_V \frac{\mathbf{i}^2}{\alpha_D T} dV + \int_V k \left(\frac{\nabla T}{T^2} \right) dV. \end{aligned} \tag{3.47}$$

The second term on the right-hand side can be transformed by employing the divergence theorem,

$$\int_V \nabla \left(\frac{\mu \cdot \mathbf{i}}{T} \right) dV = \oint_{\partial V} \frac{1}{T} \mu \mathbf{i} d\mathbf{S}, \tag{3.48}$$

and assuming that there is no flux of the light element across the core-mantle boundary $\mathbf{i} \cdot d\mathbf{S} = 0$, hence the second term on the right-hand side in eq. (3.47) is zero. Inserting this result into eq. (3.37), integrated over the whole core, yields an equation where several terms appear twice that differ only in the temperature, one term with T and one with T_{cmb}. These terms can be combined to contain a term $\frac{1}{T} - \frac{1}{T_{cmb}}$, which can be considered as an efficiency factor. Finally, the latent heat term can be included in the secular cooling term by using a modified specific heat (Gubbins, 2003) $C_p' = C_p + L\delta \frac{r - r_i}{T_m' - T_a'}$:

$$\int_V \rho C_p' \left(\frac{1}{T} - \frac{1}{T_{cmb}}\right) \frac{DT}{Dt} dV - \int_V \alpha T \left(\frac{1}{T} - \frac{1}{T_{cmb}}\right) \frac{DP}{Dt} dV - \int_V \rho \frac{\partial \mu}{\partial T} \frac{Dc}{Dt} dV$$
$$+ \int_V \rho \frac{R_H}{T_{cmb}} \frac{Dc}{Dt} dV + \frac{Q_G}{T_{cmb}} - \int_V \rho h \left(\frac{1}{T} - \frac{1}{T_{cmb}}\right) dV = \int_V k \left(\frac{\nabla T}{T}\right)^2 dV$$
$$+ \int_V \frac{\mathbf{i}^2}{\alpha_D T} dV + \int_V \frac{\Phi}{T} dV. \tag{3.49}$$

Here, R_H is the heat of reaction $R_H = \mu - T \left(\frac{\partial u}{\partial T}\right)_{P,c}$.
In analogy to the energy budget of the core, the entropy budget can be written in a slightly more concise form:

$$E_s + E_P + E_{H_1} + E_{H_2} + E_G + E_R = E_k + E_\alpha + E_\phi. \tag{3.50}$$

The left hand side comprises contributions from secular cooling including latent heat, contraction, chemical reactions, gravitation and radioactive heating, and the right hand side represents thermal diffusion, molecular conduction, and Ohmic dissipation. The aforementioned efficiency term arises due to the fact, that different terms contributing to the entropy budget are operating at different temperatures. Therefore processes occurring at the inner-core boundary are more efficient due to the higher operating temperature than processes found at the core-mantle boundary or throughout the outer core, like buoyancy, which are therefore less efficient. Latent heat therefore is the most efficient contribution, except for the gravitational term, where the efficiency factor does not occur. Therefore this term contributes most to the entropy budget, and although compositional convection is not crucial for the energy budget, it very well is for the entropy budget (Nimmo, 2009). Again this can be transformed to a shorter form by summarizing all terms depending on the core cooling rate, giving (Nimmo, 2009)

$$E_\phi = E_s + E_H + E_R + E_G - E_k = E_R - E_k + \tilde{E}_T \frac{dT_{cmb}}{dt}, \tag{3.51}$$

where E_P and E_α have been neglected due to their small contribution to the overall budget. Now that the energy and entropy budget are analytically formulated, the contributing terms could be calculated for arbitrary core structures (given the required quantities are known!). For example, in the case of the earth, if one assumes a fixed thermal and Ohmic diffusion rate (and neglecting molecular conduction), by using eq. (3.50) one can deduce the core cooling rate (see Gubbins (2003) for details and next section). If the core cooling rate is determined, the heat flow over the core mantle boundary can be calculated, since all but one term depend on this quantity (Gubbins (2003); next section). Knowing the heat flow across the core-mantle boundary this value could be used in conjunction with a scaling law (e.g., Christensen and Aubert (2006)) to estimate the magnetic field strength of a planet. Besides that, the energy and entropy budget is of course of general interest in determining the thermal history of a planet and very important to draw conclusions about the significance of different contributions to the energy and entropy budget of the planetary core, as will be explained below. In the next section the individual terms will be calculated for the earth, following Nimmo (2009) and Labrosse et al. (2001), in order to draw conclusions for the case of other (exo-)planets.

One more comment should be made on the energy and entropy budget, because rearrangement of eq. (3.36) and eq. (3.51) can yield some important insights. Expressing $\frac{dT_{cmb}}{dt}$ by rearranging eq. (3.51) and inserting the result into eq. (3.36) gives the following:

$$Q_{cmb} = Q_R + \tilde{Q}_T \left(\frac{E_\Phi + E_k - E_R}{\tilde{E}_T} \right) = Q_R \left(1 - \frac{\tilde{Q}_T E_R}{\tilde{E}_T Q_R} \right) + \frac{\tilde{Q}_T}{\tilde{E}_T} \left(E_\Phi + E_k \right).$$

Defining the effective temperature (Nimmo, 2009)

$$T_R = \frac{Q_R}{E_R} \tag{3.52}$$

and inserting it into the right-hand side of the previous equation results in

$$Q_{cmb} = Q_R \left(1 - \frac{\tilde{Q}_T}{\tilde{E}_T} \frac{1}{T_R} \right) + \frac{\tilde{Q}_T}{\tilde{E}_T} \left(E_\Phi + E_k \right). \tag{3.53}$$

Now this form of the heat flow across the core-mantle boundary allows to draw some interesting conclusions. First of all, it is obvious from the right-hand side of eq. (3.53) that the core-mantle boundary heat flow has to increase when E_Φ or E_k are becoming larger. If there is no radiogenic heat production in the core then the first term on the right-hand side vanishes and Q_{cmb} is directly proportional to the sum of Ohmic and thermal diffusion. Considering the values for $\tilde{Q}_T$ and $\tilde{E}_T$ (see Table 3.2, 3.3 and Nimmo (2009)), where heat flows are of the order of TW and entropy terms of the order of $MW\ K^{-1}$, one can see that the first term in brackets on the right-hand side in eq. (3.53) is larger than zero (since the term $\frac{\tilde{Q}_T}{\tilde{E}_T} \frac{1}{T_R}$ is ~ 0.6). This means that in the presence of radiogenic elements in the core the heat flow across the core-mantle boundary has to be larger than without those elements, or the entropy terms on the right-hand side have to decrease, in order to power the dynamo. A more thorough discussion about the interpretation of this equation regarding the thermal evolution of the earth's core can be found in Nimmo (2009), pp. 47-48. Regarding the presence of radiogenic elements in the core, rearrangement of eq. (3.36) can also be useful in order to express the core cooling rate in dependence of the radioactive heat generation:

$$\frac{dT_{cmb}}{dt} = \frac{Q_{cmb} - Q_R}{\tilde{Q}_T}. \tag{3.54}$$

In this form it becomes immediately clear that increasing radiogenic heat decreases the cooling rate, which in turn increases the lifetime of the inner core. This is an important fact, since a core that would cool too quickly would mean cessation of the dynamo rather soon in the history of a planet which would have severe implications on its habitability. An extensive discussion of the influence of potassium on the thermal evolution of the core is given in Nimmo et al. (2004), pp. 369-374. Besides that, eq. (3.54) allows to take another approach: If a fixed value of Q_{cmb} is assumed, the core cooling rate can be calculated, and the different contributions to the energy and entropy budget can be determined subsequently. This is the method used by Nimmo (2009) and also applied in this treatise.

3.4 Results for the Earth

3.4.1 Energy Balance

In order to calculate the energy balance for the earth's core, again some simplifying assumptions have to be made: spherical symmetry, constancy of quantities like specific heat capacity, thermal expansivity, or compressibility, and neglecting the density jump across the inner-core boundary for the calculcation of the gravitational acceleration. The following quantities and equations are used for calculation (see Labrosse et al. (2001) for a detailed description of these terms):

A length scale, L, for the compression within the earth:

$$L = \sqrt{\frac{3K_0 \left(\log \frac{\rho_c}{\rho_0} + 1\right)}{2\pi G \rho_0 \rho_c}}, \tag{3.55}$$

where K_0 is the compressibility at zero pressure, ρ_0 is the density at zero pressure, ρ_c is the density at the center of the earth, and G is the gravitational constant. Now the density as a function of radius can be defined as follows:

$$\rho(r) = \rho_c \exp\left(-\frac{r^2}{L^2}\right). \tag{3.56}$$

The gravity profile can be expanded as soon as the density profile is known (Appendix A in Labrosse et al. (2001)), and is given by

$$g(r) = \frac{4\pi}{3} G \rho_c r \left(1 - \frac{3r^2}{5L^2}\right) + \frac{4\pi}{3} G \Delta\rho \begin{cases} \text{r if } 0 \leqslant r \leqslant r_c, \\ \frac{r_c^3}{r^2} \text{ if } r > r_c. \end{cases} \tag{3.57}$$

The mass of the core is given by (Nimmo, 2009)

$$M_c(r_c) = \int_0^{r_c} \rho(r)dV = \frac{4\pi}{3}\rho_c \left[-\frac{L^2}{2} r \exp\left(-\frac{r^2}{L^2}\right) + \frac{L^3}{4}\sqrt{\pi}\mathrm{erf}\left(\frac{r}{L}\right)\right]_0^{r_c}. \tag{3.58}$$

and can be calculated by expanding the error function, resulting in (Nimmo, 2009)

$$M_c(r_c) = \frac{4\pi}{3}\rho_c r_c^3 \exp\left(-\frac{r_c^2}{L^2}\right)\left(1 + \frac{2}{5}\frac{r_c^2}{L^2}\right). \tag{3.59}$$

By assuming an adiabatic temperature profile, the total derivative of the temperature can be taken out of all integrals (see Gubbins (2003)) and substituted by

$$\frac{1}{T}\frac{DT}{Dt} = \frac{1}{T_{cmb}}\frac{dT_{cmb}}{dt}. \tag{3.60}$$

The inner core growth and the the rate of change of the light element concentration in the core can be related to the cooling rate (Nimmo, 2009):

$$\begin{aligned} \frac{dr_i}{dt} &= \frac{1}{\frac{dT_m}{dP} - \frac{dT}{dP}} \frac{T_i}{\rho_i g} \frac{1}{T_{cmb}} \frac{dT_{cmb}}{dt} = C_r \frac{dT_{cmb}}{dt} \\ \frac{Dc}{Dt} &= \frac{4\pi r_i^2 \rho_i c}{M_{oc}} \frac{dr_i}{dt} = C_c C_r \frac{dT_{cmb}}{dt}, \end{aligned} \tag{3.61}$$

where $\frac{dT_m}{dP}$ and $\frac{dT}{dP}$ are the slopes of the melting and adiabatic curve, respectively, ρ_i and T_i are the density and temperature at the inner-core boundary, respectively, M_{oc} is the mass of the outer core and

$$C_c = 4\pi r_i^2 \rho_i / M_{oc}. \tag{3.62}$$

The calculation of radioactive heating, Q_R, is very straightforward: assuming that radiogenic elements are distributed homogenously throughout the core and thus heat production is independent of position, as soon as the heat production by radiogenic elements in the core is known, this factor has only to be multiplied with the core mass to give the amount of radioactive heating:

$$Q_R = \int_V \rho h dV = M_c h. \tag{3.63}$$

Of course, determination of heat production by radiogenic elements within the core is less straightforward, because knowledge about the existence of various radiogenic species in the core is very sparse. Nevertheless a couple of works have dealt with this problem, which will be the topic of the next chapter.
In order to calculate the specific heat for the earth's core, Q_s, the total derivative of the temperature can be substituted as mentioned above, and the specific heat capacity C_p is taken constant, since the error introduced by this simplification is within the uncertainties of properties at core conditions (Gubbins, 2003), giving

$$Q_s = -C_p \frac{1}{T_{cmb}} \frac{dT_{cmb}}{dt} \int_V \rho T dV. \tag{3.64}$$

The integral can be integrated as given by Labrosse (2003) and further expanded (Nimmo, 2009) which results in a term

$$\int_V \rho T dV = I_s = \frac{4}{3}\pi T_c \rho_c r_c^3 \exp\left(-\frac{r_c^2}{A^2}\right)\left(1 + \frac{2}{5}\frac{r_c^2}{A^2}\right), \tag{3.65}$$

T_c and ρ_c being the temperature and the density at the center of the earth, respectively, r_c the core radius, and A a constant given by

$$A^2 = \left(\frac{1}{L^2} + \frac{1}{D^2}\right), \qquad D = \sqrt{\frac{3C_p}{2\pi\alpha\rho_c G}}. \tag{3.66}$$

The contribution of specific heat to the energy budget can therefore be written as

$$Q_s = -\frac{C_p}{T_{cmb}} \frac{dT_{cmb}}{dt} I_s. \tag{3.67}$$

Following Gubbins (2003) and Nimmo (2009), the pressure heating, Q_p, and the heat of reaction, Q_H, can be neglected in the former case (due to its small contribution to the overall energy budget, see Gubbins (2003) for details), and set equal to zero in the latter case (assuming a conservation of element species, see Gubbins (2004); Nimmo (2009) for details). In the case of latent heat, the pressure effect on freezing can be included in the latent heat term by modifying the latent heat as described above. But again, following the works cited before, where this contribution is neglected, the calculation of the latent heat is done by using the usual latent heat L_H:

$$Q_L = 4\pi r_i^2 L_H \rho_i \frac{dr_i}{dt} \tag{3.68}$$

where r_i is the radius of the inner core, ρ_i is the density at the inner-core boundary, L_H is the usual latent heat, and $\frac{dr_i}{dt}$ is the rate of advance of the inner core, which can be related to the core cooling rate as described above (eq. 3.61). Finally, the the gravitational contribution, Q_g, can be calculated by using eq. (3.57) for the gravity profile and integrating with respect to the radius. By setting adequate boundaries the potential relative to the core-mantle boundary (=zero potential) can be expressed (Nimmo, 2009):

$$\psi(r) = \left[\frac{2}{3}\pi G \rho_c r'^2 \left(1 - \frac{3r'^2}{10L^2}\right)\right]_{r_c}^{r}. \tag{3.69}$$

To evaluate the integral given in eq. (3.28), some further considerations have to be made. This integral firstly consists of contributions from the outer core, since there is no release of the light element into the inner core and therefore $\frac{Dc}{Dt} = 0$, and secondly from material freezing at the inner-core boundary. The amount of material freezing at the surface of the inner core can be estimated by (Gubbins, 2004)

$$-\psi(r_i) 4\pi r_i^2 \rho(r_i) \alpha_c c \frac{dr_i}{dt} = -\psi(r_i) \alpha_c C_c M_{oc} \frac{dr_i}{dt} \tag{3.70}$$

where r_i is the radius of the inner core, $\rho(r_i)$ is the density at the inner-core boundary, α_c is the compositional expansion coefficient, c is the concentration of the light element, C_c is the factor defined in eq. (3.62), and M_{oc} is the mass of the outer core. Combining the integral and eq. (3.70) yields the contribution of gravitational energy to the total energy budget (Gubbins, 2004):

$$Q_g = \left[\int_{oc} \rho\psi dV - M_{oc}\psi(r_i)\right] \alpha_c C_c C_r \frac{dT_c}{dt}, \tag{3.71}$$

which can be rewritten by using the definition of the compositional expansion coefficient and the relation between core cooling rate and inner-core growth, giving an equation that depends on the rate of growth of the inner-core instead of the core cooling rate (Nimmo, 2009):

$$Q_g = \left[\int_{oc} \rho\psi dV - M_{oc}\psi(r_i)\right] \Delta\rho_c \frac{c}{\Delta c} \frac{4\pi r_i^2}{M_{oc}} \frac{dr_i}{dt} \tag{3.72}$$

where $\Delta\rho_c$ is change in density across the inner-core boundary due to the change in light element concentration, c is again the concentration of the the light element in the outer core, and Δc is the change in concentration across the inner-core boundary. The integral can be expanded to give (Nimmo, 2009)

$$\int_{oc} \rho\psi dV = \frac{8\pi^2\rho_c^2 G}{3}\left[\left(\frac{3}{20}r^5 - \frac{L^2}{8}r^3 - L^2C^2r\right)\exp\left(\frac{-r^2}{L^2}\right) + \frac{C^2}{2}L^3\sqrt{\pi}erf\left(\frac{r}{L}\right)\right]_{r_i}^{r_c} \tag{3.73}$$

where

$$C^2 = \frac{3L^2}{16} - \frac{r_c^2}{2}\left(1 - \frac{3r_c^2}{10L^2}\right) \tag{3.74}$$

and the mass of the outer core is obtained by applying eq. (3.58) and changing the limits of the integration to the inner core and outer core radius, respectively.

Now the heat flow across the core mantle boundary, Q_{cmb}, can be calculated for a given core cooling rate, $\frac{dT_c}{dt}$, using the quantities listed in Table 3.1. Either the core cooling rate is obtained by assuming a fixed Ohmic dissipation rate in eq. (3.51) and rearranging to get the cooling rate, or

Q_{cmb} is assumed constant, and the core cooling rate is calculated by using eq. (3.60). Here the second approach is taken for a core-mantle boundary heat flow of 9 TW, following Nimmo (2009). This value is the mean of lower and upper bounds of CMB heat flow estimates, which range from 3 to 15 TW (Starchenko and Jones, 2002; Gubbins, 2003, 2004; Nimmo, 2009). The results of these calculations can be found in Table 3.2. The calculation of radiogenic heat produced in the core will be described in the next chapter, to determine the value of Q_R in Table 3.2 the mean abundances for radioactive species in the core have been used (see next chapter). For the calculation of Q_g it was assumed that all of the light element or elements is expelled from the inner core, which means that $c = \Delta c$ in eq. (3.72) and hence this term is equal to 1. The dependence of the cooling rate on radiogenic heat production is shown in Fig. 3.7. Calculations have been carried out using the Mathematica software package, Mathematica calculations can be found in Appendix A.

3.4.2 Entropy Balance

To calculate the entropy balance, a similar approach to the previous section is taken, and quantities derived above can also be used in this subsection. The first term in eq. (3.49) is the contribution due to secular cooling and, like the corresponding energy term, contains an integral $\int_V \rho T dV = I_s$, which can be easily shown, using eqn. (3.60) and the assumption that C_p is constant:

$$\int_c \rho C_p \left(\frac{1}{T} - \frac{1}{T_{cmb}} \right) \frac{DT}{Dt} dV = \int_c \frac{\rho C_p}{T} \frac{DT}{Dt} dV - \int_c \frac{\rho C_p}{T_{cmb}} \frac{DT}{Dt} = \frac{C_p}{T_{cmb}} \frac{dT_{cmb}}{dt} \int_c \rho dV - \frac{C_p}{T_{cmb}^2} \frac{dT_{cmb}}{dt} \int_c \rho T dV = \frac{C_p}{T_{cmb}} \left(M_c - \frac{I_s}{T_{cmb}} \right) \frac{dT_{cmb}}{dt}. \tag{3.75}$$

This expression can be calculated by using the same expansion of I_s as given in eq. (3.65). The second term in eq. (3.49) describes the effect of pressure heating on the entropy budget, and can be neglected due to the arguments given in Gubbins (2003, 2004).

E_g is determined due to eq. (3.49) by $E_g = \frac{Q_g}{T_{cmb}}$. The contribution by radioactive decay E_R is given by the last term on the left-hand side of eq. (3.49), which can be transformed in the following way

$$\int_V \rho h \left(\frac{1}{T} - \frac{1}{T_{cmb}} \right) = h \int_V \frac{\rho}{T} dV - \frac{h}{T_{cmb}} \int_V \rho dV = \\ h \int_V \frac{\rho}{T} dV - h \frac{M_c}{T_{cmb}} = h \left(I_T - \frac{M_c}{T_{cmb}} \right), \tag{3.76}$$

assuming that heat generation by radioactive elements in the core is constant. The integral $\int \frac{\rho}{T} dV$ can be expanded to give (Nimmo, 2009)

$$I_T = \frac{4\pi\rho_c}{3T_c} r_c^3 \left(1 - \frac{3}{5} \frac{r_c^2}{B^2} \right), \tag{3.77}$$

where

$$B = \left(\frac{1}{L^2} - \frac{1}{D^2} \right)^{-1}, \tag{3.78}$$

and thus, E_R can be calculated. Since the pressure freezing term, E_{PL}, is negligible it can be dropped in this calculation. The contribution of latent heat to the entropy budget, E_L, can be written as (Nimmo, 2009)

$$E_L = Q_L \frac{T_i - T_c}{T_c T_i}. \tag{3.79}$$

Unfortunately the derivation of the contribution of the heat of reaction to the entropy budget is not quite clear. The fourth term in eq. 3.49 is zero due to arguments brought forward in Gubbins (2004), so only the third term remains for a contribution. If one assumes that $\mu/T \ll \partial\mu/\partial T$ and considers $R_H = \mu - T \left(\frac{\partial \mu}{\partial T} \right)$ this term would adopt the expected form $\int_V \frac{\rho R_H}{T} \frac{Dc}{Dt} dV$ as listed in Table 1 in Nimmo (2009) (although the negative sign there is wrong). But the quoted values for μ and $\partial\mu/\partial T$ do not seem to support this approach, and therefore the derivation is not quite clear (pers. comm., F. Nimmo, 2012). Thus, eq. (64) from Nimmo (2009) is used to calculate the contribution by heat of reaction to the entropy budget, although its justification has to remain open. The occurrence of T_i in this formula is justified due to the fact that every term that depends on the rate of change of concentration contains one part from the dilution over the outer core and one part at the inner core boundary, since oxygen is removed from the solid core (eq. (37) in Gubbins (2004)). This results in the following equation:

$$E_H = R_H \left[\int_{oc} \frac{\rho}{T} dV - \frac{M_{oc}}{T_i} \right] C_c \frac{dr_i}{dt}, \tag{3.80}$$

where T_i is the temperature at the inner core boundary, and C_c is defined in eq. (3.61).

E_p and E_α are very small and can thus be ignored (Gubbins, 2003, 2004). E_Φ is the entropy production due to Ohmic dissipation and is either taken constant, as in Gubbins (2003, 2004) or calculated for a constant core-mantle boundary heat flow, as in Nimmo (2009). The adiabatic contribution E_k can be calculated by evaluating the integral from eq. (3.49)

$$E_k = \int_V k \left(\frac{\nabla T}{T} \right)^2 dV. \tag{3.81}$$

Using the adiabatic temperature $T_a(r) = T_c \exp(-r^2/D^2)$ and inserting it into the expression in brackets in the integral yields $(\nabla T_a/T_a)^2 = 4r^2/D^4$. Using spherical coordinates this can be written as

$$\frac{4k}{D^4} \int_0^{2\pi} \int_0^{\pi} \int_0^{r_c} r^4 dr \sin\theta d\theta d\phi = \frac{16\pi k r_c^5}{5D^4}. \tag{3.82}$$

The results for the calculations of the different contributions to the entropy budget are shown in Table 3.3.

Quantity	**Units**	**Value**
L	m	$7.2695 \cdot 10^{6}$
K_0 [1]	Pa	$500 \cdot 10^{9}$
ρ_c [1]	$kg\ m^{-3}$	12500
ρ_0 [1]	$kg\ m^{-3}$	7900
G [2]	$m^{-3}\ kg^{-1}\ s^{-2}$	$6.67384 \cdot 10^{-11}$
r_c [1]	m	$3.48 \cdot 10^{6}$
M_c	kg	$1.92668 \cdot 10^{24}$
h	W	$1.02182 \cdot 10^{-12}$
C_p [1]	$J\ kg^{-1}\ K^{-1}$	840
T_{cmb} [1]	K	4100
A^2	m^{-2}	$2.12753 \cdot 10^{13}$
D	m	$5.96761 \cdot 10^{6}$
I_S	$kg\ K$	$8.82541 \cdot 10^{27}$
$\frac{dT_{cmb}}{dt}$	$K\ Gyr^{-1}$	-30.186
r_i [1]	m	$1220 \cdot 10^{6}$
L_H [1]	$J\ kg^{-1}$	$750 \cdot 10^{3}$
ρ_i	$kg\ m^{-3}$	12152.9
$\frac{dT_M}{dP} - \frac{dT_a}{dP}$ [1]	$K\ GPa^{-1}$	1.3
T_i [1]	K	5520
$g(r_i)$	$m\ s^{-2}$	4.19114
C^2	m^2	$4.26975 \cdot 10^{12}$
$\int_{oc} \rho\psi dV$	J	$-1.36055 \cdot 10^{31}$
M_{oc}	kg	$1.82211 \cdot 10^{24}$
$\psi(r)$	$m^2\ s^{-2}$	$-1.71261 \cdot 10^{7}$
$\Delta\rho_c$ [1]	$kg\ m^{-3}$	575
$\frac{dr_i}{dt}$	$km\ Gyr^{-1}$	609.99

Table 3.1: Quantities used for calculation of energy balance; values that are not calculated for the purpose of this work are taken from [1] Nimmo (2009), [2] http://en.wikipedia.org/wiki/Gravitational_constant; Calculations see Appendix A

	Value	Units
Q_s	1.72	TW
Q_L	3.30	TW
Q_R	1.97	TW
Q_g	2.01	TW
Q_{cmb}	9.0	TW
dT_c/dt	−30.02	$K\ Gyr^{-1}$
dr_i/dt	609.99	$km\ Gyr^{-1}$

Table 3.2: Terms contributing to the energy balance of the core, core cooling rate, rate of advance of the inner core, and heat flow across the core-mantle boundary

	Value	Units
E_s	44.15	$MW\ K^{-1}$
E_L	206.90	$MW\ K^{-1}$
E_R	62.37	$MW\ K^{-1}$
E_g	490.09	$MW\ K^{-1}$
E_H	−178.26	$MW\ K^{-1}$
E_k	−161.83	$MW\ K^{-1}$
E_Φ	463.42	$MW\ K^{-1}$

Table 3.3: Terms contributing to the entropy balance of the core, using core cooling rate and inner core growth rate from Table 3.2

3.5 Significance of the Mantle for Core Cooling

As important as the core may be for supplying the energy to drive the geodynamo, as was shown in the last section, core cooling is the essential quantity in determining the energy and entropy budget of the core. In the case of the earth the cooling rate can be estimated by assuming the entropy generation by Ohmic and thermal dissipation to be fixed at a value enabling the geodynamo to operate (Gubbins, 2003). Another possibility would be to assess the ability of the mantle to extract heat from the core. In general it would be desirable to have a coupled core-mantle model, which would constrain the cooling of the core not only by requirements for the geodynamo but also by a thermal history model of the mantle, since

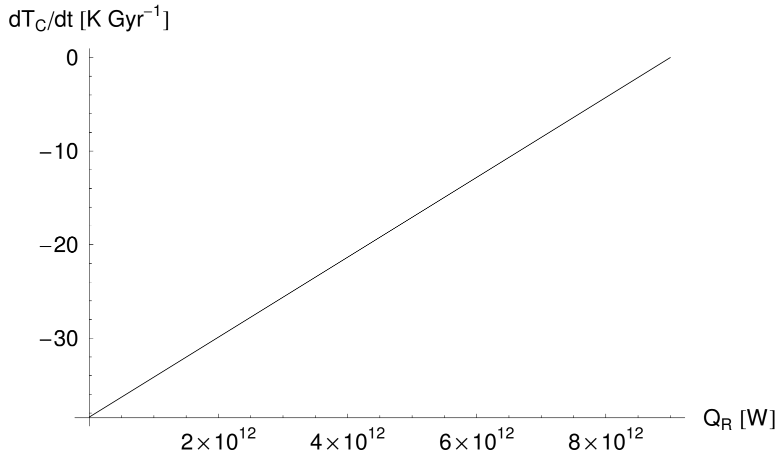

Figure 3.7: Linear dependence of the core cooling rate, dT_c/dt, on the radiogenic heat production in the core, Q_R. Calculation see Appendix A.

core cooling ultimately is controlled by the mantle. Several authors have already tried to do this. Stevenson et al. (1983) modelled the evolution of cores and mantles of terrestrial planets of the solar system using the following set of equations, describing the energy balance of core and mantle, respectively:

$$\frac{dm}{dt} = 4\pi R_i^2 \rho_c \frac{dR_i}{dt} = 4\pi R_i^2 \rho_c \frac{dR_i}{dT_{cm}} \frac{dT_{cm}}{dt}, \tag{3.83}$$

$$\frac{4}{3}\pi \left(R_p^3 - R_c^3\right) \left[Q - \rho_m C_m \eta_m \frac{dT_u}{dt}\right] = 4\pi \left[R_p^2 F_s - R_c^2 F_c\right], \tag{3.84}$$

$$\left[(L + E_G)\, 4\pi R_i^2 \rho_c \frac{dR_i}{dT_{cm}} - \frac{4}{3}\pi R_c^3 \rho_c C_c \eta_c\right] \frac{dT_{cm}}{dt} = 4\pi R_c^2 F_c, \tag{3.85}$$

where m is the mass of the inner core, R_i is the radius of the inner core, ρ_c is the constant average core density, $\frac{dR_i}{dt}$ is the rate of inner core growth, $\frac{dT_{cm}}{dt}$ is the rate of change of temperature at the core-mantle boundary, i.e. core cooling rate, R_p is the planetary radius, R_c is the core radius, Q is the heat production due to radioactive elements in the mantle, ρ_m and C_m are the average density and average heat capacity of the mantle, respectively, η_m is a constant that relates the average mantle temperature to the upper mantle temperature, T_u, $\frac{dT_u}{dt}$ is the rate of change of this upper mantle temperature, F_s and F_c are the surface and core heat flux respectively, L is the latent heat released due to inner core solidification, E_G is the gravitational energy released by exclusion of the light element at the inner-core boundary, C_c is the average heat capacity of the core, and η_c is a constant relating the average temperature in the outer core to the temperature at the core-mantle boundary. The heat fluxes, F_s and F_c, are given by

$$F = \frac{k\Delta T}{\delta}, \tag{3.86}$$

where k is the thermal conductivity, ΔT is the temperature drop across the thermal boundary layer considered, and δ is the thickness of that boundary layer. δ can be determined by different parameterized approaches, using the Rayleigh-Number Ra, the critical Rayleigh-Number Ra_{cr} or the local critical Rayleigh-Number Ra_{crb}, depending on which approach resulted in a smaller thickness (see Stevenson et al. (1983) for details). By integrating these equations the evolution of the planetary cores and mantles and the onset of inner core growth could be investigated. The six presented earth models all started with core growth between 2.3 and 3.0 Gy after planet formation and resulted in an inner-core radius between $1185 - 1234$ km. The rate of core growth listed in Table III of Stevenson et al. (1983) is between 0.17 and 0.25 mMy^{-1}, which seems unreasonably low and it has to be assumed that the units for core growth in this table should be $km\ My^{-1}$ instead. Although direct comparison with the approach in Section 3.3 and the results for the earth in Section 3.4 is difficult, a rate of inner core growth of 0.25 $km\ My^{-1} = 250\ km\ Gy^{-1}$ is only a factor 3 lower than that given in Table 3.2 and seems more plausible.

An interesting possibility of core cooling has been proposed by Labrosse et al. (1997) for the case of a low core-mantle boundary heat flux. Previous authors (e.g., Gubbins (1979); Stevenson et al. (1983)) considered the possibility, that due to the high thermal conductivity of the fluid iron in the

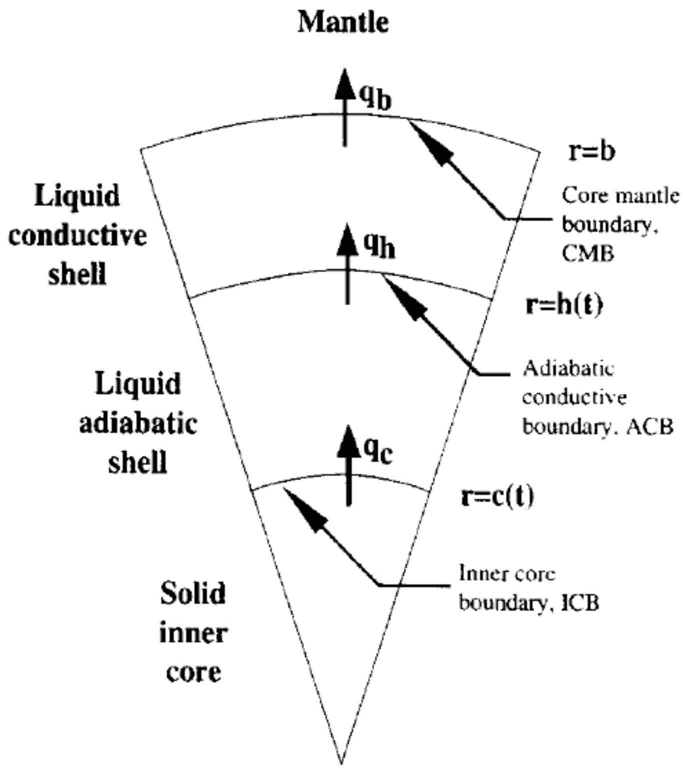

Figure 3.8: A core with a subadiabatic shell beneath the core-mantle boundary, where conduction dominates. Below, a convective shell with an adiabatic temperature gradient lies above the solid inner core. Image taken from Labrosse et al. (1997).

outer core, heat flux conducted down the adiabat across the core-mantle boundary into the mantle could be sufficiently higher than estimated so far. This could lead to a transfer of heat backwards into the core by compositional convection. But since heat transfer by compositional convection may occur rather locally than globally, Labrosse et al. (1997) suggested the existence of a shell with a subadiabatic temperature gradient just below the core-mantle boundary where heat is rather conducted than convected. This idea is illustrated in Fig. 3.8.

The work of Nimmo et al. (2004), which will be investigated amongst others in the next chapter in the context of radioactive isotopes in the core, uses a similar approach to Gubbins (2003) and Labrosse et al. (2001) to determine the thermal evolution of the core. In addition, the heat extracted from the core by the mantle is related to the heat flux across the core mantle boundary by

$$Q_C = 4\pi R_c^2 F_b, \tag{3.87}$$

where R_c is the core radius, and F_b is the heat flux across the core-mantle boundary. The thermal evolution of the mantle is given by the following approach:

$$H_m M_m - Q_M + Q_C = M_m C_{pm} \frac{dT_h}{dt}, \tag{3.88}$$

where H_m is the heat generated within the mantle, M_m is the mass of the mantle, Q_M is the heat extracted from the mantle, Q_C is the heat extracted from the core by the mantle, C_{pm} is the specific heat capacity of the mantle, and $\frac{dT_h}{dt}$ is the rate of change of the temperature half-way through the mantle, T_h, which represents the average mantle temperature. The heat extracted from the mantle, Q_M, is related to the heat flux across the lithosphere by the following equation:

$$Q_M = 4\pi R_p^2 F_t \quad , \tag{3.89}$$

with R_p the planetary radius, and F_t the heat flux across the lithosphere. Heat fluxes across the lithosphere and across the core-mantle boundary are determined analogously to the work of Stevenson et al. (1983), where the thickness of the thermal boundary layer is again determined by a $\frac{1}{3}$-power law of the critical Rayleigh number (see below), and the viscosity is determined by an exponential dependence of the mantle temperature. To determine the heat flow across the core-mantle boundary, the heat flux across the same interface has to be determined (Nimmo et al., 2004):

$$F_b = k_b(T_c - T_m)/\delta_b \quad , \tag{3.90}$$

where k_b is the thermal conductivity at the bottom of the thermal boundary layer, i.e. at the base of the mantle, T_c is the core temperature at the core-mantle boundary, T_m is the mantle temperature, and δ_b is the thickness of the bottom thermal boundary layer. Estimates of k_b range from $\sim 4 - 20\ W\ m^{-1}\ K^{-1}$ (Buffett, 2002; Manthilake et al., 2011), but experiments at high pressures up to 26 GPa suggest a thermal conductivity of 8.4 $W\ m^{-1}\ K^{-1}$. In this work a value of 5.8 $W\ m^{-1}\ K^{-1}$ is used, which is in accordance with a core-mantle boundary heat flow of 9 TW, a value used by Nimmo et al. (2004), Nimmo (2009) and also applied in this treatise, for reasons pointed out in the last paragraph of Subsection 3.4.1. The mantle temperature T_m is not explained further in Nimmo et al. (2004), but it can be derived when using the mantle viscosity employed by Nimmo et al. (2004), Table 4, of $\eta_b \sim 6.7 \cdot 10^{21} Pa\ s$, which yields $T_m = 2725\ K$. The thickness of the boundary layer is determined in the following way (Nimmo et al., 2004):

$$\delta_b = \left[\frac{Ra_c \kappa_b \eta_b(T_a)}{\rho_m g \alpha_m (T_c - T_m)} \right]^{1/3}, \tag{3.91}$$

where $Ra_c = 600$ is a generally accepted value of the critical Rayleigh number, $\kappa_b = 1 \cdot 10^{-6}$ is the thermal diffusivity at the base of the mantle, $\eta_b(T_a)$ is the dynamic viscosity determined by the temperature $T_a = \frac{T_c + T_m}{2}$, ρ_m is the mantle density, g is the gravitational acceleration at the surface, and α_m is the mantle thermal expansivity. The viscosity can be calculated as follows (Nimmo et al., 2004):

$$\eta_b(T_a) = f \eta_0 exp[-\zeta(T_a - T_1], \tag{3.92}$$

where f is a numerical factor which accounts for the higher viscosity of the deep mantle, η_0 is the viscosity at a reference temperature T_0, ζ is a quantity related to the activation energy (Nimmo et al., 2004; Solomatov, 1995), T_a is the same as for the calculation of δ_b, and T_1 is a typical temperature for the deep mantle. Using these values and those described in Table 3.1 a heat flow across the core-mantle boundary of $\sim 9.04\ TW$ was calculated. The quantities used and the resulting heat flow are summarized in Table 3.4 (see Appendix A for Mathematica calculations). This model will be used in Chapter 5 to estimate the core-mantle boundary heat flow within more massive planets than the earth to determine the cooling rate. In this case most parameters are not known and can be estimated only by employing internal structure models of terrestrial planets.

Quantity	**Units**	**Value**
R_c [1]	km	3480
T_c [3]	K	4155
T_m [4]	K	2725
T_0 [2]	K	1573
T_1 [2]	K	3400
ρ_m [2]	$kg\ m^{-3}$	4800
g [2]	$m\ s^{-2}$	9.8
Ra_c [2]	–	600
k_b [5]	$W\ m^{-1}\ K^{-1}$	5.8
κ_b [2]	$m^2\ s^{-1}$	10^{-6}
α_m [2]	K^{-1}	$2.2 \cdot 10^{-5}$
η_0 [2]	$Pa\ s$	$1.0 \cdot 10^{21}$
η_b [6]	$Pa\ s$	$6.7 \cdot 10^{21}$
f [2]	–	10
ζ [2]	K^{-1}	$1.0 \cdot 10^{-2}$
$\mathbf{Q_c}$ [7]	TW	9.045

Table 3.4: Quantities used to determine the heat flow across the core-mantle boundary in the earth, using eqs. (3.87), (3.90), and (3.91); Values taken from [1] Nimmo et al. (2004),Table 1; [2] Nimmo et al. (2004),Table 2; [3] Nimmo et al. (2004),Table 4; [4] chosen so that the viscosity has the value from Nimmo et al. (2004), Table 4; [5] chosen, so that the heat flow yields the value in Nimmo et al. (2004), Table 4; [6] calculated using eq. (3.92); [7] calculated using eq. (3.87)

Several problems arise with these parameterized models and have been criticized by Labrosse (2003). First of all, the $\frac{1}{3}$-dependence on the Rayleigh number is typically used in systems where convection is governed by high Rayleigh numbers and the dynamics of the boundary layer are independent of the flow occurring within it. This assumption does not necessarily have to hold for the bottom boundary layer of the mantle, since the dependence on the Rayleigh number is more or less unknown in this regime. The parameterized-model ansatz is another drawback, due to its quasi-static nature, which may lead to the neglect of time scales on which processes take place that should not be ignored (see Nimmo et al. (2004) for details). Nevertheless, the importance of the mantle for core cooling has to be kept in mind, and in order to determine the dependence of the planetary magnetic field on core dynamics, the regulation role of the mantle should be considered adequately.

3.6 What Can Be Said about Other Planets?

The determination of any parameters used in the discussions above for other planets than the earth is inherently difficult. The only terrestrial body except the earth for which seismic measurements are available is the moon, and even for our neighbouring planets Venus and Mars, parameters of the planetary interiors are actually non-existent. At least the magnetospheres of solar system planets out to Saturn are known pretty well, especially for the terrestrial bodies, Mercury, Venus, Mars, and the moon. Details of the planetary magnetic fields and space missions that explored them are described in Chapter 1 of this work. Knowledge about the planetary magnetic fields at least allows to reconcile different models of planetary interiors with the observed magnetic field strengths. This has been done for all "magnetic" planets in the solar system, and a good overview of this development is given in Breuer et al. (2009), Stevenson (2009), and Stanley and Glatzmaier (2010).

In the case of extrasolar planets, virtually nothing can be said about the planetary structure. Modern astronomy has just started to isolate extrasolar planets from the glaring light of their parent stars, and models of exo-planetary atmospheres are developed already (e.g., Heng and Vogt (2011), Iro and Deming (2010)), although much about these models is still very speculative. The only data that can be used in conjunction with interior models is the mass of the planet, which can be determined in several ways. The two methods employed most frequently are the radial velocity method and the transit method, where the former has enabled the identification of 358 planets and the latter the discovery of 103 planets (see Fig. 3.9). The other methods used (see Fig. 3.9) have not been as successful until today but at least complement the radial velocity and transit method, and some of these could be even more effective in the near future. A good overview of the radial velocity and the transit method are given in Beaugé et al. (2008) and Rauer and Erikson (2008), respectively, an overview of space missions to detect exoplanets can be found in Fridlund and Kaltenegger (2008).

Therefore, it is necessary to develop models with different interior structures (e.g., Valencia et al. (2006, 2007a,b); Sotin et al. (2007); Grasset et al. (2009); Wagner et al. (2011a,b)), and try to bring them into agreement with the planetary masses and radii derived from one of several observational methods mentioned above. These models usually employ one or more equations-of-state (EOS), which describe the change of density, pressure and temperature with increasing radius and relate them to each other for a given material in thermal equilibrium (Wagner et al., 2011b). Solving them in conjunction with the differential equations for mass, gravitational acceleration, pressure and temperature yields a structural model of the planet considered, i.e. for a model of a planet with a certain fragmentation into mantle and core, or crust, mantle, and core (or any other

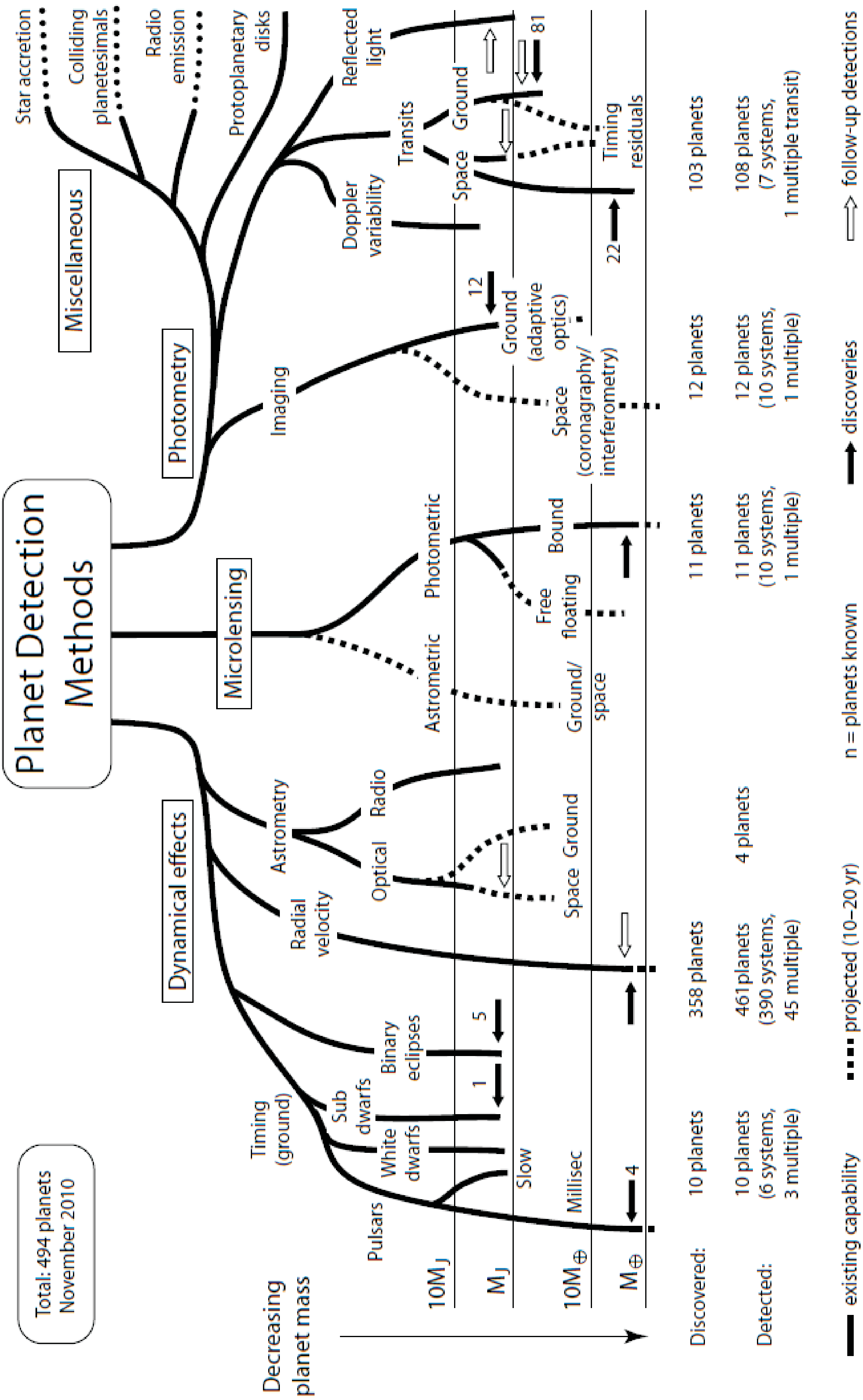

Figure 3.9: Methods used to detect extrasolar planets. Image taken from http://exoplanet.eu/papers/macp-detection-methods.pdf.

segmentation that is of interest).

Considering the analytical method presented in the previous section, one major problem with extrasolar planets is that there is no way to determine the cooling rate of the planet, which is crucial in evaluating the thermal history, and further, to make a statement about the magnetic properties of a planet. On the other hand, it is neither possible to observe the magnetosphere of the planet and estimate the dissipation rate, as exercised above, to derive the cooling rate of the planet. Therefore the chances to derive any magnetic properties of a potential exoplanet seem very grim. But there could be a possibility to gain some data about the magnetosphere of exoplanets, nevertheless. This idea is based on the fact that the stellar wind of a star interacts with the potential magnetosphere of a planet in orbit around it. The first such observation has been made with the star HD 179949, where enhancements of Ca II H and K emission lines coupled to the revolution of the planet around the host star could be detected (Shkolnik et al., 2003). A larger sample of planets has been studied by Stevens (2005), where 28 planets within 20 pc distance to the sun (29 including HD 179949, which is approx. 27 pc away) have been investigated theoretically, using stellar and planetary parameters to estimate the possible radio emissions by the planets, depending on X-ray flux of the host star, which is an indicator for the mass-loss rate of the star. One prerequisite for detection of magnetically induced radio emission is a local plasma frequency below the wave frequency of the radio emission, because otherwise the plasma frequency would screen out the radio emission caused by interaction of the magnetic field with the stellar wind. This has to be considered for planets that are in very close orbits around their parent stars, and for host stars with high mass-loss rates (Stevens, 2005). Stevens determines 5 promising stellar candidates, given in Section 4 of his paper, which would emit a flux potentially detectable by LOFAR, the

LOw **F**requency **AR**ray, although only 3 of these objects would be visible from the LOFAR site. By now (March 2012) the number of 29 exoplanets given above has increased to 96 (using data from http://exopanet.eu), where the defintion of an extrasolar giant planet (EGP) as given by Burrows et al. (1998) has been used, which defines an EGP to lie in the mass range of 0.3 $M_J - 15\ M_J$. Many of these planets cannot be used for calculations of their radio emissions, though, since important planetary or stellar parameters of these systems are still unknown. As soon as these crucial data would be determined, the expected radio emissions could be calculated for 100 planets, which would increase the chance of observing a planet's magnetosphere indirectly for the first time. With LOFAR finished this could be achieved in the near future (see http://www.lofar.org for more information and Fender (2007)).

Chapter 4

Influence of Radioactive Elements on Heat Production

4.1 Introduction

As described in the previous chapter, the energy budget of the earth's core comprises several contributions from different physical processes. One of these is thought to be the decay of the radioactive isotopes ^{40}K, ^{235}U, $^{238}U$and ^{232}Th. It has long been suggested that ^{40}K could be an important energy source for the geodynamo, (Bullard, 1949; Lewis, 1971) but divergence of geochemical and geophysical arguments have exacerbated attempts to settle this conflict (Nimmo, 2009), especially in matters of specifying the amount of radioactive species present. Nevertheless, recent high-pressure experiments contribute important facts to the solution of this question, and at least a probable range of values for radioactive isotope abundances can be given, offering the possibility to incorporate these results into calculations of the energy balance of the earth's core. This is also important in relation to models of other planets in the solar system or exoplanets, since it is crucial to know the energy sources necessary to allow a self-sustaining dynamo to work over geological time, and thus to provide a planetary habitat that does not prevent life from emerging right from the start. In the following sections recent results regarding the abundance of radioactive isotopes in the earth's core will be discussed. After assessing the amounts of these elements, the heat generated thereby can be calculated. Then the significance of this contribution to the overall energy and entropy budget can be discussed.

4.2 Abundance of Radioactive Isotopes in the Core

Since the emergence of dynamo theory, the idea existed that radioactive elements contributed to the energy available to drive the geodynamo by decaying and releasing radiogenic heat (Bullard, 1949). But until now, the abundance of these elements is a matter of discussion, although the possibility of their contribution to core energetics is more or less accepted. There are two facts that prove it very difficult to make further progress in this area of research: First of all, it is not possible to gain samples from the earth's core and conduct direct analysis of the material found. Although there could be the possibility that core material is transported to the surface via mantle plumes, it seems very implausible that it would reach the surface unaltered, considering the fact that this transport requires some time. Secondly, conditions in the earth's core are extraordinary, to say the least, with prevalent pressures beyond the possibilities of any laboratory on earth. It is therefore very hard to reproduce the correct physical conditions in order to investigate the behaviour of the above-named elements in interaction with the fluid iron and other light elements in the outer core. Nevertheless experiments have been carried out to elucidate the role of especially ^{40}K in the core of the earth. Another possibility would be to evaluate the energetic requirements of the geodynamo to work over geological time, and estimate the consequence for the existence of radioactive elements, and their necessary contribution to the energy and entropy balance.

As mentioned before, Lewis (1971) realized already 40 years ago, that potassium, which is considered lithophilic under normal circumstances, could behave chalcophilic as well, which could lead to higher abundances of ^{40}K in FeS-rich melts, which are thought to be present in the fluid outer core. In the following decades a couple of experiments have been performed to study the partitioning of radionuclides like U, Th, and K into Fe-FeS-liquids (Murrell and Burnett, 1986), but results where either not representative due to their large errors, or difficult to interpret because of inconsistent experimental preconditions. At the end of the last millennium, Chabot and Drake (1999) conducted experiments to investigate the solubility of potassium in metal under low-pressure conditions. They used a piston cylinder held at a pressure of 15 kbar and a temperature of $1900°C$, and an alumina capsule (for the first set of experiments; for the second set a graphite capsule has been used) that contained the metallic liquid and the silicate melt. After a minimum duration of 20 min the experiment was shut down, the product sliced in half when cooled down, and after polishing the surface the product could be analyzed with an electron microprobe. Two sets of experiments were conducted, one with varying sulfur content, and a second with varying silicate composition. As a result, Chabot and Drake (1999) concluded that, based on a mantle abundance for potassium of 100 *ppm*, the earth's core could contain no more than 1 *ppm* of K, which would generate a radiogenic heat of $\approx 10\ GW$, much too small to power the geodynamo or have a significant influence on the energy budget, when comparing this value with the other contributions given in Table 3.2. But the authors didn't conceal the fact, that a pressure of 15 kbar was not representative of core conditions, where pressures are in the range of tens to a few hundred Gbar. They further assumed that U and Th would contribute more to internal heating than potassium.

Four years later, Murthy et al. (2003) conducted a new set of experiments, trying to avoid error sources of the previous ones. They realized that using oil for polishing the sample could result in substantial loss of potassium from the Fe-S-phase and employed a dry polishing technique using a lubricant without any liquid, hexagonal boron nitride powder. Another source of potassium loss was the use of only one capsule, as was shown with mass-balance calculations. Therefore a double-capsule technique was applied, with an inner capsule made of graphite, containing the charge, and an outer capsule made of welded platinum. Different charges were loaded into the capsule, namely synthetic mixtures of Fe-metal, FeS, a K-silicate glass and a natural peridotite, KLB-1. Pressures were between 1 and 3 GPa and temperatures between 1200 and 1800 $^{\circ}C$, which was above the liquidus of both, metals and silicates. The partition coefficient for potassium, D_K, which describes the ratio of potassium in sulphide to potassium in silicate, was then determined as a function of pressure, temperature and composition and extrapolated to core conditions. This yielded D_K values large enough to allow for a significant amount of potassium in the core (the dependence of D_K on temperature and pressure is shown in Fig. 4.1 and Fig. 4.2). Of course the dependence on sulfur content had to be considered and a value of 10 wt % was assumed. This resulted in a range of potassium abundance in the earth's core of $60 - 130$ ppm, generating $0.4 - 0.8$ TW of radiogenic heat.

Murthy et al. (2003) argued further that the possibility of potassium being dissolved in FeS liquids also had implications on the history of the Martian dynamo. Since Mars is assumed to possess a core with a higher sulfur abundance (Bertka and Fei, 1998) than the earth, and a subsequent higher potassium content, more radiogenic heat production can occur in a core that is substantially smaller than the core of the earth. Therefore the

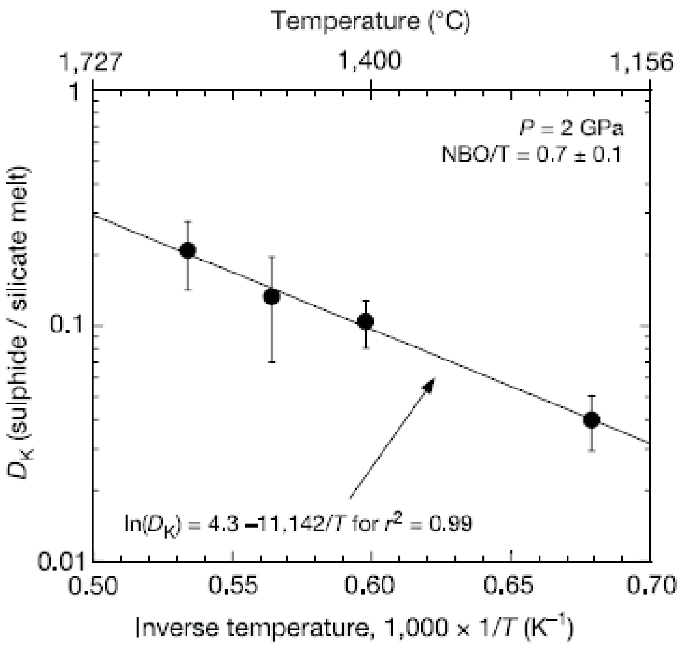

Figure 4.1: The dependence of D_K on temperature. Image taken from Murthy et al. (2003).

pressure and temperature needed to reach equilibrium between FeS-melts and silicates is lower than on earth and a partitioning coefficient of 0.1 is yielded. This means that 4 Gyr ago there could have been enough potassium in the Martian core to drive a dynamo by radiogenic heat alone and produce the magnetic signatures observed today (see Chapter 1). Due to the more rapid cooling of the core if more radiogenic material is present (see Section 3.4) the dynamo would have ceased to exist fairly soon in martian history, which would explain the observations of remanent magnetization on Mars today despite the lack of an active dynamo.

Two further experiments, conducted at higher pressures up to 15 GPa, yielded slightly different results. Bouhifd et al. (2007) determined values of 220 ± 100 ppm K in the case of a bulk silicate earth containing 250 ± 50 ppm potassium and a core with some low sulfur abundance and an oxygen content of 4 wt %, or a very low abundance of 25 ± 14 ppm K in the case

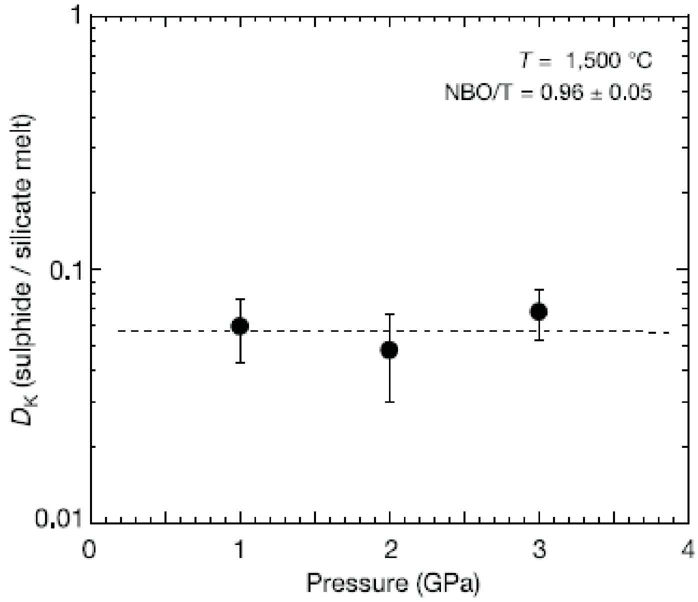

Figure 4.2: The dependence of D_K on pressure. Image taken from Murthy et al. (2003).

of a core devoid of sulfur and oxygen. Corgne et al. (2007) found that the amount of oxygen present in the core affects the partitioning of potassium, and the abundance of sulfur or carbon is more or less negligible. For a core with 2 wt % of oxygen present, a potassium abundance of $2-25$ ppm is assumed. For the most likely oxygen content of 5 wt % a potassium abundance of $\sim$ 80 ppm is suggested.

Regarding the distribution of uranium and thorium in the core very little can be found in the literature. Bao (2009) suggests the existence of two concentration centers in the outer core (see Fig. 4.3), one with a high U-,Th-concentration, the other with a low concentration, which could have a non-negligible effect on the energetics of the core. But he gives no estimation as to the abundance of uranium and thorium in these centers, or some number approximating the amount of these elements in the core. Murthy et al. (2006) conducted experiments at $3-8$ GPa and estimated the abundance of uranium in the core to be $1-2$ ppb, or $0.001-0.002$ ppm, yielding radiogenic heat of $0.1-0.3$ TW, which is approximately 1% of the total core-mantle boundary heat flow. No estimates for abundance of or heat production due to thorium in the core could be found in the literature, except an estimate by Labrosse et al. (2001), who estimates the abundance of uranium and thorium to be 5 ppb and 0.17 ppb, respectively.Considering experimental results a potassium content of $\sim$ 100 ppm in the earth's core seems plausible, although upper bounds up to $\sim$ 300 ppm could be justified experimentally.

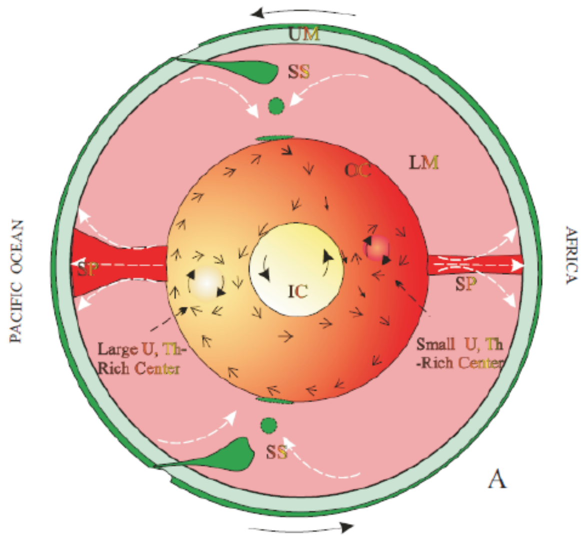

Figure 4.3: A large and a small U-Th-rich center in the earth's outer core. IC: inner core, OC: outer core, UM: upper mantle, LM: lower mantle, SS: subducted slab, SP: super-plume. Image taken from Bao (2009).

In contrast to the experimental approach, theoreticians consider the power requirements of the geodynamo and the fact that it has existed for almost 4 Gyr to constrain the abundance of radioactive isotopes in the core. Above all, the thermal history of the earth poses a major problem when regarding an early earth without a solid core. Since in the early earth no compositional convection was present to drive convection, thermal convection was the only source to power the geodynamo. But since thermal convection alone is much too weak to sustain the magnetic field, other energy sources or a different thermal history of the earth than currently assumed are needed to explain a dynamo without a solid inner core. Buffett (2002) investigated two scenarios for the dissipation rate of magnetic energy within the earth's core. Since magnetic energy is dissipated due to Ohmic diffusion, this energy loss must be compensated by convection to sustain the geodynamo. Two dissipation rates, 0.1 TW and 0.5 TW, have been assumed and the core-mantle boundary heat flow as a function of inner-core radius and the inner-core growth have been calculated for a geodynamo with these dissipation rates (see Fig. 4.4 and Fig. 4.5). By using a parameterized approach for core cooling, similar to the one described in Section (3.5), the thermal history of the core could be determined. The model with the higher dissipation rate yielded temperatures within the earth that were too high for young ages, whereas the second model could prevent these troubles by a core that was cooling very slowly. Unfortunately, this model implied a temperature contrast between the core and the mantle that was much too small and could only be achieved by either increasing the temperature at the bottom of the mantle or decreasing the temperature at the inner-core boundary, neither of which could be reconciled with current estimates of these values. This meant that thermal history models and temperature estimates at the core-mantle boundary were contradictory. One solution would be to alter the thermal profile at the core-mantle boundary, which would require a radiogenic heat production at the base of the mantle of 11 TW. This value seems pretty high, since it would imply that $\sim 39\%$ of the radioactive isotopes are in a 200 km thick layer, but it is at least comparable with the results of Coltice and Ricard (1999), who estimate that one third of the earth's radioactive elements are trapped in the D" layer. Another solution to this discrepancy would be the addition of a heat source like radiogenic heat production to the core, and Buffett (2002) concludes that 1.4 TW of radiogenic heat would be consistent with thermal history models, although it would contradict experimental results, as described above. But one has to be cautious about experimentally determined abundances due to the fact, that it is still not possible to reproduce the conditions that prevail in the earth's core in any laboratory on earth. And the progress from low-pressure to high-pressure experiments already showed that unexpected results can be obtained when the conditions come near those in the earth's core.

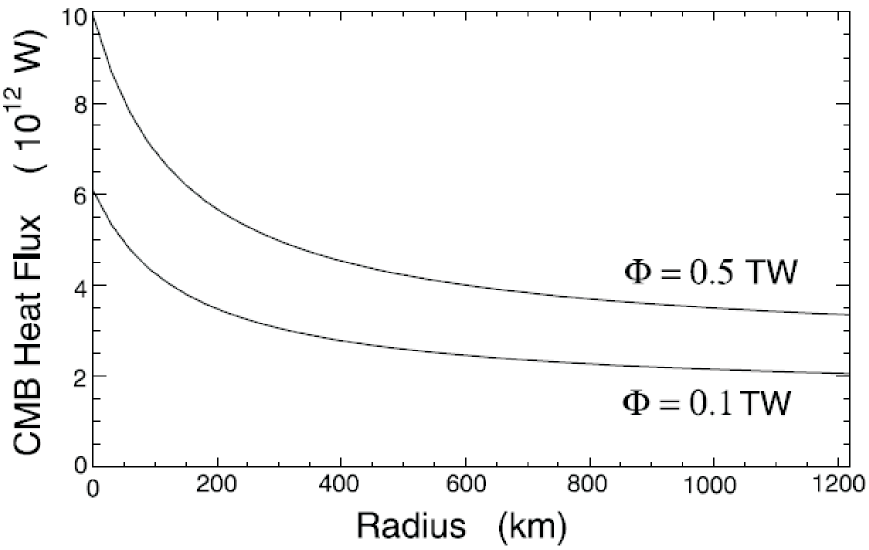

Figure 4.4: CMB heat flow required to power a geodynamo with a dissipation rate of 0.5 and 0.1 TW. Image taken from Buffett (2002).

Another theoretical approach has been taken by Nimmo et al. (2004), who calculated the energy and entropy contributions to the core analogously to the approach described in Section (3.3). By employing a parameterized approach (see Section 3.5) for mantle and core cooling a set of equations could be derived, that allow to calculate the heat flow across the core-mantle boundary and the lithosphere, respectively, and to determine the cooling rates of the core and the mantle. Subsequently, thermal evolution scenarios were investigated in terms of currently assumed values of the earth's interior, like core size, temperature, viscosity in the mantle, and of course, the existence of a magnetic field over geological time. Nimmo et al. (2004) concluded that it was very likely that potassium was present in the core and assumed an abundance of $\sim$ 400 ppm K in earth's core. Due to the results of their model, it would be rather unlikely that the core would contain no potassium, since this would make it very difficult to reconcile current observations of core size and entropy production, i.e. power requirements for the geodynamo. Nevertheless, alternatives could exist that would not require potassium in the core, but could reproduce known properties of the earth as well, some of them more likely than others. As an example, our understanding of the processes occurring at the core-mantle boundary could be incomplete or plainly wrong and the parametrization used by Nimmo et al. (2004) inadequate. As mentioned above (see Section 3.5), parameterized models could be problematic generally due to the fact that they simplify physical processes and ignore timescales that possibly should not be neglected. Potassium abundances suggested by the model of Nimmo et al. (2004) can thus be regarded as an upper boundary for current models of the earth's core

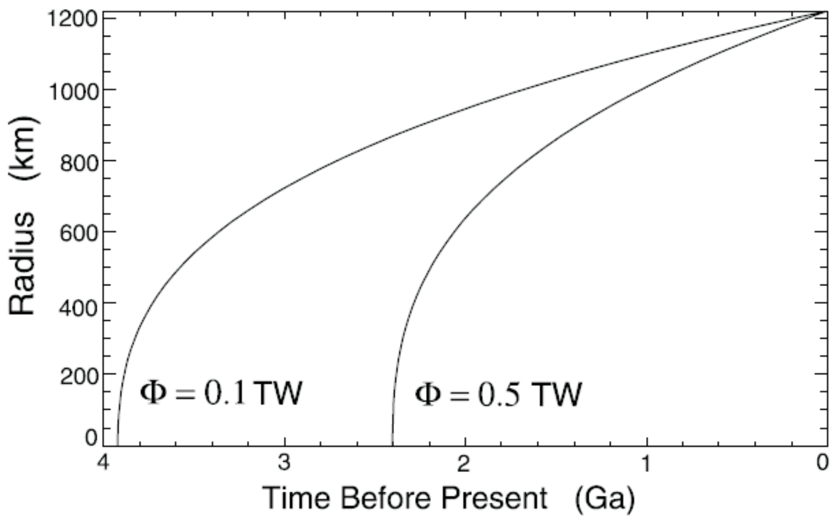

Figure 4.5: Inner core growth over the earth's history. Image taken from Buffett (2002).

As can be seen, it is still very problematic to estimate abundances of radioactive elements in the earth's core, and results obtained by different approaches are to some extent even contradictory. In the next section, the calculation of radiogenic heat in the core will be explained, and the contribution of Q_R (see Sections 3.3 and 3.4) for different abundances of ^{40}K, ^{235}U and ^{238}U, and ^{232}Th will be calculated.

4.3 Calculating the Radiogenic Heat Production

To determine the radiogenic heat in the core produced by ^{40}K, ^{235}U and ^{238}U, and ^{232}Th, a couple of steps have to be taken. First of all, the abundances of the different species have to be estimated and expressed in terms of kg of radiogenic element per kg of core material. Then the heat generated per kg of core material can be calculated. After calculating the mass of the core the total heat generated by radioactive elements, Q_R, can be determined.

Radiogenic heat production for three scenarios shall be considered. An upper bound, a lower bound, and the arithmetic mean of the both. In the case of ^{40}K, the value given by Nimmo et al. (2004) of 400 ppm is used as an upper bound, since most values in the literature lie below this number, but it still seems to be an estimation compatible with current models of the core. As a lower bound, the results by Bouhifd et al. (2007) are employed and their lower bound for the case of no oxygen and sulfur in the core, 11 ppm, is used, although this scenario seems rather unlikely (e.g., Corgne et al. (2007) suggest an oxygen abundance of 5 wt % in the core as plausible). The third value used is 205 ppm, which corresponds to the (rounded down) arithmetic mean of the upper and lower bound. It has to be considered that the isotope ^{40}K amounts to only 0.0119% of core potassium (Turcotte and Schubert, 2002). Uranium is present in the form of two isotopes, ^{235}U and ^{238}U, where most of it, 99.28%, is made up by the heavier isotope, and only 0.71% are ^{235}U (Turcotte and Schubert, 2002). Estimates of uranium in the core are very scarce in the literature, Murthy et al. (2003) estimate an abundance of 1-2 ppb, whereas Labrosse et al. (2001) consider a slightly higher amount of 5 ppb. This value shall be used as an upper bound, and the lower bound of Murthy et al. (2003) is used as a lower bound in this calculation. The arithmetic mean of these two values is then 3 ppb. When calculating the radiogenic heat, of course the different isotopes have to be accounted for. For thorium in the core, no dedicated work so far can be found in the literature. Labrosse et al. (2001) estimate a possible value of 0.17 ppb, but no arguments in favour of this value or against it are presented. Therefore their estimate is used as a lower bound, and the lower bound for uranium abundances is used as an upper bound. This results in a rounded down arithmetic mean of 0.58 ppb. Thorium appears 100% as the isotope ^{232}Th. The three scenarios for each of the radioactive elements and the corresponding mass fractions are given in Table 4.1. Now the heat generation of each species for each scenario can be calculated, following Turcotte and Schubert (2002). The total heat production by radioactive elements is given by

$$H = C^{^{40}K} H^{^{40}K} + C^{^{235}U} H^{^{235}U} + C^{^{238}U} H^{^{238}U} + C^{^{232}Th} H^{^{232}Th}, \qquad (4.1)$$

where C^X is the concentration of the respective isotope and H^X is its heat production in $W\ kg^{-1}$. Rates of heat production are given in Table 4.2 and are adopted from Turcotte and Schubert (2002). Inserting the values from Table 4.1 and Table 4.2 into equation (4.1) results in a radiogenic heat production per kg of core material as given in the first column of Table 4.3, where for each isotope the upper bound, lower bound, and arithmetic mean have been used. No combinations of upper and lower bounds and mean values are calculated, since this would result in 81 combinations which would not give any further insight.

^{238}U	**99.28%**		
	Scenario	ppb	$kg\ kg^{-1}$
	1	5	$4.96 \cdot 10^{-9}$
	2	3	$2.98 \cdot 10^{-9}$
	3	1	$9.93 \cdot 10^{-10}$
^{235}U	**0.71%**		
	Scenario	ppb	$kg\ kg^{-1}$
	1	5	$3.55 \cdot 10^{-11}$
	2	3	$2.13 \cdot 10^{-11}$
	3	1	$7.10 \cdot 10^{-12}$
^{232}Th	**100%**		
	Scenario	ppb	$kg\ kg^{-1}$
	1	1	10^{-9}
	2	0.58	$5.8 \cdot 10^{-10}$
	3	0.17	$1.7 \cdot 10^{-10}$
^{40}K	**0.0119%**		
	Scenario	ppm	$kg\ kg^{-1}$
	1	400	$4.76 \cdot 10^{-8}$
	2	205	$2.44 \cdot 10^{-8}$
	3	11	$1.31 \cdot 10^{-9}$

Table 4.1: Different scenarios and the respective abundances for U, Th, and K

To determine the total heat generation of the core, the value of H must be multiplied with the mass of the core, which can be determined using eq. (3.59) (the calculation of M_c using Mathematica is given in Appendix A), yielding a value of $1.927 \times 10^{24}\ kg$, which is in agreement with the value given in, e.g. Fowler (2005). Now the values from the first column in Table 4.3 can be multiplied for each of the three scenarios with the core mass, giving the total heat production due to radioactive elements in the core, Q_R. These values are given in the second column of Table 4.3. As is evident from eq. (4.1), the radiogenic heat production Q_R increases linearly with increasing abundance of the respective radioactive species.

Species	$H^x(W\ kg^{-1})$
^{238}U	$9.46 \cdot 10^{-5}$
^{235}U	$5.69 \cdot 10^{-4}$
^{232}Th	$2.64 \cdot 10^{-5}$
^{40}K	$2.92 \cdot 10^{-5}$

Table 4.2: Heat generation for different radioactive species; values taken from Turcotte and Schubert (2002)

The values of Q_R for a range of abundances from half the lower bound to double the upper bound for the case of ^{40}K and ^{238}U are shown in Figs. 4.6 and 4.7. In every plot the respective other abundances are kept constant at the mean value. In Fig. 5.1 the dependence of Q_R on core mass for the three scenarios, upper and lower bound, and mean value, are shown.

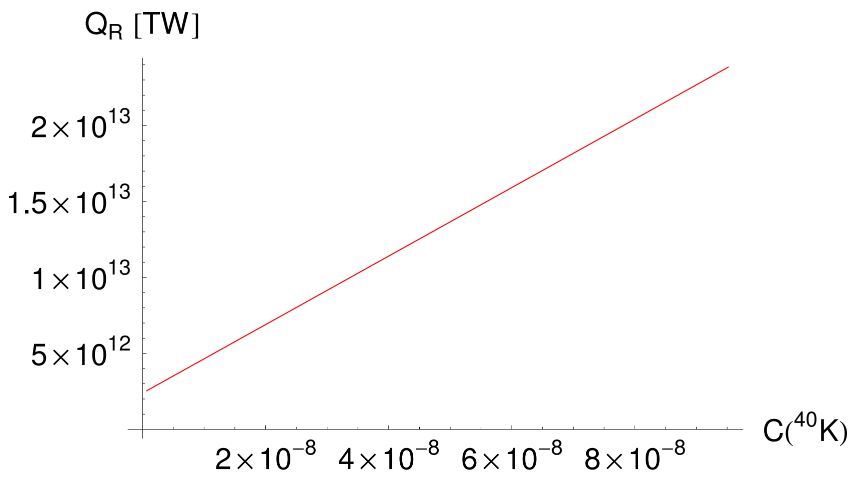

Figure 4.6: Dependence of radiogenic heat production, Q_R, on ^{40}K-abundance, where the abundances of the other radiogenic species are kept constant at the mean value (see Table 4.1). Calculation see Appendix A.

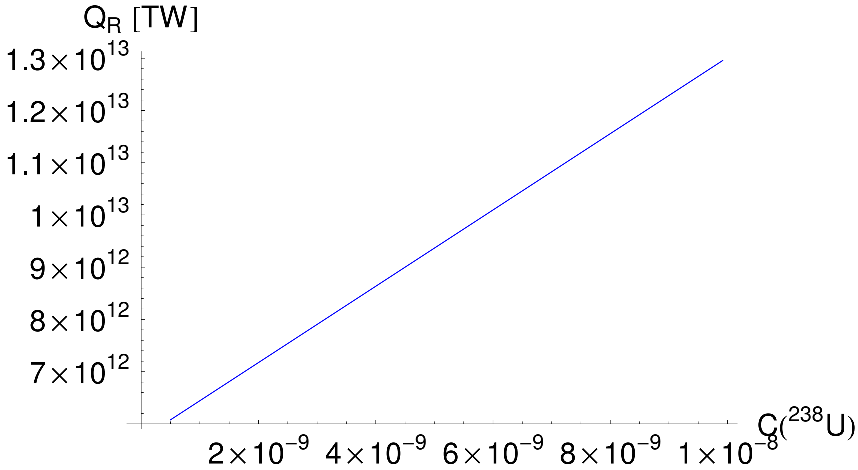

Figure 4.7: Dependence of radiogenic heat production, Q_R, on ^{238}U-abundance, where the abundances of the other radiogenic species are kept constant at the mean value (see Table 4.1). Calculation see Appendix A.

	$\mathbf{H(W\ kg^{-1})}$	$\mathbf{Q_R(W)}$
Upper Bound	$1.91 \cdot 10^{-12}$	$3.67 \cdot 10^{12}$
Mean	$1.02 \cdot 10^{-12}$	$1.97 \cdot 10^{12}$
Lower Bound	$1.41 \cdot 10^{12}$	$2.71 \cdot 10^{11}$

Table 4.3: Total heat generation by radioactive species in the core per kg of core material and heat flow by radiogenic heat production, for upper and lower bounds and for the mean values

Chapter 5

Influence of Core Size on Magnetic Field Generation

5.1 Overview

Now that the most fundamental physical processes involved in magnetic field generation have been explained, the influence of the core size on it can be assessed, if there is a relevant influence at all. First of all, one should consider the question, what a change of radius means in a physical sense. To do this, it is useful to think about each term in eq. (3.35), remembering that Q_P and Q_H do not contribute to the energy budget. Each term, except the latent heat term, is integrated over the volume of the core, where the gravitational energy is integrated over the volume of the outer core, only. Therefore, if the radius of the planet is increased from R to $R+\delta R$, these terms should increase with the third power of the ratio of these radii, $[(R+\delta R)/R]^3$. At the same time, the area of the core-mantle boundary only increases with the square of the radius. Therefore, more heat is available that has to be transported across the core-mantle boundary in order to cool the core. Considering Table 3.2 it becomes clear that in such a case latent heat would not be the dominant contribution to the energy budget anymore, since it depends only on the square of the ra-

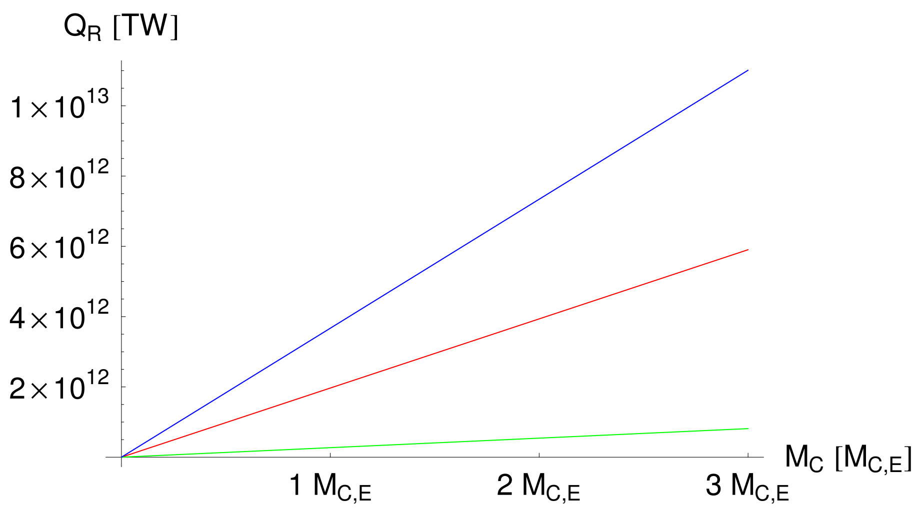

Figure 5.1: Dependence of radiogenic heat production, Q_R, on core mass for the three scenarios of radiogenic abundances described in Table 4.1. Calculation see Appendix A.

dius. Similar arguments could be applied to the terms contributing to the entropy balance. The terms describing heat conducted down the adiabat and the entropy change due to thermal diffusion, Q_k and E_k, have to be considered separately, because here the dependence on the radius is much stronger. Q_k increases with the third power of the radius, and E_k even with the fifth power.

But, of course, it is not as simple as that. Two parameters that have to be considered foremost when applying radius changes to interior models are density and pressure. If the radius of a planet increases, the density gradient changes and the pressure in its interior increases as well, as is evident from temperature changes in the earth's interior and basic thermodynamic considerations. Therefore the simple approach by applying the third power of the radius change as described above leaves out important physical processes in the planetary interior, since all other quantities that depend on density or pressure change as well (like the gravitational energy). Moreover, the pressure increase also has an influence on the viscosity of the fluid in the outer core. Since it was an elementary assumption for the derivation of the energy and entropy balance of the core that the outer core was vigorously convecting, the influence of increased pressure on the viscosity of the fluid core can not be neglected. It could be possible by all means that due to the increase in pressure a planet with a radius larger than the earth's has no fluid core anymore, since then even at higher temperatures than in the earth's core iron could solidify and then convection would be impossible.

Moreover, in a realistic model of a planet with a radius larger than the earth's, not only the core is larger in volume, but the mantle as well. Therefore, the influence of pressure on the mantle structure has to be considered in order to determine the ability of the mantle to carry away heat from the core. To achieve this, the first step would be to employ a model of the interior structure of a planet that allows to vary the radius (in the limit of terrestrial planets, i.e. up to 10 $M_{\oplus}$) but accounts for the influence of pressure change on the viscosity of mantle and core material. One such model could be, as mentioned already in Section 3.6, the model by Wagner et al. (2011b). In this model, the authors avoid common practice of previous interior models, i.e. to employ the Birch-Murnaghan- or Vinet-Equation-of-State (Eos), which are basically fits from laboratory experiments, and extrapolate to higher pressures that are prevalent in the cores of terrestrial planets and super-earths (and, hence, not accessible in laboratory experiments). Instead, they use and compare three different EoS for the lower mantle: a generalized Rydberg EoS, Stacey's reciprocal K' EoS, and the Keane EoS. The first is based on the Rydberg interatomic potential function (Stacey, 2005; Wagner et al., 2011b), the second on the reciprocal K'-relation (Stacey, 2000; Wagner et al., 2011b) and fits to PREM data (Preliminary Reference Earth Model, Dziewonski and Anderson (1981)), and the third on another relation for K' (Keane, 1954; Shanker and Singh, 2005), where K' is the pressure-related derivative of the bulk modulus. For planets with 1 $M_{\oplus}$ all three models predict values for the density, temperature, pressure, and gravitational acceleration that are in excellent agreement with PREM data and the reference geotherm (Stacey and Davis, 2008), although in the core and lower mantle deviations appear that are probably due to light elements in the core and phase transitions in the lower mantle, both of which are factors that are not accounted for in these models (see Fig. 5.2). In the case of more massive planets (see Fig. 5.3), the differences between the three EoS becomes more apparent. The central densities differ as much as 20%, which means a variation in core size of up to 5%. Central pressures also vary as much as 20%, the temperatures at the core-mantle boundary deviate up to slightly more than 20%, and the central temperatures differ up to 20% as well, where all values are for planets with 10 $M_{\oplus}$. The reason for these differences is the different treatment of the perovskite to post-perovskite transition in the lower mantle by the three EoS, and the use of a pressure- and temperature-dependent viscosity, which controls the radial temperature distribution. Therefore the models by Wagner et al. (2011b) predict higher temperatures at the core-mantle boundary than parameterized convection models used by, e.g., Valencia et al. (2006). For planets with masses up to 1 $M_{\oplus}$ the K'-EoS is the ideal choice since the fit parameters are directly obtained from seismological observations, which results in an almost perfect agreement with PREM data (Wagner et al., 2011b).

For more massive planets the Keane-EoS and the Rydberg-EoS are more suitable, since they allow for phase transitions from perovskite to post-perovskite, which is thought to represent the dominant mineral phase in the mantle of these bodies. Since it it possible that in the most massive terrestrial planets other phase transitions beyond the post-perovskite

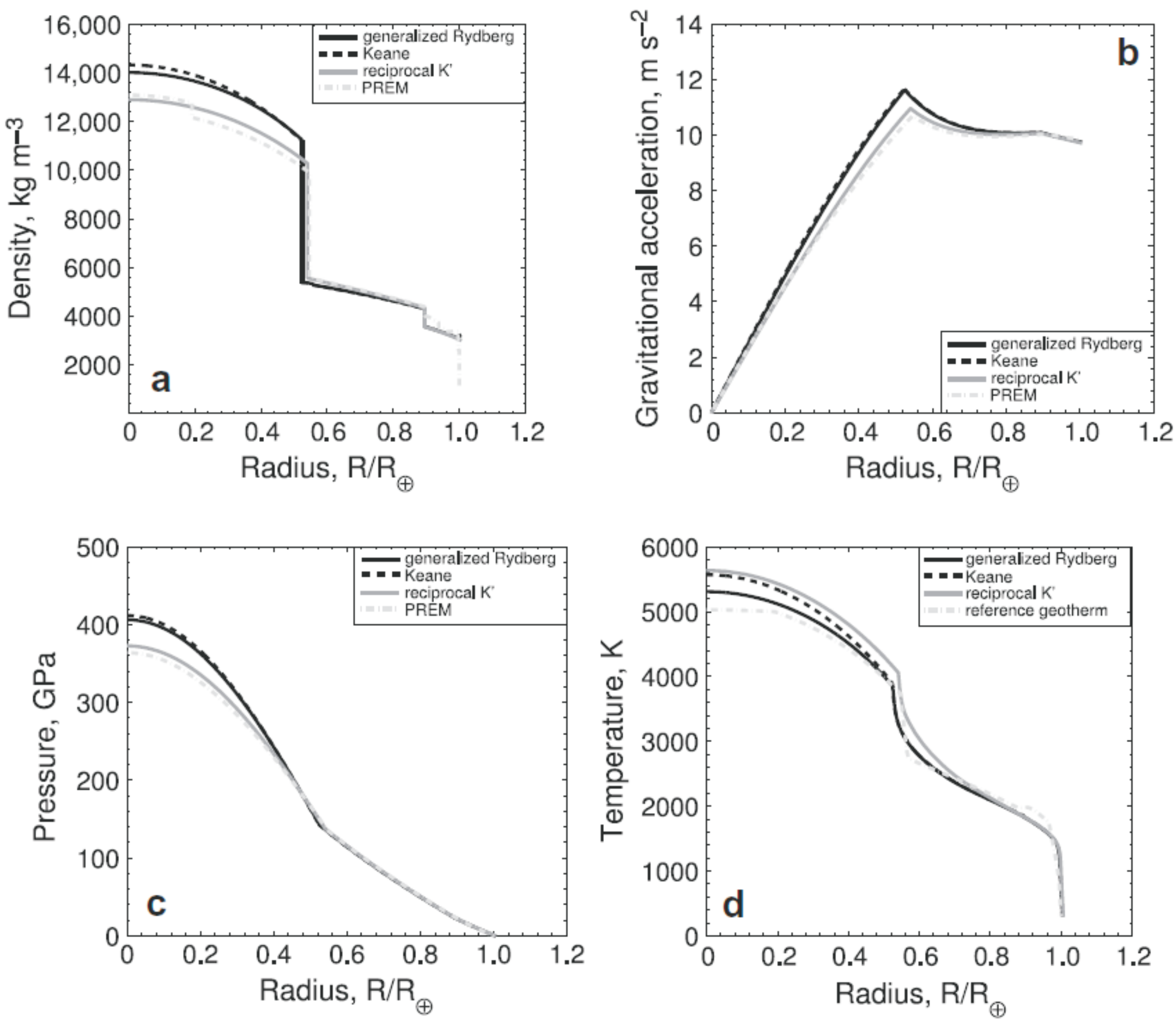

Figure 5.2: Interior structure of the earth according to the model of Wagner et al. (2011b), showing (a) the radial density structure, (b) the gradient of gravitational acceleration, (c) the pressure gradient, and (d) the temperature gradient for the case of the Rydberg-, the Keane-, and the K'-EOS and PREM data for comparison. Image taken from Wagner et al. (2011b).

phase also occur, the model results by Wagner et al. (2011b) represent a lower bound for density, pressure and temperature distribution in the interiors of massive terrestrial planets.

The results of an interior model can be used to determine the cooling rate of the core and the heat flow across the core mantle boundary, either by employing a parameterized convection model, like the one by Nimmo et

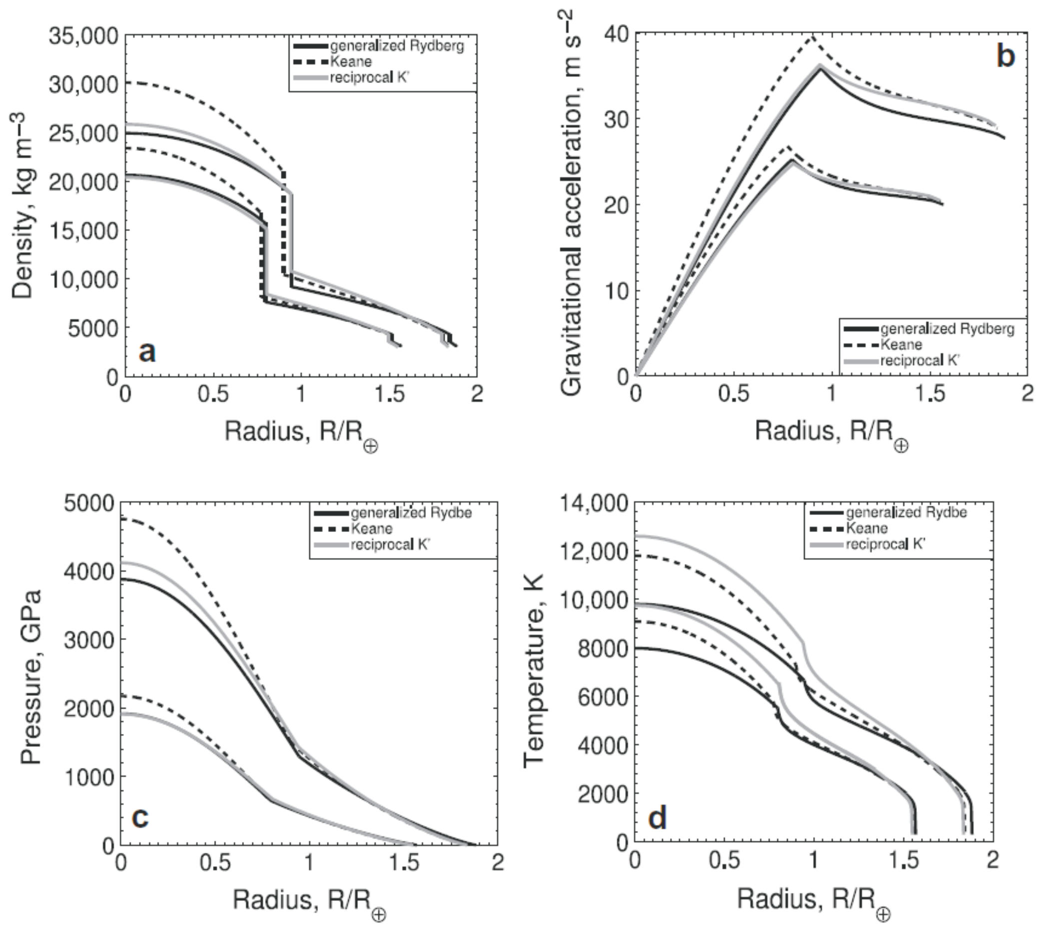

Figure 5.3: Interior structure of planets with 5 $M_{\oplus}$ and 10 $M_{\oplus}$ according to the model of Wagner et al. (2011b), showing (a) the radial density structure, (b) the gradient of gravitational acceleration, (c) the pressure gradient, and (d) the temperature gradient for the case of the Rydberg-, the Keane-, and the K'-EOS. Image taken from Wagner et al. (2011b).

al. (2004) (see Section 3.5), or a mixing length formulation, as described by Kimura et al. (2009) and Senshu et al. (2002). Then the magnetic field strength can be estimated by applying a scaling law as described in Section 2.3. As described in Chapter 3, as soon as the cooling rate is determined, the different contributions to the core energy and entropy budget can be calculated as well.

5.2 Calculations for Planets with $5\ M_\oplus$ and $10\ M_\oplus$

In this work the parameterized convection model by Nimmo et al. (2004) (see Section 3.5) is used to calculate the core-mantle boundary heat flow of planets with $5\ M_\oplus$ and $10\ M_\oplus$, using model curves published by Wagner et al. (2011b), and to determine the core cooling rate of such planets. Although parameterized models are certainly not the best approach for such a problem, and the required parameters for calculation can only be crudely estimated from the model curves by Wagner et al. (2011b) in absence of an own interior model of planets, this is an easy alternative to determine quantities needed to calculate the energy and entropy balance of cores in planets more massive than the earth, and to estimate their magnetic fields via scaling laws, both accurate to at least an order of magnitude. The quantities used to determine the heat flows for planets with $5\ M_\oplus$ and $10\ M_\oplus$, respectively, are listed in Table 5.1 , where mantle densities, temperatures, and viscosities where chosen at $1\ R_\oplus$ for planets with $5\ M_\oplus$, and at $1.2\ R_\oplus$ for planets with $10\ M_\oplus$. For both cases the results determined by Wagner et al. (2011b) using the Keane as well as the Rydberg EoS are given. As can be seen, the values for the heat flows are much smaller than for the earth, mainly due to the viscosity being two orders of magnitude higher than in the earth's mantle. Considering again eq. (3.87), when neglecting a pressure-dependent viscosity and assuming an earth-like mantle the heat flow across the core-mantle boundary would scale with the square of the radius of the planetary core, $Q_c \propto R_c^2$. This would mean for the $5\ M_\oplus$ planet listed in Table 5.1 above with a core radius of $0.8\ R_\oplus$ (which corresponds to $\sim 1.5\ R_{c,\oplus}$) in the case of the Rydberg EoS, that the heat flow would be a factor $\sim$ 2.2 higher, but instead, it is almost half the value of the earth. Of course, it is at least questionable whether this parameterized approach reproduces the conditions at the base of the mantle

		5 $M_\oplus$		10 $M_\oplus$	
Quantity	**Units**	**Keane EoS**	**Rydberg EoS**	**Keane EoS**	**Rydberg EoS**
r_c	$R_\oplus$	0.75	0.80	0.90	0.95
ρ_m	$kg\ m^{-3}$	7500	7000	9000	8500
ρ_c	$kg\ m^{-3}$	8560	8090	10500	9430
ρ_{cen}	$kg\ m^{-3}$	23400	20600	30100	24900
T_m	K	4500	4400	5600	5200
T_c	K	5770	5510	7280	6650
T_{cen}	K	9080	7970	11800	9790
η_b	$10^{23}\ Pa\ s$	2.5	2.5	2	2
F_b	$W\ m^{-2}$	0.020	0.014	0.029	0.024
$\mathbf{Q_c}$	TW	5.606	4.708	1.213	1.090

Table 5.1: Quantities used to determine the heat flow across the core-mantle boundary in 5 $M_\oplus$ and 10 $M_\oplus$ planets, using eqs. (3.87), (3.90), and (3.91), and the resulting heat flows; values, except Q_c, taken from Wagner et al. (2011b) using Fig.2 and Fig.3

within massive terrestrial planets adequately, let alone the fact that the parameters are either estimated from model curves from the results by Wagner et al. (2011b) or taken from calculations for the earth by Nimmo et al. (2004), and are not calculated independently. But it is very probable that the higher uncertainties arise from the parameterized approach instead of the estimation procedure. Comparing the heat fluxes in Table 5.1 with predicted heat fluxes for 10 $M_\oplus$ planets from Stamenković and Breuer (2010) shows that the results from above are an order of magnitude smaller than those from Stamenković and Breuer (2010). This has a huge impact on the cooling rate, as will be shown in the following. In principle, as soon as the core-mantle boundary heat flow is determined, the cooling rate can be calculated as described in Section 3.4.1 for the case of the earth. For this purpose the following set of assumptions is made, whose implications are discussed below. First of all, the radius of the inner core is required. Since the model by Wagner et al. (2011b) does not reproduce an inner core/outer core structure, no inner core radius is yielded. Theoretically it would be possible to determine it by combining a phase diagram of iron (or its melting curve) with the temperature gradient determined by a structure model like the ones by Wagner et al. (2011b) or Valencia et al. (2006), and using the intersection of the both as the point where the iron solidifies in the core. To simplify matters, it is assumed that the ratio of inner core to outer core radius is similar to the earth. Of course, it is difficult to justify this from a physical point of view, since it is thoroughly possible that terrestrial planets more massive than the earth have either smaller solid cores, or no inner cores at all (Gaidos et al., 2010), but in the absence of a structure model that can be employed it is the simplest scenario, and in this respect it can be regarded as an upper bound. Besides, it would be interesting to investigate the possibility of Mercury-like cores in terrestrial planets, although the arguments brought forward in Gaidos et al. (2010) seem to make this rather implausible. With the inner core radius determined in this way, the temperature at the inner core boundary is estimated from the diagrams in Wagner et al. (2011b), and the values are listed in Table 5.2. The specific heat capacity, C_p, and the thermal expansivity, α, are assumed constant throughout the core. This is probably an oversimplification, since α changes with radius, and also C_p will change in the cores of massive terrestrial planets, but the dependence on planetary radius of both quantities is poorly constrained, even more so for high-pressure phases of iron. The change in density across the inner core boundary due to the change in light element concentration, $\delta\rho_c$, is rather uncertain in the earth, and no information is available regarding other planets, hence the value from the earth is adopted. The difference in the temperature-pressure gradients of the melting curve and the adiabatic curve, $\frac{dT_m}{dP} - \frac{dT_a}{dP}$, is also unknown for other planets than the earth, and therefore the value of 1.3 is used, although the results by Gaidos

		5 $M_\oplus$		10 $M_\oplus$	
Quantity	**Units**	**Keane EoS**	**Rydberg EoS**	**Keane EoS**	**Rydberg EoS**
r_i	$R_\oplus$	0.263	0.281	0.316	0.333
T_i	K	8800	7900	11400	9600

Table 5.2: Values for inner core radius and temperature at the inner core boundary used to calculate energy and entropy budgets

et al. (2010) indicate that the ratio of these two gradients decreases with increasing planetary mass. This is also an issue that could be clarified by an adequate interior structure model. All other quantities are either used as listed in Table 5.1, or adopted from the earth, see Table 3.1.

If the energy budget for the cores of 5 $M_\oplus$ and 10 $M_\oplus$ planets is calculated using the values from scenario 2 in Table 4.1, one problem arises, as can be seen in Table 5.3. Since the radiogenic heat generated in the cores is distinctly larger than the heat flow across the core-mantle boundary, calculated as described above, a positive core cooling rate is obtained, which would mean that the core would not lose heat but heat up constantly. This is a result of the fact that core calculations were carried out assuming vigorous convection in the core, but as can be seen in Table 5.3, the heat conducted down the adiabat is much larger than the core-mantle boundary heat flow. Of course Q_k depends on the choice of values of α, C_p, and k, where the first two quantities are most uncertain. Moreover, deviations from a purely adiabatic core are ignored, and the cores in these planets are probably subadiabatic. Nevertheless, it is very unlikely that Q_k would be lower than Q_c as listed in Table 5.2, unless very low values for k or α would be used. This means that heat would be primarily transported by conduction and convection would probably come to a halt at all, in which case no dynamo would be possible.

Calculating the energy budget for the case of negligible radioactive contributions results in heat flows as displayed in Table 5.4, and in the

		5 $M_\oplus$		10 $M_\oplus$	
Quantity	**Units**	**Keane EoS**	**Rydberg EoS**	**Keane EoS**	**Rydberg EoS**
Q_c	TW	5.61	4.71	12.13	10.90
Q_k	TW	33.37	34.05	93.60	83.18
Q_R	TW	7.89	8.25	14.32	13.91
dT_c/dt	$K\ Gyr^{-1}$	7.12	10.00	7.15	8.37

Table 5.3: CMB heat flow determined by parameterized approach, Q_c, heat conducted down the adiabat, Q_k, radiogenic heat production in the core, Q_R, and core cooling rate, dT_c/dt; note that cooling rates are positive, which means heating up instead of cooling! Calculations see Appendix A and C.

		5 $M_\oplus$		10 $M_\oplus$	
Quantity	**Units**	**Keane EoS**	**Rydberg EoS**	**Keane EoS**	**Rydberg EoS**
Q_k	TW	33.37	34.05	93.60	83.18
Q_g	TW	1.68	1.63	4.58	4.58
Q_L	TW	1.64	1.42	3.66	3.29
Q_s	TW	2.29	1.66	3.90	3.03
Q_c	TW	5.61	4.71	12.13	10.90
dT_c/dt	$K\ Gyr^{-1}$	−17.49	−13.28	−39.54	−30.22
dr_i/dt	$km\ Gyr^{-1}$	89.42	77.79	112.64	109.93

Table 5.4: CMB heat flow determined by parameterized approach, Q_c, heat conducted down the adiabat, Q_k, and core cooling rate, dT_c/dt, for the case of negligible radiogenic core heat.Calculations see Appendix A and C.

case of scenario 3 from Table 4.1, i.e. for very low abundances, the heat flows are listed in Table 5.5. For these two cases negative cooling rates are obtained, though they are rather low compared to the value determined for the earth (see Table 3.2) considering the fact that these cores are much larger than the earth's core. Furthermore, these values have to be considered with caution, since one key assumption of core calculations, vigorous convection and subsequent homogeneity of the core, is violated.

Calculations of the entropy budget for 5 $M_\oplus$ and 10 $M_\oplus$ planets, which is primarily of interest in conjunction with the dynamo, are omitted, since

		5 $M_\oplus$		10 $M_\oplus$	
Quantity	**Units**	**Keane EoS**	**Rydberg EoS**	**Keane EoS**	**Rydberg EoS**
Q_k	TW	33.37	34.05	93.60	83.18
Q_R	TW	1.09	1.14	1.97	1.92
Q_g	TW	1.35	1.24	3.83	3.77
Q_L	TW	1.32	1.08	3.06	2.71
Q_s	TW	1.85	1.26	3.26	2.50
Q_c	TW	5.61	4.71	12.13	10.90
dT_c/dt	$K\ Gyr^{-1}$	-14.10	-10.07	-33.11	-24.91
dr_i/dt	$km\ Gyr^{-1}$	72.09	59.01	94.32	90.60

Table 5.5: CMB heat flow determined by parameterized approach, Q_c, heat conducted down the adiabat, Q_k, radiogenic heat production in the core, Q_R, and core cooling rate, dT_c/dt for the case of radiogenic element abundances described by scenario 3 in Table 4.1. Calculations see Appendix A and C.

convection in the cores of these planets is questionable. Therefore the attempt to estimate the magnetic fields of such planets is in vain, at least using the parameterized approach described above, because the difference of conductive and convective heat flows as shown above is much too large to assume significant convection in the core, which is a key assumption for the whole derivation described in Chapter 3. As can be seen in Fig 5.4, the heat conducted down the adiabat changes very rapidly with planetary radius. Calculations have been carried out using the Mathematica software package, Mathematica scripts can be found in Appendix B and Appendix C. As mentioned above, the parameterized approach is problematic, and probably does not capture the physical processes that prevail in the thermal boundary layers correctly. Thus, an improved model of heat transport in the mantle and in thermal boundary layers could yield more realistic values for Q_c, but at the moment such models are out of reach. Nevertheless, it seems very probable that conduction becomes more and more important with increasing mass in the cores of massive terrestrial planets and therefore magnetic fields are more and more unlikely. A possible influence of radiogenic heat production in the core, which increases linearly with core mass (see Fig 5.1), on the viscosity has not been scrutinized so far, but could possibly have a counteracting effect and decrease the viscosity enough to enable thermal and/or compositional convection in the cores of super-earths.

Finally, it should be stated that always the thermal evolution of a planet

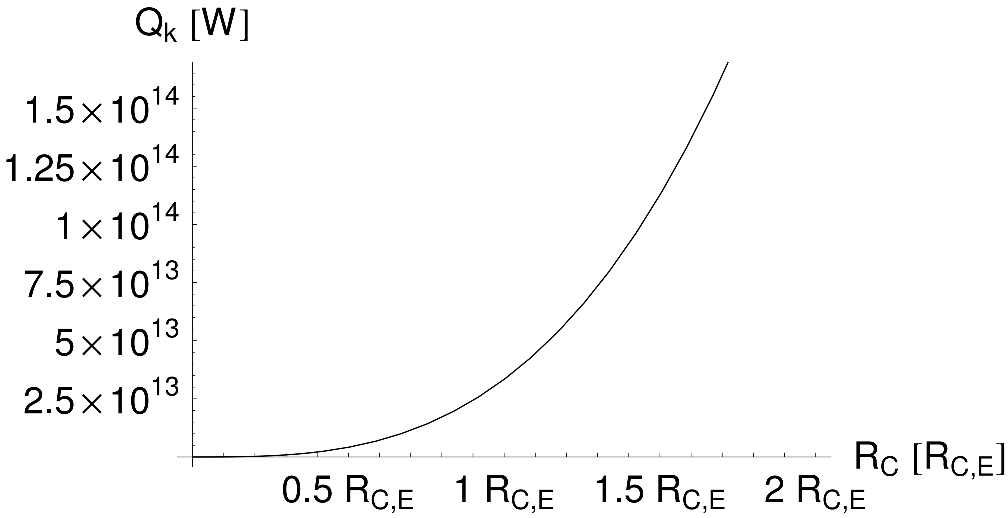

Figure 5.4: Dependence of heat conducted down the adiabat, Q_k, on planetary radius in units of earth radii. Calculation see Appendix B.

should be considered to evaluate its ability to generate a magnetic field over a significant period of time, and considering the planet only at a given moment in time is not sufficient. Therefore the cooling rate, and thus, the ability of the mantle to extract heat from the core is crucial. If the core cools too quickly, the dynamo will shut down rather early in the history of the planet and the whole core will be frozen out. The presence of radiogenic elements will probably delay this process and allow the outer core to stay fluid over longer time and thus enable the dynamo to operate accordingly longer. Moreover, for the dynamo the entropy production in the core is the decisive factor, not the energy budget. In this respect, radioactive heat contributes to this entropy budget, although it is dominated by entropy due to gravitational energy and latent heat.

Chapter 6

Impact on Super-Earths

6.1 Magnetic Fields in Super-Earths?

As mentioned in the last chapter, an increase in the planetary radius causes an according increase in pressure, which means that the viscosity of material in the lower mantle as well as in the outer core will be higher than in the interior of the earth. Thus, the question arises whether this increase in viscosity still enables convection vigorous enough to power a planetary dynamo. Gómez-Pérez and López-Morales (2010) developed a simple 1-D, two layer model for terrestrial planets employing a Birch-Murnaghan equation of state to calculate the seismic parameter ϕ. A fifth-order Runge-Kutta scheme was used to integrate the equations for density, pressure and mass from the surface to the center, assuming an earth-like composition of the mantle and pure iron in the core. To estimate the magnetic moment, the scaling law by Olsen and Christensen (2006) was used:

$$M \sim 4\pi r_0^3 \gamma \left(\overline{\rho_0} \mu_0\right)^{1/2} (FD)^{1/3}, \qquad (6.1)$$

where r_o is the radius of the iron core, $\gamma \sim 0.2$ is a numerical parameter, $\overline{\rho_0}$ is the bulk density in the core, μ_0 is the vacuum magnetic permeability, F is the convective heat flux, and D is the thickness of the fluid shell where convection occurs. In the view of Gómez-Pérez and López-Morales

(2010) magnetic fields of planets in close orbits will have significant magnetospheres (which is important for close-in planets around M dwarfs) and they conclude that planetary magnetic fields in the environment of strong, external magnetic fields are not impossible.
This is in contrast to the results of the parameterized 1D boundary layer model by Stamenković and Breuer (2010). Using a pressure- and temperature-dependent viscosity,

$$\eta(p,T) \propto exp\left(\frac{(E^* + pV^*(p))T_{ref} - (E^* + p_{ref}V^*_{ref})T)}{RT_{ref}T}\right), \tag{6.2}$$

where V^* and E^* are activation volume and energy, respectively, and p_{ref}, T_{ref}, and V^*_{ref} are the reference pressure, temperature, and activation volume, respectively, and employing the Wiedemann-Franz law and the Bloch-Grüneisen theory, Stamenković and Breuer (2010) arrive at a derivation for the critical heat flux across the core-mantle boundary, which determines the heat flux needed in order to drive a dynamo purely by thermal convection:

$$F_{crit} \propto \frac{\rho^{3.6}_{cmb} T_{cmb} g_{cmb}}{K_{T,cmb}}, \tag{6.3}$$

where $K_{T,cmb}$ is the bulk modulus, and all values are taken at the core side of the core-mantle boundary. In Fig. 6.1 the results are displayed, where it becomes obvious that in this model super-earths have heat fluxes too low to generate magnetic fields by thermal convection alone. This, of course, would not permit them to have convection driven by compositional buoyancy, but this would require at least a significant part of the core to be fluid. But it has to be considered that Stamenković and Breuer (2010) assumed a core-mass fraction, similar to the earth, of 32.59 %, which has not to be the case for super-earths. By applying a mixing length formulation for the temperature gradient in the mantle and using an Arrhenius law for a pressure- and temperature-dependent viscosity, Wagner et al. (2010) came to the conclusion that terrestrial exoplanets more massive than the earth have entirely solid iron cores due to the high pressure and subsequent high viscosity, impeding self-sustaining dynamos in these planets. Thus, it is still unclear whether massive terrestrial exoplanets have interior structures comparable to the earth.

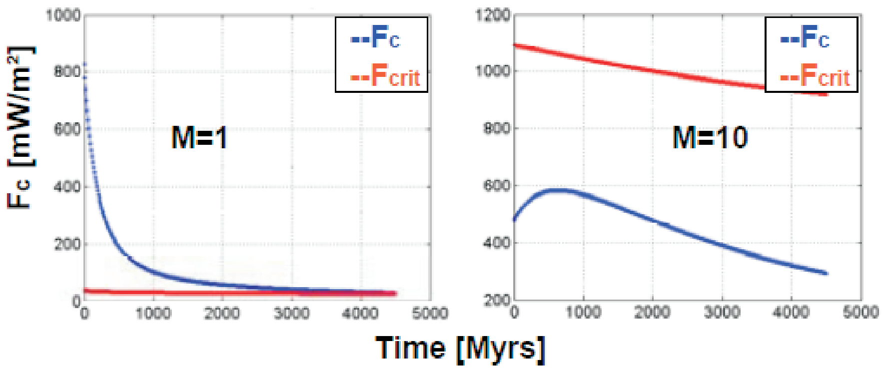

Figure 6.1: Critical heat flux across the core-mantle boundary necessary to drive a purely thermal dynamo, for 1 $M_{\oplus}$ and 10 $M_{\oplus}$. Image taken from Stamenković and Breuer (2010).

A more elaborate attempt to model thermodynamics in super-earths and its influence on magnetic field generation has been undertaken by Gaidos et al. (2010), using a third-order Birch-Murnaghan equation of state to model the planetary interior, and employing energy, entropy and heat flow calculations similar to Labrosse (2003), Nimmo et al. (2004), and Nimmo (2009), where the determination of heat transport in the mantle and the viscosity used is slightly different from Nimmo et al. (2004). The magnetic field is estimated using a scaling law following Christensen and Aubert (2006). Gaidos et al. (2010) also come to the conclusion that the probability for a long-lived dynamo decreases with increasing planetary mass, although this can be changed by higher surface temperatures like on planets in orbits close to their host stars. Whether a solid core grows from the center outwards or by "iron snow", i.e. crystallizing and sinking iron, towards the center depends on the ratio of the pressure-temperature slopes of the adiabat and the solidus. As can be seen in Fig. 6.2 the calculations of Gaidos et al. (2010) predict a decrease of this ratio for increasing planetary mass, and for a ratio smaller than 1 a stratified core is expected, which probably prevents a dynamo from being active. The results of this model regarding the dynamo lifetime are shown in Fig. 6.3. It has to be pointed out that this model neglects some possibly important effects, like the properties of iron and silicates at very high pressures or the depression of the melting point caused by light elements in the core. Furthermore it maybe employs erroneous or inadequate approaches, like the use of a third-order Birch-Murnaghan equation of state, instead of a Keane-EoS, which could describe high-pressure conditions more adequately, and the assumption of a fully convecting mantle, which other authors consider improbable in a massive terrestrial planet (see below). And again, a parameterized convection model for the mantle could disregard important effects and lead to unrealistic heat flows across the core mantle boundary.

Recently, Stamenković et al. (2011) derived a series of quantities, like thermal expansivity and heat capacity, for the mantles of super-earths. They derived a viscosity increase for 10 $M_{\oplus}$ planets of 15 orders of magnitude, an increase of thermal conductivity by a factor of 7, and a decrease of thermal expansivity by a factor of 8, all throughout an adiabatic mantle. This implies that heat transfer is dominantly carried out by conduction, and significant convection does not take place. Moreover, it raises questions whether such planets are differentiated at all. In light of these results, whole mantle convection seems very improbable, and the generation of self-sustaining magnetic fields as well as the ability to sustain plate tectonics is very questionable. It should be noted that Van Heck and Tackley (2011) arrived at contrary results with their model, and derived an increasing

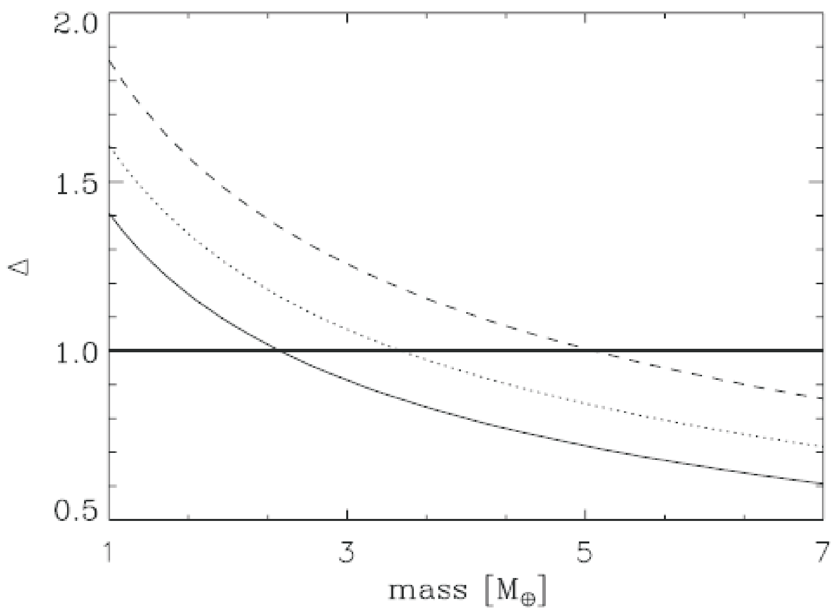

Figure 6.2: Dependence of the ratio of the pressure-temperature slopes for the adiabat and the solidus, Δ, vs. planetary mass. Image taken from Gaidos et al. (2010).

probability for plate tectonics with increasing planetary mass. But their model assumed constant physical properties taken from the earth, a ratio of core-mantle radii similar to the earth, and neglected the dependence of the viscosity on pressure, which is unlikely to produce reliable results, as described above. An effect that is neglected in all current models is the influence radiogenic heat produced in these cores could have on the viscosity, as mentioned in the last chapter. Since this contribution is not negligible, as can be seen in Table 5.3, it would be interesting to investigate the possibility of vigorously convecting cores due to their radiogenic heat production in massive terrestrial planets despite the counteracting influence of pressure.

6.2 Habitability of Super-Earths

Habitability is the theoretical possibility of life-supporting conditions on a planetary body and is governed by a number of prerequisites a planet and

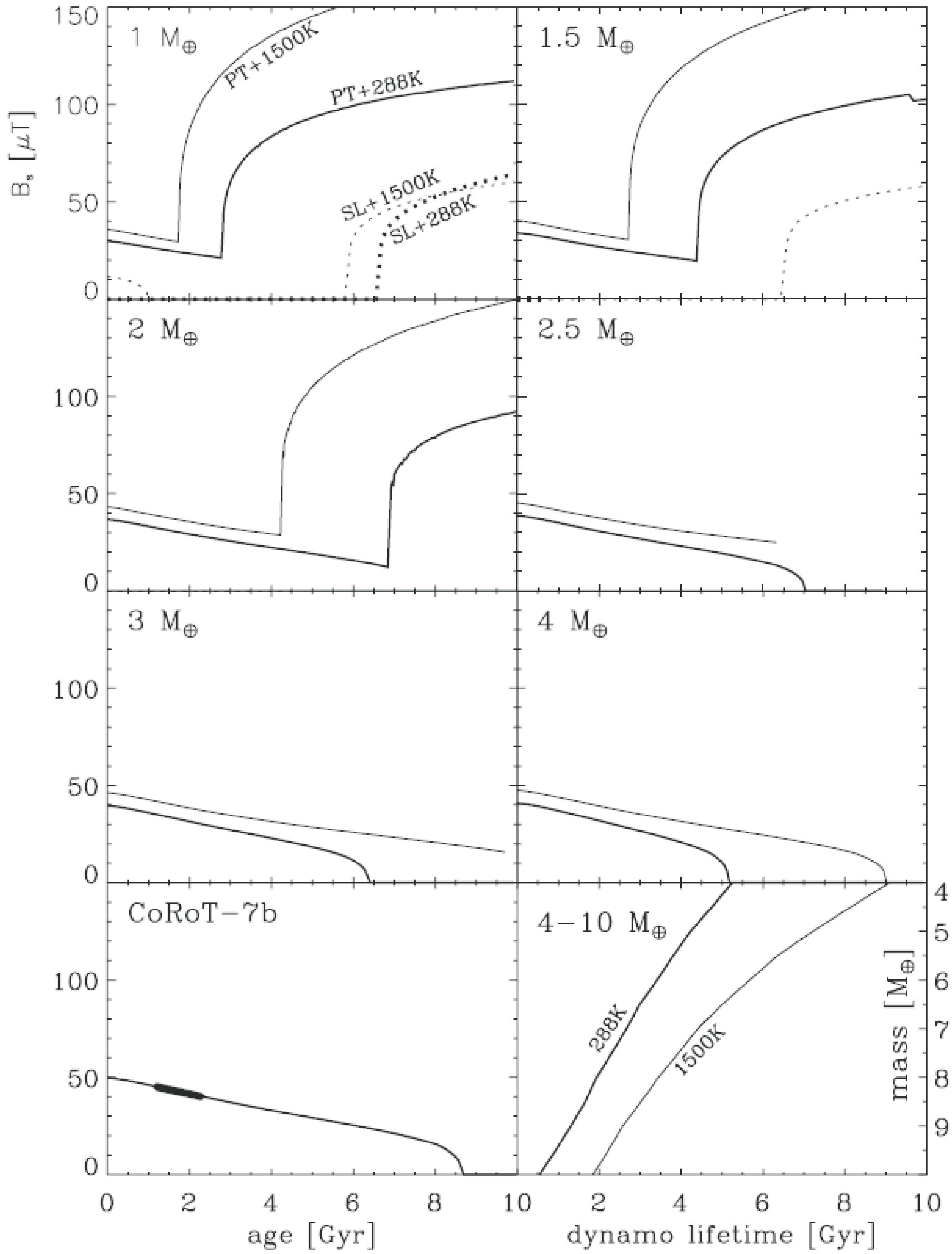

Figure 6.3: Development of the average surface field strength for exoplanets with different masses. Detailed description see Gaidos et al. (2010). Image taken from Gaidos et al. (2010).

its host star must satisfy. One key term in this context is the habitable zone (HZ). This is a zone around a star that allows liquid water to exist and first of all depends on the orbital distance of a planet from its host star. Secondly, it is affected by the spectral type of the star, which determines the radiative energy emitted in different parts of the spectrum, and the composition of the planetary atmosphere, which determines the amount of light that is reflected or scattered into space or transmitted to the surface. This concept has been reproduced for earth-like conditions by Kasting et al. (1993), and other types of HZs have been proposed, like the UV-HZ by Buccino et al. (2006), which accounts for the influence of UV-radiation, the galactic HZ (Lineweaver et al., 2004), which considers the position of the star system in the galaxy and its influence on heavy element abundance or the impact of potential super-novae on the emergence and evolution of life. An extension of this idea is the "life supporting zone" (LSZ, Leitner et al. (2010); Neubauer et al. (2011)), in which the geocentric view of water as the only possible solvent to support life is abandoned. Therefore it has to be considered that different solvents are in the liquid phase over different temperature ranges, which determines the width of the habitable zone for each solvent or composite of solvent with water. The HZs for all these solvents and composites compose the LSZ of a planet.

Another key feature of a habitable planet for life as we know it is its ability to generate a self-sustaining magnetic field over geological time, in order to shield life forms from high-energetic particles from space, which have a devastating effect on cells, at least in earth-like organisms. Although the question of how and when life emerged on earth is still unanswered, it seems evident that the magnetosphere of the earth had a positive effect on its evolution, and although life forms are known that can deal with very high dosages of radiation (Deinococcus radiodurans, e.g. Cox and Battista (2005), Fig. 6.4), it is very unlikely that life would have emerged on the surface of a planet that is constantly bombarded by particles from its parent star or the cosmos. But theories supporting an emergence of life in either the oceans (Wächtershäuser, 1992) or the upper 5-10 km of the crust, the so-called "deep hot biosphere" (Gold, 1999), are not in need of a magnetic field that protects the first organisms from cosmic radiation. Therefore, only in the context of surface life, the magnetic field of a planet is crucial for its emergence. Thus, the ability of super-earths to generate magnetic fields is of vital importance in order to evaluate their potential habitability for, at least, primitive life at the surface of a planet. Since current models predict a decreasing probability for magnetic fields of massive terrestrial planets with increasing mass over geological time, it is doubtful whether super-earths that are more massive than 2-3 times the mass of the earth (see discussion in Gaidos et al. (2010)) can harbor life at their surface. Nevertheless, that does probably not prevent life from emerging either in an ocean or in the crust of a planet.

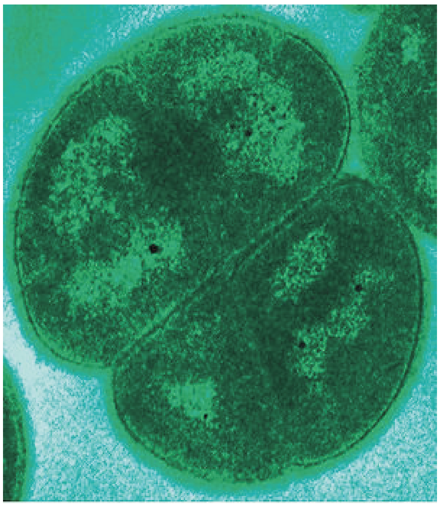

Figure 6.4: The extremophilic bacterium Deinococcus Radiodurans is able to deal with radiation levels of more than 10.000 Gy (for humans 6 Gy are deadly) and can be found in the cooling ponds of nuclear power plants. Image taken from http://de.wikipedia.org/wiki/Deinococcus_radiodurans.

Chapter 7

Concluding Remarks

The problem of evaluating a terrestrial planet's ability to generate a self-sustaining magnetic field and its dependence on planetary mass or cores size is a very complex one and many aspects have to be considered in order to yield reasonable and physically sound results. An ideal model would have to incorporate a complete model of the inner structure of the planet, ideally employing an equation of state that allows for high-pressure conditions in the lower mantle and the core, like the Keane-EoS, to yield gradients of density, pressure, and temperature inside the planet and at boundaries like the core-mantle boundary. Furthermore, an adequate modelling of heat flow from the core into the mantle should be included, possibly avoiding parameterized convection models and using more advanced schemes, if available, to get reasonable heat flows across the core mantle boundary. As explained above, core cooling is controlled by the mantle, and therefore this part decides on success or defeat of the whole model. Moreover, it yields the core cooling rate, which can further be used to calculate the different contributions to the energy and entropy budget of the core as described in Chapter 3. By applying a scaling law, as explained in Section 2.3, the magnetic moment of the planet can be estimated, as soon as the heat flows are determined (given that significant convection takes place in the core). What should be kept in mind is the fact, that significant amounts of radioactive elements could be present in the core, which would have an influence on the core cooling rate and the lifetime of a potential dynamo. Although the radiogenic heat in the core only depends linearly on the element abundances and the mass of the core, its importance for the thermal history of a planet can not be neglected. Moreover, it possibly could influence the viscosity in massive terrestrial planets sufficiently to sustain convection, although this is a very speculative idea.

In the simple model described in the previous chapters it has been shown that high viscosities in massive terrestrial planets lead to heat flows across the core-mantle boundary much lower than expected, especially if radioactive species are accounted for. Although due to the parameterized approach these values have to be considered carefully, it is probable that the qualitative trend is correct, viz. the increasing relevance of conduction as a transport mechanism of heat, instead of convection. This would mean that convection in the cores of massive terrestrial planets is questionable as well as a full differentiation of the planet. Therefore an influence of the core size on the magnetic field is not given, since the very existence of a core depends on the conditions prevalent at very high-pressures within super-earths, and these are still very speculative. Thus, if there exists a mechanism that allows thermal or compositional convection in the cores of planets more massive than the earth over geological time, magnetic fields will be present long enough to protect potential life from high-energetic radiation, otherwise these planets will be rather unpleasant places, but possibly that is just another challenge life has to cope with, to succeed as it did on earth.

Appendix A

Mathematica Scripts - Calculations for the Earth

A.1 Q_g

rho0 = 7900

7900

rc = 3480 * 1000

3480000

ri = 1220 * 1000

1220000

K0 = 500 * 10^9

500000000000

$\boldsymbol{G = 6.67384 * 10\char`^ - 11}$

6.67384×10^{-11}

rhocen = 12500

12500

$\boldsymbol{L = \mathrm{Sqrt}[(3 * \mathrm{K0} * (\mathrm{Log}[\mathrm{rhocen/rho0}] + 1))/(2 * \pi * G * \mathrm{rho0} * \mathrm{rhocen})]}$

7.26954×10^{6}

$\boldsymbol{\psi = (2/3 * \pi * G * \mathrm{rhocen} * \mathrm{ri}\char`^2 * (1 - (3 * \mathrm{ri}\char`^2)/(10 * L\char`^2))) -}$

$\boldsymbol{(2/3 * \pi * G * \mathrm{rhocen} * \mathrm{rc}\char`^2 * (1 - (3 * \mathrm{rc}\char`^2)/(10 * L\char`^2)))}$

-1.71261×10^{7}

$\boldsymbol{\mathrm{Moc} = (4/3 * \pi * \mathrm{rhocen} * \mathrm{rc}\char`^3 * \mathrm{Exp}[-\mathrm{rc}\char`^2/L\char`^2] * (1 + (2/5) * (\mathrm{rc}\char`^2/L\char`^2))) -}$

$\boldsymbol{(4/3 * \pi * \mathrm{rhocen} * \mathrm{ri}\char`^3 * \mathrm{Exp}[-\mathrm{ri}\char`^2/L\char`^2] * (1 + (2/5) * (\mathrm{ri}\char`^2/L\char`^2)))}$

1.82211×10^{24}

Δrhoc = 575

575

$\mathbf{dri = 609.9896322325887 * 1000/(10\text{^}9 * 86400 * 365)}$

1.93426×10^{-11}

$\mathbf{C^2 = (3 * \mathit{L}\text{^}2)/16 - ((rc\text{^}2)/2) * (1 - ((3 * rc\text{^}2)/(10 * \mathit{L}\text{^}2)))}$

4.26975×10^{12}

$\mathbf{integralterm = ((8 * \pi\text{^}2 * rhocen\text{^}2 * \mathit{G})/3)*}$
$\mathbf{(((((3/20 * rc\text{^}5) - (\mathit{L}\text{^}2/8 * rc\text{^}3) - (\mathit{L}\text{^}2 * C^2 * rc)) * Exp[-rc\text{^}2/\mathit{L}\text{^}2])+}$
$\mathbf{(C^2/2) * \mathit{L}\text{^}3 * Sqrt[\pi] * Erf[rc/\mathit{L}])-}$
$\mathbf{((((3/20 * ri\text{^}5) - (\mathit{L}\text{^}2/8 * ri\text{^}3) - (\mathit{L}\text{^}2 * C^2 * ri)) * Exp[-ri\text{^}2/\mathit{L}\text{^}2])+}$
$\mathbf{(C^2/2) * \mathit{L}\text{^}3 * Sqrt[\pi] * Erf[ri/\mathit{L}]))}$

-1.36055×10^{31}

$\mathbf{Qg = (integralterm - Moc * \psi) * \Delta rhoc * ((4 * \pi * ri\text{^}2)/Moc) * dri}$

2.00935×10^{12}

A.2 Q_k

rc = 3480 * 1000

3480000

k = 40

40

Tc = 4100

4100

cp = 840

840

α = 1.35 * 10^ − 5

0.0000135

rhocen = 12500

12500

G = 6.67384 * 10^ − 11

6.67384×10^{-11}

Dd = Sqrt[(3 * cp)/(2 * π * α * rhocen * G)]

5.96761×10^{6}

Qk = (8 * π * rc^3 * k * Tc)/Dd^2

4.87776×10^{12}

A.3 Q_L

ri = 1220 ∗ 1000

1220000

LH = 750000

750000

rhocen = 12500

12500

rho0 = 7900

7900

K0 = 500 ∗ 10^9

500000000000

***G* = 6.67384 ∗ 10^ − 11**

6.67384×10^{-11}

***L* = Sqrt[(3 ∗ K0 ∗ (Log[rhocen/rho0] + 1))/(2 ∗ π ∗ *G* ∗ rho0 ∗ rhocen)]**

7.26954×10^{6}

rhoi = rhocen ∗ Exp[−ri^2/*L*^2]

12152.9

ΔdTdP = 1.3/10^9

1.3×10^{-9}

Ti = 5520

5520

Tc = 4100

4100

dTc = −30/(10^9 ∗ 86400 ∗ 365)

$-\frac{1}{1051200000000000}$

***g* = (4 ∗ π/3) ∗ *G* ∗ rhocen ∗ ri ∗ (1 − ((3 ∗ ri^2)/(5 ∗ *L*^2)))**

4.19114

QL = −(4 ∗ π ∗ ri^2 ∗ LH ∗ Ti)/(ΔdTdP ∗ *g*) ∗ (1/Tc) ∗ dTc

3.2975×10^{12}

A.4 Q_R

CK40 = 2.44 * 10^ − 8

2.44×10^{-8}

CU238 = 2.98 * 10^ − 9

2.98×10^{-9}

CU235 = 2.13 * 10^ − 11

2.13×10^{-11}

CTh232 = 5.8 * 10^ − 10

5.8×10^{-10}

HK40 = 2.92 * 10^ − 5

0.0000292

HTh232 = 2.64 * 10^ − 5

0.0000264

HU238 = 9.46 * 10^ − 5

0.0000946

HU235 = 5.69 * 10^ − 4

0.000569

H0 = CU235 * HU235 + CU238 * HU238 + CTh232 * HTh232 + CK40 * HK40

1.02182×10^{-12}

***L* = 7269.54 * 10^3**

7.26954×10^{6}

***G* = 6.6873 * 10^ − 11**

6.6873×10^{-11}

rho0 = 7019

7019

rhocen = 12500

12500

K0 = (*L*^2 * 2 * π * *G* * rho0 * rhocen)/(3 * Log[(rhocen/rho0) + 1])

6.34938×10^{11}

***R* = 3480 * 10^3**

3480000

Mc = 4 * π * rhocen * (((−*L*^2)/2) * *R* * Exp[(−*R*^2)/(*L*^2)] + ((*L*^3)/4) * Sqrt[π]
***N*[Erf[*R*/*L*], 5]) − 4 * π * rhocen * (((*L*^3)/4) * Sqrt[π] * *N*[Erf[0], 5])**

1.92668×10^{24}

QR = Mc * H0

1.96872×10^{12}

A.5 Q_s

K0 = 500 * 10^9

500000000000

rhocen = 12500

12500

rho0 = 7900

7900

G = 6.67384 * 10^ − 11

6.67384×10^{-11}

L = Sqrt[(3 * K0 * (Log[rhocen/rho0] + 1))/(2 * π * G * rho0 * rhocen)]

7.26954×10^{6}

Cp = 840

840

α = 1.35 * 10^ − 5

0.0000135

Dd = Sqrt[(3 * Cp)/(2 * π * α * rhocen * G)]

5.96761×10^{6}

A^2 = ((1/L^2) + (1/Dd^2))^(−1)

2.12753×10^{13}

Tcen = 5756

5756

Tc = 4100

4100

rc = 3480 * 1000

3480000

Is = (4/3) * π * Tcen * rhocen * rc^3 * Exp[−rc^2/A^2] * (1 + (2/5) * (rc^2/A^2))

8.82541×10^{27}

dTc = −30/(10^9 * 86400 * 365)

$-\frac{1}{1051200000000000}$

Qs = −(Cp/Tc) * dTc * Is

1.72006×10^{12}

A.6 $\tilde{Q}_T$

K0 = 500 * 10^9

500000000000

LH = 750000

750000

rhocen = 12500

12500

rho0 = 7900

7900

$\boldsymbol{G = 6.67384 * 10\hat{\ } - 11}$

6.67384×10^{-11}

L = Sqrt[(3 * K0 * (Log[rhocen/rho0] + 1))/(2 * π * G * rho0 * rhocen)]

7.26954×10^{6}

Cp = 840

840

α = 1.35 * 10^ − 5

0.0000135

Dd = Sqrt[(3 * Cp)/(2 * π * α * rhocen * G)]

5.96761×10^{6}

A^2 = ((1/L^2) + (1/Dd^2))^(−1)

2.12753×10^{13}

Tcen = 5756

5756

Tc = 4100

4100

rc = 3480 * 1000

3480000

Is = (4/3) * π * Tcen * rhocen * rc^3 * Exp[−rc^2/A^2] * (1 + (2/5) * (rc^2/A^2))

8.82541×10^{27}

ri = 1220 * 1000

1220000

ψ = (2/3 * π * G * rhocen * ri^2 * (1 − (3 * ri^2)/(10 * L^2))) − (2/3 * π * G * rhocen * rc^2 *(1 − (3 * rc^2)/(10 * L^2)))

-1.71261×10^{7}

Moc = (4/3 * π * rhocen * rc^3 * Exp[−rc^2/L^2] * (1 + (2/5) * (rc^2/L^2)))− (4/3 * π * rhocen * ri^3 * Exp[−ri^2/L^2] * (1 + (2/5) * (ri^2/L^2)))

1.82211×10^{24}

ΔdTdP = −1.3/10^9

-1.3×10^{-9}

Δrhoc = 575

575

Ti = 5520

5520

rhoi = rhocen ∗ Exp[−ri^2/L^2]

12152.9

g = (4 ∗ π/3) ∗ G ∗ rhocen ∗ ri ∗ (1 − ((3 ∗ ri^2)/(5 ∗ L^2)))

4.19114

dri = (1/ΔdTdP) ∗ (Ti/(rhoi ∗ g)) ∗ (1/Tc)

−20333.

C^2 = (3 ∗ L^2)/16 − ((rc^2)/2) ∗ (1 − ((3 ∗ rc^2)/(10 ∗ L^2)))

4.26975×10^{12}

qstilde = −(Cp/Tc) ∗ Is

-1.80813×10^{27}

integralterm =
((8 ∗ π^2 ∗ rhocen^2 ∗ G)/3)∗
(((((3/20 ∗ rc^5) − (L^2/8 ∗ rc^3) − (L^2 ∗ C^2 ∗ rc)) ∗ Exp[−rc^2/L^2]) + (C^2/2) ∗ L^3 ∗ Sqrt[π]
∗Erf[rc/L])−
((((3/20 ∗ ri^5) − (L^2/8 ∗ ri^3) − (L^2 ∗ C^2 ∗ ri)) ∗ Exp[−ri^2/L^2]) + (C^2/2) ∗ L^3 ∗ Sqrt[π]
∗Erf[ri/L]))

-1.36055×10^{31}

qgtilde = (integralterm − Moc ∗ ψ) ∗ Δrhoc ∗ ((4 ∗ π ∗ ri^2)/Moc) ∗ dri

-2.11223×10^{27}

qltilde = (4 ∗ π ∗ ri^2 ∗ LH ∗ rhoi) ∗ dri

-3.46633×10^{27}

qttilde = qstilde + qgtilde + qltilde

-7.3867×10^{27}

QR = 1.968716214453684*^12

1.96872×10^{12}

dTc = ((9 ∗ 10^12 − QR)/qttilde) ∗ 86400 ∗ 365 ∗ 10^9

−30.0186

Plot [((9 ∗ 10^12 − QR)/qttilde) ∗ 86400 ∗ 365 ∗ 10^9, {QR, 0, 9 ∗ 10^12}, AxesOrigin → {0, −38.5},
AxesLabel-> {"Q_R [W]", "dT_C/dt [K Gyr^{-1}]"} , TextStyle → {FontFamily → Arial, FontSize → 14}]

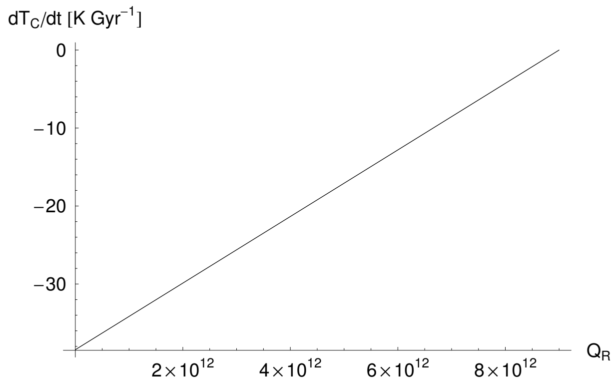

−Graphics−

A.7 dr_i/dt

$\mathbf{\Delta dTdP = 1.3/10\hat{}9}$

1.3×10^{-9}

$\mathbf{Ti = 5520}$

5520

$\mathbf{Tc = 4100}$

4100

$\mathbf{dTc = -30/(10\hat{}9 * 86400 * 365)}$

$-\frac{1}{1051200000000000}$

$\mathbf{ri = 1220 * 1000}$

1220000

$\mathbf{rho0 = 7900}$

7900

$\mathbf{K0 = 500 * 10\hat{}9}$

500000000000

$\boldsymbol{G = 6.67384 * 10\hat{}\ -11}$

6.67384×10^{-11}

$\mathbf{rhocen = 12500}$

12500

$\boldsymbol{L = \mathrm{Sqrt}[(3 * \mathrm{K0} * (\mathrm{Log}[\mathrm{rhocen/rho0}] + 1))/(2 * \pi * G * \mathrm{rho0} * \mathrm{rhocen})]}$

7.26954×10^{6}

$\boldsymbol{\mathrm{rhoi} = \mathrm{rhocen} * \mathrm{Exp}[-\mathrm{ri}\hat{}2/L\hat{}2]}$

12152.9

$\boldsymbol{g = (4 * \pi/3) * G * \mathrm{rhocen} * \mathrm{ri} * (1 - ((3 * \mathrm{ri}\hat{}2)/(5 * L\hat{}2)))}$

4.19114

$\boldsymbol{\mathrm{dri} = -(((1/(\Delta \mathrm{dTdP})) * (\mathrm{Ti}/(\mathrm{rhoi} * g)) * (1/\mathrm{Tc}) * \mathrm{dTc}) * 10\hat{}9 * 86400 * 365)/1000}$

609.99

A.8 Q_C

$\mathbf{R = 3480000}$

3480000

$\mathbf{kb = 5.8}$

5.8

$\boldsymbol{\kappa}\mathbf{b = 10 * 10\hat{}\ -7}$

$\frac{1}{1000000}$

$\mathbf{Tc = 4155}$

4155

$\mathbf{Rac = 600}$

600

$\mathbf{rhom = 4800}$

4800

$\boldsymbol{g}\mathbf{ = 9.8}$

9.8

$\boldsymbol{\alpha}\mathbf{m = 2.2 * 10\hat{}\ -5}$

0.000022

$\mathbf{Tm = 2725}$

2725

$\mathbf{Ta = (Tc + Tm)/2.}$

$3440.$

$\boldsymbol{f}\mathbf{ = 10}$

10

$\boldsymbol{\eta}\mathbf{0 = 1.0 * 10\hat{}21}$

$1. \times 10^{21}$

$\boldsymbol{\zeta}\mathbf{ = 1.0 * 10\hat{}\ -2}$

0.01

$\mathbf{T1 = 3400}$

3400

$\boldsymbol{\eta}\mathbf{b = }\boldsymbol{f}\mathbf{ * }\boldsymbol{\eta}\mathbf{0 * Exp[-}\boldsymbol{\zeta}\mathbf{ * (Ta - T1)]}$

6.7032×10^{21}

$\boldsymbol{\delta}\mathbf{b = ((Rac * }\boldsymbol{\kappa}\mathbf{b * }\boldsymbol{\eta}\mathbf{b)/(rhom * }\boldsymbol{g}\mathbf{ * }\boldsymbol{\alpha}\mathbf{m * (Tc - Tm)))\hat{}(1/3)}$

$139552.$

$\mathbf{Fb = kb * (Tc - Tm)/}\boldsymbol{\delta}\mathbf{b}$

0.0594331

$\mathbf{Qc = 4 * }\boldsymbol{\pi}\mathbf{ * }\boldsymbol{R}\mathbf{\hat{}2 * Fb}$

9.04475×10^{12}

A.9 E_g

Qg = 2.00935 * 10^12

2.00935×10^{12}

Tc = 4100

4100

Eg = Qg/Tc

4.90085×10^{8}

A.10 E_k

$\boldsymbol{k = 40}$

40

rc = 3480 ∗ 1000

3480000

Cp = 840

840

$\boldsymbol{\alpha = 1.35 * 10\hat{} - 5}$

0.0000135

rhocen = 12500

12500

$\boldsymbol{G = 6.67384 * 10\hat{} - 11}$

6.67384×10^{-11}

Dd = Sqrt[(3 ∗ Cp)/(2 ∗ π ∗ α ∗ rhocen ∗ G)]

5.96761×10^{6}

Ek = −(16 ∗ π ∗ k ∗ rc^5)/(5 ∗ Dd^4)

-1.61828×10^{8}

A.11 E_L

QL = 3.2975 * 10^12

3.2975×10^{12}

Tc = 4100

4100

Ti = 5520

5520

EL = QL * (Ti − Tc)/(Tc * Ti)

2.06895×10^{8}

A.12 E_R

K0 = 500 * 10^9

500000000000

rhocen = 12500

12500

rho0 = 7900

7900

G = 6.67384 * 10^ − 11

6.67384×10^{-11}

L = Sqrt[(3 * K0 * (Log[rhocen/rho0] + 1))/
(2 * π * G * rho0 * rhocen)]

7.26954×10^{6}

Cp = 840

840

α = 1.35 * 10^ − 5

0.0000135

Dd = Sqrt[(3 * Cp)/(2 * π * α * rhocen * G)]

5.96761×10^{6}

B^2 = ((1/L^2) − (1/Dd^2))^(−1)

-1.09203×10^{14}

Tcen = 5756

5756

Tc = 4100

4100

rc = 3480 * 1000

3480000

It = ((4 * π * rhocen)/(3 * Tcen)) * rc^3*
(1 − (3/5) * (rc^2/B^2))

4.08877×10^{20}

Mc =
4 * π * rhocen*
(((−L^2)/2) * rc * Exp[(−rc^2)/(L^2)]+
((L^3)/4) * Sqrt[π] * N[Erf[rc/L], 5])−
4 * π * rhocen * (((L^3)/4) * Sqrt[π] * N[Erf[0], 5])

1.92668×10^{24}

CK40 = 2.44 * 10^ − 8

2.44×10^{-8}

$\mathbf{CU238 = 2.98 * 10^\wedge - 9}$

2.98×10^{-9}

$\mathbf{CU235 = 2.13 * 10^\wedge - 11}$

2.13×10^{-11}

$\mathbf{CTh232 = 5.8 * 10^\wedge - 10}$

5.8×10^{-10}

$\mathbf{HK40 = 2.92 * 10^\wedge - 5}$

0.0000292

$\mathbf{HTh232 = 2.64 * 10^\wedge - 5}$

0.0000264

$\mathbf{HU238 = 9.46 * 10^\wedge - 5}$

0.0000946

$\mathbf{HU235 = 5.69 * 10^\wedge - 4}$

0.000569

$\mathbf{H0 = CU235 * HU235 + CU238 * HU238 + CTh232 * HTh232 +}$

$\mathbf{CK40 * HK40}$

1.02182×10^{-12}

$\mathbf{Er = (Mc/Tc - It) * H0}$

6.23765×10^{7}

A.13 E_s

K0 = 500 * 10^9

500000000000

rhocen = 12500

12500

rho0 = 7900

7900

G = 6.67384 * 10^ − 11

6.67384×10^{-11}

L = Sqrt[(3 * K0 * (Log[rhocen/rho0] + 1))/
(2 * π * G * rho0 * rhocen)]

7.26954×10^{6}

Cp = 840

840

α = 1.35 * 10^ − 5

0.0000135

Dd = Sqrt[(3 * Cp)/(2 * π * α * rhocen * G)]

5.96761×10^{6}

A00B2 = ((1/L^2) + (1/Dd^2))^(−1)

2.12753×10^{13}

Tcen = 5756

5756

Tc = 4100

4100

rc = 3480 * 1000

3480000

Is = (4/3) * π * Tcen * rhocen * rc^3 * Exp[−rc^2/A00B2]*
(1 + (2/5) * (rc^2/A00B2))

8.82541×10^{27}

Mc =
4 * π * rhocen*
(((−L^2)/2) * rc * Exp[(−rc^2)/(L^2)]+
((L^3)/4) * Sqrt[π] * N[Erf[rc/L], 5])−
4 * π * rhocen * (((L^3)/4) * Sqrt[π] * N[Erf[0], 5])

1.92668×10^{24}

dT = −30.086/(86400 * 365 * 10^9)

-9.54021×10^{-16}

$$\mathbf{Es = (Cp/Tc) * (Mc - (Is/Tc)) * dT}$$

4.41464×10^{7}

Appendix B

Mathematica Scripts - Calculations for $5M_{\oplus}$ Planets

B.1 Keane EoS - Normal

B.1.1 Q_k

rc = 0.75 * 6378 * 1000

4.7835×10^{6}

k = 40

40

Tc = 5770

5770

cp = 840

840

α = 1.35 * 10^ − 5

0.0000135

rhocen = 23400

23400

G = 6.67384 * 10^ − 11

6.67384×10^{-11}

Dd = Sqrt[(3 * cp)/(2 * π * α * rhocen * G)]

4.36162×10^{6}

Qk = (8 * π * rc^3 * k * Tc)/Dd^2

3.33747×10^{13}

Plot [(8 * π * rc^3 * k * Tc)/Dd^2, {rc, 0, 2 * rc}, AxesLabel-> {"R_C [$R_{C,E}$]", "Q_k [W]"} , AxesOrigin → {0, 0}, Ticks → {{{0 * rc, ""}, {0.1 * rc, ""}, {0.2 * rc, ""}, {0.3 * rc, ""}, {0.4 * rc, ""},

```
{0.5 * rc, "0.5 R_{C,E}"} , {0.6 * rc, ""}, {0.7 * rc, ""}, {0.8 * rc, ""}, {0.9 * rc, ""}, {1 * rc, "1 R_{C,E}"} ,
{1.1 * rc, ""}, {1.2 * rc, ""}, {1.3 * rc, ""}, {1.4 * rc, ""}, {1.5 * rc, "1.5 R_{C,E}"} ,
 {1.6 * rc, ""}, {1.7 * rc, ""}, {1.8 * rc, ""}, {1.9 * rc, ""}, {2 * rc, "2 R_{C,E}"}} ,
Automatic}, TextStyle → {FontFamily → Arial, FontSize → 14}]
```

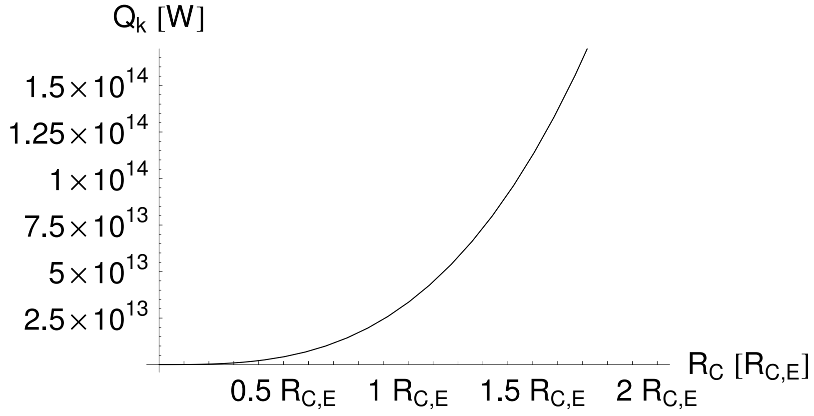

−Graphics−

B.1.2 Q_R

$\mathbf{CK40upper = 4.76 * 10^{\wedge} - 8}$

4.76×10^{-8}

$\mathbf{CK40mean = 2.44 * 10^{\wedge} - 8}$

2.44×10^{-8}

$\mathbf{CK40lower = 1.31 * 10^{\wedge} - 9}$

1.31×10^{-9}

$\mathbf{CU238upper = 4.96 * 10^{\wedge} - 9}$

4.96×10^{-9}

$\mathbf{CU238mean = 2.98 * 10^{\wedge} - 9}$

2.98×10^{-9}

$\mathbf{CU238lower = 9.93 * 10^{\wedge} - 10}$

9.93×10^{-10}

$\mathbf{CU235upper = 3.55 * 10^{\wedge} - 11}$

3.55×10^{-11}

$\mathbf{CU235mean = 2.13 * 10^{\wedge} - 11}$

2.13×10^{-11}

$\mathbf{CU235lower = 7.1 * 10^{\wedge} - 12}$

7.1×10^{-12}

$\mathbf{CTh232upper = 1.0 * 10^{\wedge} - 9}$

$1. \times 10^{-9}$

$\mathbf{CTh232mean = 5.8 * 10^{\wedge} - 10}$

5.8×10^{-10}

$\mathbf{CTh232lower = 1.7 * 10^{\wedge} - 10}$

1.7×10^{-10}

$\mathbf{HK40 = 2.92 * 10^{\wedge} - 5}$

0.0000292

$\mathbf{HTh232 = 2.64 * 10^{\wedge} - 5}$

0.0000264

$\mathbf{HU238 = 9.46 * 10^{\wedge} - 5}$

0.0000946

$\mathbf{HU235 = 5.69 * 10^{\wedge} - 4}$

0.000569

$\mathbf{H0 = CU235mean * HU235 + CU238mean * HU238 + CTh232mean * HTh232 + CK40mean * HK40}$

1.02182×10^{-12}

$\mathbf{H1 = CU235lower * HU235 + CU238lower * HU238 + CTh232lower * HTh232 + CK40lower * HK40}$

1.40718×10^{-13}

```
H2 = CU235upper * HU235 + CU238upper * HU238 + CTh232upper * HTh232 + CK40upper * HK40
```

1.90574×10^{-12}

```
rhocen = 23400
```

23400

```
rho0 = 7900
```

7900

```
K0 = 500 * 10^9
```

500000000000

```
G = 6.67384 * 10^ - 11
```

6.67384×10^{-11}

```
L = Sqrt[(3 * K0 * (Log[rhocen/rho0] + 1))/(2 * π * G * rho0 * rhocen)]
```

6.35317×10^{6}

```
G = 6.6873 * 10^ - 11
```

6.6873×10^{-11}

```
R = 0.75 * 6378 * 10^3
```

4.7835×10^{6}

```
Mc =
4 * π * rhocen*
(((−L^2)/2) * R * Exp[(−R^2)/(L^2)] + ((L^3)/4) * Sqrt[π] * N[Erf[R/L], 5])−
4 * π * rhocen * (((L^3)/4) * Sqrt[π] * N[Erf[0], 5])
```

7.72105×10^{24}

```
QR = Mc * H0
```

7.88952×10^{12}

```
M_{C,E} = 1.926 * 10^24
```

1.926×10^{24}

```
Plot[{Mc * H0, Mc * H1, Mc * H2}, {Mc, 0, 3 * 1.926 * 10^24},
PlotStyle → {Red, Green, Blue}, AxesLabel-> {"M_C [M_{C,E}]", "Q_R [TW]"},
Ticks → {{{1 * M_{C,E}, "1 M_{C,E}"}, {2 * M_{C,E}, "2 M_{C,E}"}, {3 * M_{C,E}, "3 M_{C,E}"},
 {4 * M_{C,E}, "4 M_{C,E}"}, {5 * M_{C,E}, "5M_{C,E}"}}, Automatic},
TextStyle → {FontFamily → Arial, FontSize → 14}]
```

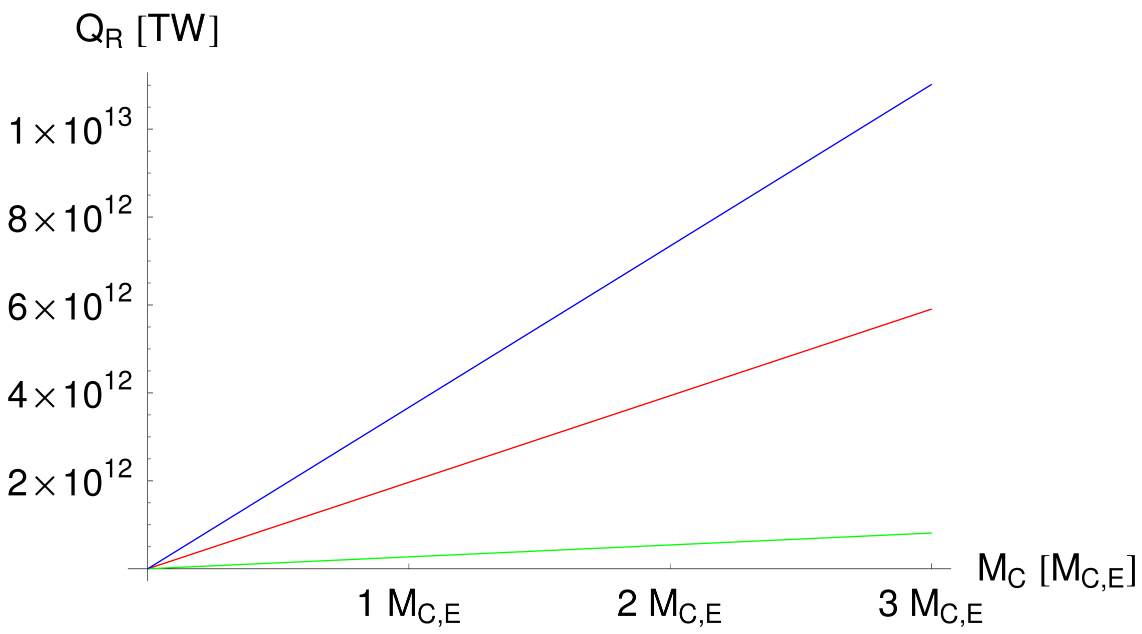

−Graphics−

Plot[
Mc ∗ (CU235mean ∗ HU235 + CU238mean ∗ HU238 + CTh232mean ∗ HTh232 + CK40mean ∗ HK40),
{CK40mean, CK40lower/2, CK40upper ∗ 2}, PlotStyle → Red,
AxesLabel-> {"C(^{40}K)", "Q_R [TW]"} , TextStyle → {FontFamily → Arial, FontSize → 14}]

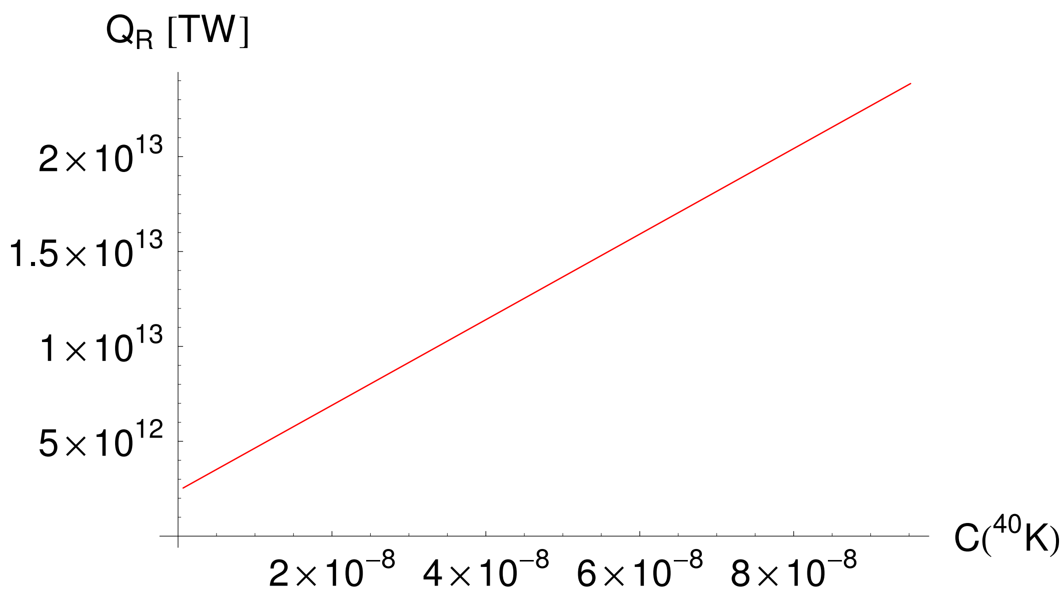

−Graphics−

Plot[
Mc ∗ (CU235mean ∗ HU235 + CU238mean ∗ HU238 + CTh232mean ∗ HTh232 + CK40mean ∗ HK40),

{CU238mean, CU238lower/2, CU238upper * 2}, PlotStyle → Blue,
AxesLabel-> {"C(^{238}U)", "Q_R [TW]"} , TextStyle → {FontFamily → Arial, FontSize → 14}]

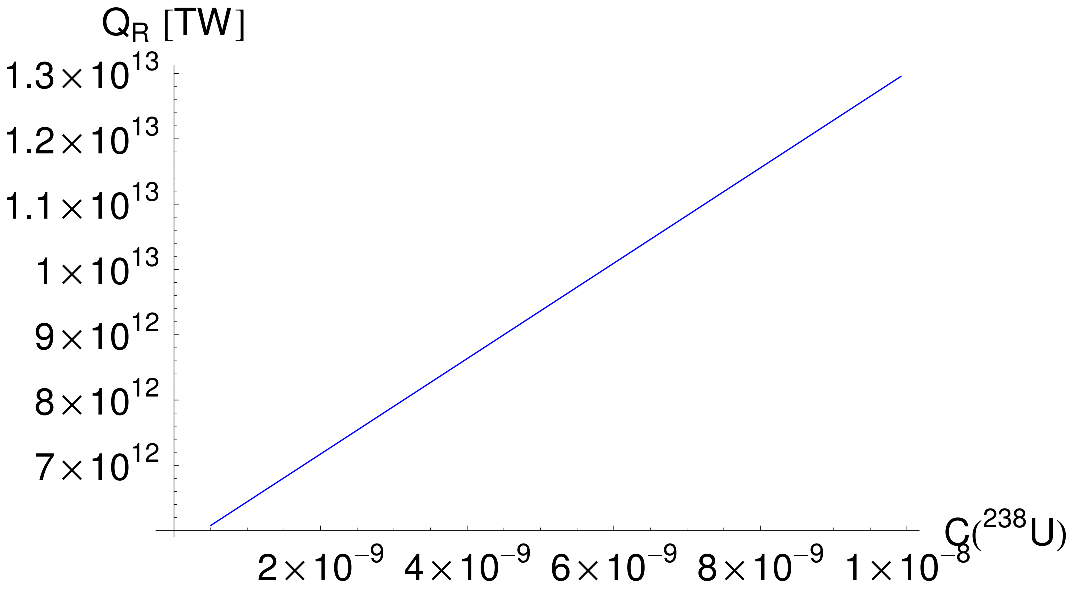

–Graphics–

Plot[
Mc * (CU235mean * HU235 + CU238mean * HU238 + CTh232mean * HTh232 + CK40mean * HK40),
{CU235mean, CU235lower/2, CU235upper * 2}, AxesOrigin → {0.1 * 10^ − 11, 7.81 * 10^12},
PlotStyle → Green, AxesLabel-> {"C(^{235}U)", "Q_R [TW]"} ,
TextStyle → {FontFamily → Arial, FontSize → 14}]

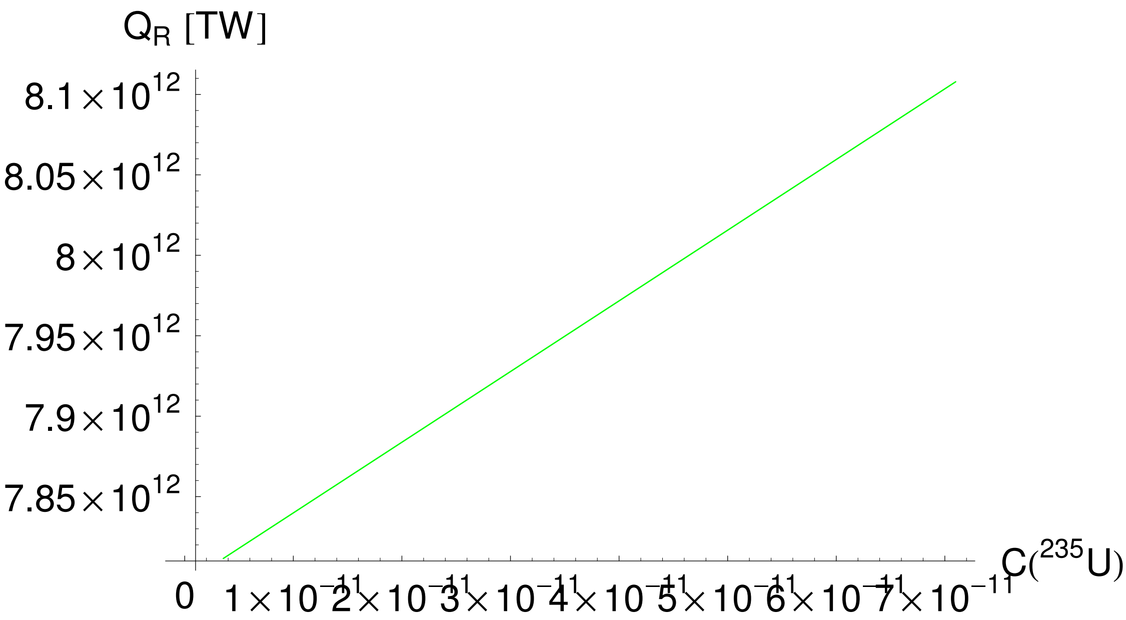

−Graphics−

B.1.3 $\tilde{Q}_T$

K0 = 500 ∗ 10^9

500000000000

rhocen = 23400

23400

rho0 = 7900

7900

G **= 6.67384 ∗ 10^ − 11**

6.67384×10^{-11}

L **= Sqrt[(3 ∗ K0 ∗ (Log[rhocen/rho0] + 1))/(2 ∗ π ∗** G **∗ rho0 ∗ rhocen)]**

6.35317×10^{6}

Cp = 840

840

LH = 750000

750000

α **= 1.35 ∗ 10^ − 5**

0.0000135

Dd = Sqrt[(3 ∗ Cp)/(2 ∗ π ∗ α **∗ rhocen ∗** G**)]**

4.36162×10^{6}

A² = ((1/L**^2) + (1/Dd^2))^(−1)**

1.29297×10^{13}

Tcen = 9080

9080

Tc = 5770

5770

rc = 0.75 ∗ 6378 ∗ 1000

4.7835×10^{6}

Is = (4/3) ∗ π ∗ Tcen ∗ rhocen ∗ rc^3 ∗ Exp[−rc^2/A²] ∗ (1 + (2/5) ∗ (rc^2/A²))

2.83472×10^{28}

ri = 0.75 ∗ (1220/3480) ∗ 6378 ∗ 1000

1.67697×10^{6}

ψ **= (2/3 ∗ π ∗** G **∗ rhocen ∗ ri^2 ∗ (1 − (3 ∗ ri^2)/(10 ∗** L**^2)))−**
(2/3 ∗ π ∗ G **∗ rhocen ∗ rc^2 ∗ (1 − (3 ∗ rc^2)/(10 ∗** L**^2)))**

-5.3107×10^{7}

Moc = (4/3 ∗ π ∗ rhocen ∗ rc^3 ∗ Exp[−rc^2/L**^2] ∗ (1 + (2/5) ∗ (rc^2/**L**^2)))−**
(4/3 ∗ π ∗ rhocen ∗ ri^3 ∗ Exp[−ri^2/L**^2] ∗ (1 + (2/5) ∗ (ri^2/**L**^2)))**

7.02301×10^{24}

$\Delta dTdP = -1.3/10^{\wedge}9$

-1.3×10^{-9}

$\Delta rhoc = 575$

575

$Ti = 8800$

8800

$rhoi = rhocen * Exp[-ri^{\wedge}2/L^{\wedge}2]$

21825.1

$g = (4 * \pi/3) * G * rhocen * ri * (1 - ((3 * ri^{\wedge}2)/(5 * L^{\wedge}2)))$

10.5114

$dri = (1/\Delta dTdP) * (Ti/(rhoi * g)) * (1/Tc)$

-5113.83

$C^2 = (3 * L^{\wedge}2)/16 - ((rc^{\wedge}2)/2) * (1 - ((3 * rc^{\wedge}2)/(10 * L^{\wedge}2)))$

-1.92714×10^{12}

$qstilde = -(Cp/Tc) * Is$

-4.1268×10^{27}

$integralterm = ((8 * \pi^{\wedge}2 * rhocen^{\wedge}2 * G)/3)*$
$(((((3/20 * rc^{\wedge}5) - (L^{\wedge}2/8 * rc^{\wedge}3) - (L^{\wedge}2 * C^2 * rc)) * Exp[-rc^{\wedge}2/L^{\wedge}2])+$
$(C^2/2) * L^{\wedge}3 * Sqrt[\pi] * Erf[rc/L])-$
$((((3/20 * ri^{\wedge}5) - (L^{\wedge}2/8 * ri^{\wedge}3) - (L^{\wedge}2 * C^2 * ri)) * Exp[-ri^{\wedge}2/L^{\wedge}2])+$
$(C^2/2) * L^{\wedge}3 * Sqrt[\pi] * Erf[ri/L]))$

-1.68515×10^{32}

$qgtilde = (integralterm - Moc * \psi) * \Delta rhoc * ((4 * \pi * ri^{\wedge}2)/Moc) * dri$

-3.02519×10^{27}

$qltilde = (4 * \pi * ri^{\wedge}2 * LH * rhoi) * dri$

-2.95819×10^{27}

$qttilde = qstilde + qgtilde + qltilde$

-1.01102×10^{28}

QR = 7.889521076951764*^12

7.88952×10^{12}

dTc = ((5.60569877911644*^12 − QR)/qttilde) * 86400 * 365 * 10^9

7.12377

Plot[((QC − QR)/qttilde) * 86400 * 365 * 10^9, {QR, 0, 5 * 10^12}, AxesOrigin → {0, −17.5},
AxesLabel-> {"Q_R [W]", "dT_C/dt [K Gyr^{-1}]"} , TextStyle → {FontFamily → Arial, FontSize → 14}]

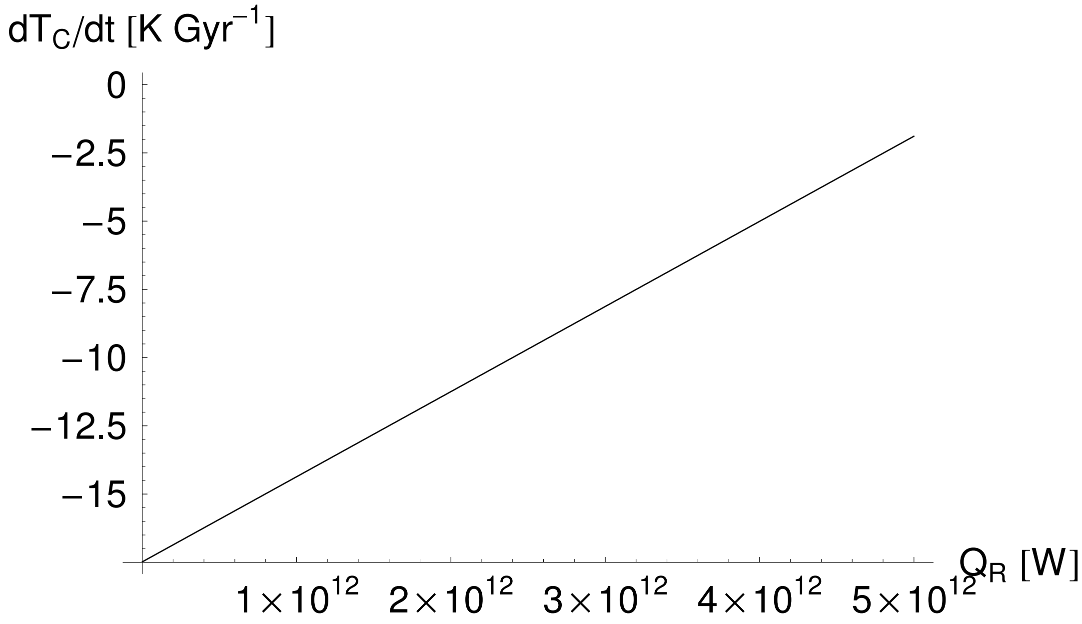
dTC/dt [K Gyr−1]
0
−2.5
−5
−7.5
−10
−12.5
−15
QR [W]
1×10^12
2×10^12
3×10^12
4×10^12
5×10^12

−Graphics−

B.1.4 Q_C

$\boldsymbol{R = 0.75 * 6378 * 1000}$

4.7835×10^{6}

$\mathbf{kb = 5.8}$

5.8

$\boldsymbol{\kappa}\mathbf{b = 10 * 10\hat{}\ -7}$

$\frac{1}{1000000}$

$\mathbf{Tc = 5770}$

5770

$\mathbf{Rac = 600}$

600

$\mathbf{rhom = 7500}$

7500

$\boldsymbol{g = 9.8}$

9.8

$\boldsymbol{\alpha}\mathbf{m = 2.2 * 10\hat{}\ -5}$

0.000022

$\mathbf{Tm = 4400}$

4400

$\boldsymbol{\eta}\mathbf{b = 2.5 * 10\hat{}23}$

2.5×10^{23}

$\boldsymbol{\delta}\mathbf{b = ((Rac *} \boldsymbol{\kappa}\mathbf{b *} \boldsymbol{\eta}\mathbf{b)/(rhom *} \boldsymbol{g *\alpha}\mathbf{m * (Tc - Tm)))\hat{}(1/3)}$

$407587.$

$\mathbf{Fb = kb * (Tc - Tm)/}\boldsymbol{\delta}\mathbf{b}$

0.0194952

$\mathbf{Qc = 4 *} \boldsymbol{\pi * R}\mathbf{\hat{}2 * Fb}$

5.6057×10^{12}

B.2 Keane EoS - $Q_R = 0$

B.2.1 Q_g

$\mathrm{rho0} = 7900$

7900

$\mathrm{rc} = 0.75 * 6378 * 1000$

4.7835×10^{6}

$\mathrm{ri} = 0.75 * (1220/3480) * 6378 * 1000$

1.67697×10^{6}

$\mathrm{K0} = 500 * 10\hat{\ }9$

500000000000

$G = 6.67384 * 10\hat{\ } - 11$

6.67384×10^{-11}

$\mathrm{rhocen} = 23400$

23400

$L = \mathrm{Sqrt}[(3 * \mathrm{K0} * (\mathrm{Log}[\mathrm{rhocen}/\mathrm{rho0}] + 1))/(2 * \pi * G * \mathrm{rho0} * \mathrm{rhocen})]$

6.35317×10^{6}

$\psi = (2/3 * \pi * G * \mathrm{rhocen} * \mathrm{ri}\hat{\ }2 * (1 - (3 * \mathrm{ri}\hat{\ }2)/(10 * L\hat{\ }2))) -$
$(2/3 * \pi * G * \mathrm{rhocen} * \mathrm{rc}\hat{\ }2 * (1 - (3 * \mathrm{rc}\hat{\ }2)/(10 * L\hat{\ }2)))$

-5.3107×10^{7}

$\mathrm{Moc} = (4/3 * \pi * \mathrm{rhocen} * \mathrm{rc}\hat{\ }3 * \mathrm{Exp}[-\mathrm{rc}\hat{\ }2/L\hat{\ }2] * (1 + (2/5) * (\mathrm{rc}\hat{\ }2/L\hat{\ }2))) -$
$(4/3 * \pi * \mathrm{rhocen} * \mathrm{ri}\hat{\ }3 * \mathrm{Exp}[-\mathrm{ri}\hat{\ }2/L\hat{\ }2] * (1 + (2/5) * (\mathrm{ri}\hat{\ }2/L\hat{\ }2)))$

7.02301×10^{24}

$\Delta\mathrm{rhoc} = 575$

575

$\mathrm{dri} = 89.41768625642986 * 1000/(10\hat{\ }9 * 86400 * 365)$

2.83542×10^{-12}

$\mathrm{C}^2 = (3 * L\hat{\ }2)/16 - ((\mathrm{rc}\hat{\ }2)/2) * (1 - ((3 * \mathrm{rc}\hat{\ }2)/(10 * L\hat{\ }2)))$

-1.92714×10^{12}

$\mathrm{integralterm} = ((8 * \pi\hat{\ }2 * \mathrm{rhocen}\hat{\ }2 * G)/3) *$
$(((((3/20 * \mathrm{rc}\hat{\ }5) - (L\hat{\ }2/8 * \mathrm{rc}\hat{\ }3) - (L\hat{\ }2 * \mathrm{C}^2 * \mathrm{rc})) * \mathrm{Exp}[-\mathrm{rc}\hat{\ }2/L\hat{\ }2]) +$
$(\mathrm{C}^2/2) * L\hat{\ }3 * \mathrm{Sqrt}[\pi] * \mathrm{Erf}[\mathrm{rc}/L]) -$
$((((3/20 * \mathrm{ri}\hat{\ }5) - (L\hat{\ }2/8 * \mathrm{ri}\hat{\ }3) - (L\hat{\ }2 * \mathrm{C}^2 * \mathrm{ri})) * \mathrm{Exp}[-\mathrm{ri}\hat{\ }2/L\hat{\ }2]) +$
$(\mathrm{C}^2/2) * L\hat{\ }3 * \mathrm{Sqrt}[\pi] * \mathrm{Erf}[\mathrm{ri}/L]))$

-1.68515×10^{32}

$\mathrm{Qg} = (\mathrm{integralterm} - \mathrm{Moc} * \psi) * \Delta\mathrm{rhoc} * ((4 * \pi * \mathrm{ri}\hat{\ }2)/\mathrm{Moc}) * \mathrm{dri}$

1.67735×10^{12}

B.2.2 Q_L

$\mathbf{ri = 0.75 * (1220/3480) * 6378 * 1000}$

1.67697×10^6

$\mathbf{LH = 750000}$

750000

$\mathbf{rhocen = 23400}$

23400

$\mathbf{rho0 = 7900}$

7900

$\mathbf{K0 = 500 * 10\hat{}9}$

500000000000

$\boldsymbol{G} = \mathbf{6.67384 * 10\hat{}-11}$

6.67384×10^{-11}

$\boldsymbol{L} = \mathbf{Sqrt[(3 * K0 * (Log[rhocen/rho0] + 1))/(2 * \pi * \boldsymbol{G} * rho0 * rhocen)]}$

6.35317×10^6

$\mathbf{rhoi = rhocen * Exp[-ri\hat{}2/\boldsymbol{L}\hat{}2]}$

21825.1

$\mathbf{\Delta dTdP = 1.3/10\hat{}9}$

1.3×10^{-9}

$\mathbf{Ti = 8800}$

8800

$\mathbf{Tc = 5770}$

5770

$\mathbf{dTc = -17.48547276238309\grave{}/(10\hat{}9 * 86400 * 365)}$

-5.54461×10^{-16}

$\boldsymbol{g} = \mathbf{(4 * \pi/3) * \boldsymbol{G} * rhocen * ri * (1 - ((3 * ri\hat{}2)/(5 * \boldsymbol{L}\hat{}2)))}$

10.5114

$\mathbf{QL = -(4 * \pi * ri\hat{}2 * LH * Ti)/(\Delta dTdP * \boldsymbol{g}) * (1/Tc) * dTc}$

1.6402×10^{12}

B.2.3 Q_s

$\mathbf{K0 = 500 * 10\hat{}9}$

500000000000

$\mathbf{rhocen = 23400}$

23400

$\mathbf{rho0 = 7900}$

7900

$\boldsymbol{G = 6.67384 * 10\hat{}-11}$

6.67384×10^{-11}

$\boldsymbol{L = \mathrm{Sqrt}[(3 * \mathrm{K0} * (\mathrm{Log}[\mathrm{rhocen}/\mathrm{rho0}] + 1))/(2 * \pi * G * \mathrm{rho0} * \mathrm{rhocen})]}$

6.35317×10^{6}

$\mathbf{Cp = 840}$

840

$\boldsymbol{\alpha = 1.35 * 10\hat{}-5}$

0.0000135

$\boldsymbol{\mathrm{Dd} = \mathrm{Sqrt}[(3 * \mathrm{Cp})/(2 * \pi * \alpha * \mathrm{rhocen} * G)]}$

4.36162×10^{6}

$\boldsymbol{\mathrm{A}^2 = ((1/L\hat{}2) + (1/\mathrm{Dd}\hat{}2))\hat{}(-1)}$

1.29297×10^{13}

$\mathbf{Tcen = 9080}$

9080

$\mathbf{Tc = 5770}$

5770

$\mathbf{rc = 0.75 * 6378 * 1000}$

4.7835×10^{6}

$\boldsymbol{\mathrm{Is} = (4/3) * \pi * \mathrm{Tcen} * \mathrm{rhocen} * \mathrm{rc}\hat{}3 * \mathrm{Exp}[-\mathrm{rc}\hat{}2/\mathrm{A}^2] * (1 + (2/5) * (\mathrm{rc}\hat{}2/\mathrm{A}^2))}$

2.83472×10^{28}

$\mathbf{dTc = -17.48547276238309/(10\hat{}9 * 86400 * 365)}$

-5.54461×10^{-16}

$\mathbf{Qs = -(Cp/Tc) * dTc * Is}$

2.28815×10^{12}

B.2.4 $\tilde{Q}_T$

$\mathbf{K0 = 500 * 10\verb|^|9}$

500000000000

$\mathbf{rhocen = 23400}$

23400

$\mathbf{rho0 = 7900}$

7900

$\boldsymbol{G} \mathbf{= 6.67384 * 10\verb|^| - 11}$

6.67384×10^{-11}

$\boldsymbol{L} \mathbf{= Sqrt[(3 * K0 * (Log[rhocen/rho0] + 1))/(2 * \pi *} \boldsymbol{G} \mathbf{* rho0 * rhocen)]}$

6.35317×10^{6}

$\mathbf{Cp = 840}$

840

$\mathbf{LH = 750000}$

750000

$\boldsymbol{\alpha} \mathbf{= 1.35 * 10\verb|^| - 5}$

0.0000135

$\mathbf{Dd = Sqrt[(3 * Cp)/(2 * \pi * \alpha * rhocen *} \boldsymbol{G} \mathbf{)]}$

4.36162×10^{6}

$\mathbf{A^2 = ((1/}\boldsymbol{L}\mathbf{\verb|^|2) + (1/Dd\verb|^|2))\verb|^|(-1)}$

1.29297×10^{13}

$\mathbf{Tcen = 9080}$

9080

$\mathbf{Tc = 5770}$

5770

$\mathbf{rc = 0.75 * 6378 * 1000}$

4.7835×10^{6}

$\mathbf{Is = (4/3) * \pi * Tcen * rhocen * rc\verb|^|3 * Exp[-rc\verb|^|2/A^2] * (1 + (2/5) * (rc\verb|^|2/A^2))}$

2.83472×10^{28}

$\mathbf{ri = 0.75 * (1220/3480) * 6378 * 1000}$

1.67697×10^{6}

$\boldsymbol{\psi} \mathbf{= (2/3 * \pi *} \boldsymbol{G} \mathbf{* rhocen * ri\verb|^|2 * (1 - (3 * ri\verb|^|2)/(10 *} \boldsymbol{L}\mathbf{\verb|^|2)))-}$
$\mathbf{(2/3 * \pi *} \boldsymbol{G} \mathbf{* rhocen * rc\verb|^|2 * (1 - (3 * rc\verb|^|2)/(10 *} \boldsymbol{L}\mathbf{\verb|^|2)))}$

-5.3107×10^{7}

$\mathbf{Moc = (4/3 * \pi * rhocen * rc\verb|^|3 * Exp[-rc\verb|^|2/}\boldsymbol{L}\mathbf{\verb|^|2] * (1 + (2/5) * (rc\verb|^|2/}\boldsymbol{L}\mathbf{\verb|^|2)))-}$
$\mathbf{(4/3 * \pi * rhocen * ri\verb|^|3 * Exp[-ri\verb|^|2/}\boldsymbol{L}\mathbf{\verb|^|2] * (1 + (2/5) * (ri\verb|^|2/}\boldsymbol{L}\mathbf{\verb|^|2)))}$

7.02301×10^{24}

$\mathbf{\Delta dTdP = 1.3/10\^{}9}$

1.3×10^{-9}

$\mathbf{\Delta rhoc = 575}$

575

$\mathbf{Ti = 8800}$

8800

$\mathbf{rhoi = rhocen * Exp[-ri\^{}2/\mathit{L}\^{}2]}$

21825.1

$\mathbf{\mathit{g} = (4 * \pi/3) * \mathit{G} * rhocen * ri * (1 - ((3 * ri\^{}2)/(5 * \mathit{L}\^{}2)))}$

10.5114

$\mathbf{dri = -(1/\Delta dTdP) * (Ti/(rhoi * \mathit{g})) * (1/Tc)}$

-5113.83

$\mathbf{C^2 = (3 * \mathit{L}\^{}2)/16 - ((rc\^{}2)/2) * (1 - ((3 * rc\^{}2)/(10 * \mathit{L}\^{}2)))}$

-1.92714×10^{12}

$\mathbf{qstilde = -(Cp/Tc) * Is}$

-4.1268×10^{27}

$\mathbf{integralterm = ((8 * \pi\^{}2 * rhocen\^{}2 * \mathit{G})/3) *}$
$\mathbf{(((((3/20 * rc\^{}5) - (\mathit{L}\^{}2/8 * rc\^{}3) - (\mathit{L}\^{}2 * C^2 * rc)) * Exp[-rc\^{}2/\mathit{L}\^{}2]) +}$
$\mathbf{(C^2/2) * \mathit{L}\^{}3 * Sqrt[\pi] * Erf[rc/\mathit{L}]) -}$
$\mathbf{((((3/20 * ri\^{}5) - (\mathit{L}\^{}2/8 * ri\^{}3) - (\mathit{L}\^{}2 * C^2 * ri)) * Exp[-ri\^{}2/\mathit{L}\^{}2]) +}$
$\mathbf{(C^2/2) * \mathit{L}\^{}3 * Sqrt[\pi] * Erf[ri/\mathit{L}]))}$

-1.68515×10^{32}

$\mathbf{qgtilde = (integralterm - Moc * \psi) * \Delta rhoc * ((4 * \pi * ri\^{}2)/Moc) * dri}$

-3.02519×10^{27}

$\mathbf{qltilde = (4 * \pi * ri\^{}2 * LH * rhoi) * dri}$

-2.95819×10^{27}

$\mathbf{qttilde = qstilde + qgtilde + qltilde}$

-1.01102×10^{28}

$\mathbf{QR = 7.889521076951764{*}\^{}12}$

7.88952×10^{12}

$\mathbf{Qc = 5.60569877911644{*}\^{}12}$

5.6057×10^{12}

$\mathbf{dTc = (Qc/qttilde) * 86400 * 365 * 10\^{}9}$

-17.4855

B.2.5 dr_i/dt

ΔdTdP = 1.3/10^9

1.3×10^{-9}

Ti = 8800

8800

Tc = 5770

5770

dTc = −17.48547276238309`/(10^9 * 86400 * 365)

-5.54461×10^{-16}

ri = 0.75 * (1220/3480) * 6378 * 1000

1.67697×10^{6}

rho0 = 7900

7900

K0 = 500 * 10^9

500000000000

***G* = 6.67384 * 10^ − 11**

6.67384×10^{-11}

rhocen = 23400

23400

***L* = Sqrt[(3 * K0 * (Log[rhocen/rho0] + 1))/(2 * π * *G* * rho0 * rhocen)]**

6.35317×10^{6}

rhoi = rhocen * Exp[−ri^2/*L*^2]

21825.1

***g* = (4 * π/3) * *G* * rhocen * ri * (1 − ((3 * ri^2)/(5 * *L*^2)))**

10.5114

dri = −(((1/(ΔdTdP)) * (Ti/(rhoi * *g*)) * (1/Tc) * dTc) * 10^9 * 86400 * 365)/1000

89.4177

B.3 Keane EoS - $Q_R \rightarrow$ Lower Bound

B.3.1 Q_g

rho0 = 7900

7900

rc = 0.75 * 6378 * 1000

4.7835×10^{6}

ri = 0.75 * (1220/3480) * 6378 * 1000

1.67697×10^{6}

K0 = 500 * 10^9

500000000000

***G* = 6.67384 * 10^ − 11**

6.67384×10^{-11}

rhocen = 23400

23400

***L* = Sqrt[(3 * K0 * (Log[rhocen/rho0] + 1))/(2 * π * *G* * rho0 * rhocen)]**

6.35317×10^{6}

***ψ* = (2/3 * π * *G* * rhocen * ri^2 * (1 − (3 * ri^2)/(10 * *L*^2)))−**
(2/3 * π * *G* * rhocen * rc^2 * (1 − (3 * rc^2)/(10 * *L*^2)))

-5.3107×10^{7}

Moc = (4/3 * π * rhocen * rc^3 * Exp[−rc^2/*L*^2] * (1 + (2/5) * (rc^2/*L*^2)))−
(4/3 * π * rhocen * ri^3 * Exp[−ri^2/*L*^2] * (1 + (2/5) * (ri^2/*L*^2)))

7.02301×10^{24}

Δrhoc = 575

575

dri = 72.08687996489924 * 1000/(10^9 * 86400 * 365)

2.28586×10^{-12}

C^2 = (3 * *L*^2)/16 − ((rc^2)/2) * (1 − ((3 * rc^2)/(10 * *L*^2)))

-1.92714×10^{12}

integralterm = ((8 * π^2 * rhocen^2 * *G*)/3)*
(((((3/20 * rc^5) − (*L*^2/8 * rc^3) − (*L*^2 * C^2 * rc)) * Exp[−rc^2/*L*^2])+
(C^2/2) * *L*^3 * Sqrt[π] * Erf[rc/*L*])−
((((3/20 * ri^5) − (*L*^2/8 * ri^3) − (*L*^2 * C^2 * ri)) * Exp[−ri^2/*L*^2])+
(C^2/2) * *L*^3 * Sqrt[π] * Erf[ri/*L*]))

-1.68515×10^{32}

Qg = (integralterm − Moc * *ψ*) * Δrhoc * ((4 * π * ri^2)/Moc) * dri

1.35225×10^{12}

B.3.2 Q_L

$\mathbf{ri = 0.75 * (1220/3480) * 6378 * 1000}$

1.67697×10^6

$\mathbf{LH = 750000}$

750000

$\mathbf{rhocen = 23400}$

23400

$\mathbf{rho0 = 7900}$

7900

$\mathbf{K0 = 500 * 10\hat{}9}$

500000000000

$\boldsymbol{G = 6.67384 * 10\hat{}-11}$

6.67384×10^{-11}

$\boldsymbol{L = \mathrm{Sqrt}[(3 * K0 * (\mathrm{Log}[rhocen/rho0] + 1))/(2 * \pi * G * rho0 * rhocen)]}$

6.35317×10^6

$\boldsymbol{rhoi = rhocen * \mathrm{Exp}[-ri\hat{}2/L\hat{}2]}$

21825.1

$\mathbf{\Delta dTdP = 1.3/10\hat{}9}$

1.3×10^{-9}

$\mathbf{Ti = 8800}$

8800

$\mathbf{Tc = 5770}$

5770

$\mathbf{dTc = -14.096463786109055/(10\hat{}9 * 86400 * 365)}$

-4.46996×10^{-16}

$\boldsymbol{g = (4 * \pi/3) * G * rhocen * ri * (1 - ((3 * ri\hat{}2)/(5 * L\hat{}2)))}$

10.5114

$\boldsymbol{QL = -(4 * \pi * ri\hat{}2 * LH * Ti)/(\Delta dTdP * g) * (1/Tc) * dTc}$

1.3223×10^{12}

B.3.3 Q_R

$\mathbf{CK40 = 1.31 * 10\hat{\ } - 9}$

1.31×10^{-9}

$\mathbf{CU238 = 9.93 * 10\hat{\ } - 10}$

9.93×10^{-10}

$\mathbf{CU235 = 7.1 * 10\hat{\ } - 12}$

7.1×10^{-12}

$\mathbf{CTh232 = 1.7 * 10\hat{\ } - 10}$

1.7×10^{-10}

$\mathbf{HK40 = 2.92 * 10\hat{\ } - 5}$

0.0000292

$\mathbf{HTh232 = 2.64 * 10\hat{\ } - 5}$

0.0000264

$\mathbf{HU238 = 9.46 * 10\hat{\ } - 5}$

0.0000946

$\mathbf{HU235 = 5.69 * 10\hat{\ } - 4}$

0.000569

$\mathbf{H0 = CU235 * HU235 + CU238 * HU238 + CTh232 * HTh232 + CK40 * HK40}$

1.40718×10^{-13}

$\mathbf{rhocen = 23400}$

23400

$\mathbf{rho0 = 7900}$

7900

$\mathbf{K0 = 500 * 10\hat{\ }9}$

500000000000

$\boldsymbol{G} \mathbf{= 6.67384 * 10\hat{\ } - 11}$

6.67384×10^{-11}

$\boldsymbol{L} \mathbf{= Sqrt[(3 * K0 * (Log[rhocen/rho0] + 1))/(2 * \pi * \boldsymbol{G} * rho0 * rhocen)]}$

6.35317×10^{6}

$\boldsymbol{G} \mathbf{= 6.6873 * 10\hat{\ } - 11}$

6.6873×10^{-11}

$\boldsymbol{R} \mathbf{= 0.75 * 6378 * 10\hat{\ }3}$

4.7835×10^{6}

$\mathbf{Mc = 4 * \pi * rhocen * (((-\boldsymbol{L}\hat{\ }2)/2) * \boldsymbol{R} * Exp[(-\boldsymbol{R}\hat{\ }2)/(\boldsymbol{L}\hat{\ }2)] + ((\boldsymbol{L}\hat{\ }3)/4) * Sqrt[\pi] * \boldsymbol{N}[Erf[\boldsymbol{R}/\boldsymbol{L}], 5])}$
$\mathbf{-4 * \pi * rhocen * (((\boldsymbol{L}\hat{\ }3)/4) * Sqrt[\pi] * \boldsymbol{N}[Erf[0], 5])}$

7.72105×10^{24}

$\mathbf{QR = Mc * H0}$

1.08649×10^{12}

B.3.4 Q_s

K0 = 500 * 10^9

500000000000

rhocen = 23400

23400

rho0 = 7900

7900

G = 6.67384 * 10^ − 11

6.67384×10^{-11}

L = Sqrt[(3 * K0 * (Log[rhocen/rho0] + 1))/(2 * π * G * rho0 * rhocen)]

6.35317×10^{6}

Cp = 840

840

α = 1.35 * 10^ − 5

0.0000135

Dd = Sqrt[(3 * Cp)/(2 * π * α * rhocen * G)]

4.36162×10^{6}

A^2 = ((1/L^2) + (1/Dd^2))^(−1)

1.29297×10^{13}

Tcen = 9080

9080

Tc = 5770

5770

rc = 0.75 * 6378 * 1000

4.7835×10^{6}

Is = (4/3) * π * Tcen * rhocen * rc^3 * Exp[−rc^2/A^2] * (1 + (2/5) * (rc^2/A^2))

2.83472×10^{28}

dTc = −14.096463786109055/(10^9 * 86400 * 365)

-4.46996×10^{-16}

Qs = −(Cp/Tc) * dTc * Is

1.84466×10^{12}

B.3.5 $\tilde{Q}_T$

K0 = 500 * 10^9

500000000000

rhocen = 23400

23400

rho0 = 7900

7900

G = 6.67384 * 10^ − 11

6.67384×10^{-11}

L = Sqrt[(3 * K0 * (Log[rhocen/rho0] + 1))/(2 * π * G * rho0 * rhocen)]

6.35317×10^{6}

Cp = 840

840

LH = 750000

750000

α = 1.35 * 10^ − 5

0.0000135

Dd = Sqrt[(3 * Cp)/(2 * π * α * rhocen * G)]

4.36162×10^{6}

A^2 = ((1/L^2) + (1/Dd^2))^(−1)

1.29297×10^{13}

Tcen = 9080

9080

Tc = 5770

5770

rc = 0.75 * 6378 * 1000

4.7835×10^{6}

Is = (4/3) * π * Tcen * rhocen * rc^3 * Exp[−rc^2/A^2] * (1 + (2/5) * (rc^2/A^2))

2.83472×10^{28}

ri = 0.75 * (1220/3480) * 6378 * 1000

1.67697×10^{6}

ψ = (2/3 * π * G * rhocen * ri^2 * (1 − (3 * ri^2)/(10 * L^2)))−
(2/3 * π * G * rhocen * rc^2 * (1 − (3 * rc^2)/(10 * L^2)))

-5.3107×10^{7}

Moc = (4/3 * π * rhocen * rc^3 * Exp[−rc^2/L^2] * (1 + (2/5) * (rc^2/L^2)))−
(4/3 * π * rhocen * ri^3 * Exp[−ri^2/L^2] * (1 + (2/5) * (ri^2/L^2)))

7.02301×10^{24}

```
ΔdTdP = 1.3/10^9
1.3 × 10^-9
Δrhoc = 575
575
Ti = 8800
8800
rhoi = rhocen * Exp[-ri^2/L^2]
21825.1
g = (4 * π/3) * G * rhocen * ri * (1 - ((3 * ri^2)/(5 * L^2)))
10.5114
dri = -(1/ΔdTdP) * (Ti/(rhoi * g)) * (1/Tc)
-5113.83
C^2 = (3 * L^2)/16 - ((rc^2)/2) * (1 - ((3 * rc^2)/(10 * L^2)))
-1.92714 × 10^12
qstilde = -(Cp/Tc) * Is
-4.1268 × 10^27
integralterm = ((8 * π^2 * rhocen^2 * G)/3)*
(((( (3/20 * rc^5) - (L^2/8 * rc^3) - (L^2 * C^2 * rc)) * Exp[-rc^2/L^2])+
(C^2/2) * L^3 * Sqrt[π] * Erf[rc/L])-
((((3/20 * ri^5) - (L^2/8 * ri^3) - (L^2 * C^2 * ri)) * Exp[-ri^2/L^2])+
(C^2/2) * L^3 * Sqrt[π] * Erf[ri/L]))
-1.68515 × 10^32
qgtilde = (integralterm - Moc * ψ) * Δrhoc * ((4 * π * ri^2)/Moc) * dri
-3.02519 × 10^27
qltilde = (4 * π * ri^2 * LH * rhoi) * dri
-2.95819 × 10^27
qttilde = qstilde + qgtilde + qltilde
-1.01102 × 10^28
QR = 1.0864884089141903*^12
1.08649 × 10^12
Qc = 5.60569877911644*^12
5.6057 × 10^12
dTc = ((Qc - QR)/qttilde) * 86400 * 365 * 10^9
-14.0965
Plot[((Qc - QR)/qttilde) * 86400 * 365 * 10^9, {QR, 0, 5 * 10^12}, AxesOrigin → {0, -17.5},
AxesLabel-> {"Q_R [W]", "dT_C/dt [K Gyr^-1]"}, TextStyle → {FontFamily → Arial, FontSize → 14}]
```

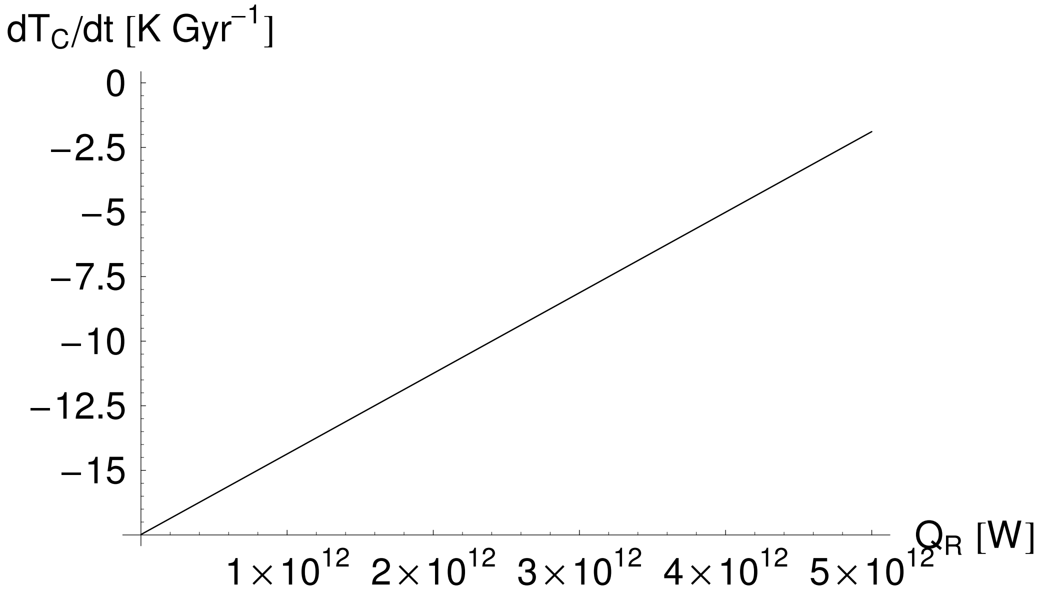
dTC/dt [K Gyr−1]
0
−2.5
−5
−7.5
−10
−12.5
−15
QR [W]
1×10^12
2×10^12
3×10^12
4×10^12
5×10^12

−Graphics−

B.3.6 dr_i/dt

ΔdTdP = 1.3/10^9

1.3×10^{-9}

Ti = 8800

8800

Tc = 5770

5770

dTc = −14.096463786109055/(10^9 * 86400 * 365)

-4.46996×10^{-16}

ri = 0.75 * (1220/3480) * 6378 * 1000

1.67697×10^{6}

rho0 = 7900

7900

K0 = 500 * 10^9

500000000000

***G* = 6.67384 * 10^ − 11**

6.67384×10^{-11}

rhocen = 23400

23400

***L* = Sqrt[(3 * K0 * (Log[rhocen/rho0] + 1))/(2 * π * *G* * rho0 * rhocen)]**

6.35317×10^{6}

rhoi = rhocen * Exp[−ri^2/*L*^2]

21825.1

***g* = (4 * π/3) * *G* * rhocen * ri * (1 − ((3 * ri^2)/(5 * *L*^2)))**

10.5114

dri = −(((1/(ΔdTdP)) * (Ti/(rhoi * *g*)) * (1/Tc) * dTc) * 10^9 * 86400 * 365)/1000

72.0869

B.4 Rydberg EoS - Normal

B.4.1 Q_k

$\mathbf{rc = 0.8 * 6378 * 1000}$

5.1024×10^6

$\boldsymbol{k = 40}$

40

$\mathbf{Tc = 5510}$

5510

$\mathbf{cp = 840}$

840

$\boldsymbol{\alpha = 1.35 * 10\hat{}\ -5}$

0.0000135

$\mathbf{rhocen = 20600}$

20600

$\boldsymbol{G = 6.67384 * 10\hat{}\ -11}$

6.67384×10^{-11}

$\mathbf{Dd = Sqrt[(3 * cp)/(2 * \boldsymbol{\pi} * \boldsymbol{\alpha} * rhocen * \boldsymbol{G})]}$

4.6486×10^6

$\mathbf{Qk = (8 * \boldsymbol{\pi} * rc\hat{}3 * \boldsymbol{k} * Tc)/Dd\hat{}2}$

3.40511×10^{13}

B.4.2 Q_R

$\mathbf{CK40 = 2.44 * 10\char`^ - 8}$

2.44×10^{-8}

$\mathbf{CU238 = 2.98 * 10\char`^ - 9}$

2.98×10^{-9}

$\mathbf{CU235 = 2.13 * 10\char`^ - 11}$

2.13×10^{-11}

$\mathbf{CTh232 = 5.8 * 10\char`^ - 10}$

5.8×10^{-10}

$\mathbf{HK40 = 2.92 * 10\char`^ - 5}$

0.0000292

$\mathbf{HTh232 = 2.64 * 10\char`^ - 5}$

0.0000264

$\mathbf{HU238 = 9.46 * 10\char`^ - 5}$

0.0000946

$\mathbf{HU235 = 5.69 * 10\char`^ - 4}$

0.000569

$\mathbf{H0 = CU235 * HU235 + CU238 * HU238 + CTh232 * HTh232 + CK40 * HK40}$

1.02182×10^{-12}

$\mathbf{rhocen = 20600}$

20600

$\mathbf{rho0 = 7900}$

7900

$\mathbf{K0 = 500 * 10\char`^9}$

500000000000

$\boldsymbol{G} \mathbf{= 6.67384 * 10\char`^ - 11}$

6.67384×10^{-11}

$\boldsymbol{L} \mathbf{= Sqrt[(3 * K0 * (Log[rhocen/rho0] + 1))/(2 * \pi *} \boldsymbol{G} \mathbf{* rho0 * rhocen)]}$

6.56107×10^{6}

$\boldsymbol{G} \mathbf{= 6.6873 * 10\char`^ - 11}$

6.6873×10^{-11}

$\boldsymbol{R} \mathbf{= 0.8 * 6378 * 10\char`^3}$

5.1024×10^{6}

$\mathbf{Mc = 4 * \pi * rhocen * (((-}\boldsymbol{L}\mathbf{\char`^2)/2) *} \boldsymbol{R} \mathbf{* Exp[(-}\boldsymbol{R}\mathbf{\char`^2)/(}\boldsymbol{L}\mathbf{\char`^2)] + ((}\boldsymbol{L}\mathbf{\char`^3)/4) * Sqrt[\pi] *} \boldsymbol{N}\mathbf{[Erf[}\boldsymbol{R/L}\mathbf{], 5])}$

$\mathbf{-4 * \pi * rhocen * (((}\boldsymbol{L}\mathbf{\char`^3)/4) * Sqrt[\pi] *} \boldsymbol{N}\mathbf{[Erf[0], 5])}$

8.07643×10^{24}

$\mathbf{QR = Mc * H0}$

8.25265×10^{12}

B.4.3 $\tilde{Q}_T$

$\mathbf{K0 = 500 * 10\hat{}9}$

500000000000

$\mathbf{rhocen = 20600}$

20600

$\mathbf{rho0 = 7900}$

7900

$\mathbf{G = 6.67384 * 10\hat{} - 11}$

6.67384×10^{-11}

$\mathbf{L = Sqrt[(3 * K0 * (Log[rhocen/rho0] + 1))/(2 * \pi * G * rho0 * rhocen)]}$

6.56107×10^{6}

$\mathbf{Cp = 840}$

840

$\boldsymbol{\alpha} \mathbf{= 1.35 * 10\hat{} - 5}$

0.0000135

$\mathbf{Dd = Sqrt[(3 * Cp)/(2 * \pi * \alpha * rhocen * G)]}$

4.6486×10^{6}

$\mathbf{A^2 = ((1/L\hat{}2) + (1/Dd\hat{}2))\hat{}(-1)}$

1.43872×10^{13}

$\mathbf{Tcen = 7970}$

7970

$\mathbf{Tc = 5510}$

5510

$\mathbf{rc = 0.8 * 6378 * 1000}$

5.1024×10^{6}

$\mathbf{Is = (4/3) * \pi * Tcen * rhocen * rc\hat{}3 * Exp[-rc\hat{}2/A^2] * (1 + (2/5) * (rc\hat{}2/A^2))}$

2.5784×10^{28}

$\mathbf{ri = 0.8 * (1220/3480) * 6378 * 1000}$

1.78877×10^{6}

$\boldsymbol{\psi} \mathbf{= (2/3 * \pi * G * rhocen * ri\hat{}2 * (1 - (3 * ri\hat{}2)/(10 * L\hat{}2)))-}$

$\mathbf{(2/3 * \pi * G * rhocen * rc\hat{}2 * (1 - (3 * rc\hat{}2)/(10 * L\hat{}2)))}$

-5.23548×10^{7}

$\mathbf{Moc = (4/3 * \pi * rhocen * rc\hat{}3 * Exp[-rc\hat{}2/L\hat{}2] * (1 + (2/5) * (rc\hat{}2/L\hat{}2)))-}$

$\mathbf{(4/3 * \pi * rhocen * ri\hat{}3 * Exp[-ri\hat{}2/L\hat{}2] * (1 + (2/5) * (ri\hat{}2/L\hat{}2)))}$

7.30315×10^{24}

$\mathbf{\Delta dTdP = 1.3/10\hat{}9}$

1.3×10^{-9}

$\Delta\mathrm{rhoc} = 575$

575

$\mathrm{Ti} = 7900$

7900

$\mathrm{rhoi} = \mathrm{rhocen} * \mathrm{Exp}[-\mathrm{ri}\hat{}2/L\hat{}2]$

19124.3

$g = (4 * \pi/3) * G * \mathrm{rhocen} * \mathrm{ri} * (1 - ((3 * \mathrm{ri}\hat{}2)/(5 * L\hat{}2)))$

9.84177

$\mathrm{dri} = -(1/\Delta\mathrm{dTdP}) * (\mathrm{Ti}/(\mathrm{rhoi} * g)) * (1/\mathrm{Tc})$

-5859.67

$\mathrm{C}^2 = (3 * L\hat{}2)/16 - ((\mathrm{rc}\hat{}2)/2) * (1 - ((3 * \mathrm{rc}\hat{}2)/(10 * L\hat{}2)))$

-2.58403×10^{12}

$\mathrm{qstilde} = -(\mathrm{Cp}/\mathrm{Tc}) * \mathrm{Is}$

-3.93077×10^{27}

$\mathrm{integralterm} = ((8 * \pi\hat{}2 * \mathrm{rhocen}\hat{}2 * G)/3) *$
$(((((3/20 * \mathrm{rc}\hat{}5) - (L\hat{}2/8 * \mathrm{rc}\hat{}3) - (L\hat{}2 * \mathrm{C}^2 * \mathrm{rc})) * \mathrm{Exp}[-\mathrm{rc}\hat{}2/L\hat{}2]) +$
$(\mathrm{C}^2/2) * L\hat{}3 * \mathrm{Sqrt}[\pi] * \mathrm{Erf}[\mathrm{rc}/L]) -$
$((((3/20 * \mathrm{ri}\hat{}5) - (L\hat{}2/8 * \mathrm{ri}\hat{}3) - (L\hat{}2 * \mathrm{C}^2 * \mathrm{ri})) * \mathrm{Exp}[-\mathrm{ri}\hat{}2/L\hat{}2]) +$
$(\mathrm{C}^2/2) * L\hat{}3 * \mathrm{Sqrt}[\pi] * \mathrm{Erf}[\mathrm{ri}/L]))$

-1.73556×10^{32}

$\mathrm{qgtilde} = (\mathrm{integralterm} - \mathrm{Moc} * \psi) * \Delta\mathrm{rhoc} * ((4 * \pi * \mathrm{ri}\hat{}2)/\mathrm{Moc}) * \mathrm{dri}$

-3.87329×10^{27}

$\mathrm{qltilde} = (4 * \pi * \mathrm{ri}\hat{}2 * \mathrm{LH} * \mathrm{rhoi}) * \mathrm{dri}$

-3.37941×10^{27}

$\mathrm{qttilde} = \mathrm{qstilde} + \mathrm{qgtilde} + \mathrm{qltilde}$

-1.11835×10^{28}

$\mathrm{QR} = 8.252652352083379\mathrm{*}\hat{}12$

8.25265×10^{12}

$\mathrm{Qc} = 4.707995209388494\mathrm{*}\hat{}12$

4.708×10^{12}

$\mathrm{dTc} = ((\mathrm{Qc} - \mathrm{QR})/\mathrm{qttilde}) * 86400 * 365 * 10\hat{}9$

9.9955

B.4.4 Q_C

$\boldsymbol{R = 0.8 * 6378 * 1000}$

5.1024×10^6

$\mathbf{kb = 5.8}$

5.8

$\boldsymbol{\kappa}\mathbf{b = 10 * 10\hat{}\, - 7}$

$\frac{1}{1000000}$

$\mathbf{Tc = 5510}$

5510

$\mathbf{Rac = 600}$

600

$\mathbf{rhom = 7000}$

7000

$\boldsymbol{g = 9.8}$

9.8

$\boldsymbol{\alpha}\mathbf{m = 2.2 * 10\hat{}\, - 5}$

0.000022

$\mathbf{Tm = 4400}$

4400

$\boldsymbol{\eta}\mathbf{b = 2.5 * 10\hat{}23}$

2.5×10^{23}

$\boldsymbol{\delta}\mathbf{b = ((Rac * \boldsymbol{\kappa} b * \boldsymbol{\eta} b)/(rhom * \boldsymbol{g} * \boldsymbol{\alpha} m * (Tc - Tm)))\hat{}(1/3)}$

$447377.$

$\mathbf{Fb = kb * (Tc - Tm)/\boldsymbol{\delta} b}$

0.0143905

$\mathbf{Qc = 4 * \boldsymbol{\pi} * \boldsymbol{R}\hat{}2 * Fb}$

4.708×10^{12}

B.5 Rydberg EoS - $Q_R = 0$

B.5.1 Q_g

rho0 = 7900

7900

rc = 0.8 * 6378 * 1000

5.1024×10^6

ri = 0.8 * (1220/3480) * 6378 * 1000

1.78877×10^6

K0 = 500 * 10^9

500000000000

G = 6.67384 * 10^ − 11

6.67384×10^{-11}

rhocen = 20600

20600

L = Sqrt[(3 * K0 * (Log[rhocen/rho0] + 1))/(2 * π * G * rho0 * rhocen)]

6.56107×10^6

ψ = (2/3 * π * G * rhocen * ri^2 * (1 − (3 * ri^2)/(10 * L^2)))−
(2/3 * π * G * rhocen * rc^2 * (1 − (3 * rc^2)/(10 * L^2)))

-5.23548×10^7

Moc = (4/3 * π * rhocen * rc^3 * Exp[−rc^2/L^2] * (1 + (2/5) * (rc^2/L^2)))−
(4/3 * π * rhocen * ri^3 * Exp[−ri^2/L^2] * (1 + (2/5) * (ri^2/L^2)))

7.30315×10^{24}

Δrhoc = 575

575

dri = 77.79272701335886 * 1000/(10^9 * 86400 * 365)

2.46679×10^{-12}

C^2 = (3 * L^2)/16 − ((rc^2)/2) * (1 − ((3 * rc^2)/(10 * L^2)))

-2.58403×10^{12}

integralterm = ((8 * π^2 * rhocen^2 * G)/3)*
(((((3/20 * rc^5) − (L^2/8 * rc^3) − (L^2 * C^2 * rc)) * Exp[−rc^2/L^2])+
(C^2/2) * L^3 * Sqrt[π] * Erf[rc/L])−
((((3/20 * ri^5) − (L^2/8 * ri^3) − (L^2 * C^2 * ri)) * Exp[−ri^2/L^2])+
(C^2/2) * L^3 * Sqrt[π] * Erf[ri/L]))

-1.73556×10^{32}

Qg = (integralterm − Moc * ψ) * Δrhoc * ((4 * π * ri^2)/Moc) * dri

1.63057×10^{12}

B.5.2 Q_L

```
ri = 0.8 * (1220/3480) * 6378 * 1000
1.78877 × 10^6
LH = 750000
750000
rhocen = 20600
20600
rho0 = 7900
7900
K0 = 500 * 10^9
500000000000
G = 6.67384 * 10^ - 11
6.67384 × 10^-11
L = Sqrt[(3 * K0 * (Log[rhocen/rho0] + 1))/(2 * π * G * rho0 * rhocen)]
6.56107 × 10^6
rhoi = rhocen * Exp[-ri^2/L^2]
19124.3
ΔdTdP = 1.3/10^9
1.3 × 10^-9
Ti = 7900
7900
Tc = 5510
5510
dTc = -13.275967362134109/(10^9 * 86400 * 365)
-4.20978 × 10^-16
g = (4 * π/3) * G * rhocen * ri * (1 - ((3 * ri^2)/(5 * L^2)))
9.84177
QL = -(4 * π * ri^2 * LH * Ti)/(ΔdTdP * g) * (1/Tc) * dTc
1.42266 × 10^12
```

B.5.3 Q_s

K0 = 500 * 10^9

500000000000

rhocen = 20600

20600

rho0 = 7900

7900

G = 6.67384 * 10^ − 11

6.67384×10^{-11}

L = Sqrt[(3 * K0 * (Log[rhocen/rho0] + 1))/(2 * π * G * rho0 * rhocen)]

6.56107×10^{6}

Cp = 840

840

α = 1.35 * 10^ − 5

0.0000135

Dd = Sqrt[(3 * Cp)/(2 * π * α * rhocen * G)]

4.6486×10^{6}

A^2 = ((1/L^2) + (1/Dd^2))^(−1)

1.43872×10^{13}

Tcen = 7970

7970

Tc = 5510

5510

rc = 0.8 * 6378 * 1000

5.1024×10^{6}

Is = (4/3) * π * Tcen * rhocen * rc^3 * Exp[−rc^2/A^2] * (1 + (2/5) * (rc^2/A^2))

2.5784×10^{28}

dTc = −13.275967362134109/(10^9 * 86400 * 365)

-4.20978×10^{-16}

Qs = −(Cp/Tc) * dTc * Is

1.65477×10^{12}

B.5.4 $\tilde{Q}_T$

$\mathbf{K0 = 500 * 10\hat{\ }9}$

500000000000

$\mathbf{rhocen = 20600}$

20600

$\mathbf{rho0 = 7900}$

7900

$\boldsymbol{G = 6.67384 * 10\hat{\ } - 11}$

6.67384×10^{-11}

$\boldsymbol{L = \mathrm{Sqrt}[(3 * \mathrm{K0} * (\mathrm{Log}[\mathrm{rhocen/rho0}] + 1))/(2 * \pi * G * \mathrm{rho0} * \mathrm{rhocen})]}$

6.56107×10^{6}

$\mathbf{Cp = 840}$

840

$\boldsymbol{\alpha = 1.35 * 10\hat{\ } - 5}$

0.0000135

$\boldsymbol{\mathrm{Dd} = \mathrm{Sqrt}[(3 * \mathrm{Cp})/(2 * \pi * \alpha * \mathrm{rhocen} * G)]}$

4.6486×10^{6}

$\boldsymbol{\mathrm{A}^2 = ((1/L\hat{\ }2) + (1/\mathrm{Dd}\hat{\ }2))\hat{\ }(-1)}$

1.43872×10^{13}

$\mathbf{Tcen = 7970}$

7970

$\mathbf{Tc = 5510}$

5510

$\mathbf{rc = 0.8 * 6378 * 1000}$

5.1024×10^{6}

$\boldsymbol{\mathrm{Is} = (4/3) * \pi * \mathrm{Tcen} * \mathrm{rhocen} * \mathrm{rc}\hat{\ }3 * \mathrm{Exp}[-\mathrm{rc}\hat{\ }2/\mathrm{A}^2] * (1 + (2/5) * (\mathrm{rc}\hat{\ }2/\mathrm{A}^2))}$

2.5784×10^{28}

$\mathbf{ri = 0.8 * (1220/3480) * 6378 * 1000}$

1.78877×10^{6}

$\boldsymbol{\psi = (2/3 * \pi * G * \mathrm{rhocen} * \mathrm{ri}\hat{\ }2 * (1 - (3 * \mathrm{ri}\hat{\ }2)/(10 * L\hat{\ }2))) -}$
$\boldsymbol{(2/3 * \pi * G * \mathrm{rhocen} * \mathrm{rc}\hat{\ }2 * (1 - (3 * \mathrm{rc}\hat{\ }2)/(10 * L\hat{\ }2)))}$

-5.23548×10^{7}

$\boldsymbol{\mathrm{Moc} = (4/3 * \pi * \mathrm{rhocen} * \mathrm{rc}\hat{\ }3 * \mathrm{Exp}[-\mathrm{rc}\hat{\ }2/L\hat{\ }2] * (1 + (2/5) * (\mathrm{rc}\hat{\ }2/L\hat{\ }2))) -}$
$\boldsymbol{(4/3 * \pi * \mathrm{rhocen} * \mathrm{ri}\hat{\ }3 * \mathrm{Exp}[-\mathrm{ri}\hat{\ }2/L\hat{\ }2] * (1 + (2/5) * (\mathrm{ri}\hat{\ }2/L\hat{\ }2)))}$

7.30315×10^{24}

$\boldsymbol{\Delta\mathrm{dTdP} = 1.3/10\hat{\ }9}$

1.3×10^{-9}

```
Δrhoc = 575
575
Ti = 7900
7900
rhoi = rhocen * Exp[−ri^2/L^2]
19124.3
g = (4 * π/3) * G * rhocen * ri * (1 − ((3 * ri^2)/(5 * L^2)))
9.84177
dri = −(1/ΔdTdP) * (Ti/(rhoi * g)) * (1/Tc)
−5859.67
C^2 = (3 * L^2)/16 − ((rc^2)/2) * (1 − ((3 * rc^2)/(10 * L^2)))
−2.58403 × 10^12
qstilde = −(Cp/Tc) * Is
−3.93077 × 10^27
integralterm = ((8 * π^2 * rhocen^2 * G)/3)*
(((( (3/20 * rc^5) − (L^2/8 * rc^3) − (L^2 * C^2 * rc)) * Exp[−rc^2/L^2])+
(C^2/2) * L^3 * Sqrt[π] * Erf[rc/L])−
((((3/20 * ri^5) − (L^2/8 * ri^3) − (L^2 * C^2 * ri)) * Exp[−ri^2/L^2])+
(C^2/2) * L^3 * Sqrt[π] * Erf[ri/L]))
−1.73556 × 10^32
qgtilde = (integralterm − Moc * ψ) * Δrhoc * ((4 * π * ri^2)/Moc) * dri
−3.87329 × 10^27
qltilde = (4 * π * ri^2 * LH * rhoi) * dri
−3.37941 × 10^27
qttilde = qstilde + qgtilde + qltilde
−1.11835 × 10^28
Qc = 4.707995209388494*^12
4.708 × 10^12
dTc = (Qc/qttilde) * 86400 * 365 * 10^9
−13.276
```

B.5.5 dr_i/dt

ΔdTdP = 1.3/10^9

1.3×10^{-9}

Ti = 7900

7900

Tc = 5510

5510

dTc = −13.275967362134109/(10^9 * 86400 * 365)

-4.20978×10^{-16}

ri = 0.8 * (1220/3480) * 6378 * 1000

1.78877×10^{6}

rho0 = 7900

7900

K0 = 500 * 10^9

500000000000

***G* = 6.67384 * 10^ − 11**

6.67384×10^{-11}

rhocen = 20600

20600

***L* = Sqrt[(3 * K0 * (Log[rhocen/rho0] + 1))/(2 * π * *G* * rho0 * rhocen)]**

6.56107×10^{6}

rhoi = rhocen * Exp[−ri^2/*L*^2]

19124.3

***g* = (4 * π/3) * *G* * rhocen * ri * (1 − ((3 * ri^2)/(5 * *L*^2)))**

9.84177

dri = −(((1/(ΔdTdP)) * (Ti/(rhoi * *g*)) * (1/Tc) * dTc) * 10^9 * 86400 * 365)/1000

77.7927

B.6 Rydberg EoS - $Q_R \rightarrow$ Lower Bound

B.6.1 Q_g

rho0 = 7900

7900

rc = 0.8 * 6378 * 1000

5.1024×10^6

ri = 0.8 * (1220/3480) * 6378 * 1000

1.78877×10^6

K0 = 500 * 10^9

500000000000

G **= 6.67384 * 10^ − 11**

6.67384×10^{-11}

rhocen = 20600

20600

L **= Sqrt[(3 * K0 * (Log[rhocen/rho0] + 1))/(2 *** π *** G * rho0 * rhocen)]**

6.56107×10^6

ψ **= (2/3 *** π *** G * rhocen * ri^2 * (1 − (3 * ri^2)/(10 *** L**^2)))−**
(2/3 * π *** G * rhocen * rc^2 * (1 − (3 * rc^2)/(10 *** L**^2)))**

-5.23548×10^7

Moc = (4/3 * π *** rhocen * rc^3 * Exp[−rc^2/**L**^2] * (1 + (2/5) * (rc^2/**L**^2)))−**
(4/3 * π *** rhocen * ri^3 * Exp[−ri^2/**L**^2] * (1 + (2/5) * (ri^2/**L**^2)))**

7.30315×10^{24}

Δrhoc = 575

575

dri = 59.013790619839746 * 1000/(10^9 * 86400 * 365)

1.87132×10^{-12}

C^2 = (3 * L**^2)/16 − ((rc^2)/2) * (1 − ((3 * rc^2)/(10 *** L**^2)))**

-2.58403×10^{12}

integralterm = ((8 * π**^2 * rhocen^2 *** G**)/3)***
(((((3/20 * rc^5) − (L**^2/8 * rc^3) − (**L**^2 * C^2 * rc)) * Exp[−rc^2/**L**^2])+**
(C^2/2) * L**^3 * Sqrt[**π**] * Erf[rc/**L**])−**
((((3/20 * ri^5) − (L**^2/8 * ri^3) − (**L**^2 * C^2 * ri)) * Exp[−ri^2/**L**^2])+**
(C^2/2) * L**^3 * Sqrt[**π**] * Erf[ri/**L**]))**

-1.73556×10^{32}

Qg = (integralterm − Moc * ψ**) * Δrhoc * ((4 *** π *** ri^2)/Moc) * dri**

1.23696×10^{12}

B.6.2 Q_L

ri = 0.8 * (1220/3480) * 6378 * 1000

1.78877×10^6

LH = 750000

750000

rhocen = 20600

20600

rho0 = 7900

7900

K0 = 500 * 10^9

500000000000

G = 6.67384 * 10^ − 11

6.67384×10^{-11}

L = Sqrt[(3 * K0 * (Log[rhocen/rho0] + 1))/(2 * π * G * rho0 * rhocen)]

6.56107×10^6

rhoi = rhocen * Exp[−ri^2/L^2]

19124.3

ΔdTdP = 1.3/10^9

1.3×10^{-9}

Ti = 7900

7900

Tc = 5510

5510

dTc = −10.071187735201375/(10^9 * 86400 * 365)

-3.19355×10^{-16}

g = (4 * π/3) * G * rhocen * ri * (1 − ((3 * ri^2)/(5 * L^2)))

9.84177

QL = −(4 * π * ri^2 * LH * Ti)/(ΔdTdP * g) * (1/Tc) * dTc

1.07923×10^{12}

B.6.3 Q_R

CK40 = 1.31 * 10^ − 9

1.31×10^{-9}

CU238 = 9.93 * 10^ − 10

9.93×10^{-10}

CU235 = 7.1 * 10^ − 12

7.1×10^{-12}

CTh232 = 1.7 * 10^ − 10

1.7×10^{-10}

HK40 = 2.92 * 10^ − 5

0.0000292

HTh232 = 2.64 * 10^ − 5

0.0000264

HU238 = 9.46 * 10^ − 5

0.0000946

HU235 = 5.69 * 10^ − 4

0.000569

H0 = CU235 * HU235 + CU238 * HU238 + CTh232 * HTh232 + CK40 * HK40

1.40718×10^{-13}

rhocen = 20600

20600

rho0 = 7900

7900

K0 = 500 * 10^9

500000000000

***G* = 6.67384 * 10^ − 11**

6.67384×10^{-11}

***L* = Sqrt[(3 * K0 * (Log[rhocen/rho0] + 1))/(2 * π * *G* * rho0 * rhocen)]**

6.56107×10^{6}

***R* = 0.8 * 6378 * 10^3**

5.1024×10^{6}

Mc = 4 * π * rhocen * (((−*L*^2)/2) * *R* * Exp[(−*R*^2)/(*L*^2)] + ((*L*^3)/4) * Sqrt[π] * *N*[Erf[*R*/*L*], 5])
−4 * π * rhocen * (((*L*^3)/4) * Sqrt[π] * *N*[Erf[0], 5])

8.07643×10^{24}

QR = Mc * H0

1.1365×10^{12}

B.6.4 Q_s

$\mathbf{K0 = 500 * 10\hat{}9}$

500000000000

$\mathbf{rhocen = 20600}$

20600

$\mathbf{rho0 = 7900}$

7900

$G = \mathbf{6.67384 * 10\hat{} - 11}$

6.67384×10^{-11}

$L = \mathbf{Sqrt[(3 * K0 * (Log[rhocen/rho0] + 1))/(2 * \pi * } G \mathbf{ * rho0 * rhocen)]}$

6.56107×10^{6}

$\mathbf{Cp = 840}$

840

$\alpha = \mathbf{1.35 * 10\hat{} - 5}$

0.0000135

$\mathbf{Dd = Sqrt[(3 * Cp)/(2 * \pi * } \alpha \mathbf{ * rhocen * } G \mathbf{)]}$

4.6486×10^{6}

$\mathbf{A^2 = ((1/} L \mathbf{\hat{}2) + (1/Dd\hat{}2))\hat{}(-1)}$

1.43872×10^{13}

$\mathbf{Tcen = 7970}$

7970

$\mathbf{Tc = 5510}$

5510

$\mathbf{rc = 0.8 * 6378 * 1000}$

5.1024×10^{6}

$\mathbf{Is = (4/3) * \pi * Tcen * rhocen * rc\hat{}3 * Exp[-rc\hat{}2/A^2] * (1 + (2/5) * (rc\hat{}2/A^2))}$

2.5784×10^{28}

$\mathbf{dTc = -10.071187735201375/(10\hat{}9 * 86400 * 365)}$

-3.19355×10^{-16}

$\mathbf{Qs = -(Cp/Tc) * dTc * Is}$

1.25531×10^{12}

B.6.5 $\tilde{Q}_T$

$\mathbf{K0 = 500 * 10\hat{}9}$

500000000000

$\mathbf{rhocen = 20600}$

20600

$\mathbf{rho0 = 7900}$

7900

$\boldsymbol{G = 6.67384 * 10\hat{} - 11}$

6.67384×10^{-11}

$\boldsymbol{L = \mathrm{Sqrt}[(3 * \mathrm{K0} * (\mathrm{Log}[\mathrm{rhocen/rho0}] + 1))/(2 * \pi * G * \mathrm{rho0} * \mathrm{rhocen})]}$

6.56107×10^{6}

$\mathbf{Cp = 840}$

840

$\mathbf{LH = 750000}$

750000

$\boldsymbol{\alpha = 1.35 * 10\hat{} - 5}$

0.0000135

$\boldsymbol{\mathrm{Dd} = \mathrm{Sqrt}[(3 * \mathrm{Cp})/(2 * \pi * \alpha * \mathrm{rhocen} * G)]}$

4.6486×10^{6}

$\boldsymbol{\mathrm{A}^2 = ((1/L\hat{}2) + (1/\mathrm{Dd}\hat{}2))\hat{}(-1)}$

1.43872×10^{13}

$\mathbf{Tcen = 7970}$

7970

$\mathbf{Tc = 5510}$

5510

$\mathbf{rc = 0.8 * 6378 * 1000}$

5.1024×10^{6}

$\boldsymbol{\mathrm{Is} = (4/3) * \pi * \mathrm{Tcen} * \mathrm{rhocen} * \mathrm{rc}\hat{}3 * \mathrm{Exp}[-\mathrm{rc}\hat{}2/\mathrm{A}^2] * (1 + (2/5) * (\mathrm{rc}\hat{}2/\mathrm{A}^2))}$

2.5784×10^{28}

$\mathbf{ri = 0.8 * (1220/3480) * 6378 * 1000}$

1.78877×10^{6}

$\boldsymbol{\psi = (2/3 * \pi * G * \mathrm{rhocen} * \mathrm{ri}\hat{}2 * (1 - (3 * \mathrm{ri}\hat{}2)/(10 * L\hat{}2))) -}$
$\boldsymbol{(2/3 * \pi * G * \mathrm{rhocen} * \mathrm{rc}\hat{}2 * (1 - (3 * \mathrm{rc}\hat{}2)/(10 * L\hat{}2)))}$

-5.23548×10^{7}

$\boldsymbol{\mathrm{Moc} = (4/3 * \pi * \mathrm{rhocen} * \mathrm{rc}\hat{}3 * \mathrm{Exp}[-\mathrm{rc}\hat{}2/L\hat{}2] * (1 + (2/5) * (\mathrm{rc}\hat{}2/L\hat{}2))) -}$
$\boldsymbol{(4/3 * \pi * \mathrm{rhocen} * \mathrm{ri}\hat{}3 * \mathrm{Exp}[-\mathrm{ri}\hat{}2/L\hat{}2] * (1 + (2/5) * (\mathrm{ri}\hat{}2/L\hat{}2)))}$

7.30315×10^{24}

$\Delta\mathbf{dTdP = 1.3/10\hat{}9}$

1.3×10^{-9}

$\Delta\mathbf{rhoc = 575}$

575

$\mathbf{Ti = 7900}$

7900

$\mathbf{rhoi = rhocen * Exp[-ri\hat{}2/}\boldsymbol{L}\mathbf{\hat{}2]}$

19124.3

$\boldsymbol{g}\mathbf{ = (4 * }\boldsymbol{\pi}\mathbf{/3) * }\boldsymbol{G}\mathbf{ * rhocen * ri * (1 - ((3 * ri\hat{}2)/(5 * }\boldsymbol{L}\mathbf{\hat{}2)))}$

9.84177

$\mathbf{dri = -(1/\Delta dTdP) * (Ti/(rhoi * }\boldsymbol{g}\mathbf{)) * (1/Tc)}$

-5859.67

$\mathbf{C^2 = (3 * }\boldsymbol{L}\mathbf{\hat{}2)/16 - ((rc\hat{}2)/2) * (1 - ((3 * rc\hat{}2)/(10 * }\boldsymbol{L}\mathbf{\hat{}2)))}$

-2.58403×10^{12}

$\mathbf{qstilde = -(Cp/Tc) * Is}$

-3.93077×10^{27}

$\mathbf{integralterm = ((8 * }\boldsymbol{\pi}\mathbf{\hat{}2 * rhocen\hat{}2 * }\boldsymbol{G}\mathbf{)/3)*}$
$\mathbf{(((((3/20 * rc\hat{}5) - (}\boldsymbol{L}\mathbf{\hat{}2/8 * rc\hat{}3) - (}\boldsymbol{L}\mathbf{\hat{}2 * C^2 * rc)) * Exp[-rc\hat{}2/}\boldsymbol{L}\mathbf{\hat{}2])+}$
$\mathbf{(C^2/2) * }\boldsymbol{L}\mathbf{\hat{}3 * Sqrt[}\boldsymbol{\pi}\mathbf{] * Erf[rc/}\boldsymbol{L}\mathbf{])-}$
$\mathbf{((((3/20 * ri\hat{}5) - (}\boldsymbol{L}\mathbf{\hat{}2/8 * ri\hat{}3) - (}\boldsymbol{L}\mathbf{\hat{}2 * C^2 * ri)) * Exp[-ri\hat{}2/}\boldsymbol{L}\mathbf{\hat{}2])+}$
$\mathbf{(C^2/2) * }\boldsymbol{L}\mathbf{\hat{}3 * Sqrt[}\boldsymbol{\pi}\mathbf{] * Erf[ri/}\boldsymbol{L}\mathbf{]))}$

-1.73556×10^{32}

$\mathbf{qgtilde = (integralterm - Moc * }\boldsymbol{\psi}\mathbf{) * \Delta rhoc * ((4 * }\boldsymbol{\pi}\mathbf{ * ri\hat{}2)/Moc) * dri}$

-3.87329×10^{27}

$\mathbf{qltilde = (4 * }\boldsymbol{\pi}\mathbf{ * ri\hat{}2 * LH * rhoi) * dri}$

-3.37941×10^{27}

$\mathbf{qttilde = qstilde + qgtilde + qltilde}$

-1.11835×10^{28}

$\mathbf{QR = 1.136496250644574*\hat{}12}$

1.1365×10^{12}

$\mathbf{Qc = 4.707995209388494*\hat{}12}$

4.708×10^{12}

$\mathbf{dTc = ((Qc - QR)/qttilde) * 86400 * 365 * 10\hat{}9}$

-10.0712

B.6.6 dr_i/dt

ΔdTdP = 1.3/10^9

1.3×10^{-9}

Ti = 7900

7900

Tc = 5510

5510

dTc = −10.071187735201375/(10^9 ∗ 86400 ∗ 365)

-3.19355×10^{-16}

ri = 0.8 ∗ (1220/3480) ∗ 6378 ∗ 1000

1.78877×10^{6}

rho0 = 7900

7900

K0 = 500 ∗ 10^9

500000000000

G = 6.67384 ∗ 10^ − 11

6.67384×10^{-11}

rhocen = 20600

20600

L = Sqrt[(3 ∗ K0 ∗ (Log[rhocen/rho0] + 1))/(2 ∗ π ∗ G ∗ rho0 ∗ rhocen)]

6.56107×10^{6}

rhoi = rhocen ∗ Exp[−ri^2/L^2]

19124.3

g = (4 ∗ π/3) ∗ G ∗ rhocen ∗ ri ∗ (1 − ((3 ∗ ri^2)/(5 ∗ L^2)))

9.84177

dri = −(((1/(ΔdTdP)) ∗ (Ti/(rhoi ∗ g)) ∗ (1/Tc) ∗ dTc) ∗ 10^9 ∗ 86400 ∗ 365)/1000

59.0138

Appendix C

Mathematica Scripts - Calculations for $10M_{\oplus}$ Planets

C.1 Keane EoS - Normal

C.1.1 Q_k

```
rc = 0.9 * 6378 * 1000
```
5.7402×10^{6}
```
k = 40
```
40
```
Tc = 7280
```
7280
```
cp = 840
```
840
```
α = 1.35 * 10^ − 5
```
0.0000135
```
rhocen = 30100
```
30100
```
G = 6.67384 * 10^ − 11
```
6.67384×10^{-11}
```
Dd = Sqrt[(3 * cp)/(2 * π * α * rhocen * G)]
```
3.84567×10^{6}
```
Qk = (8 * π * rc^3 * k * Tc)/Dd^2
```
9.35982×10^{13}
```
Plot[(8 * π * rc^3 * k * Tc)/Dd^2, {rc, 3480 * 1000, 6378 * 1000}, Ticks → {{3.4 * 10^6, 3480 * 1000,
6378 * 1000}, Automatic}]
```

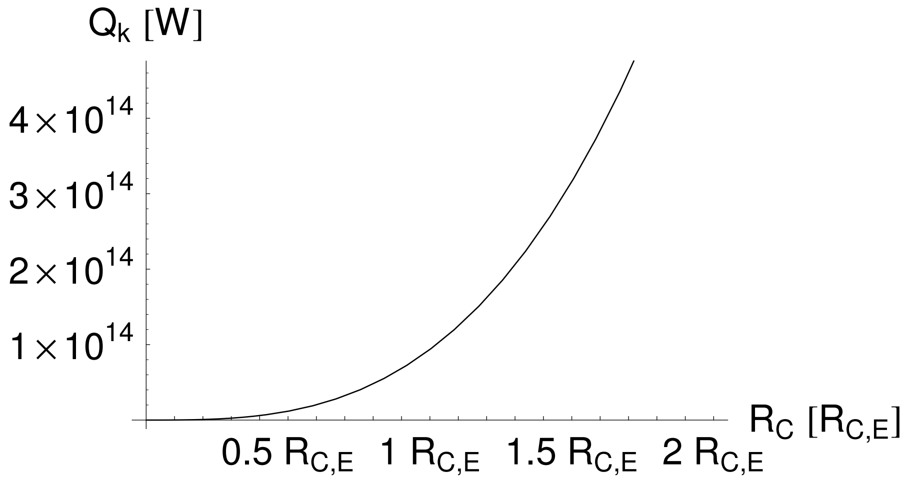

Q_k [W]
4×10^{14}
3×10^{14}
2×10^{14}
1×10^{14}
R_C [$R_{C,E}$]
0.5 $R_{C,E}$
1 $R_{C,E}$
1.5 $R_{C,E}$
2 $R_{C,E}$

−Graphics−

C.1.2 Q_R

$\mathbf{CK40 = 2.44 * 10\hat{\ } - 8}$

2.44×10^{-8}

$\mathbf{CU238 = 2.98 * 10\hat{\ } - 9}$

2.98×10^{-9}

$\mathbf{CU235 = 2.13 * 10\hat{\ } - 11}$

2.13×10^{-11}

$\mathbf{CTh232 = 5.8 * 10\hat{\ } - 10}$

5.8×10^{-10}

$\mathbf{HK40 = 2.92 * 10\hat{\ } - 5}$

0.0000292

$\mathbf{HTh232 = 2.64 * 10\hat{\ } - 5}$

0.0000264

$\mathbf{HU238 = 9.46 * 10\hat{\ } - 5}$

0.0000946

$\mathbf{HU235 = 5.69 * 10\hat{\ } - 4}$

0.000569

$\mathbf{H0 = CU235 * HU235 + CU238 * HU238 + CTh232 * HTh232 + CK40 * HK40}$

1.02182×10^{-12}

$\mathbf{rhocen = 30100}$

30100

$\mathbf{rho0 = 7900}$

7900

$\mathbf{K0 = 500 * 10\hat{\ }9}$

500000000000

$\boldsymbol{G} \mathbf{= 6.67384 * 10\hat{\ } - 11}$

6.67384×10^{-11}

$\boldsymbol{L} \mathbf{= Sqrt[(3 * K0 * (Log[rhocen/rho0] + 1))/(2 * \pi *} \boldsymbol{G} \mathbf{* rho0 * rhocen)]}$

5.9301×10^{6}

$\boldsymbol{R} \mathbf{= 0.9 * 6378 * 10\hat{\ }3}$

5.7402×10^{6}

$\mathbf{Mc = 4 * \pi * rhocen * (((-}\boldsymbol{L}\mathbf{\hat{\ }2)/2) *} \boldsymbol{R} \mathbf{* Exp[(-}\boldsymbol{R}\mathbf{\hat{\ }2)/(}\boldsymbol{L}\mathbf{\hat{\ }2)] + ((}\boldsymbol{L}\mathbf{\hat{\ }3)/4) * Sqrt[\pi] *} \boldsymbol{N}\mathbf{[Erf[}\boldsymbol{R/L}\mathbf{], 5]) -}$
$\mathbf{4 * \pi * rhocen * (((}\boldsymbol{L}\mathbf{\hat{\ }3)/4) * Sqrt[\pi] *} \boldsymbol{N}\mathbf{[Erf[0], 5])}$

1.40168×10^{25}

$\mathbf{QR = Mc * H0}$

1.43227×10^{13}

C.1.3 $\tilde{Q}_T$

K0 = 500 * 10^9

500000000000

rhocen = 30100

30100

rho0 = 7900

7900

***G* = 6.67384 * 10^ − 11**

6.67384×10^{-11}

***L* = Sqrt[(3 * K0 * (Log[rhocen/rho0] + 1))/(2 * π * *G* * rho0 * rhocen)]**

5.9301×10^{6}

Cp = 840

840

α = 1.35 * 10^ − 5

0.0000135

Dd = Sqrt[(3 * Cp)/(2 * π * α * rhocen * *G*)]

3.84567×10^{6}

A^2 = ((1/*L*^2) + (1/Dd^2))^(−1)

1.04109×10^{13}

Tcen = 11800

11800

Tc = 7280

7280

rc = 0.9 * 6378 * 1000

5.7402×10^{6}

Is = (4/3) * π * Tcen * rhocen * rc^3 * Exp[−rc^2/A^2] * (1 + (2/5) * (rc^2/A^2))

2.69187×10^{28}

ri = 0.9 * (1220/3480) * 6378 * 1000

2.01237×10^{6}

ψ = (2/3 * π * *G* * rhocen * ri^2 * (1 − (3 * ri^2)/(10 * *L*^2)))−
(2/3 * π * *G* * rhocen * rc^2 * (1 − (3 * rc^2)/(10 * *L*^2)))

-8.32121×10^{7}

Moc = (4/3 * π * rhocen * rc^3 * Exp[−rc^2/*L*^2] * (1 + (2/5) * (rc^2/*L*^2)))−
(4/3 * π * rhocen * ri^3 * Exp[−ri^2/*L*^2] * (1 + (2/5) * (ri^2/*L*^2)))

1.18875×10^{25}

ΔdTdP = 1.3/10^9

1.3×10^{-9}

$\mathbf{\Delta rhoc = 575}$

575

Ti = 11400

11400

$\mathbf{rhoi = rhocen * Exp[-ri\hat{}2/\mathit{L}\hat{}2]}$

26825.9

$\mathbf{\mathit{g} = (4 * \pi/3) * \mathit{G} * rhocen * ri * (1 - ((3 * ri\hat{}2)/(5 * \mathit{L}\hat{}2)))}$

15.7632

$\mathbf{dri = -(1/\Delta dTdP) * (Ti/(rhoi * \mathit{g})) * (1/Tc)}$

-2848.6

$\mathbf{C^2 = (3 * \mathit{L}\hat{}2)/16 - ((rc\hat{}2)/2) * (1 - ((3 * rc\hat{}2)/(10 * \mathit{L}\hat{}2)))}$

-5.2503×10^{12}

$\mathbf{qstilde = -(Cp/Tc) * Is}$

-3.106×10^{27}

$\mathbf{integralterm = ((8 * \pi\hat{}2 * rhocen\hat{}2 * \mathit{G})/3)*}$
$\mathbf{(((((3/20 * rc\hat{}5) - (\mathit{L}\hat{}2/8 * rc\hat{}3) - (\mathit{L}\hat{}2 * C^2 * rc)) * Exp[-rc\hat{}2/\mathit{L}\hat{}2])+}$
$\mathbf{(C^2/2) * \mathit{L}\hat{}3 * Sqrt[\pi] * Erf[rc/\mathit{L}])-}$
$\mathbf{((((3/20 * ri\hat{}5) - (\mathit{L}\hat{}2/8 * ri\hat{}3) - (\mathit{L}\hat{}2 * C^2 * ri)) * Exp[-ri\hat{}2/\mathit{L}\hat{}2])+}$
$\mathbf{(C^2/2) * \mathit{L}\hat{}3 * Sqrt[\pi] * Erf[ri/\mathit{L}]))}$

-4.68603×10^{32}

$\mathbf{qgtilde = (integralterm - Moc * \psi) * \Delta rhoc * ((4 * \pi * ri\hat{}2)/Moc) * dri}$

-3.65025×10^{27}

$\mathbf{qltilde = (4 * \pi * ri\hat{}2 * LH * rhoi) * dri}$

-2.91657×10^{27}

qttilde = qstilde + qgtilde + qltilde

-9.67282×10^{27}

QR = 1.4322656783193984`*^13

1.43227×10^{13}

Qc = 1.2128514782867988`*^13

1.21285×10^{13}

$\mathbf{dTc = ((Qc - QR)/qttilde) * 86400 * 365 * 10\hat{}9}$

7.15349

$\mathbf{Plot[((Qc - QR)/qttilde) * 86400 * 365 * 10\hat{}9, \{QR, 0, 5 * 10\hat{}12\}]}$

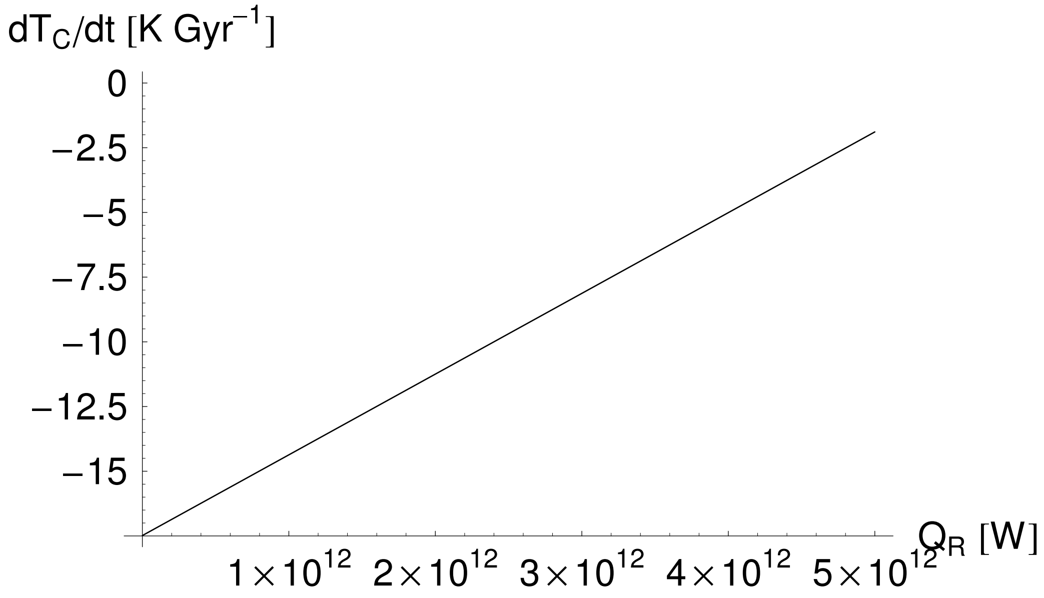

dTC/dt [K Gyr−1]
0
−2.5
−5
−7.5
−10
−12.5
−15
QR [W]
1×10^12
2×10^12
3×10^12
4×10^12
5×10^12

−Graphics−

C.1.4 Q_C

$\boldsymbol{R = 0.9 * 6378 * 1000}$

5.7402×10^6

$\mathbf{kb = 5.8}$

5.8

$\boldsymbol{\kappa\mathbf{b} = 10 * 10\hat{} - 7}$

$\frac{1}{1000000}$

$\mathbf{Tc = 7280}$

7280

$\mathbf{Rac = 600}$

600

$\mathbf{rhom = 9000}$

9000

$\boldsymbol{g = 9.8}$

9.8

$\boldsymbol{\alpha\mathbf{m} = 2.2 * 10\hat{} - 5}$

0.000022

$\mathbf{Tm = 5600}$

5600

$\boldsymbol{\eta\mathbf{b} = 2.0 * 10\hat{}23}$

$2. \times 10^{23}$

$\boldsymbol{\delta\mathbf{b} = ((\mathbf{Rac} * \kappa\mathbf{b} * \eta\mathbf{b})/(\mathbf{rhom} * g * \alpha\mathbf{m} * (\mathbf{Tc} - \mathbf{Tm})))\hat{}(1/3)}$

$332655.$

$\boldsymbol{\mathbf{Fb} = \mathbf{kb} * (\mathbf{Tc} - \mathbf{Tm})/\delta\mathbf{b}}$

0.0292916

$\boldsymbol{\mathbf{Qc} = 4 * \pi * R\hat{}2 * \mathbf{Fb}}$

1.21285×10^{13}

C.2 Keane EoS - $Q_R = 0$

C.2.1 Q_g

rho0 = 7900

7900

rc = 0.9 * 6378 * 1000

5.7402×10^6

ri = 0.9 * (1220/3480) * 6378 * 1000

2.01237×10^6

K0 = 500 * 10^9

500000000000

***G* = 6.67384 * 10^ − 11**

6.67384×10^{-11}

rhocen = 30100

30100

***L* = Sqrt[(3 * K0 * (Log[rhocen/rho0] + 1))/(2 * *π* * *G* * rho0 * rhocen)]**

5.9301×10^6

***ψ* = (2/3 * *π* * *G* * rhocen * ri^2 * (1 − (3 * ri^2)/(10 * *L*^2)))−**
(2/3 * *π* * *G* * rhocen * rc^2 * (1 − (3 * rc^2)/(10 * *L*^2)))

-8.32121×10^7

Moc = (4/3 * *π* * rhocen * rc^3 * Exp[−rc^2/*L*^2] * (1 + (2/5) * (rc^2/*L*^2)))−
(4/3 * *π* * rhocen * ri^3 * Exp[−ri^2/*L*^2] * (1 + (2/5) * (ri^2/*L*^2)))

1.18875×10^{25}

Δrhoc = 575

575

dri = 112.64001390185491` * 1000/(10^9 * 86400 * 365)

3.57179×10^{-12}

C^2 = (3 * *L*^2)/16 − ((rc^2)/2) * (1 − ((3 * rc^2)/(10 * *L*^2)))

-5.2503×10^{12}

integralterm = ((8 * *π*^2 * rhocen^2 * *G*)/3)*
(((((3/20 * rc^5) − (*L*^2/8 * rc^3) − (*L*^2 * C^2 * rc)) * Exp[−rc^2/*L*^2])+
(C^2/2) * *L*^3 * Sqrt[*π*] * Erf[rc/*L*])−
((((3/20 * ri^5) − (*L*^2/8 * ri^3) − (*L*^2 * C^2 * ri)) * Exp[−ri^2/*L*^2])+
(C^2/2) * *L*^3 * Sqrt[*π*] * Erf[ri/*L*]))

-4.68603×10^{32}

Qg = (integralterm − Moc * *ψ*) * Δrhoc * ((4 * *π* * ri^2)/Moc) * dri

4.57696×10^{12}

C.2.2 Q_L

$\mathbf{ri = 0.9 * (1220/3480) * 6378 * 1000}$

2.01237×10^6

$\mathbf{LH = 750000}$

750000

$\mathbf{rhocen = 30100}$

30100

$\mathbf{rho0 = 7900}$

7900

$\mathbf{K0 = 500 * 10\hat{\ }9}$

500000000000

$\boldsymbol{G} \mathbf{= 6.67384 * 10\hat{\ } - 11}$

6.67384×10^{-11}

$\boldsymbol{L} \mathbf{= Sqrt[(3 * K0 * (Log[rhocen/rho0] + 1))/(2 * \pi *} \boldsymbol{G} \mathbf{* rho0 * rhocen)]}$

5.9301×10^6

$\mathbf{rhoi = rhocen * Exp[-ri\hat{\ }2/}\boldsymbol{L}\mathbf{\hat{\ }2]}$

26825.9

$\mathbf{\Delta dTdP = 1.3/10\hat{\ }9}$

1.3×10^{-9}

$\mathbf{Ti = 11400}$

11400

$\mathbf{Tc = 7280}$

7280

$\mathbf{dTc = -39.542221196997566/(10\hat{\ }9 * 86400 * 365)}$

-1.25388×10^{-15}

$\boldsymbol{g} \mathbf{= (4 * \pi/3) *} \boldsymbol{G} \mathbf{* rhocen * ri * (1 - ((3 * ri\hat{\ }2)/(5 *} \boldsymbol{L}\mathbf{\hat{\ }2)))}$

15.7632

$\mathbf{QL = -(4 * \pi * ri\hat{\ }2 * LH * Ti)/(\Delta dTdP *} \boldsymbol{g}\mathbf{) * (1/Tc) * dTc}$

3.65702×10^{12}

C.2.3 Q_s

K0 = 500 * 10^9

500000000000

rhocen = 30100

30100

rho0 = 7900

7900

G = 6.67384 * 10^ − 11

6.67384×10^{-11}

L = Sqrt[(3 * K0 * (Log[rhocen/rho0] + 1))/(2 * π * G * rho0 * rhocen)]

5.9301×10^{6}

Cp = 840

840

α = 1.35 * 10^ − 5

0.0000135

Dd = Sqrt[(3 * Cp)/(2 * π * α * rhocen * G)]

3.84567×10^{6}

A^2 = ((1/L^2) + (1/Dd^2))^(−1)

1.04109×10^{13}

Tcen = 11800

11800

Tc = 7280

7280

rc = 0.9 * 6378 * 1000

5.7402×10^{6}

Is = (4/3) * π * Tcen * rhocen * rc^3 * Exp[−rc^2/A^2] * (1 + (2/5) * (rc^2/A^2))

2.69187×10^{28}

dTc = −39.542221196997566/(10^9 * 86400 * 365)

-1.25388×10^{-15}

Qs = −(Cp/Tc) * dTc * Is

3.89454×10^{12}

C.2.4 $\tilde{Q}_T$

K0 = 500 * 10^9

500000000000

rhocen = 30100

30100

rho0 = 7900

7900

***G* = 6.67384 * 10^ − 11**

6.67384×10^{-11}

***L* = Sqrt[(3 * K0 * (Log[rhocen/rho0] + 1))/(2 * π * *G* * rho0 * rhocen)]**

5.9301×10^{6}

Cp = 840

840

LH = 750000

750000

***α* = 1.35 * 10^ − 5**

0.0000135

Dd = Sqrt[(3 * Cp)/(2 * π * *α* * rhocen * *G*)]

3.84567×10^{6}

A^2 = ((1/*L*^2) + (1/Dd^2))^(−1)

1.04109×10^{13}

Tcen = 11800

11800

Tc = 7280

7280

rc = 0.9 * 6378 * 1000

5.7402×10^{6}

Is = (4/3) * π * Tcen * rhocen * rc^3 * Exp[−rc^2/A^2] * (1 + (2/5) * (rc^2/A^2))

2.69187×10^{28}

ri = 0.9 * (1220/3480) * 6378 * 1000

2.01237×10^{6}

***ψ* = (2/3 * π * *G* * rhocen * ri^2 * (1 − (3 * ri^2)/(10 * *L*^2)))−**
(2/3 * π * *G* * rhocen * rc^2 * (1 − (3 * rc^2)/(10 * *L*^2)))

-8.32121×10^{7}

Moc = (4/3 * π * rhocen * rc^3 * Exp[−rc^2/*L*^2] * (1 + (2/5) * (rc^2/*L*^2)))−
(4/3 * π * rhocen * ri^3 * Exp[−ri^2/*L*^2] * (1 + (2/5) * (ri^2/*L*^2)))

1.18875×10^{25}

$\Delta\mathbf{dTdP = 1.3/10\hat{\ }9}$

1.3×10^{-9}

$\Delta\mathbf{rhoc = 575}$

575

$\mathbf{Ti = 11400}$

11400

$\mathbf{rhoi = rhocen * Exp[-ri\hat{\ }2/\mathit{L}\hat{\ }2]}$

26825.9

$\mathbf{\mathit{g} = (4 * \pi/3) * \mathit{G} * rhocen * ri * (1 - ((3 * ri\hat{\ }2)/(5 * \mathit{L}\hat{\ }2)))}$

15.7632

$\mathbf{dri = -(1/\Delta dTdP) * (Ti/(rhoi * \mathit{g})) * (1/Tc)}$

-2848.6

$\mathbf{C^2 = (3 * \mathit{L}\hat{\ }2)/16 - ((rc\hat{\ }2)/2) * (1 - ((3 * rc\hat{\ }2)/(10 * \mathit{L}\hat{\ }2)))}$

-5.2503×10^{12}

$\mathbf{qstilde = -(Cp/Tc) * Is}$

-3.106×10^{27}

$\mathbf{integralterm = ((8 * \pi\hat{\ }2 * rhocen\hat{\ }2 * \mathit{G})/3)*}$
$\mathbf{(((((3/20 * rc\hat{\ }5) - (\mathit{L}\hat{\ }2/8 * rc\hat{\ }3) - (\mathit{L}\hat{\ }2 * C^2 * rc)) * Exp[-rc\hat{\ }2/\mathit{L}\hat{\ }2])+}$
$\mathbf{(C^2/2) * \mathit{L}\hat{\ }3 * Sqrt[\pi] * Erf[rc/\mathit{L}])-}$
$\mathbf{((((3/20 * ri\hat{\ }5) - (\mathit{L}\hat{\ }2/8 * ri\hat{\ }3) - (\mathit{L}\hat{\ }2 * C^2 * ri)) * Exp[-ri\hat{\ }2/\mathit{L}\hat{\ }2])+}$
$\mathbf{(C^2/2) * \mathit{L}\hat{\ }3 * Sqrt[\pi] * Erf[ri/\mathit{L}]))}$

-4.68603×10^{32}

$\mathbf{qgtilde = (integralterm - Moc * \psi) * \Delta rhoc * ((4 * \pi * ri\hat{\ }2)/Moc) * dri}$

-3.65025×10^{27}

$\mathbf{qltilde = (4 * \pi * ri\hat{\ }2 * LH * rhoi) * dri}$

-2.91657×10^{27}

$\mathbf{qttilde = qstilde + qgtilde + qltilde}$

-9.67282×10^{27}

$\mathbf{Qc = 1.2128514782867988{*}\hat{\ }13}$

1.21285×10^{13}

$\mathbf{dTc = (Qc/qttilde) * 86400 * 365 * 10\hat{\ }9}$

-39.5422

$\mathbf{Plot[((Qc - QR)/qttilde) * 86400 * 365 * 10\hat{\ }9, \{QR, 0, 5 * 10\hat{\ }12\}]}$

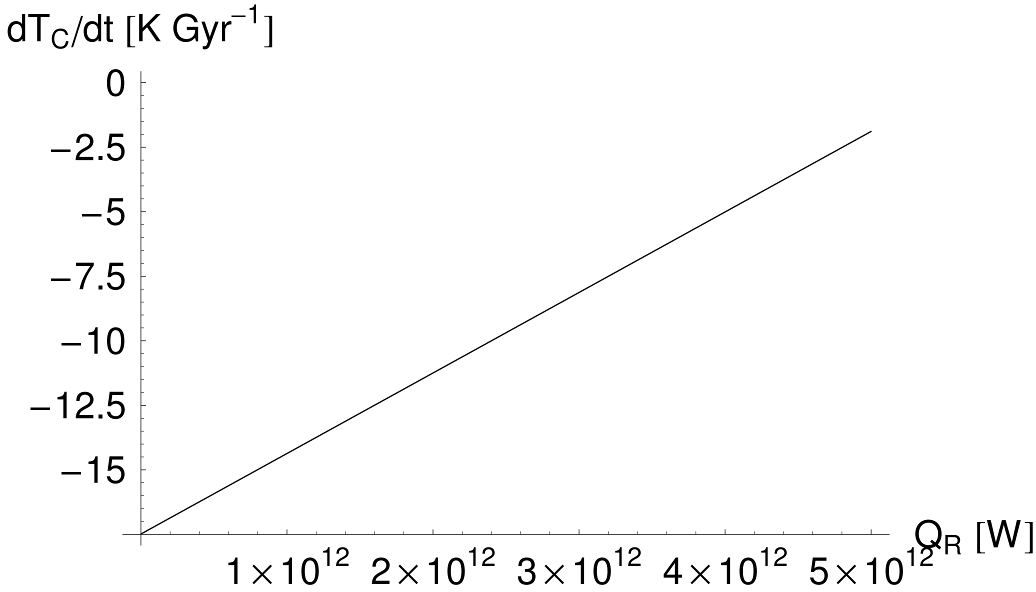
dT_C/dt [K Gyr^-1]
0
−2.5
−5
−7.5
−10
−12.5
−15
Q_R [W]
1×10^12
2×10^12
3×10^12
4×10^12
5×10^12

−Graphics−

C.2.5 dr_i/dt

ΔdTdP = 1.3/10^9

1.3×10^{-9}

Ti = 11400

11400

Tc = 7280

7280

dTc = −39.542221196997566/(10^9 ∗ 86400 ∗ 365)

-1.25388×10^{-15}

ri = 0.9 ∗ (1220/3480) ∗ 6378 ∗ 1000

2.01237×10^{6}

rho0 = 7900

7900

K0 = 500 ∗ 10^9

500000000000

G = 6.67384 ∗ 10^ − 11

6.67384×10^{-11}

rhocen = 30100

30100

L = Sqrt[(3 ∗ K0 ∗ (Log[rhocen/rho0] + 1))/(2 ∗ π ∗ G ∗ rho0 ∗ rhocen)]

5.9301×10^{6}

rhoi = rhocen ∗ Exp[−ri^2/L^2]

26825.9

g = (4 ∗ π/3) ∗ G ∗ rhocen ∗ ri ∗ (1 − ((3 ∗ ri^2)/(5 ∗ L^2)))

15.7632

dri = −(((1/(ΔdTdP)) ∗ (Ti/(rhoi ∗ g)) ∗ (1/Tc) ∗ dTc) ∗ 10^9 ∗ 86400 ∗ 365)/1000

112.64

C.3 Keane EoS - $Q_R \rightarrow$ Lower Bound

C.3.1 Q_g

rho0 = 7900

7900

rc = 0.9 * 6378 * 1000

5.7402×10^{6}

ri = 0.9 * (1220/3480) * 6378 * 1000

2.01237×10^{6}

K0 = 500 * 10^9

500000000000

G = 6.67384 * 10^ − 11

6.67384×10^{-11}

rhocen = 30100

30100

L = Sqrt[(3 * K0 * (Log[rhocen/rho0] + 1))/(2 * π * G * rho0 * rhocen)]

5.9301×10^{6}

ψ = (2/3 * π * G * rhocen * ri^2 * (1 − (3 * ri^2)/(10 * L^2)))−
(2/3 * π * G * rhocen * rc^2 * (1 − (3 * rc^2)/(10 * L^2)))

-8.32121×10^{7}

Moc = (4/3 * π * rhocen * rc^3 * Exp[−rc^2/L^2] * (1 + (2/5) * (rc^2/L^2)))−
(4/3 * π * rhocen * ri^3 * Exp[−ri^2/L^2] * (1 + (2/5) * (ri^2/L^2)))

1.18875×10^{25}

Δrhoc = 575

575

dri = 94.32180045421302 * 1000/(10^9 * 86400 * 365)

2.99092×10^{-12}

C^2 = (3 * L^2)/16 − ((rc^2)/2) * (1 − ((3 * rc^2)/(10 * L^2)))

-5.2503×10^{12}

integralterm = ((8 * π^2 * rhocen^2 * G)/3)*
(((((3/20 * rc^5) − (L^2/8 * rc^3) − (L^2 * C^2 * rc)) * Exp[−rc^2/L^2])+
(C^2/2) * L^3 * Sqrt[π] * Erf[rc/L])−
((((3/20 * ri^5) − (L^2/8 * ri^3) − (L^2 * C^2 * ri)) * Exp[−ri^2/L^2])+
(C^2/2) * L^3 * Sqrt[π] * Erf[ri/L]))

-4.68603×10^{32}

Qg = (integralterm − Moc * ψ) * Δrhoc * ((4 * π * ri^2)/Moc) * dri

3.83263×10^{12}

C.3.2 Q_L

ri = 0.9 * (1220/3480) * 6378 * 1000

2.01237×10^6

LH = 750000

750000

rhocen = 30100

30100

rho0 = 7900

7900

K0 = 500 * 10^9

500000000000

***G* = 6.67384 * 10^ − 11**

6.67384×10^{-11}

***L* = Sqrt[(3 * K0 * (Log[rhocen/rho0] + 1))/(2 * π * *G* * rho0 * rhocen)]**

5.9301×10^6

rhoi = rhocen * Exp[−ri^2/*L*^2]

26825.9

ΔdTdP = 1.3/10^9

1.3×10^{-9}

Ti = 11400

11400

Tc = 7280

7280

dTc = −33.111621421756034/(10^9 * 86400 * 365)

-1.04996×10^{-15}

***g* = (4 * π/3) * *G* * rhocen * ri * (1 − ((3 * ri^2)/(5 * *L*^2)))**

15.7632

QL = −(4 * π * ri^2 * LH * Ti)/(ΔdTdP * *g*) * (1/Tc) * dTc

3.06229×10^{12}

C.3.3 Q_R

$\mathbf{CK40 = 1.31 * 10^\wedge - 9}$

1.31×10^{-9}

$\mathbf{CU238 = 9.93 * 10^\wedge - 10}$

9.93×10^{-10}

$\mathbf{CU235 = 7.1 * 10^\wedge - 12}$

7.1×10^{-12}

$\mathbf{CTh232 = 1.7 * 10^\wedge - 10}$

1.7×10^{-10}

$\mathbf{HK40 = 2.92 * 10^\wedge - 5}$

0.0000292

$\mathbf{HTh232 = 2.64 * 10^\wedge - 5}$

0.0000264

$\mathbf{HU238 = 9.46 * 10^\wedge - 5}$

0.0000946

$\mathbf{HU235 = 5.69 * 10^\wedge - 4}$

0.000569

$\mathbf{H0 = CU235 * HU235 + CU238 * HU238 + CTh232 * HTh232 + CK40 * HK40}$

1.40718×10^{-13}

$\mathbf{rhocen = 30100}$

30100

$\mathbf{rho0 = 7900}$

7900

$\mathbf{K0 = 500 * 10^\wedge 9}$

500000000000

$\boldsymbol{G} \mathbf{= 6.67384 * 10^\wedge - 11}$

6.67384×10^{-11}

$\boldsymbol{L} \mathbf{= Sqrt[(3 * K0 * (Log[rhocen/rho0] + 1))/(2 * \pi *} \boldsymbol{G} \mathbf{* rho0 * rhocen)]}$

5.92413×10^{6}

$\boldsymbol{R} \mathbf{= 0.9 * 6378 * 10^\wedge 3}$

5.7402×10^{6}

$\mathbf{Mc =}$

$\mathbf{4 * \pi * rhocen *}$

$\mathbf{(((-\boldsymbol{L}^\wedge 2)/2) * \boldsymbol{R} * Exp[(-\boldsymbol{R}^\wedge 2)/(\boldsymbol{L}^\wedge 2)] + ((\boldsymbol{L}^\wedge 3)/4) * Sqrt[\pi] * \boldsymbol{N}[Erf[\boldsymbol{R}/\boldsymbol{L}], 5]) -}$

$\mathbf{4 * \pi * rhocen * (((\boldsymbol{L}^\wedge 3)/4) * Sqrt[\pi] * \boldsymbol{N}[Erf[0], 5])}$

1.40027×10^{25}

$\mathbf{QR = Mc * H0}$

1.97043×10^{12}

C.3.4 Q_s

$\mathbf{K0 = 500 * 10\hat{\ }9}$

500000000000

$\mathbf{rhocen = 30100}$

30100

$\mathbf{rho0 = 7900}$

7900

$\boldsymbol{G = 6.67384 * 10\hat{\ } - 11}$

6.67384×10^{-11}

$\boldsymbol{L = \mathrm{Sqrt}[(3 * \mathrm{K0} * (\mathrm{Log}[\mathrm{rhocen}/\mathrm{rho0}] + 1))/(2 * \pi * G * \mathrm{rho0} * \mathrm{rhocen})]}$

5.9301×10^{6}

$\mathbf{Cp = 840}$

840

$\boldsymbol{\alpha = 1.35 * 10\hat{\ } - 5}$

0.0000135

$\boldsymbol{\mathrm{Dd} = \mathrm{Sqrt}[(3 * \mathrm{Cp})/(2 * \pi * \alpha * \mathrm{rhocen} * G)]}$

3.84567×10^{6}

$\boldsymbol{\mathrm{A}^2 = ((1/L\hat{\ }2) + (1/\mathrm{Dd}\hat{\ }2))\hat{\ }(-1)}$

1.04109×10^{13}

$\mathbf{Tcen = 11800}$

11800

$\mathbf{Tc = 7280}$

7280

$\mathbf{rc = 0.9 * 6378 * 1000}$

5.7402×10^{6}

$\boldsymbol{\mathrm{Is} = (4/3) * \pi * \mathrm{Tcen} * \mathrm{rhocen} * \mathrm{rc}\hat{\ }3 * \mathrm{Exp}[-\mathrm{rc}\hat{\ }2/\mathrm{A}^2] * (1 + (2/5) * (\mathrm{rc}\hat{\ }2/\mathrm{A}^2))}$

2.69187×10^{28}

$\mathbf{dTc = -33.111621421756034\grave{}/(10\hat{\ }9 * 86400 * 365)}$

-1.04996×10^{-15}

$\mathbf{Qs = -(Cp/Tc) * dTc * Is}$

3.26119×10^{12}

C.3.5 $\tilde{Q}_T$

K0 = 500 * 10^9

500000000000

rhocen = 30100

30100

rho0 = 7900

7900

G = 6.67384 * 10^ − 11

6.67384×10^{-11}

L = Sqrt[(3 * K0 * (Log[rhocen/rho0] + 1))/(2 * π * G * rho0 * rhocen)]

5.9301×10^{6}

Cp = 840

840

LH = 750000

750000

α = 1.35 * 10^ − 5

0.0000135

Dd = Sqrt[(3 * Cp)/(2 * π * α * rhocen * G)]

3.84567×10^{6}

A^2 = ((1/L^2) + (1/Dd^2))^(−1)

1.04109×10^{13}

Tcen = 11800

11800

Tc = 7280

7280

rc = 0.9 * 6378 * 1000

5.7402×10^{6}

Is = (4/3) * π * Tcen * rhocen * rc^3 * Exp[−rc^2/A^2] * (1 + (2/5) * (rc^2/A^2))

2.69187×10^{28}

ri = 0.9 * (1220/3480) * 6378 * 1000

2.01237×10^{6}

ψ = (2/3 * π * G * rhocen * ri^2 * (1 − (3 * ri^2)/(10 * L^2)))−
(2/3 * π * G * rhocen * rc^2 * (1 − (3 * rc^2)/(10 * L^2)))

-8.32121×10^{7}

Moc = (4/3 * π * rhocen * rc^3 * Exp[−rc^2/L^2] * (1 + (2/5) * (rc^2/L^2)))−
(4/3 * π * rhocen * ri^3 * Exp[−ri^2/L^2] * (1 + (2/5) * (ri^2/L^2)))

1.18875×10^{25}

$$\Delta \mathbf{dTdP} = \mathbf{1.3/10{}^\wedge 9}$$

$$1.3 \times 10^{-9}$$

$$\Delta \mathbf{rhoc} = \mathbf{575}$$

$$575$$

$$\mathbf{Ti} = \mathbf{11400}$$

$$11400$$

$$\mathbf{rhoi} = \mathbf{rhocen} * \mathbf{Exp}[-\mathbf{ri}{}^\wedge 2/L{}^\wedge 2]$$

$$26825.9$$

$$g = (4 * \pi/3) * G * \mathbf{rhocen} * \mathbf{ri} * (1 - ((3 * \mathbf{ri}{}^\wedge 2)/(5 * L{}^\wedge 2)))$$

$$15.7632$$

$$\mathbf{dri} = -(1/\Delta\mathbf{dTdP}) * (\mathbf{Ti}/(\mathbf{rhoi} * g)) * (1/\mathbf{Tc})$$

$$-2848.6$$

$$\mathbf{C}^2 = (3 * L{}^\wedge 2)/16 - ((\mathbf{rc}{}^\wedge 2)/2) * (1 - ((3 * \mathbf{rc}{}^\wedge 2)/(10 * L{}^\wedge 2)))$$

$$-5.2503 \times 10^{12}$$

$$\mathbf{qstilde} = -(\mathbf{Cp}/\mathbf{Tc}) * \mathbf{Is}$$

$$-3.106 \times 10^{27}$$

$$\mathbf{integralterm} = ((8 * \pi{}^\wedge 2 * \mathbf{rhocen}{}^\wedge 2 * G)/3)*$$
$$(((((3/20 * \mathbf{rc}{}^\wedge 5) - (L{}^\wedge 2/8 * \mathbf{rc}{}^\wedge 3) - (L{}^\wedge 2 * \mathbf{C}^2 * \mathbf{rc})) * \mathbf{Exp}[-\mathbf{rc}{}^\wedge 2/L{}^\wedge 2])+$$
$$(\mathbf{C}^2/2) * L{}^\wedge 3 * \mathbf{Sqrt}[\pi] * \mathbf{Erf}[\mathbf{rc}/L])-$$
$$((((3/20 * \mathbf{ri}{}^\wedge 5) - (L{}^\wedge 2/8 * \mathbf{ri}{}^\wedge 3) - (L{}^\wedge 2 * \mathbf{C}^2 * \mathbf{ri})) * \mathbf{Exp}[-\mathbf{ri}{}^\wedge 2/L{}^\wedge 2])+$$
$$(\mathbf{C}^2/2) * L{}^\wedge 3 * \mathbf{Sqrt}[\pi] * \mathbf{Erf}[\mathbf{ri}/L]))$$

$$-4.68603 \times 10^{32}$$

$$\mathbf{qgtilde} = (\mathbf{integralterm} - \mathbf{Moc} * \psi) * \Delta\mathbf{rhoc} * ((4 * \pi * \mathbf{ri}{}^\wedge 2)/\mathbf{Moc}) * \mathbf{dri}$$

$$-3.65025 \times 10^{27}$$

$$\mathbf{qltilde} = (4 * \pi * \mathbf{ri}{}^\wedge 2 * \mathbf{LH} * \mathbf{rhoi}) * \mathbf{dri}$$

$$-2.91657 \times 10^{27}$$

$$\mathbf{qttilde} = \mathbf{qstilde} + \mathbf{qgtilde} + \mathbf{qltilde}$$

$$-9.67282 \times 10^{27}$$

$$\mathbf{QR} = \mathbf{1.9724138421097737{*}{}^\wedge 12}$$

$$1.97241 \times 10^{12}$$

$$\mathbf{Qc} = \mathbf{1.2128514782867988{*}{}^\wedge 13}$$

$$1.21285 \times 10^{13}$$

$$\mathbf{dTc} = ((\mathbf{Qc} - \mathbf{QR})/\mathbf{qttilde}) * 86400 * 365 * 10{}^\wedge 9$$

$$-33.1116$$

$$\mathbf{Plot}[((\mathbf{Qc} - \mathbf{QR})/\mathbf{qttilde}) * 86400 * 365 * 10{}^\wedge 9, \{\mathbf{QR}, 0, 5 * 10{}^\wedge 12\}]$$

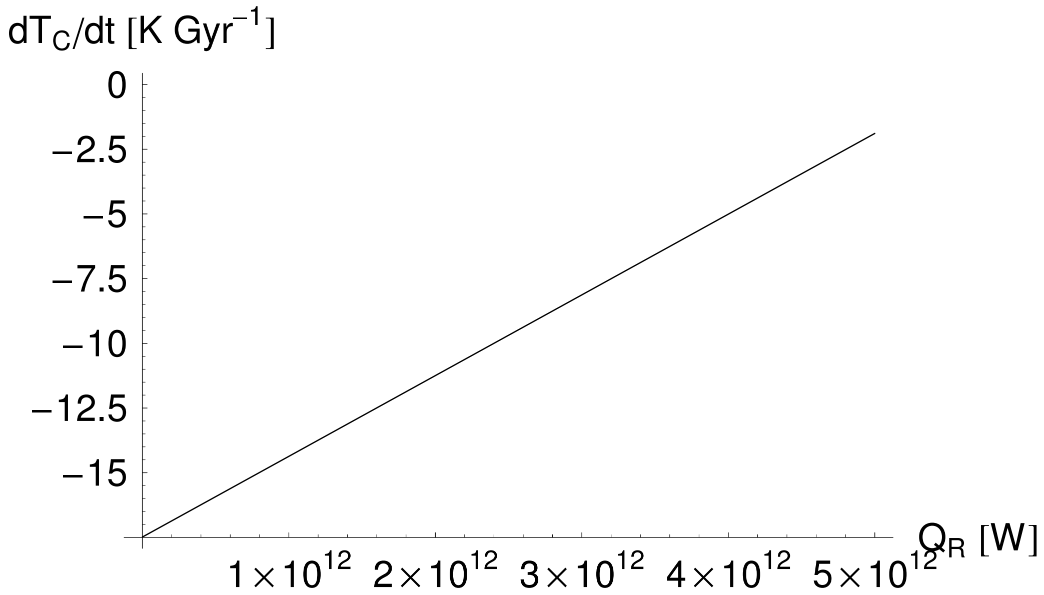

dTC/dt [K Gyr−1]
0
−2.5
−5
−7.5
−10
−12.5
−15
QR [W]
1×10^12
2×10^12
3×10^12
4×10^12
5×10^12

−Graphics−

C.3.6 dr_i/dt

ΔdTdP = 1.3/10^9

1.3×10^{-9}

Ti = 11400

11400

Tc = 7280

7280

dTc = −33.111621421756034/(10^9 * 86400 * 365)

-1.04996×10^{-15}

ri = 0.9 * (1220/3480) * 6378 * 1000

2.01237×10^{6}

rho0 = 7900

7900

K0 = 500 * 10^9

500000000000

***G* = 6.67384 * 10^ − 11**

6.67384×10^{-11}

rhocen = 30100

30100

***L* = Sqrt[(3 * K0 * (Log[rhocen/rho0] + 1))/(2 * π * *G* * rho0 * rhocen)]**

5.9301×10^{6}

rhoi = rhocen * Exp[−ri^2/*L*^2]

26825.9

***g* = (4 * π/3) * *G* * rhocen * ri * (1 − ((3 * ri^2)/(5 * *L*^2)))**

15.7632

dri = −(((1/(ΔdTdP)) * (Ti/(rhoi * *g*)) * (1/Tc) * dTc) * 10^9 * 86400 * 365)/1000

94.3218

C.4 Rydberg EoS - Normal

C.4.1 Q_k

rc = 0.95 * 6378 * 1000

6.0591×10^{6}

k = 40

40

Tc = 6650

6650

cp = 840

840

α = 1.35 * 10^ − 5

0.0000135

rhocen = 24900

24900

G = 6.67384 * 10^ − 11

6.67384×10^{-11}

Dd = Sqrt[(3 * cp)/(2 * π * α * rhocen * G)]

4.2282×10^{6}

Qk = (8 * π * rc^3 * k * Tc)/Dd^2

8.31829×10^{13}

Plot[(8 * π * rc^3 * k * Tc)/Dd^2, {rc, 3480 * 1000, 6378 * 1000}]

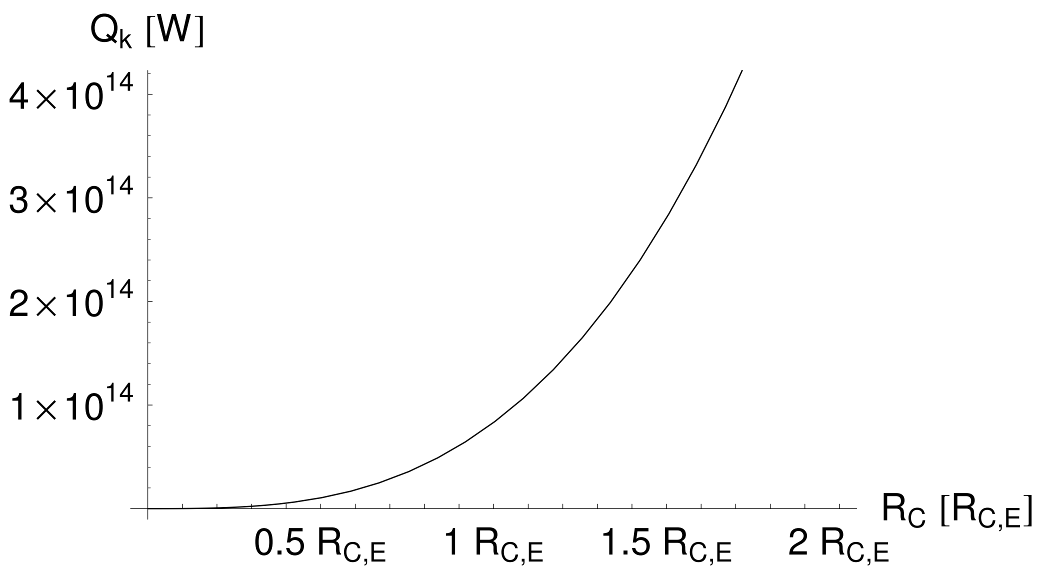

−Graphics−

C.4.2 Q_R

$\mathbf{CK40 = 2.44 * 10\hat{} - 8}$

2.44×10^{-8}

$\mathbf{CU238 = 2.98 * 10\hat{} - 9}$

2.98×10^{-9}

$\mathbf{CU235 = 2.13 * 10\hat{} - 11}$

2.13×10^{-11}

$\mathbf{CTh232 = 5.8 * 10\hat{} - 10}$

5.8×10^{-10}

$\mathbf{HK40 = 2.92 * 10\hat{} - 5}$

0.0000292

$\mathbf{HTh232 = 2.64 * 10\hat{} - 5}$

0.0000264

$\mathbf{HU238 = 9.46 * 10\hat{} - 5}$

0.0000946

$\mathbf{HU235 = 5.69 * 10\hat{} - 4}$

0.000569

$\mathbf{H0 = CU235 * HU235 + CU238 * HU238 + CTh232 * HTh232 + CK40 * HK40}$

1.02182×10^{-12}

$\mathbf{rhocen = 24900}$

24900

$\mathbf{rho0 = 7900}$

7900

$\mathbf{K0 = 500 * 10\hat{}9}$

500000000000

$\boldsymbol{G} \mathbf{= 6.67384 * 10\hat{} - 11}$

6.67384×10^{-11}

$\boldsymbol{L} \mathbf{= Sqrt[(3 * K0 * (Log[rhocen/rho0] + 1))/(2 * \pi *} \boldsymbol{G} \mathbf{* rho0 * rhocen)]}$

6.24989×10^{6}

$\boldsymbol{R} \mathbf{= 0.95 * 6378 * 10\hat{}3}$

6.0591×10^{6}

$\mathbf{Mc = 4 * \pi * rhocen * (((-} \boldsymbol{L} \mathbf{\hat{}2)/2) *} \boldsymbol{R} \mathbf{* Exp[(-} \boldsymbol{R} \mathbf{\hat{}2)/(} \boldsymbol{L} \mathbf{\hat{}2)] + ((} \boldsymbol{L} \mathbf{\hat{}3)/4) * Sqrt[\pi] *} \boldsymbol{N} \mathbf{[Erf[} \boldsymbol{R/L} \mathbf{], 5])}$
$\mathbf{-4 * \pi * rhocen * (((} \boldsymbol{L} \mathbf{\hat{}3)/4) * Sqrt[\pi] *} \boldsymbol{N} \mathbf{[Erf[0], 5])}$

1.36161×10^{25}

$\mathbf{QR = Mc * H0}$

1.39132×10^{13}

C.4.3 $\tilde{Q}_T$

$\mathbf{K0 = 500 * 10\hat{}9}$

500000000000

$\mathbf{rhocen = 24900}$

24900

$\mathbf{rho0 = 7900}$

7900

$\boldsymbol{G = 6.67384 * 10\hat{}-11}$

6.67384×10^{-11}

$\boldsymbol{L = \mathrm{Sqrt}[(3 * \mathrm{K0} * (\mathrm{Log}[\mathrm{rhocen/rho0}] + 1))/(2 * \pi * G * \mathrm{rho0} * \mathrm{rhocen})]}$

6.24989×10^{6}

$\mathbf{Cp = 840}$

840

$\boldsymbol{\alpha = 1.35 * 10\hat{}-5}$

0.0000135

$\boldsymbol{\mathrm{Dd} = \mathrm{Sqrt}[(3 * \mathrm{Cp})/(2 * \pi * \alpha * \mathrm{rhocen} * G)]}$

4.2282×10^{6}

$\boldsymbol{\mathrm{A}^2 = ((1/L\hat{}2) + (1/\mathrm{Dd}\hat{}2))\hat{}(-1)}$

1.22644×10^{13}

$\mathbf{Tcen = 9790}$

9790

$\mathbf{Tc = 6650}$

6650

$\mathbf{rc = 0.95 * 6378 * 1000}$

6.0591×10^{6}

$\boldsymbol{\mathrm{Is} = (4/3) * \pi * \mathrm{Tcen} * \mathrm{rhocen} * \mathrm{rc}\hat{}3 * \mathrm{Exp}[-\mathrm{rc}\hat{}2/\mathrm{A}^2] * (1 + (2/5) * (\mathrm{rc}\hat{}2/\mathrm{A}^2))}$

2.50133×10^{28}

$\mathbf{ri = 0.95 * (1220/3480) * 6378 * 1000}$

2.12417×10^{6}

$\boldsymbol{\psi = (2/3 * \pi * G * \mathrm{rhocen} * \mathrm{ri}\hat{}2 * (1 - (3 * \mathrm{ri}\hat{}2)/(10 * L\hat{}2))) -}$

$\boldsymbol{(2/3 * \pi * G * \mathrm{rhocen} * \mathrm{rc}\hat{}2 * (1 - (3 * \mathrm{rc}\hat{}2)/(10 * L\hat{}2)))}$

-7.65881×10^{7}

$\boldsymbol{\mathrm{Moc} = (4/3 * \pi * \mathrm{rhocen} * \mathrm{rc}\hat{}3 * \mathrm{Exp}[-\mathrm{rc}\hat{}2/L\hat{}2] * (1 + (2/5) * (\mathrm{rc}\hat{}2/L\hat{}2))) -}$

$\boldsymbol{(4/3 * \pi * \mathrm{rhocen} * \mathrm{ri}\hat{}3 * \mathrm{Exp}[-\mathrm{ri}\hat{}2/L\hat{}2] * (1 + (2/5) * (\mathrm{ri}\hat{}2/L\hat{}2)))}$

1.15401×10^{25}

$\boldsymbol{\Delta \mathrm{dTdP} = 1.3/10\hat{}9}$

1.3×10^{-9}

$\Delta\text{rhoc} = 575$

575

$\text{Ti} = 9600$

9600

$\text{rhoi} = \text{rhocen} * \text{Exp}[-\text{ri}\hat{\ }2/L\hat{\ }2]$

22183.6

$g = (4 * \pi/3) * G * \text{rhocen} * \text{ri} * (1 - ((3 * \text{ri}\hat{\ }2)/(5 * L\hat{\ }2)))$

13.7613

$\text{dri} = -(1/\Delta\text{dTdP}) * (\text{Ti}/(\text{rhoi} * g)) * (1/\text{Tc})$

-3637.6

$\text{C}^2 = (3 * L\hat{\ }2)/16 - ((\text{rc}\hat{\ }2)/2) * (1 - ((3 * \text{rc}\hat{\ }2)/(10 * L\hat{\ }2)))$

-5.85657×10^{12}

$\text{qstilde} = -(\text{Cp}/\text{Tc}) * \text{Is}$

-3.15957×10^{27}

$\text{integralterm} = ((8 * \pi\hat{\ }2 * \text{rhocen}\hat{\ }2 * G)/3)*$
$(((((3/20 * \text{rc}\hat{\ }5) - (L\hat{\ }2/8 * \text{rc}\hat{\ }3) - (L\hat{\ }2 * \text{C}^2 * \text{rc})) * \text{Exp}[-\text{rc}\hat{\ }2/L\hat{\ }2])+$
$(\text{C}^2/2) * L\hat{\ }3 * \text{Sqrt}[\pi] * \text{Erf}[\text{rc}/L])-$
$((((3/20 * \text{ri}\hat{\ }5) - (L\hat{\ }2/8 * \text{ri}\hat{\ }3) - (L\hat{\ }2 * \text{C}^2 * \text{ri})) * \text{Exp}[-\text{ri}\hat{\ }2/L\hat{\ }2])+$
$(\text{C}^2/2) * L\hat{\ }3 * \text{Sqrt}[\pi] * \text{Erf}[\text{ri}/L]))$

-4.18852×10^{32}

$\text{qgtilde} = (\text{integralterm} - \text{Moc} * \psi) * \Delta\text{rhoc} * ((4 * \pi * \text{ri}\hat{\ }2)/\text{Moc}) * \text{dri}$

-4.77857×10^{27}

$\text{qltilde} = (4 * \pi * \text{ri}\hat{\ }2 * \text{LH} * \text{rhoi}) * \text{dri}$

-3.4316×10^{27}

$\text{qttilde} = \text{qstilde} + \text{qgtilde} + \text{qltilde}$

-1.13697×10^{28}

$\text{QR} = 1.3913228024287514\text{*}\hat{\ }13$

1.39132×10^{13}

$\text{Qc} = 1.0895326426751783\text{*}\hat{\ }13$

1.08953×10^{13}

$\text{dTc} = ((\text{Qc} - \text{QR})/\text{qttilde}) * 86400 * 365 * 10\hat{\ }9$

8.37069

$\text{Plot}[((9 * 10\hat{\ }12 - \text{QR})/\text{qttilde}) * 86400 * 365 * 10\hat{\ }9, \{\text{QR}, 0, 5 * 10\hat{\ }12\}]$

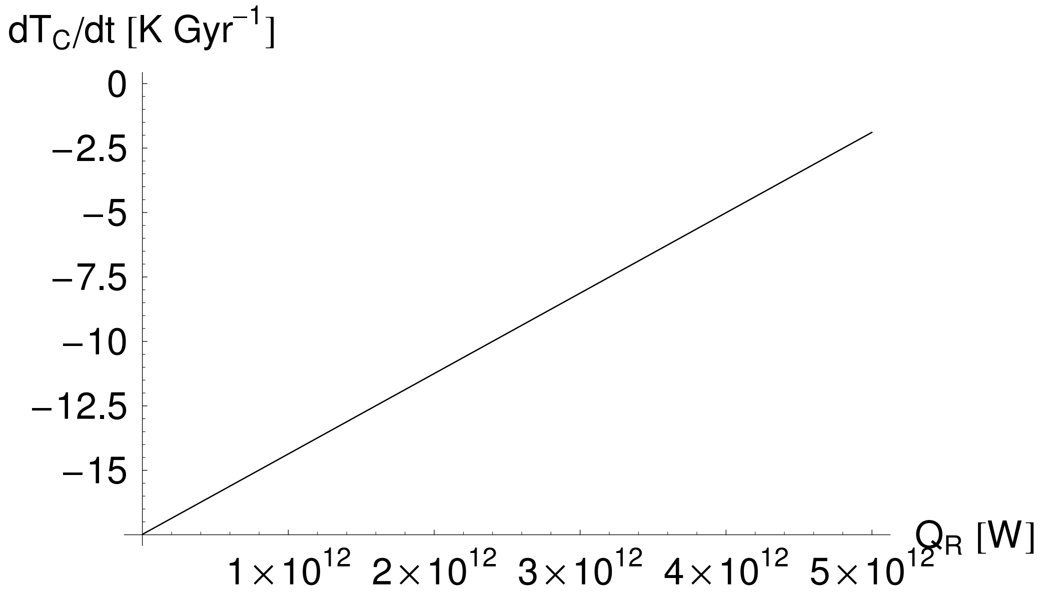
dT_C/dt [K Gyr^-1]
0
−2.5
−5
−7.5
−10
−12.5
−15
Q_R [W]
1×10^12
2×10^12
3×10^12
4×10^12
5×10^12

−Graphics−

C.4.4 Q_C

$\boldsymbol{R = 0.95 * 6378 * 1000}$

6.0591×10^6

$\mathbf{kb = 5.8}$

5.8

$\boldsymbol{\kappa}\mathbf{b = 10 * 10\hat{} - 7}$

$\frac{1}{1000000}$

$\mathbf{Tc = 6650}$

6650

$\mathbf{Rac = 600}$

600

$\mathbf{rhom = 8500}$

8500

$\boldsymbol{g = 9.8}$

9.8

$\boldsymbol{\alpha}\mathbf{m = 2.2 * 10\hat{} - 5}$

0.000022

$\mathbf{Tm = 5200}$

5200

$\boldsymbol{\eta}\mathbf{b = 2.0 * 10\hat{}23}$

$2. \times 10^{23}$

$\boldsymbol{\delta}\mathbf{b = ((Rac * \boldsymbol{\kappa} b * \boldsymbol{\eta} b)/(rhom * \boldsymbol{g} * \boldsymbol{\alpha} m * (Tc - Tm)))\hat{}(1/3)}$

$356108.$

$\mathbf{Fb = kb * (Tc - Tm)/\boldsymbol{\delta} b}$

0.0236164

$\mathbf{Qc = 4 * \boldsymbol{\pi} * \boldsymbol{R}\hat{}2 * Fb}$

1.08953×10^{13}

C.5 Rydberg EoS - $Q_R = 0$

C.5.1 Q_g

rho0 = 7900

7900

rc = 0.95 * 6378 * 1000

6.0591×10^6

ri = 0.95 * (1220/3480) * 6378 * 1000

2.12417×10^6

K0 = 500 * 10^9

500000000000

***G* = 6.67384 * 10^ − 11**

6.67384×10^{-11}

rhocen = 24900

24900

***L* = Sqrt[(3 * K0 * (Log[rhocen/rho0] + 1))/(2 * π * *G* * rho0 * rhocen)]**

6.24989×10^6

***ψ* = (2/3 * π * *G* * rhocen * ri^2 * (1 − (3 * ri^2)/(10 * *L*^2)))−**
(2/3 * π * *G* * rhocen * rc^2 * (1 − (3 * rc^2)/(10 * *L*^2)))

-7.65881×10^7

Moc = (4/3 * π * rhocen * rc^3 * Exp[−rc^2/*L*^2] * (1 + (2/5) * (rc^2/*L*^2)))−
(4/3 * π * rhocen * ri^3 * Exp[−ri^2/*L*^2] * (1 + (2/5) * (ri^2/*L*^2)))

1.15401×10^{25}

Δrhoc = 575

575

dri = 109.92893047197018 * 1000/(10^9 * 86400 * 365)

3.48582×10^{-12}

C² = (3 * *L*^2)/16 − ((rc^2)/2) * (1 − ((3 * rc^2)/(10 * *L*^2)))

-5.85657×10^{12}

integralterm = ((8 * π^2 * rhocen^2 * *G*)/3)*
(((((3/20 * rc^5) − (*L*^2/8 * rc^3) − (*L*^2 * C² * rc)) * Exp[−rc^2/*L*^2])+
(C²/2) * *L*^3 * Sqrt[π] * Erf[rc/*L*])−
((((3/20 * ri^5) − (*L*^2/8 * ri^3) − (*L*^2 * C² * ri)) * Exp[−ri^2/*L*^2])+
(C²/2) * *L*^3 * Sqrt[π] * Erf[ri/*L*]))

-4.18852×10^{32}

Qg = (integralterm − Moc * *ψ*) * Δrhoc * ((4 * π * ri^2)/Moc) * dri

4.57918×10^{12}

C.5.2 Q_L

ri = 0.95 * (1220/3480) * 6378 * 1000

2.12417×10^{6}

LH = 750000

750000

rhocen = 24900

24900

rho0 = 7900

7900

K0 = 500 * 10^9

500000000000

***G* = 6.67384 * 10^ − 11**

6.67384×10^{-11}

***L* = Sqrt[(3 * K0 * (Log[rhocen/rho0] + 1))/(2 * π * *G* * rho0 * rhocen)]**

6.24989×10^{6}

rhoi = rhocen * Exp[−ri^2/*L*^2]

22183.6

ΔdTdP = 1.3/10^9

1.3×10^{-9}

Ti = 9600

9600

Tc = 6650

6650

dTc = −30.220147963524436/(10^9 * 86400 * 365)

-9.58275×10^{-16}

***g* = (4 * π/3) * *G* * rhocen * ri * (1 − ((3 * ri^2)/(5 * *L*^2)))**

13.7613

QL = −(4 * π * ri^2 * LH * Ti)/(ΔdTdP * *g*) * (1/Tc) * dTc

3.28841×10^{12}

C.5.3 Q_s

$\mathbf{K0 = 500 * 10^{\wedge}9}$

500000000000

$\mathbf{rhocen = 24900}$

24900

$\mathbf{rho0 = 7900}$

7900

$\boldsymbol{G = 6.67384 * 10^{\wedge} - 11}$

6.67384×10^{-11}

$\boldsymbol{L = \text{Sqrt}[(3 * \text{K0} * (\text{Log}[\text{rhocen/rho0}] + 1))/(2 * \pi * G * \text{rho0} * \text{rhocen})]}$

6.24989×10^{6}

$\mathbf{Cp = 840}$

840

$\boldsymbol{\alpha = 1.35 * 10^{\wedge} - 5}$

0.0000135

$\boldsymbol{\text{Dd} = \text{Sqrt}[(3 * \text{Cp})/(2 * \pi * \alpha * \text{rhocen} * G)]}$

4.2282×10^{6}

$\boldsymbol{\text{A}^2 = ((1/L^{\wedge}2) + (1/\text{Dd}^{\wedge}2))^{\wedge}(-1)}$

1.22644×10^{13}

$\mathbf{Tcen = 9790}$

9790

$\mathbf{Tc = 6650}$

6650

$\mathbf{rc = 0.95 * 6378 * 1000}$

6.0591×10^{6}

$\boldsymbol{\text{Is} = (4/3) * \pi * \text{Tcen} * \text{rhocen} * \text{rc}^{\wedge}3 * \text{Exp}[-\text{rc}^{\wedge}2/\text{A}^2] * (1 + (2/5) * (\text{rc}^{\wedge}2/\text{A}^2))}$

2.50133×10^{28}

$\boldsymbol{\text{dTc} = -30.220147963524436/(10^{\wedge}9 * 86400 * 365)}$

-9.58275×10^{-16}

$\boldsymbol{\text{Qs} = -(\text{Cp/Tc}) * \text{dTc} * \text{Is}}$

3.02774×10^{12}

C.5.4 $\tilde{Q}_T$

K0 = 500 * 10^9

500000000000

rhocen = 24900

24900

rho0 = 7900

7900

***G* = 6.67384 * 10^ − 11**

6.67384×10^{-11}

***L* = Sqrt[(3 * K0 * (Log[rhocen/rho0] + 1))/(2 * π * *G* * rho0 * rhocen)]**

6.24989×10^{6}

Cp = 840

840

LH = 750000

750000

***α* = 1.35 * 10^ − 5**

0.0000135

Dd = Sqrt[(3 * Cp)/(2 * π * *α* * rhocen * *G*)]

4.2282×10^{6}

A^2 = ((1/*L*^2) + (1/Dd^2))^(−1)

1.22644×10^{13}

Tcen = 9790

9790

Tc = 6650

6650

rc = 0.95 * 6378 * 1000

6.0591×10^{6}

Is = (4/3) * π * Tcen * rhocen * rc^3 * Exp[−rc^2/A^2] * (1 + (2/5) * (rc^2/A^2))

2.50133×10^{28}

ri = 0.95 * (1220/3480) * 6378 * 1000

2.12417×10^{6}

***ψ* = (2/3 * π * *G* * rhocen * ri^2 * (1 − (3 * ri^2)/(10 * *L*^2)))−
(2/3 * π * *G* * rhocen * rc^2 * (1 − (3 * rc^2)/(10 * *L*^2)))**

-7.65881×10^{7}

**Moc = (4/3 * π * rhocen * rc^3 * Exp[−rc^2/*L*^2] * (1 + (2/5) * (rc^2/*L*^2)))−
(4/3 * π * rhocen * ri^3 * Exp[−ri^2/*L*^2] * (1 + (2/5) * (ri^2/*L*^2)))**

1.15401×10^{25}

$\Delta \text{dTdP} = 1.3/10\wedge 9$

1.3×10^{-9}

$\Delta \text{rhoc} = 575$

575

$\text{Ti} = 9600$

9600

$\text{rhoi} = \text{rhocen} * \text{Exp}[-\text{ri}\wedge 2/L\wedge 2]$

22183.6

$g = (4 * \pi/3) * G * \text{rhocen} * \text{ri} * (1 - ((3 * \text{ri}\wedge 2)/(5 * L\wedge 2)))$

13.7613

$\text{dri} = -(1/\Delta \text{dTdP}) * (\text{Ti}/(\text{rhoi} * g)) * (1/\text{Tc})$

-3637.6

$\text{C}^2 = (3 * L\wedge 2)/16 - ((\text{rc}\wedge 2)/2) * (1 - ((3 * \text{rc}\wedge 2)/(10 * L\wedge 2)))$

-5.85657×10^{12}

$\text{qstilde} = -(\text{Cp}/\text{Tc}) * \text{Is}$

-3.15957×10^{27}

$\text{integralterm} = ((8 * \pi\wedge 2 * \text{rhocen}\wedge 2 * G)/3) *$
$(((((3/20 * \text{rc}\wedge 5) - (L\wedge 2/8 * \text{rc}\wedge 3) - (L\wedge 2 * \text{C}^2 * \text{rc})) * \text{Exp}[-\text{rc}\wedge 2/L\wedge 2]) +$
$(\text{C}^2/2) * L\wedge 3 * \text{Sqrt}[\pi] * \text{Erf}[\text{rc}/L]) -$
$((((3/20 * \text{ri}\wedge 5) - (L\wedge 2/8 * \text{ri}\wedge 3) - (L\wedge 2 * \text{C}^2 * \text{ri})) * \text{Exp}[-\text{ri}\wedge 2/L\wedge 2]) +$
$(\text{C}^2/2) * L\wedge 3 * \text{Sqrt}[\pi] * \text{Erf}[\text{ri}/L]))$

-4.18852×10^{32}

$\text{qgtilde} = (\text{integralterm} - \text{Moc} * \psi) * \Delta \text{rhoc} * ((4 * \pi * \text{ri}\wedge 2)/\text{Moc}) * \text{dri}$

-4.77857×10^{27}

$\text{qltilde} = (4 * \pi * \text{ri}\wedge 2 * \text{LH} * \text{rhoi}) * \text{dri}$

-3.4316×10^{27}

$\text{qttilde} = \text{qstilde} + \text{qgtilde} + \text{qltilde}$

-1.13697×10^{28}

$\text{Qc} = 1.0895326426751783\text{*}\wedge 13$

1.08953×10^{13}

$\text{dTc} = (\text{Qc}/\text{qttilde}) * 86400 * 365 * 10\wedge 9$

-30.2201

$\text{Plot}[((\text{Qc} - \text{QR})/\text{qttilde}) * 86400 * 365 * 10\wedge 9, \{\text{QR}, 0, 5 * 10\wedge 12\}]$

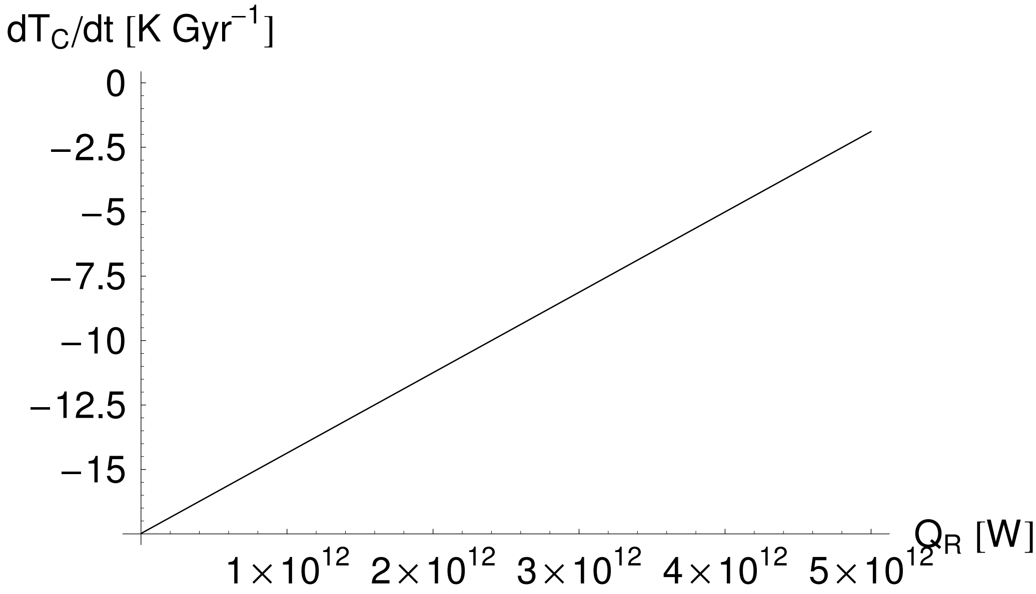
dTC/dt [K Gyr−1]
0
−2.5
−5
−7.5
−10
−12.5
−15
QR [W]
1×10^12
2×10^12
3×10^12
4×10^12
5×10^12

−Graphics−

C.5.5 dr_i/dt

ΔdTdP = 1.3/10^9

1.3×10^{-9}

Ti = 9600

9600

Tc = 6650

6650

dTc = −30.220147963524436/(10^9 ∗ 86400 ∗ 365)

-9.58275×10^{-16}

ri = 0.95 ∗ (1220/3480) ∗ 6378 ∗ 1000

2.12417×10^{6}

rho0 = 7900

7900

K0 = 500 ∗ 10^9

500000000000

***G* = 6.67384 ∗ 10^ − 11**

6.67384×10^{-11}

rhocen = 24900

24900

***L* = Sqrt[(3 ∗ K0 ∗ (Log[rhocen/rho0] + 1))/(2 ∗ π ∗ *G* ∗ rho0 ∗ rhocen)]**

6.24989×10^{6}

rhoi = rhocen ∗ Exp[−ri^2/*L*^2]

22183.6

***g* = (4 ∗ π/3) ∗ *G* ∗ rhocen ∗ ri ∗ (1 − ((3 ∗ ri^2)/(5 ∗ *L*^2)))**

13.7613

dri = −(((1/(ΔdTdP)) ∗ (Ti/(rhoi ∗ *g*)) ∗ (1/Tc) ∗ dTc) ∗ 10^9 ∗ 86400 ∗ 365)/1000

109.929

C.6 Rydberg EoS - $Q_R \rightarrow$ Lower Bound

C.6.1 Q_g

rho0 = 7900

7900

rc = 0.95 * 6378 * 1000

6.0591×10^6

ri = 0.95 * (1220/3480) * 6378 * 1000

2.12417×10^6

K0 = 500 * 10^9

500000000000

G = 6.67384 * 10^ − 11

6.67384×10^{-11}

rhocen = 24900

24900

L = Sqrt[(3 * K0 * (Log[rhocen/rho0] + 1))/(2 * π * G * rho0 * rhocen)]

6.24989×10^6

ψ = (2/3 * π * G * rhocen * ri^2 * (1 − (3 * ri^2)/(10 * L^2)))−
(2/3 * π * G * rhocen * rc^2 * (1 − (3 * rc^2)/(10 * L^2)))

-7.65881×10^7

Moc = (4/3 * π * rhocen * rc^3 * Exp[−rc^2/L^2] * (1 + (2/5) * (rc^2/L^2)))−
(4/3 * π * rhocen * ri^3 * Exp[−ri^2/L^2] * (1 + (2/5) * (ri^2/L^2)))

1.15401×10^{25}

Δrhoc = 575

575

dri = 90.59704935029396 * 1000/(10^9 * 86400 * 365)

2.87281×10^{-12}

C^2 = (3 * L^2)/16 − ((rc^2)/2) * (1 − ((3 * rc^2)/(10 * L^2)))

-5.85657×10^{12}

integralterm = ((8 * π^2 * rhocen^2 * G)/3)*
(((((3/20 * rc^5) − (L^2/8 * rc^3) − (L^2 * C^2 * rc)) * Exp[−rc^2/L^2])+
(C^2/2) * L^3 * Sqrt[π] * Erf[rc/L])−
((((3/20 * ri^5) − (L^2/8 * ri^3) − (L^2 * C^2 * ri)) * Exp[−ri^2/L^2])+
(C^2/2) * L^3 * Sqrt[π] * Erf[ri/L]))

-4.18852×10^{32}

Qg = (integralterm − Moc * ψ) * Δrhoc * ((4 * π * ri^2)/Moc) * dri

3.77389×10^{12}

C.6.2 Q_L

$\mathbf{ri = 0.95 * (1220/3480) * 6378 * 1000}$

2.12417×10^6

$\mathbf{LH = 750000}$

750000

$\mathbf{rhocen = 24900}$

24900

$\mathbf{rho0 = 7900}$

7900

$\mathbf{K0 = 500 * 10\hat{}9}$

500000000000

$\boldsymbol{G = 6.67384 * 10\hat{} - 11}$

6.67384×10^{-11}

$\boldsymbol{L = \mathrm{Sqrt}[(3 * \mathrm{K0} * (\mathrm{Log}[\mathrm{rhocen/rho0}] + 1))/(2 * \pi * G * \mathrm{rho0} * \mathrm{rhocen})]}$

6.24989×10^6

$\boldsymbol{\mathrm{rhoi} = \mathrm{rhocen} * \mathrm{Exp}[-\mathrm{ri}\hat{}2/L\hat{}2]}$

22183.6

$\mathbf{\Delta dTdP = 1.3/10\hat{}9}$

1.3×10^{-9}

$\mathbf{Ti = 9600}$

9600

$\mathbf{Tc = 6650}$

6650

$\mathbf{dTc = -24.905693384533667/(10\hat{}9 * 86400 * 365)}$

-7.89754×10^{-16}

$\boldsymbol{g = (4 * \pi/3) * G * \mathrm{rhocen} * \mathrm{ri} * (1 - ((3 * \mathrm{ri}\hat{}2)/(5 * L\hat{}2)))}$

13.7613

$\boldsymbol{\mathrm{QL} = -(4 * \pi * \mathrm{ri}\hat{}2 * \mathrm{LH} * \mathrm{Ti})/(\Delta\mathrm{dTdP} * g) * (1/\mathrm{Tc}) * \mathrm{dTc}}$

2.71012×10^{12}

C.6.3 Q_R

$\mathbf{CK40 = 1.31 * 10^\wedge - 9}$

1.31×10^{-9}

$\mathbf{CU238 = 9.93 * 10^\wedge - 10}$

9.93×10^{-10}

$\mathbf{CU235 = 7.1 * 10^\wedge - 12}$

7.1×10^{-12}

$\mathbf{CTh232 = 1.7 * 10^\wedge - 10}$

1.7×10^{-10}

$\mathbf{HK40 = 2.92 * 10^\wedge - 5}$

0.0000292

$\mathbf{HTh232 = 2.64 * 10^\wedge - 5}$

0.0000264

$\mathbf{HU238 = 9.46 * 10^\wedge - 5}$

0.0000946

$\mathbf{HU235 = 5.69 * 10^\wedge - 4}$

0.000569

$\mathbf{H0 = CU235 * HU235 + CU238 * HU238 + CTh232 * HTh232 + CK40 * HK40}$

1.40718×10^{-13}

$\mathbf{rhocen = 24900}$

24900

$\mathbf{rho0 = 7900}$

7900

$\mathbf{K0 = 500 * 10^\wedge 9}$

500000000000

$\boldsymbol{G = 6.67384 * 10^\wedge - 11}$

6.67384×10^{-11}

$\boldsymbol{L = \mathrm{Sqrt}[(3 * \mathrm{K0} * (\mathrm{Log}[\mathrm{rhocen}/\mathrm{rho0}] + 1))/(2 * \pi * G * \mathrm{rho0} * \mathrm{rhocen})]}$

6.24989×10^{6}

$\boldsymbol{R = 0.95 * 6378 * 10^\wedge 3}$

6.0591×10^{6}

$\mathbf{Mc} =$

$\boldsymbol{4 * \pi * \mathrm{rhocen} *}$

$\boldsymbol{(((-L^\wedge 2)/2) * R * \mathrm{Exp}[(-R^\wedge 2)/(L^\wedge 2)] +}$

$\boldsymbol{((L^\wedge 3)/4) * \mathrm{Sqrt}[\pi] * N[\mathrm{Erf}[R/L], 5]) -}$

$\boldsymbol{4 * \pi * \mathrm{rhocen} * (((L^\wedge 3)/4) * \mathrm{Sqrt}[\pi] * N[\mathrm{Erf}[0], 5])}$

1.36161×10^{25}

$\mathbf{QR = Mc * H0}$

1.91603×10^{12}

C.6.4 Q_s

$\mathbf{K0 = 500 * 10\hat{}9}$

500000000000

$\mathbf{rhocen = 24900}$

24900

$\mathbf{rho0 = 7900}$

7900

$\boldsymbol{G} \mathbf{= 6.67384 * 10\hat{} - 11}$

6.67384×10^{-11}

$\boldsymbol{L} \mathbf{= Sqrt[(3 * K0 * (Log[rhocen/rho0] + 1))/(2 * \pi * G * rho0 * rhocen)]}$

6.24989×10^{6}

$\mathbf{Cp = 840}$

840

$\boldsymbol{\alpha} \mathbf{= 1.35 * 10\hat{} - 5}$

0.0000135

$\mathbf{Dd = Sqrt[(3 * Cp)/(2 * \pi * \alpha * rhocen * G)]}$

4.2282×10^{6}

$\mathbf{A^2 = ((1/L\hat{}2) + (1/Dd\hat{}2))\hat{}(-1)}$

1.22644×10^{13}

$\mathbf{Tcen = 9790}$

9790

$\mathbf{Tc = 6650}$

6650

$\mathbf{rc = 0.95 * 6378 * 1000}$

6.0591×10^{6}

$\mathbf{Is = (4/3) * \pi * Tcen * rhocen * rc\hat{}3 * Exp[-rc\hat{}2/A^2] * (1 + (2/5) * (rc\hat{}2/A^2))}$

2.50133×10^{28}

$\mathbf{dTc = -24.905693384533667/(10\hat{}9 * 86400 * 365)}$

-7.89754×10^{-16}

$\mathbf{Qs = -(Cp/Tc) * dTc * Is}$

C.6.5 $\tilde{Q}_T$

K0 = 500 * 10^9

500000000000

rhocen = 24900

24900

rho0 = 7900

7900

G **= 6.67384 * 10^ − 11**

6.67384×10^{-11}

L **= Sqrt[(3 * K0 * (Log[rhocen/rho0] + 1))/(2 * π *** G *** rho0 * rhocen)]**

6.24989×10^{6}

Cp = 840

840

LH = 750000

750000

α **= 1.35 * 10^ − 5**

0.0000135

Dd = Sqrt[(3 * Cp)/(2 * π * α *** rhocen *** G**)]**

4.2282×10^{6}

A² = ((1/*L***^2) + (1/Dd^2))^(−1)**

1.22644×10^{13}

Tcen = 9790

9790

Tc = 6650

6650

rc = 0.95 * 6378 * 1000

6.0591×10^{6}

Is = (4/3) * π * Tcen * rhocen * rc^3 * Exp[−rc^2/A²] * (1 + (2/5) * (rc^2/A²))

2.50133×10^{28}

ri = 0.95 * (1220/3480) * 6378 * 1000

2.12417×10^{6}

ψ **= (2/3 * π *** G *** rhocen * ri^2 * (1 − (3 * ri^2)/(10 *** L**^2)))−**
(2/3 * π * G *** rhocen * rc^2 * (1 − (3 * rc^2)/(10 *** L**^2)))**

-7.65881×10^{7}

Moc = (4/3 * π * rhocen * rc^3 * Exp[−rc^2/*L***^2] * (1 + (2/5) * (rc^2/***L***^2)))−**
(4/3 * π * rhocen * ri^3 * Exp[−ri^2/*L***^2] * (1 + (2/5) * (ri^2/***L***^2)))**

1.15401×10^{25}

Δ**dTdP = 1.3/10^9**

1.3×10^{-9}

Δ**rhoc = 575**

575

Ti = 9600

9600

rhoi = rhocen * Exp[−ri^2/L^2]

22183.6

g **= (4 * π/3) * G * rhocen * ri * (1 − ((3 * ri^2)/(5 * L^2)))**

13.7613

dri = −(1/ΔdTdP) * (Ti/(rhoi * g)) * (1/Tc)

−3637.6

C^2 = (3 * L^2)/16 − ((rc^2)/2) * (1 − ((3 * rc^2)/(10 * L^2)))

-5.85657×10^{12}

qstilde = −(Cp/Tc) * Is

-3.15957×10^{27}

integralterm = ((8 * π^2 * rhocen^2 * G)/3)*
(((((3/20 * rc^5) − (L^2/8 * rc^3) − (L^2 * C^2 * rc)) * Exp[−rc^2/L^2])+
(C^2/2) * L^3 * Sqrt[π] * Erf[rc/L])−
((((3/20 * ri^5) − (L^2/8 * ri^3) − (L^2 * C^2 * ri)) * Exp[−ri^2/L^2])+
(C^2/2) * L^3 * Sqrt[π] * Erf[ri/L]))

-4.18852×10^{32}

qgtilde = (integralterm − Moc * ψ) * Δrhoc * ((4 * π * ri^2)/Moc) * dri

-4.77857×10^{27}

qltilde = (4 * π * ri^2 * LH * rhoi) * dri

-3.4316×10^{27}

qttilde = qstilde + qgtilde + qltilde

-1.13697×10^{28}

QR = 1.9160302420801665*^12

1.91603×10^{12}

Qc = 1.0895326426751783*^13

1.08953×10^{13}

dTc = ((Qc − QR)/qttilde) * 86400 * 365 * 10^9

−24.9057

Plot[((Qc − QR)/qttilde) * 86400 * 365 * 10^9, {QR, 0, 5 * 10^12}]

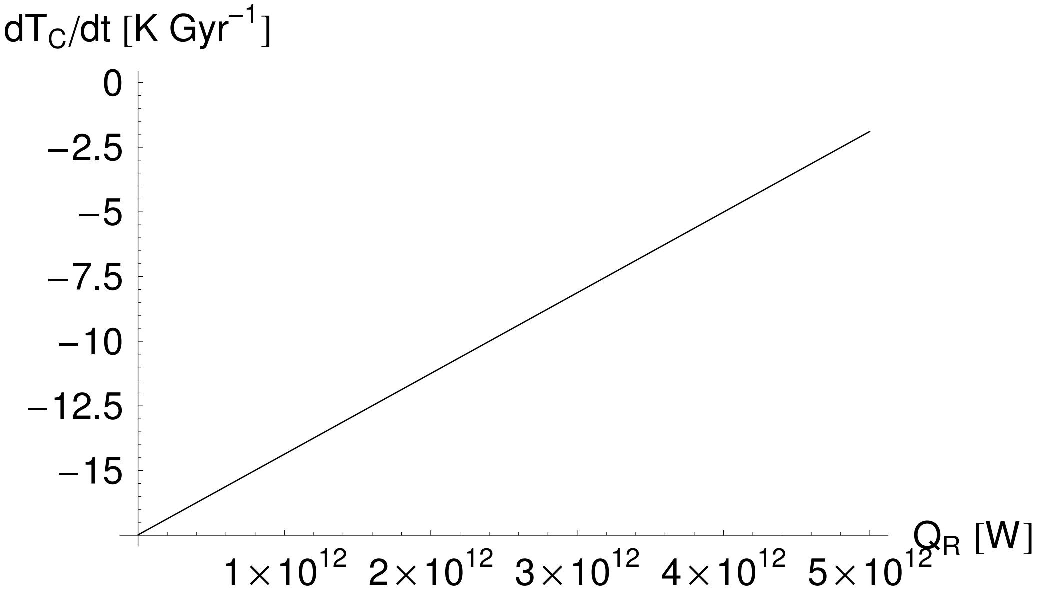
dT_C/dt [K Gyr^-1]
0
−2.5
−5
−7.5
−10
−12.5
−15
Q_R [W]
1×10^12
2×10^12
3×10^12
4×10^12
5×10^12

−Graphics−

C.6.6 dr_i/dt

ΔdTdP = 1.3/10^9

1.3×10^{-9}

Ti = 9600

9600

Tc = 6650

6650

dTc = −24.905693384533667/(10^9 * 86400 * 365)

-7.89754×10^{-16}

ri = 0.95 * (1220/3480) * 6378 * 1000

2.12417×10^{6}

rho0 = 7900

7900

K0 = 500 * 10^9

500000000000

***G* = 6.67384 * 10^ − 11**

6.67384×10^{-11}

rhocen = 24900

24900

***L* = Sqrt[(3 * K0 * (Log[rhocen/rho0] + 1))/(2 * π * *G* * rho0 * rhocen)]**

6.24989×10^{6}

rhoi = rhocen * Exp[−ri^2/*L*^2]

22183.6

***g* = (4 * π/3) * *G* * rhocen * ri * (1 − ((3 * ri^2)/(5 * *L*^2)))**

13.7613

dri = −(((1/(ΔdTdP)) * (Ti/(rhoi * *g*)) * (1/Tc) * dTc) * 10^9 * 86400 * 365)/1000

90.597

Bibliography

Acuña, M.H. et al. (1998): Magnetic Field and Plasma Observations at Mars: Initial Results of the Mars Global Surveyor Mission, Science 279, 1676

Acuña, M.H. et al. (1999): Global Distribution of Crustal Magnetization Discovered by the Mars Global Surveyor MAG/ER Experiment, Science 284, 790

Alfe, D., Gillan, M.J., Price, G.D. (2002): Ab initio chemical potentials of solid and liquid solutions and the chemistry of the Earth's core, Journal of Chemical Physics, 116, 7127

Alfvén, H. (1957): On the Theory of Comet Tails, Tellus, 9, 1, 92

Anderson, J.D. (1996): Gravitational constraints on the internal structure of Ganymede, Nature, 384, 541

Anderson, J.D., Jacobson, R.A., Lau, E.L., et al. (2001): Io's gravity field and interior structure, Journal of Geophysical Research, 106, E12, 32963

Anderson, B.J., Acuña, M.H., Korth, H., et al. (2009): The Magnetic Field of Mercury, Space Sci. Rev., 152, 1-4, 307

Backes, H. et al. (2005): Titan's Magnetic Field Signature During the First Cassini Encounter, Science, 308, 992

Backus, G. (1958): A class of self-sustaining dissipative spherical dynamos, Annals of Physics, 4, 372

Bagenal, F. et al. (2006): Jupiter - The Planet, Satellites and Magnetosphere, Cambridge University Press

Balogh, A., Grard, R., Solomon, S.C., Schulz, R., Langevin, Y., Kasaba, Y., Fujimoto, M. (2007): Missions to Mercury, Space Sci. Rev., 132, 611

Beaugé, C., Ferraz-Mello, S., Michtchenko, T.A. (2008): Planetary Masses and Orbital Parameters from Radial Velocity Measurements, in Extrasolar Planets, chap. 1, pp. 1, edited by Dvorak, R., Wiley-VCH

Bertka, C.M., Fei, Y. (1998): Implications of Mars Pathfinder data for the accretion history of the terrestrial planets, Science, 281, 1838

Binder, A.B. (1998): Lunar Prospector: Overview, Science, 281, 1475

Birch, F. (1952): Elasticity and constitution of the Earth's interior, J. Geophys. Res., 57, 227

Blackett, P.M.S (1947): The magnetic field of massive rotating bodies, Nature, 159, 658

Bland, M.T., Showman, A.P., Tobie, G. (2007): Ganymede's orbital and thermal evolution and its effect on magnetic field generation, Lunar and Planetary Science XXXVIII (2007), 2020

Bland, M.T., Showman, A.P., Tobie, G. (2008): The production of Ganymede's magnetic field, Icarus, 198, 384

Bland, M.T., Showman, A.P., Tobie, G. (2009): The generation of Ganymede's magnetic field, EPSC abstracts, 4, EPSC2009-556, European Planetary Science Congress 2009

Braginsky, S.I. (1963): Structure of the F layer and reasons for convection in the Earth's core, Soviet Physics - Doklady 149: 8-10

Braginsky, S.I. (1964): Self-excitation of a magnetic field during the motion of a highly conducting fluid, Soviet Physics JETP, 20, 726

Braginsky, S.I., Roberts, P.H. (1995): Equations governing Earth's core and the geodynamo, Geoophys. astrophys. Fluid Dyn., 79, 1

Breuer, D., Labrosse, S., Spohn, T. (2009): Thermal Evolution and Magnetic Field Generation in Terrestrial Planets and Satellites, Space Sci. Rev., 152, 449

Bouhifd, M.A., Gautron, L., Bolfan-Casanova, N., Malavergne, V., Hammouda, T., Andrault, D., Jephcoat, A.P. (2007): Potassium partitioning into molten iron alloys at high-pressure: Implications for Earth's core, Physics of the Earth and Planetary Interiors, 160, 22

Buccino, A.P., Lemarchand, G.A., Mauas, P.J.D. (2006): Ultraviolet radiation constraints around the circumstellar habitable zones, Icarus, 183, 491

Buffett, B.A. (2002): Estimates of heat flow in the deep mantle based on the power requirements for the geodynamo, Geoph. Res. Let., 29, 12, 1566

Bullard, E.C. (1949): The magnetic field within the Earth, Proc. R. Soc. Lond A 197, 433

Bullard, E., Gellman, H. (1954): Homogeneous Dynamos and Terrestrial Magnetism, Phil. Trans. Roy. Soc. Lond. A, 247, 928, 213

Burrows, A., Sudarsky, D., Sharp, C., Marley, M., Hubbard, W.B., Lunine, J.I., Guillot, T., Saumon, D., Freedman, R. (1998): Advances in the Theory of Brown Dwarfs and Extrasolar Giant Planets, ASP Conference Series, Vol. 134, 354

Busse, F.H. (1970): Thermal instabilities in rapidly rotating systems, Journal of Fluid Mechanics, 44, 3, 441

Busse, F.H. (1976): Generation of Planetary Magnetismj by Convection, Physics of Earth and Planetary Interiors, 12, 350

Cao, A.M., Romanowicz, B. (2004): Constraints on density and shear velocity contrasts at the inner core boundary, Geophysical Journal International, 157, 1146

Chabot, N.L., Drake, M.J. (1999): Potassium solubility in metal: the effects of composition at 15kbar and 1900$^{\circ}C$ on partitioning between iron alloys and silicate melts, Earth and Planetary Science Letters, 172, 323

Christensen, U.R., Aubert, J. (2006): Scaling properties of convection-driven dynamos in rotating spherical shells and application to planetary magnetic fields, Geophys. J. Int., 166, 97

Christensen, U.R., Wicht, J. (2009): Numerical Dynamo Simulations, in Treatise on Geophysics, Vol. 8, Ch. 8, pp. 245, Elsevier

Christensen, U.R. (2010): Dynamo Scaling Laws and Applications to the Planets, Space Sci. Rev., 152, 565

Colomb, F.R., Alonso, C., Hofmann, C., Nollmann, I. (2004): SAC-C mission, an example of international cooperation, Adv. Space Res., 34, 2194

Coltice, N., Ricard, Y. (1999): Geochemical observations and one layer mantle convection, Earth and Planetary Science Letters, 174, 125

Connerney, J.E.P., Acuña, M.H., Wasilewski, P.J., et al. (2001): The Global Magnetic Field of Mars and Implications for Crustal Evolution, Geophys. Res. Lett., 28, 21, 4015

Corgne, A., Keshav, S., Fei, Y., McDonough, W.F. (2007): How much potassium is in the Earth's core? New insights from partitioning experiments, Earth and Planetary Science Letters, 256, 567

Cowling, T.G. (1934): The magnetic field of sunspots, Monthly Notices of the Royal Astronomical Society, 94, 39

Cowling, T.G. (1957): The dynamo maintenance of steady magnetic fields, Quarterly Journal of Mechanics and Applied Mathematics, 10, 129

Cox, M.M., Battista, J.R. (2005): Deinococcus Radiodurans - the consummate survivor, Nature Reviews Microbiology, 3, 882

Crary, F.J, Bagenal, F. (1998): Remanent ferromagnetism and the interior structure of Ganymede, Journal of Geophysical Research, 103, E11, 25757

Curtis, S.A., Ness, N.F. (1986): Magnetostrophic balance in planetary dynamos - Predictions for Neptune's magnetosphere, Journal of Geophysical Research A, 91, 11003

Dolginov, Sh.Sh., Yeroshenko, Ye.G., and Zhuzgov, L.N. (1973): Magnetic Field in the Very Close Neighborhood of Mars According to Data from the Mars 2 and Mars 3 Spacecraft, Journal of Geophysical Research 78, 22, 4779

Dolginov, Sh.Sh, Pushkov, A.N. (1978): Abstracts of Papers Presented to the Conference on Origins of Planetary Magnetism. A Lunar and Planetary Institute Topical Conference held November 8-11, 1978. LPI Contribution 348, edited by P. C. Robertson, published by the Lunar and Planetary Institute, 3303 Nasa Road 1, Houston, TX 77058, 1978, p.28

Dolginov, Sh.Sh. (1978): On the Magnetic Field of Mars: Mars 2 and 3 Evidence, Geophysical Research Letters, 5, 1, 89

Dolginov, Sh.Sh. (1978): On the Magnetic Field of Mars: Mars 5 Evidence, Geophysical Research Letters 5, 1, 93

Dorfi, E.A. (2007): Lecture notes in "Basics of mathematics and physics for astronomers II", held at the Universtiy of Vienna, Institute of Astronomy, Summer 2007.

Dyal, P., Parkin, C.W., Daily, W.D. (1974): Magnetism and the Interior of the Moon, Reviews of Geophysics and Space Physics, 12, 4, 568

Dyal, P., Parkin, C.W., Daily, W.D. (1976): Structure of the lunar interior from magnetic field measurements, Proc. Lunar Sci. Conf. 7th, 3077

Dziewonski, A.M., Anderson, D.L. (1981): Preliminary Reference Earth Model, Physics of the Earth and Planetary Interiors 25, 297

Earth Science in Maine Wiki (2012): http://earthscienceinmaine.wikispaces.com/6.3+Seafloor+Spreading

Eltayeb, I.A., Roberts, P.H. (1970): On the hydromagnetics of rotating fluids, ApJ, 162, 699

Elsasser, W.M. (1946): Induction Effects in Terrestrial Magnetism, Part I. Theory, Physical Review, Vol. 69, Nos. 3 and 4, 106

Elsasser, W.M. (1946): Induction Effects in Terrestrial Magnetism, Part II. The Secular Variation, Physical Review, Vol. 70, Nos. 3 and 4, 202

Elsasser, W.M. (1946): Induction Effects in Terrestrial Magnetism, Part III. Electric Modes, Physical Review, Vol. 72, Nos. 3 and 4, 821

Elsasser, W.M. (1950): The Earth's Interior and Geomagnetism, Reviews of Modern Physics, 22, 1, 1

ESA Website (2012): http://sci.esa.int/science-e/www/area/index.cfm?fareaid=30

Fender, R.P. (2007): LOFAR Transients and the Radio Sky Monitor, Proceedings of "Bursts, Pulses and Flickering: wide-field monitoring of the dynamic radio sky". 12-15 June 2007, Kerastari, Tripolis, Greece., p.30

Fowler, C.M.R. (2005): The Solid Earth - An Introduction to Global Geophysics, Second Edition, Appendix 7, p. 648, Cambridge University Press

Fridlund, M., Kaltenegger, L. (2008): Mission Requirements: How to Search for Extrasolar Planets, in Extrasolar Planets, ch. 3, pp. 51, edited by Dvorak, R., Wiley-VCH

Gaidos, E., Conrad, C.P., Manga, M., Hernlund, J. (2010): Thermodynamic Limits on Magnetodynamos in Rocky Exoplanets, ApJ, 718, 2, 596

Gailitis, A. (1970): Self-excitation of a magnetic field by a pair of annular vortices, Magnetohydrodynamics, 6, 1, 14

Gauß, C.F. (1839): Allgemeine Theorie des Erdmagnetismus, Leipzig

Geomagnetism Website (2012): http://geomag.org/info/equatorial_electrojet.html

Geomagnetism Website (2012): http://www.geomag.us/info/magnetosphere.html

Glatzmaier, G., Roberts, P. (1995): A three-dimensional self-consistent computer simulation of a geomagnetic field reversal, Nature, 337, 203

Gold, Th. (1999): The Deep Hot Biosphere - The Myth of Fossil Fuels, Springer

Goldstein, B.E., Phillips, R.J., Russell, C.T. (1976): Magnetic evidence concerning a lunar core, Proc. Lunar Sci. Conf 4th, 3321

Gómez-Pérez, N., López-Morales, M. (2010): Predicted dynamos for terrestrial extra-solar planets and their influence in habitability, EPSC Abstracts, Vol.5, EPSC2010-299

Grasset, O., Schneider, J., Sotin, C. (2009): A study of the accuracy of mass-radius relationship for silicate-rich and ice-rich planets up to 100 Earth-masses, ApJ, 693, 722

Greff-Lefftz, M., Legros, H. (1999): Core rotational dynamics and geological events, Science, 286, 1707

Gubbins, D., Masters, T.G., Jacobs, J.A. (1979): Thermal evolution of the Earth's core, Geophys. J. R. astr. Soc., 59, 57

Gubbins D., Alfè, D., Masters, G., Price, G.D., Gillan, M.J. (2003): Can the Earth's dynamo run on heat alone?, Geophys. J. Int., 155, 609

Gubbins, D., Alfè, D., Masters, G., Price, G.D., Gillan, M. (2004): Gross thermodynamics of two-component core convection, Geophys. J. Int., 157, 1407

Gurnett, D.A. (1996): Evidence for a magnetosphere at Ganymede from plasma-wave observations by the Galileo spacecraft, Nature, 384, 535

Hauck, S.A. et al. (2006): Sulfur's impact on core evolution and magnetic field generation on Ganymde, Journal of Geophysical Research, 111, E09008

Heng, K., Vogt, S.S. (2011): Gliese 581g as a scaled-up version of Earth: atmospheric circulation simulations, MNRAS, 415, 2145

Herbert, F., Wiskerchen, M., Sonett, C.P., Chao, J.K. (1976): Solar Wind Induction in Mercury: Constraints on the Formation of a Magnetosphere, Icarus, 28, 489

Herzenberg, A. (1958): Geomagnetic dynamos, Phil. Trans. Roy. Soc. Lond. A, 250, 543

Hewitt, J., McKenzie, D.P., Weiss, N.O. (1975): Dissipative heating in convective flows, Journal of Fluid Mechanics, 68, 721

Hoffmeyer, P. (2000): The Ørsted Satellite Project, Air & Space Europe, 2, 5, 74

Hulot, G., Finlay, C.C., Constable, C.G., Olsen, N., Mandea, M. (2010): The Magnetic Field of Planet Earth, Space Sci. Rev., 152, 1-4, 159

Iess, L., Rappaport, N.J., Jacobson, R.A., et al. (2010): Gravity Field, Shape, and Moment of Inertia of Titan, Science, 327, 1367

Iro, N., Deming, L.D. (2010): A Time-Dependent Radiative Model for the Atmosphere of the Eccentric Exoplanets, ApJ, 712, 218

Jakosky, B.M. (2011): The 2013 Mars Atmosphere and Volatile EvolutioN (MAVEN) Mission to Mars, The Fourth International Workshop on the Mars Atmosphere: Modelling and observation, held 8-11 February, 2011, in Paris, France, Published online at http://www-mars.lmd.jussieu.fr/paris2011/program.html, pp.477-477

JAXA Website (2012): http://www.stp.isas.jaxa.jp/mercury/p_bepi.html

Jeffreys, H. (1926): The rigidity of the Earth's central core, Monthly Notices of the Royal Astronomical Society Geophysical Supplement, 1, 371

Jia, X. et al. (2010): Magnetic Fields of the Satellites of Jupiter and Saturn, Space Sci. Rev., 152, 271

Jones, D.E. et al. (1980): A Possible Magnetic Wake of Titan: Pioneer 11 Observations, Journal of Geophysical Research, 85, A11, 5835

Jones, C.A (2007): Les Houches Summer School 2007 Notes on Dynamo Theory, http://www.maths.leeds.ac.uk/c̃ajones/LesHouches/chapter.pdf

Jones, C.A (2007): NORDITA Winter School 2010, Graduate Lecture "Planetary magnetic fields and interior structure", http://www.maths.leeds.ac.uk/c̃ajones/NORDITA/Nordita_1.pdf

Kageyama, A., Sato, T. (1995): Computer simulation of a magnetohydrodynamic dynamo. II, Physics of Plasmas 2, 1421

Kasting, J.F., Whitmire, D.P., Reynolds, R.T. (1993): Habitable zones around main sequence stars, Icarus, 101, 108

Keane, A. (1954): An Investigation of Finite Strain in an Isotropic Material Subjected to Hydrostatic Pressure and Its Seismological Applications, Australian Journal of Physics, 7, 322

Kimura, J., Nakagawa, T., Kurita, K. (2009): Size and compositional constraints of Ganymede's metallic core for driving an active dynamo, Icarus, 202, 216

Kivelson, M.G. et al. (1996): A Magnetic Signature at Io: Initial Report from the Galileo Magnetometer, Science, 273, 337

Kivelson, M.G. et al. (1996): Io's Interaction with the Plasma Torus: Galileo Magnetometer Report, Science, 274, 396

Kivelson, M.G. et al. (1996): Discovery of Ganymede's magnetic field by the Galileo spacecraft, Nature, 384, 537

Kivelson, M.G. et al. (1997): The magnetic field and magnetosphere of Ganymede, Geophysical Research Letters, 24, 17, 2155

Kivelson, M.G. (2002): The Permanent and Inductive Magnetic Moments of Ganymede, Icarus, 157, 507

Kuang, W., Bloxham, J. (1999): Numerical Modeling of Magnetohydrodynamic Convection in a Rapidly Rotating Spherical Shell: Weak and Strong Field Dynamo Action, Journal of Computational Physics, 153, 51

Labrosse, S., Poirier, J.-P., Le Mouël, J.-L. (1997): On cooling of the Earth's core, Physics of the Earth and Planetary Interiors, 99, 1

Labrosse, S., Poirier, J.-P., Le Mouël, J.-L. (2001): The age of the inner core, Earth and Planetary Science Letters, 2001, 111

Labrosse, S. (2003): Thermal and magnetic evolution of the Earth's core, Physics of the Earth and Planetary Interiors, 140, 127

Labrosse, S., Hernlund, J.W., Coltice, N. (2007): A crystallizing dense magma ocean at the base of the Earth's mantle, Nature, 450, 866

Landau, L.D., Lifschitz, E.M. (1959): Course of Theoretical Physics, Vol. 6, Fluid Mechanics. London: Pergamon

Larmor, J. (1920): How could a Rotating Body such as the Sun become a Magnet?, Report of 87th meeting of the British Association for the Advancement of Science, September, 1919. Published by John Murray.

Lehmann, I. (1936): publications of the International geodetic & geophysical Union, Association of seismology, Seria A, Travaux Scientifiques 14, 87

Leitner, J (2006): Heat Transport Mechanisms through the Venusian Lithosphere, Diploma Thesis, Institute for Astronomy, University of Vienna

Leitner J. J., Firneis M. G., Hitzenberger R. (2010): Potential Habitats for Exotic Life Within the Life Supporting Zone, Geophysical Research Abstracts, Vol. 12, Abstract No. EGU2010-12544

Lewis, J.S. (1971): Consequences of the presence of sulfur in the core of the Earth, Earth and Planetary Science Letters, 11, 130

Lin, R.P., Mitchell, D.L., Curtis, D.W., et al. (1998): Lunar Surface Magnetic Fields and Their Interaction with the Solar Wind: Results from Lunar Prospector, Science, 281, 1480

Lineweaver, C.H., Fenner, Y., Gibson, B.K. (2004): The galactic habitable zone and the age distribution of complex life in the Milky Way, Science, 303, 59

Lowrie, W. (2006): Fundamentals of Geophysics, Cambridge University Press, Seventh Printing 2006.

Manthilake, G.M., de Koker, N., Frost, D.J., McCammon, C.A. (2011): Lattice thermal conductivity of lower mantle minerals and heat flux from Earth's core, PNAS, 10.1073/pnas.1110594108

Master, G., Gubbins, D. (2003): On the resolution of density within the Earth, Physics of the Earth and Planetary Interiors, 140, 159

Mitchell, D.L., Halekas, J.S., Lin, R.P., et al. (2008): Global mapping of lunar crustal magnetic fields by Lunar Prospector, Icarus, 194, 401

Mizutani, H., Yamamoto, T., Fujimura, A. (1992): A New Scaling Law of the Planetary Magnetic Fields, Adv. Space Res., 12, 8, (8)265

Moffatt, H.K. (1978): Magnetic field generation in electrically conducting fluids, Cambridge University Press.

Mouël, J.-L., Shebalin, P., Chulliat, A. (2006): The field of the equatorial electrojet from CHAMP data, Ann. Geophys., 24, 515

Möhlmann, D. et al. (1991): The Question of an Internal Martian Magnetic Field, Planet. Space Sci. 39, 1/2, 83

Möhlmann, D. et al. (1992): Magnetic Field Environment of Mars as Studied by Phobos-2, Adv. Space Res. 12, 9, (9)221

Murphy, K.L., Patterson, E.T (1998): Mars Global Surveyor Aerobraking - A Collaborative Team Approach in the Physics Classroom, The Physics Teacher, 36, 154

Murrell, M.T., Burnett, D.S. (1986): Partitioning of K, U, and Th Between Sulfide and Silicate Liquids: Implications for Radioactive Heating of Planetary Cores, J. Geophys. Res., 91, 8126

Murthy, V.R., van Westrenen, W., Fei, Y. (2003): Experimental evidence that potassium is a substantial radioactive heat source in planetary cores, Nature, 423, 163

Murthy, V.R., Draper, D.S., Agee, C.B. (2006): Uranium in the Earth's Core? Metal-silicate partitioning of Uranium at High Pressure and Temperature and Highly Reducing Conditions, Workshop on Early Planetary Differentiation 2006, 4036

NASA's Cosmos Website (2012): http://ase.tufts.edu/cosmos/print_images.asp?id=7

NASA Website(2012): http://www.nasa.gov/mission_pages/juno/main/index.html

NASA Website(2012): http://www.nasa.gov/mission_pages/maven/main/index.html

Neubauer, F.M. (1978): Possible Strengths of Dynamo Magnetic Fields of the Galilean Satellites and of Titan, Geophysical Research Letter, 5, 11, 905

Neubauer, F.M. et al. (1984): Titan's Magnetospheric Interaction, in Saturn, ed. by T. Gehrels, M.S. Matthews (University of Arizona Press, Tuscon, 1984), pp. 760-787

Neubauer, F.M. et al. (2006): Titan's near magnetotail from magnetic field and electron plasma observations and modeling: Cassini flybys TA, TB, and T3, Journal of Geophysical Research, 11, A10220

Ness, N.F., Behannon, K.W., Lepping, R.P., Whang, Y.C., Schatten, K.H. (1974): Magnetic Field Observations near Mercury: Preliminary Results from Mariner 10, 185, 151

Ness, N.F., Behannon, K.W., Lepping, R.P. (1975): The Magnetic Field of Mercury, 1; Journal of Geophysical Research, 80, 19, 2708

Ness, N.F. et al. (1982): The Induced Magnetosphere of Titan, Journal of Geophysical Research, 87, A3, 136

Neubauer, D., Vrtala, A., Leitner, J.J., Firneis, M.G., Hitzenberger, G. (2011): Development of a model to computate the extension of life supporting zones for earth-like exoplanets, Origin of life and evolution of biospheres, DOI: 10.1007/s11084-011-9259-9, in press

Nimmo, F., Price, G.D., Brodholt, J., Gubbins, D. (2004): The influence of potassium on core and geodynamo evolution, Geophys. J. Int., 156, 363

Nimmo, F. (2009): Energetics of the Core, in Treatise on Geophysics, Vol. 8, Ch. 2, p. 33, Elsevier

Olsen P.,Christensen, U.R. (2006): Dipole moment scaling for convection driven planetary dynamos, Earth Planet. Sci. Lett., 250, 3-4, 561

Olsen, N., Lühr, H., Sabaka, T.J., et al. (2006): CHAOS - a model of the Earth's magnetic field derived from CHAMP, Ørsted, and SAC-C magnetic satellite data, Geophys. J. Int., 166, 67

Olsen, P. (2009): Overview, in Treatise on Geophysics, Vol. 8, Ch. 1, p. 13, Elsevier

Onwumechili, C.A., Agu, C.E. (1980): General Features of the Magnetic Field of the Equatorial Electrojet Measured by the POGO Satellites, Planet. Space Sci., 28, 1125

Paty, C., Winglee, R. (2006): The role of ion cyclotron motion at Ganymede: Magnetic field morphology and magnetospheric dynamics, Geophysical Research Letters, 33, L10106

Parker, E.N. (1955): Hydromagnetic dynamo models, Astrophysical Journal, 122, 293

Phillips, J.K., Russel, C.T. (1987): Upper Limit on the Intrinsic Magnetic Field of Venus, Journal of Geophysical Research, 92, A3, 2253

Poirier, J.-P. (1994): Light elements in the Earth's outer core: A critical review, Physics of the Earth and Planetary Interiors, 85, 319

Ponomarenko, Y.B. (1973): On the theory of the hydromagnetic dynamo, J. Appl. Mech. Tech. Phys., 14, 775

Priest, E., Forbes, T. (2006): Magnetic Reconnection - MHD Theory and Applications, Cambridge University Press

Rädler, K.-H. (1968): On the electrodynamics of conducting fluids in turbulent motion. II. Turbulent conductivity and turbulent permeability, Zeitschrift für Naturforschung, 23a, 1851

Rajaram, M. (1993): MAGSAT's Contribution to Geophysical Surveys, Adv. Space Res., 13, 11, (11)33

Rauer, H., Erikson, A. (2008): The Transit Method, in Extrasolar Planets, chap. 9, pp. 207, edited by Dvorak, R., Wiley-VCH

Reigber, Ch., Lühr, H., Schwintzner, P. (2002): CHAMP Mission Stauts, Adv. Space Res., 30, 2, 129

Roberts, P.H., Stix, M. (1971): The Turbulent Dynamo - A Translation of a series of papers by F. Krause, K.-H. Rädler, and M. Steenbeck, Technical Note NCAR-TN/IA-60 from National Center for Atmospheric Research, Boulder, Colorado

Roberts, P.H., Glatzmaier, G.A. (2000): Geodynamo theory and simulations, Reviews of Modern Physics, 72, 4, 1081

Roberts, P.H. (2009): Theory of the Geodynamo, in Treatise on Geophysics, Vol.8 - Core Dynamics, Elsevier, 2009

Russell, C.T., Coleman Jr., P.J., Lichtenstein, B.R., Schubert, G., Sharp, L.R. (1973): Subsatellite measurements of the lunar magnetic field, Proc. Lunar Sci. Conf. 4th, Suppl. 4, Vol. 3, 2833

Russell, C.T., Lichtenstein, B.R. (1975): On the Source of Lunar Limb Compression, Journal of Geophysical Research, 80, 34, 4700

Russell, C.T., Coleman Jr., P.J., Fleming, B.K., et al. (1975): The fine-scale lunar magnetic field, Proc. Lunar Sci. Conf. 6th, 2955

Russell, C.T., Goldstein, B.E. (1976): The geomagnetic dynamo of the Moon and Venus: Comparisons with a recent scaling law, Proc. Lunar Sci. Conf. 7th, 3343

Russell, C.T. (1978): Re-evaluating Bode's law of planetary magnetism, Nature, 272, 147

Russell, C.T. (1978): Lunar and Planetary Science Conference, 9th, Houston, Tex., March 13-17, 1978, Proceedings. Volume 3. (A79-39253 16-91) New York, Pergamon Press, Inc., 1978, p. 3137-3149.

Russell, C.T. (1978): The Magnetic Field of Mars: Mars 5 Evidence Re-examined, Geophysical Research Letters, 5, 1, 85

Russell, C.T. (1981): The Magnetic Fields of Mercury, Venus and Mars, Adv. Space Res. 1, 3

Sage, L.J (1997): Second Light, JRASC, 91, 18

Sarson, G.R., et al. (1997): Magnetoconvection Dynamos and the Magnetic Fields of Io and Ganymede, Science, 276, 1106

Schubert, G. et al. (1996): The magnetic field an internal structure of Ganymede, Nature, 384, 544

Schubert, G., Limonadi, D. (1994): Gravitational Coefficients and Internal Structures of the Icy Galilean Satellites: An Assessment of the Galileo Orbiter Mission, Icarus, 111, 433

Senshu, H., Kuramoto, K., Matsui, T. (2002): Thermal evolution of a growing Mars, J. Geophys. Res (Planets), 107, E12, 1

Shanker, J., Singh, B.P. (2005): A comparative study of Keane's and Stacey's equations of state, Physica B, 370, 78

Shearer, P., Masters, G. (1990): The density and shear velocity contrast at the inner core boundary, Geophysical Journal International, 102, 491, ApJ, 597, 1092

Shkolnik, E., Walker, G.A.H., Bohlender, D.A. (2003): Evidence for planet-induced chromospheric activity on HD 179949

Slavin, J.A., Acuña, M.H., Anderson, B.J., et al. (2008): Mercury's Magnetosphere After MESSENGER's First Flyby, Science, 321, 85

Solomatov, V.S. (1995): Scaling of temperature- and stress-dependent viscosity convection, Phys. Fluids, 7, 266

Sotin, C., Grasset, O., Mocquet, A. (2007): Mass-radius curve for extrasolar Earth-like planets and ocean planets, Icarus, 191, 337

Stacey, F.D. (2000): The K-primed approach to high-pressure equations of state, Geophys. J. Int, 143, 621

Stacey, F.D. (2005): High pressure equations of state and planetary interiors, Rep. Prog. Phys., 68, 341

Stacey, F.D., Davis, P.M. (2008): Physics of the Earth, Cambridge University Press.

Stamenković, V., Breuer, D. (2010): No Magnetic Fields on Super-Earths?, EPSC Abstracts, Vol.5, EPSC2010-910

Stamenković, V., Breuer, D., Spohn, T. (2011): Thermal and transport properties of mantle rock at high pressure: Applications to super-Earths, Icarus, 216, 572

Stanley, S., Glatzmaier, G.A. (2010): Dynamo Models for Planets Other Than Earth, Space Sci. Rev., 152, 617

Starchenko, S.V., Jones, C.A. (2002): Typical Velocities and Magnetic Field Strengths in Planetary Interiors, Icarus, 157, 426

Steenbeck, M., Krause, F., Rädler, K.-H. (1966): Berechnung der mittleren Lorentz-Feldstärke $\overline{\mathbf{v} \times \mathbf{B}}$ für ein elektrisch leitendes Medium in turbulenter, durch Coriolis-Kräfte beeinflußter Bewegung, Zeitschrift für Naturforschung, 21a, 369

Steenbeck, M., Krause, F. (1969): Zur Dynamotheorie stellarer und planetarer Magnetfelder II. Berechnung planetenähnlicher Gleichfeldgeneratoren, Astronomische Nachrichten, 291, 271

Stevens, I.R. (2005): Magnetospheric radio emission from extrasolar giant planets: the role of the host stars, Mon. Not. R. Astron. Soc., 356, 1053

Stevenson, D.J., Spohn, T., Schubert, G. (1983): Magnetism and Thermal Evolution of the Terrestrial Planets, Icarus, 54, 466

Stevenson, D.J. (2009): Planetary Magnetic Fields: Achievements and Prospects, Space Sci. Rev., 152, 651

Tarduno, J.A., Cottrell, R.D., Watkeys, M.K., Bauch, D. (2007): Geomagnetic field strength 3.2 billion years ago recorded by single silicate crystals, Nature, 446, 657

Taylor, J. (1963): The magnetohydrodynamics of a rotating fluid and the earth's dynamo problem, Proc. Roy. Soc. London A, 274, 274

Titov, D.V., Svedhem, H., Taylor, F.W., et al. (2009): Venus Express: Highlights of the Nominal Mission, Solar System Research, 43, 185

Touma, J., Wisdom, J. (2001): Nonlinear core-mantle coupling, Astronomical Journal, 122, 1030

Tsunakawa, H., Shibuya, H., Takahashi, F., et al. (2010): Lunar Magnetic Field Observations and Inital Global Mapping of Lunar Magnetic Anomalies by MAP-LMAG Onboard SELENE(Kaguya), Space Sci. Rev., 154, 1-4, 219

Turcotte, D.L., Schubert, G. (2002): Geodynamics, chap. 4, pp. 136-137, Cambridge University Press

Valencia, D., O'Connell, R., Sasselov, D.D. (2006): Internal structure of massive terrestrial exoplanets, Icarus, 181, 545

Valencia, D., Sasselov, D.D., O'Connell, R.O. (2007): Radius and structure models of the first Super-Earth planet, ApJ, 656, 545

Valencia, D., Sasselov, D.D., O'Connell, R.O. (2007): Detailed models of Super-Earths: How well can we infer bulk properties?, ApJ, 665, 1413

Vallée, J.P. (1998): Observations of the Magnetic Fields Inside and Outside the Solar System: From Meteorites (10 attoparsecs), Asteroids, Planets, Stars, Pulsars, Masers, To Protostellar Cloudlets ($<$ 1 parsec), Fundamentals of Cosmic Physics, Vol. 19, pp. 319-422

van Heck, H.J., Tackley, P.J. (2011): Plate tectonics on super-Earths: Equally or more likely than on Earth, Earth and Planetary Science Letters, 310, 252

Wagner, F.W., Sohlm, F., Rauer, H. (2010): Thermal State of Terrestrial Exoplanet Interiors, EPSC Abstracts, Vol. 5, EPSC2010-909

Wagner, F.W., Sohl, F., Rückriemen, T., Rauer, H. (2011): Physical State of the Deep Interior of the CoRoT-7b Exoplanet, eprint arXiv:1105.1271

Wagner, F.W., Sohl, F., Hussmann, H., Grott, M., Rauer, H. (2011): Interior structure models of solid exoplanets using material laws in the infinite pressure limit, Icarus, 214, 366

Wächershäuser, G. (1992): Groundworks for an evolutionary biochemistry - the iron-sulfur world, Prog. Biophys. Mol. Biol. 58, 85

Wen, L., Helmberger, D.V. (1998): Ultra-Low Velocity Zones Near the Core-Mantle Boundary from Broadband PKP Precursors, Science, 279, 1701

Wieczorek, Weiss, B.P. (2010): Testing the Lunar Dynamo Hypothesis Using Global Magnetic Field Data, 41st Lunar and Planetary Science Conference, 1625

Wienbruch, U., Spohn, T. (1995): A self sustained magnetic field on Io?, Planet. Space Sci., 43, 9, 1045

WIKIPEDIA (2012): http://en.wikipedia.org/wiki/Mars_Climate_Orbiter

Bao, X. (2009): Distribution of U and Th and Their Nuclear Fission in the Outer Core of the Earth and Their Effects on the Geodynamics, eprint arXiv: 0903.1566

Zeldovich, Y.B. (1956): The magnetic field in the two-dimensional motion of a conducting fluid, Soviet Physics JETP, 31, 154

Abstract (in German)

Die Erde ist bis heute der einzige Planet, den wir kennen, der die Bedingungen für Leben erfüllt. Einerseits befindet sie sich gerade in der richtigen Entfernung von der Sonne, um flüssiges Wasser zu ermöglichen, andererseits schirmt sie hochenergetische Strahlung von der Sonne und aus den Tiefen des Alls durch ihr Magnetfeld ab und schützt somit Leben auf der Oberfläche vor deren tödlichen Wirkung. Die Erde ist einer von nur zwei terrestrischen Planeten in unserem Sonnensystem, der über diesen Schutzmechanismus verfügt - Merkur ist der andere Planet, wenngleich er auch mit einem weit schwächeren Magnetfeld ausgestattet ist als die Erde. Der Mars verfügte zwar nach heutigem Wissensstand über ein Magnetfeld in seiner frühen Geschichte, der dafür verantwortliche Mechanismus ist aber seit langem zum Erliegen gekommen. Die Venus, so vermutet man heute, hatte niemals diese Fähigkeit, trotz vieler anderen Ähnlichkeiten zur Erde. Damit stellt sich die Frage, was einen terrestrischen Planeten befähigt, ein Magnetfeld zu erzeugen und dieses über geologische Zeitskalen aufrecht zu erhalten. Da in den letzten Jahren die Zahl der bekannten extrasolarer Planeten (oder Exoplaneten) sprunghaft angestiegen ist, ist dies auch im Zusammenhang mit terrestrischen Planeten bei anderen Sternen von Bedeutung. Was für Eigenschaften müssen diese aufweisen, um ein Magnetfeld erzeugen zu können? Können Super-Erden, terrestrische Exoplaneten mit mehreren Erdmassen, Magnetfelder erzeugen und so eine der vermeintlichen Grundvoraussetzungen für die Entstehung von Leben erfüllen? Der Mechanismus, der für die Entstehung eines Magnetfeldes in einem Planeten verantwortlich ist, wird als planetarer Dynamo bezeichnet. Durch die Bewegung eines elektrisch leitenden Mediums in einem äußeren Magnetfeld wird durch Induktion das planetare Feld erzeugt. In der Erde finden im äußeren Kern Konvektionsbewegungen des dort vorhandenen flüssigen Eisens statt. Da sich die Erde im interplanetaren Magnetfeld und dem der Sonne befindet, erzeugen diese Konvektionsbewegungen durch Induktion selbst ein Magnetfeld. Da jedes reale, leitende Medium allerdings keinen unendlich kleinen elektrischen Widerstand aufweisen kann, kommt es durch den ohmschen Widerstand zu Verlusten, die das Magnetfeld in relativ kurzer Zeit zum Erliegen bringen würden. Um einen selbsterhaltenden Dynamo zu gewährleisten muß dieser Verlust durch neuerliche

Induktion ausgeglichen werden. Nur dann kann ein Planet ein über geologisch relevante Zeitskalen aktives Magnetfeld aufrecht erhalten, wie es in der Erde der Fall ist. Da das Magnetfeld eines Planeten in dessen Kern entsteht, stellt sich die Frage, welche Eigenschaften ein planetarer Kern aufweisen muß, um ausreichend starke Konvektion zu ermöglichen und welche Rolle seine Größe dabei spielt. Desweiteren ist die Rolle von radioaktiven Elementen im Kern auf die Konvektion und damit das Magnetfeld ein wichtiger Punkt, der zu beachten ist. Es stellt sich heraus, dass die Rate, mit der der planetare Kern auskühlt, eine entscheidende Rolle spielt. Da hierfür die Fähigkeit des Mantels, Wärme aus dem Kern abzuleiten, ebenfalls entscheidend ist, kann der Kern nicht isoliert betrachtet werden und muß als System zusammen mit dem Mantel untersucht werden. Durch die Verwendung eines Energie- und Entropiebilanzmodells des Kerns, basierend auf der Erde, sowie eines parametrisierten Mantelkonvektionsmodells, wird der Wärmefluß vom Kern in den Mantel und die einzelnen Beiträge zu diesem berechnet, sowie die Fähigkeit bestimmt, ein Magnetfeld zu erzeugen und aufrecht zu erhalten. Wenn Konvektion dominiert, kann die Stärke des Magnetfeldes durch ein Skalierungsgesetz abgeschätzt werden. Durch die Verwendung der Ergebnisse eines Strukturmodells kann dies dann auf Exoplaneten mit unterschiedlicher Masse angewandt werden. Allerdings muß berücksichtigt werden, daß nur dann Konvektion stattfindet, wenn die adiabatisch geleitete Wärme nicht größer ist, als der Wärmefluß über die Kern-Mantel-Grenze. Da Konvektion eine Grundvoraussetzung für die Anwendung des Energie- und Entropiebilanzmodells darstellt, ist diese Beschränkung durch die Wärmeflüsse ebenfalls eine Beschränkung für die Bilanzmodelle. Die Berechnungen für Exoplaneten mit 5 und 10 Erdmassen zeigen, daß in solchen Planeten wahrscheinlich keine Konvektion im Kern vorhanden ist. Aufgrund der zu erwartenden hohen Viskosität und des hohen Drucks im Inneren dieser Planeten ist es sehr wahrscheinlich, daß Wärmeleitung den dominierenden Transportmechanismus darstellt. Für den Fall der Keane-Zustandsgleichung ergibt sich für einen Planeten mit 5 Erdmassen ein Wärmefluß über die Kernmantelgrenze von 5.61 TW im Vergleich zu einem Wärmefluß durch Wärmeleitung von 33.37 TW, bzw. von 12.13 TW und 93.60 TW im Falle eines Planeten mit 10 Erdmassen. Trotz der Probleme, die die verwendeten Ansätze mit sich bringen, ist zu erwarten, dass der Trend qualitativ richtig ist, nämlich eine zunehmende Bedeutung von Wärmeleitung mit zunehmender planetarer Masse und gleichzeitige Abnahme von Konvektion. Daher ist es eher unwahrscheinlich, dass terrestrische Exoplaneten mit mehreren Erdmassen ein Magnetfeld über geologische Zeitskalen aufrechterhalten können und deren Habitabilität ist daher, zumindest aus diesem Blickwinkel, zu bezweifeln.

Abstract (in English)

The earth is the only habitable planet known to date. One reason for this is the fact that the distance to the sun is just the proper one to enable water to exist in its liquid phase. On the other hand, earth's magnetic field shields highly energetic radiation from the sun and the depths of space, and thus protects life at the surface from its lethal effect. The earth is one of only two terrestrial planets in the solar system which possesses this protective mechanism, the other being Mercury, but with a magnetic field much weaker than the earth's. From what we know today, Mars did possess one in its early history, but the field has decayed long ago. Venus probably never had the ability to generate a magnetic field, although it is so similar to earth in many other respects. Therefore the question arises what prerequisites a planet has to exhibit in order to generate and sustain a magnetic field over geological time. Since the number of known exoplanets has increased dramatically in the last years, this question is also of interest with regard to terrestrial planets around other stars. What planetary characteristics are needed in order to enable a planet to generate a magnetic field? Are super-earths, terrestrial exoplanets with many times the mass of the earth, capable of producing magnetic fields and fulfilling one of the prerequisites for the emergence of life? The mechanism responsible for the generation of a planetary magnetic field is called a planetary dynamo. By the motion of an electrically conducting medium in an external magnetic field the planetary field is created via induction processes. In the earths' outer core convective motions of fluid iron take place, which create an induction field due to the fact that the earth is enclosed by the interplanetary and the sun's magnetic field. Since every conducting medium suffers from Ohmic dissipation, the magnetic field would decay rather soon. For a self-sustaining dynamo to be possible, this Ohmic losses have to be compensated for by continuous induction, which generates new magnetic flux, and only then can a planet sustain a magnetic field over geological time, like it is the case for the earth. Since the magnetic field of a planet originates in its core, the question arises, which properties a planetary core must exhibit to enable convection vigorously enough for the generation of a magnetic field, and which role the size of the core is playing. Furthermore, the influence of radioactive elements in the core on convection and thus the magnetic field is of crucial importance, which should not be neglected. It turns out that the rate of core cooling plays a decisive role. Since the ability of the mantle to extract heat from the core is also essential in this context, mantle and core cannot be considered isolated from each other but their

interaction has to be accounted for. By calculating the energy and entropy budget of the core, based on a model for the earth, and employing a parameterized convection model for the mantle, the heat flow from the core towards the mantle and the different contributions to it are determined, as well as the ability to generate and sustain a magnetic field. If convection is dominating, the strength of the magnetic field can be determined by applying an appropriate scaling law. Using the results from a model of the inner structure of terrestrial planets allows to apply these findings to exoplanets with different masses than the earth. However, it has to be considered that the heat conducted down the adiabat must not exceed the heat flow across the core-mantle boundary in order to allow convection to take place. Since convection is one of the key assumptions for the calculation of the energy and entropy budget of the core, this constraint of conductive and convective heat flows also is a constraint for the determination of the energy and entropy budget. Calculations for planets with 5 and 10 earth masses, respectively, show that in such planets probably no convection takes place. Due to the expected high viscosities and pressures in the interiors of these bodies it is very likely that conduction becomes the dominant mechanism of heat transport. Using the Keane-EoS in the case of a planet with 5 earth masses results in a heat flow across the core-mantle boundary of 5.61 TW, in contrast to heat conducted down the adiabat of 33.37 TW, and of 12.13 TW and 93.60 TW in the case of planets with 10 earth masses. Despite the shortcomings of the approaches used, it is expected that the qualitative trend of increasing importance of heat conduction with increasing mass and subsequent decreasing importance of convection is correct. Thus, it is unlikely that terrestrial exoplanets more massive than the earth will sustain a magnetic field over geological time, and therefore their habitability is questionable, at least from this point of view.

Curriculum Vitae

General

Name: Manfred Gold

Adress: Keltenweg 1/1/5, 7100 Neusiedl am See, Austria

Day of birth: 19.07.1977

Place of birth: Vienna

Nationality: Austria

Education

1983 - 1987: elementary school in Vienna

1987 - 1991: Goethe gymnasium in Vienna

1991 - 1996: school for EDP and management HTBLVA Wien V, Spengergasse

1998 - 2003: studies in Jazz guitar at the Vienna Konservatorium

2004: start of university studies in astronomy

2007: start of university studies in physics

Scientific Memberships

AGU - American Geophysical Union (since 2009)

Scientific Publications

Gold, M.W., Leitner, J.J., Firneis, M.G. (2012): Self-sustaining Dynamos in Massive Terrestrial Exoplanets?, 43rd Lunar and Planetary Science Conference, print-only abstract

Gold, M.W., Leitner, J.J., Firneis, M.G. (2012): Do Super-Earths Have Convective Cores?, Geophys. Res. Abstracts, Vol. 14, EGU2012-PREVIEW, EGU General Assembly 2012

Work Experience

1997 - 2001: software developer, BEKO Ing. P. Kotauczek GmbH

2001 - 2002: software developer, Database Marketing GmbH

2002 - 2005: software developer, UNIKAT Hochschulinformationssysteme GmbH

2005 - 2006: software developer, AV Büroservice GmbH
since 2002: additionally free-lancing
2007 - 2009: free-lancing software developer, supervising the website of the Österreichischer Versicherungsmaklerring (ÖVM)
2010 - 2012: tutor for the Astronomical Laboratory Exercises for Beginners at the Institute of Astronomy, during summer terms 2010, 2011 and 2012
2010 - 2012: tutor for Physics Laboratory Course for Nutritional Sciences at the Insitute of Physics, University of Vienna
2009 - 2012: staff member of the Research Platform: ExoLife, University of Vienna

Other Activities

2009-2011: Chairman of the Student's Council at the Institute of Astronomy, University of Vienna